University of California, Merced

Sierra Nevada isotope hydrology, tracking links between forest water sources, subsurface storage and major river runoff

A dissertation submitted in partial satisfaction of the requirements

for the degree Doctor of Philosophy

in

Environmental Systems

By

Melissa Nicole Thaw

Committee in charge

Professor Martha H. Conklin, Chair
Dr. Ate Visser
Professor Teamrat A. Ghezzehei
Professor Roger C. Bales

2019

University of California, Merced

The Dissertation of Melissa Nicole Thaw is approved, and it is acceptable in quality and form for publication on microfilm and electronically:

Professor Roger C. Bales

Professor Teamrat A. Ghezzehei

Dr. Ate Visser

Professor Martha H. Conklin, Chair

University of California, Merced
2019

Table of Contents

Table of Figures

Chapter 2 Figures:

Chapter 2 Appendix Figures:

List of Tables

Chapter 2 Tables:

Chapter 2 Appendix Tables:

Acknowledgements

Funding sources: National Science Foundation Critical Zone Observatory, NSF Award Number 1331939, Lawrence Livermore National Laboratory, University of California Chancellor's Fellowship, Southern California Edison. Prepared by LLNL under Contract DE-AC52-07NA27344; LLNL-JRNL (LDRD 15-ER-042).

I am thankful for the many people who guided me in this endeavor. My advisor, Martha Conklin was instrumental in securing and maintaining funding, and providing insightful mentorship in mountain hydrology, scientific writing, presentations and data interpretation. My mentor, Ate Visser, took me under his wing and taught me many aspects of isotope hydrology: from sample collection and processing, to data analysis and visualization. Ate taught me scientific writing, as well as how to navigate existing literature. He opened the door for me to engage with a broader research community through international conferences and connected me with his research network. Ate served as a role model for academic professionalism, integrity and exemplar work ethic. I would like to thank Roger Bales for helping to me to become resilient in the face of challenges, helping me in data analysis and for reminding me to think about the broader importance of my research. Teamrat Ghezzehei taught me about soil evaporation; his patient, encouraging and insightful input helped me to think and understand topics in soil water isotopes and soil data analysis.

I would like to thank my snowmobiling mentor, Mollie Mason, who taught me the skills to be able to collect the thousands of field samples during difficult winter conditions. I am grateful for moral support from my father, who always encouraged me to "think outside the box," and gave me the outdoors skills to do field work in the Sierra Nevada. I would like to thank Daniel Arce for teaching me academic material including math, chemistry and biology that was the bridge from a Bachelor of Arts to an academic career in science and allowed me to pursue a graduate degree. I am grateful for the innumerable instances of moral support from Daniel on my journey to this PhD. I am thankful for the support from the Gerodias family and Cardenas families.

I would like to thank Qin Ma, Peter Hartsough, Ryan Ferrell, Michelle Gilmore, Michael Pickard and Anthony Everhart for assistance in sample collection and logistics. I would also like to thank Liying Zhao for assistance using the LGR instrument, Erik Oerter for insightful discussions, Marty Frisbee for assistance with passive capillary samplers and Todd Dawson for assistance with cryogenic vacuum distillation. Jean Moran and Brad Esser assisted me in data interpretation and visualization. I would like to thank Richard Bibby, Amanda Deinhart and Mike Sharp for teaching and mentoring me in cryogenic vacuum distillation, radiochemistry and isotope hydrology. Professional mentoring and moral support from Jennifer Pett-Ridge helped me to gain success beyond the science. I am grateful for mentoring and encouragement from Robert Rice. His enthusiasm for gender equality in engineering and Earth sciences was very encouraging and helped me to maintain confidence through challenging situations.

Curriculum Vitae

Melissa N. Thaw
Lawrence Scholar
Lawrence Livermore National Laboratory
7000 East Avenue L-231
Livermore, CA 94551

Education

PhD. Candidate, Environmental Systems. University of California, Merced. 2019
Adviser: Dr. Martha Conklin

M.S. Water Resources Management, University of Nevada, Las Vegas. 2013
Adviser: Dr. Kumud Acharya, Desert Research Institute

Post-Baccalaureate Coursework
Lake Tahoe Community College

B.A. East Asian Studies. Lewis & Clark College, 2004.

Publications

Visser, A., Thaw, M., Deinhart, A., Bibby, R., Safeeq, M., Conklin, M., ... & Van der Velde, Y. (2019). Cosmogenic Isotopes Unravel the Hydrochronology and Water Storage Dynamics of the Southern Sierra Critical Zone. *Water Resources Research*, *55*(2), 1429-1450.

Oerter, E. J., Singleton, M., **Thaw, M.,** & Davisson, M. L. (2019). Water vapor exposure chamber for constant humidity and hydrogen and oxygen stable isotope composition. *Rapid Communications in Mass Spectrometry*, *33*(1), 89-96.

Visser, A., **Thaw, M.**, & Esser, B. (2018). Analysis of air mass trajectories to explain observed variability of tritium in precipitation at the Southern Sierra Critical Zone Observatory, California, USA. Journal of environmental radioactivity, 181, 42-51.

Thaw, M., Nicholl, M. J., & Acharya, K. (2014). Sensitivity of post-settlement Dreissena rostriformis bugensis to UVB radiation at Earth surface intensity levels. *Journal of Great Lakes Research*, *40*(4), 934-939.

Bisiaux, M. M., Edwards, R., Heyvaert, A. C., Thomas, J. M., Fitzgerald, B., Susfalk, R. B., ... & **Thaw, M**. (2011). Stormwater and fire as sources of black carbon nanoparticles to Lake Tahoe. *Environmental science & technology*, *45*(6), 2065-2071.

Caldwell, T. J., Rosen, M. R., Chandra, S., Acharya, K., Caires, A. M., Davis, C. J., **Thaw, M** & Webster, D. M. (2015). Temporal and basin-specific population trends of quagga mussels on soft sediment of a multi-basin reservoir.

Manuscripts in preparation

Thaw, M. Visser, A., Conklin, M.., Sierra Nevada precipitation and snowmelt stable isotope signatures

Thaw, M., Visser, A., Bibby, R., Deinhart, A., Oerter, E., Conklin, M. Forest vegetation water sources investigated with stable isotopes and tritium in the Sierra Nevada, California

Thaw, M., Visser, A., Conklin, M., Sierra Nevada river source elevation using stable isotope lapse rates

Presentations

Thaw, M., (2018) Sierra Nevada isotope hydrology, tracking water at different scales. Yosemite Hydroclimate symposium

Thaw, M., Visser, A., Conklin, M., Deinhart, A., Bibby, R. (2017) Headwater Catchments to Mountain Range River Runoff, American Geophysical Union Annual Meeting, New Orleans.

Thaw, M., Visser, A., Deinhart, A., Bibby, R., Everhart, A., Conklin, M., (2017) Investigating drought vulnerability using stable water isotopes and tritium in a montane system. European Geosciences Union General Assembly, Vienna

Thaw, M., Visser, A., Deinhart, A., Bibby, R., Sharp., M., Everhart, A., Conklin, M. (2016) Tracking water through the Southern Sierra Critical Zone Observatory using radioactive and stable isotopes. American Geophysical Union Annual Meeting, San Francisco.

Thaw, M. (2016) Variability in Sierra Nevada forest water sources during a severe drought. Yosemite Hydroclimate Meeting, Yosemite National Park, CA.

Thaw, M. (2012) Nutrient transport to Lake Taihu. U.S. - China Young Scientists Forum, Beijing, China, July 2012

Thaw, M., Visser, A., Deinhart, A., Bibby, R., Sharp, M., Conklin, M. Cosmogenic tracers reveal groundwater contributions to major Sierra Nevada rivers. Lawrence Livermore National Laboratory Student Poster Symposium.

Thaw, M., Visser, A., Deinhart, A., Bibby, R., Sharp, M., Conklin, M. (2018) Tracking California river water sources with sulfur-35, tritium and stable isotopes. Groundwater Resources Association of California Annual Conference.

Thaw, M., Visser, A., Deinhart, A., Bibby, R., Sharp, M., Conklin, M. (2018) Vegetation Water Sources and Links to Storage in the Sierra Nevada. Lawrence Livermore National Laboratory Postdoc Poster Symposium.

Thaw, M. Visser, A., Conklin, M., Deinhart, A., Bibby, R., Sharp, M. (2017) Surface Water-Groundwater Interactions in a Sierra Nevada Headwater Catchment using tritium and stable isotopes. Groundwater Resources Association of California Annual Conference.

Thaw, M. Everhart, A. (2016) Winter field hydrology: Strategies developed in the Southern Sierra Critical Zone Observatory. (Poster) Southern Sierra Critical Zone Observatory Annual Meeting, Merced, CA.

Thaw, **M.** (2013) Collaborative Crossover in Protecting Lake Tahoe: Aquatic Invasive Species & Commercial Development. (Oral Presentation) International Protected Areas Exchange Symposium, University of Nevada, Las Vegas.

Thaw, M., Gao F., Acharya, K., Yu, Z. (2012) Nutrient characterization of rainwater, soil and groundwater from two different watersheds, Lake Taihu, China (Poster), American Geophysical Union Annual Meeting, San Francisco.

Thaw, M. & LaCroix, T. (2012) Effects of Ultra-Violet radiation on quagga mussel (*Dreissena bugensis*) mortality (Poster), Tahoe Science Conference.

Thaw, M. (2012) Influence of solar radiation on the quagga mussel (*Dreissena bugensis*) invasion in Lake Mead (Poster), University of Nevada, Las Vegas GeoSymposium.

Thaw, M., Gaurino, J., Zsi, J., Burton, A., Cox, K. (2011) Lake Tahoe Community College goes to NASA (Poster), American Association of Physics Teachers Conference, Ontario, CA

Awards and Fellowships

2017-2019 Lawrence Livermore National Laboratory Lawrence Scholar ($51,450/year)
UC Merced GSA Conference Travel Award, 2017 ($500)
Southern California Edison Graduate Fellowship, summer 2016 ($12,000)
University of California, Merced - Chancellor's Fellowship, 2014-2015 ($30,000)
NSF East Asia and Pacific Summer Institute Fellowship, 2013 ($6,000)
NASA - Reduced Gravity Student Flight Opportunities, 2011 (~$14,000)
California Community College Mathematics Council, Annual Speaker Scholarship ($500)

Service & Outreach

UC Merced Environmental Systems Seminar Committee (2017-2018)
Merced River Days science education volunteer, 2016 & 2017
Southern California Edison Days science education volunteer, 2015/2016/2017

Research Experience

University of California, Merced, Conklin & Mountain Hydrology Research Group 2014-2019
Isotope hydrology in the Sierra Nevada.

Lawrence Livermore National Laboratory 2017-2019
Laboratory techniques for isotope hydrology, including development of new hydrologic tracers; cryogenic vacuum distillation, water stable isotopes, tritium, sulfur-35 and sodium-22.

Desert Research Institute 2011-2013
Acharya Ecological Engineering Laboratory group, invasive species and ecohydrology.

East Asia and Pacific Summer Institute, NSF (Fellow) 2012
International collaboration with Hohai University, Nanjing China, investigating water quality in Lake Taihu basin, China.

University of California, Davis Tahoe Environmental Research Center 2011
Subalpine limnology research intern with focus on water quality, physical dynamics and water quality impacts from invasive species.

Desert Research Institute 2009
Edwards clean lab; ice core and water sample analysis for black carbon.

Teaching

Teaching Assistant, University of California, Merced, spring 2016/2017/2018
Course: Field methods in snow hydrology

Guest Lecturer, University of California, Davis, fall, 2018
Course: Intercultural Communication and grant writing

Instructional Aide, Lake Tahoe Community College, Fall, 2013

Professional Experience

Natural Resources Manager, League to Save Lake Tahoe 2013-2014
Associate Program Advocate, League to Save Lake Tahoe 2009-2011

Abstract

Sierra Nevada isotope hydrology: tracking links between forest water sources, subsurface storage and major river runoff

by

Melissa Nicole Thaw

Doctor of Philosophy in Environmental Systems

University of California, Merced, 2019

Professor Martha Conklin, Chair

The work presented here was motivated by the importance of the Sierra Nevada to California's water resources and the need for understanding fluxes of water across expanded spatial and temporal scales through the critical zone, the area from bedrock to atmosphere, in which fluxes of energy and water support life on Earth. A new set of isotopic data is presented, characterizing each component of the hydrologic cycle (precipitation, evapotranspiration, runoff and storage), on two scales: headwater catchment scale and mountain range scale. These analyses are preceded by analyses of factors affecting precipitation signatures. From initial precipitation, links between headwater catchment evapotranspiration sources, subsurface storage and runoff, were tracked and, finally, the source-elevation of river water was determined across the entire Sierra Nevada using isotopic data from major rivers.

Precipitation input stable isotope signatures represent the starting point to track water through the critical zone's atmosphere – vegetation – subsurface continuum and allow interpretation of streams, deeply stored saturated zone water, soil water and xylem water signatures. Elevation, season and canopy interception are factors affecting precipitation stable isotope signatures in the Sierra Nevada. Precipitation $\delta^{18}O$ signatures decreased with elevation at a rate of -3.3 (± 1.8) ‰/km in the northern central Sierra Nevada and -2.8 (± 1.8) ‰/km in the southern central Sierra Nevada. By measuring a total of 31 isotopic lapse rates along two elevation transects, temporal and spatial variability was observed. Individual isotopic lapse rates were compared to mean amount weighted lapse rates to determine that individual lapse rates do not represent the aggregate input into the system, concluding that aggregate lapse rates should be measured. Similarly, the Local Meteoric Water Line (LMWL) in the Sierra Nevada changed seasonally, but lacked interannual variability. The LMWL for the entire Sierra Nevada had a slope of 7.2 (± 0.1) and an offset of 3.1 (± 1.2). Seasonality in the Central Sierra Nevada was modeled with a sinusoidal function, which varied with elevation. Snowmelt signatures beneath canopy and in open areas were measured every ten days throughout two snowmelt seasons, showing that canopy interaction significantly affected snowmelt stable isotope signatures.

By measuring both water stable isotopes and tritium (^3H) in each component of the hydrologic cycle on the catchment scale, it was determined that although evapotranspiration and deeper subsurface saturated zone water originated as snowmelt, vegetation in all seasons used a younger component of water compared to deeper subsurface saturated zone water. Even when stable isotope signatures of xylem water and saturated zone water matched, ^3H data showed that the age of xylem water and saturated zone water were distinct, demonstrating the utility of using multiple tracers to track water through vegetation. Likewise, water stable isotopes $\delta^{18}O$ and $\delta^{2}H$

showed that vegetation responded to new water inputs over time, while saturated zone water did not, further confirming that vegetation accessed younger water compared to saturated zone water. These findings contribute to current debate in recent literature regarding the concept of ecohydrological separation, in which it is argued that vegetation uses a separate source water compared to runoff. Additionally, by understanding how vegetation source water is connected to saturated zone water on this expanded temporal scale, the implication is that older water provides drought resilience to runoff from the saturated zone and new precipitation provides drought resilience to vegetation.

Previous studies have shown that water from upper elevations in the Sierra Nevada contributed a disproportionate amount of water to runoff, partially due to additional subsurface stores of water and lower evapotranspiration at upper elevations. This dissertation uses isotopic data to confirm these previous findings through new Sierra Nevada river $\delta^{18}O$ and $\delta^{2}H$ data applied to isotopic lapse rates. Even across geologically heterogeneous catchments, river source waters originated above their mean catchment elevation, with higher elevation source waters correlating to higher elevation catchments. Isotopic results agree with results and findings derived from a spatially distributed mass balance approach.

Chapter 1: Introduction

Tracking water through the critical zone's atmosphere – vegetation – subsurface continuum on expanded spatial and temporal scales, requires a comprehensive and cross-disciplinary approach (Brantley et al., 2007), which can be accomplished through the use of isotopic tracers. Precipitation input stable isotope signatures represent the starting point to investigate hydrologic connectivity through the critical zone (Clark & Fritz, 1997). Coupled physical and biological critical zone processes, such as fluxes of water through surface-subsurface interactions have been identified as key processes to improve representation of hydrologic processes in Earth Systems Models (Clark et al., 2015). These processes can be tracked using isotopic tracers, starting by characterizing the isotopic input of precipitation, from which evapotranspiration, runoff and stored water originate. Elevation gradients, temperature and precipitation variability due to climate, and variability in forest density and transpiration, represent some of the key critical zone heterogeneities that affect energy and water fluxes through the Sierra Nevada (Bales et al., 2018; Goulden & Bales, 2014; O'Geen et al., 2018).

These heterogeneities also affect precipitation stable isotope signatures, leading to distinct "fingerprints" that can be used to track water through the critical zone. For example, the effect of altitude on precipitation stable isotope signatures has been characterized for different areas around the world, and a limited set of data has been collected for the Sierra Nevada (Friedman & Smith, 1970; Ingraham & Taylor, 1991; Poage & Chamberlain, 2002; Winograd & Friedman, 1972). These studies provide data collected from limited time intervals, and make use of some aged snow, in which isotopic signatures may have been altered over time (Unnikrishna et al., 2002); furthermore, the Sierra Nevada receives most of its precipitation through a few large storms, often categorized as atmospheric rivers (Dettinger et al., 2011), pointing to the importance of aggregating precipitation signatures in a way that represents the proportional input. Aggregating seasonally variable input is also applied in developing Local Meteoric Water Lines (LMWL). LMWLs are fundamental to tracing vadose zone processes with stable isotopes, systematically determining evaporative processes and interpreting xylem water stable isotope signatures (Evaristo et al., 2015; Landwehr, 2006; Sprenger et al., 2016). Previously LMWLs for the Sierra Nevada have been constructed of limited data and often a combination of surface water and precipitation (Kendall & Coplen, 2001; Rose et al., 2003); surface water may not accurately represent precipitation as evaporation and storage selection processes may alter the resulting signatures (Gat, 1996; Visser et al., 2019). In addition to LMWLs, observed seasonality in precipitation stable isotope signatures is useful in determining seasonal contributions to vegetation, streams and groundwater and can be captured using sine waves (Allen et al., 2019; Allen et al., 2018; Dewalle et al., 1997; Jasechko et al., 2014; Jodar et al., 2016). On a finer scale, sub-canopy forest heterogeneities have been found to affect snow and the stable isotope signatures of snow (von Freyberg et al., 2019).

Chapter 2 of this dissertation seeks to characterize the precipitation input stable isotope signatures for the Sierra Nevada through a new data set collected over expanded temporal and spatial scales. In particular, the effects of elevation on precipitation stable isotopes were characterized by constructing two amount weighted stable isotope lapse rates at two different latitudes in the Sierra Nevada. By measuring multiple lapse rates over the course of an entire water year, variability within storms and across different storms showed that lapse rates constructed of precipitation over a short period of time were not representative of the aggregate mean isotopic lapse rate. LMWLs for several locations in the Sierra Nevada were constructed and spatial and temporal variability was examined, including seasonal variability in LMWLs. By fitting sinusoidal functions to precipitation isotope values over time, seasonality was modeled. On a finer scale, snow melt stable isotope signatures were measured every ten days over two snowmelt seasons. Snowmelt

signatures beneath canopy interaction and in forest gaps were significantly different, providing evidence that canopy interception can affect the input of snow isotopic signatures similarly to other areas in the world (Gustafson et al., 2010; von Freyberg et al., 2019).

With the foundation of precipitation input stable isotope signatures established, the third and fourth chapters of this dissertation seek to use isotopic tracers as a complementary approach to support the hypothesis that most Sierra Nevada river water originates in the upper elevations. We build upon existing Sierra Nevada critical zone research which has established the importance of upper elevation contributions to runoff, due to lower evapotranspiration at higher elevations and additional higher elevation subsurface storage which contributes runoff during drought (Bales et al., 2018; Goulden & Bales, 2014; Rungee, 2019). While these previous studies have used mass balance and remote sensing data, stable isotopes can also be used to determine river source elevations (Tsujimura et al., 2007; Zhu et al., 2018). Not dependent on hydrometeorological data, this independent approach is complementary to mass balance approaches in which hydrometeorological data is used (Rungee, 2019).

Water stable isotopes are also particularly useful for tracking water through complex critical zone processes as conservative tracers (Clark & Fritz, 1997; Sprenger et al., 2016). However, recent research into methods used to measure water stable isotopes in soil moisture, combined with recent debate in ecohydrology literature proposing that vegetation uses a source water that is distinct from runoff and groundwater (Brooks et al., 2010; Evaristo et al., 2015), provide motivation to use ^{3}H as a third, cross-disciplinary tracer to understand fluxes of water through the critical zone atmosphere – plant – subsurface continuum to shed light on expanded temporal scales of ecohydrologic connectivity.

The third chapter of this dissertation addressed the call in critical zone science to "trace the water" through trees and also applied a novel set of tracers to approach the critical zone hypothesis: "Trees rely on matrix water in the unsaturated zone that at times may have an isotopic composition distinct from the gravity-drained water that transits from the hillslope to groundwater and streamflow" (Brantley et al., 2017). This question is important to address in the Sierra Nevada critical zone where declines in evapotranspiration from forest die-off, thinning and wildfire have led to increases in soil moisture and runoff (Bales et al., 2018; Boisrame et al., 2017; Roche et al., 2018; Saksa et al., 2017). We investigated ecohydrologic connectivity in a Sierra Nevada headwater catchment by tracking water through each component of the hydrologic cycle (precipitation, evapotranspiration, storage and runoff) using three complementary tracers, $\delta^{18}O$, $\delta^{2}H$ and ^{3}H. Water stable isotopes $\delta^{18}O$ and $\delta^{2}H$ data showed forest evapotranspiration and subsurface saturated zone water were both composed of water that originated as snowmelt, and at the same time, ^{3}H data showed that vegetation accessed young water, while saturated zone meadow water contributing to runoff was composed of a mix of water ages including older water from deeper flow paths. During normal summer conditions in which the dry season followed snowmelt input, water stable isotopes of vegetation and saturated zone meadow water matched, but only through examination of ^{3}H data, was it apparent that vegetation accessed a younger water source.

In the fourth chapter, water stable isotope data from Sierra Nevada rivers were combined with stable isotope lapse rates to determine Sierra Nevada river water source elevations, which were compared to results from a spatially distributed mass balance approach. Evaporative processes were examined through analysis of deuterium-excess (d-excess) and line conditioned-excess (lc-excess) of river water compared to that of precipitation and groundwater. D-excess and lc-excess reflected evaporative fractionation occurring in river water, which was enhanced at low elevations following the dry summer season, suggesting the importance of determining evaporative processes when sampling surface water from warm, Mediterranean climates.

References

Allen, S. T., Kirchner, J. W., Braun, S., Siegwolf, R. T. W., & Goldsmith, G. R. (2019). Seasonal origins of soil water used by trees. *Hydrology and Earth System Sciences, 23*(2), 1199-1210.

Allen, S. T., Kirchner, J. W., & Goldsmith, G. R. (2018). Predicting Spatial Patterns in Precipitation Isotope (delta H-2 and delta O-18) Seasonality Using Sinusoidal Isoscapes. *Geophysical Research Letters, 45*(10), 4859-4868.

Bales, R. C., Goulden, M. L., Hunsaker, C. T., Conklin, M. H., Hartsough, P. C., O'Geen, A. T., et al. (2018). Mechanisms controlling the impact of multi-year drought on mountain hydrology. *Scientific Reports, 8*.

Boisrame, G., Thompson, S., Collins, B., & Stephens, S. (2017). Managed Wildfire Effects on Forest Resilience and Water in the Sierra Nevada. *Ecosystems, 20*(4), 717-732.

Brantley, S. L., Eissenstat, D. M., Marshall, J. A., Godsey, S. E., Balogh-Brunstad, Z., Karwan, D. L., et al. (2017). Reviews and syntheses: on the roles trees play in building and plumbing the critical zone. *Biogeosciences, 14*(22), 5115-5142.

Brantley, S. L., Goldhaber, M. B., & Ragnarsdottir, K. V. (2007). Crossing disciplines and scales to understand the Critical Zone. *Elements, 3*(5), 307-314.

Brooks, J. R., Barnard, H. R., Coulombe, R., & McDonnell, J. J. (2010). Ecohydrologic separation of water between trees and streams in a Mediterranean climate. *Nature Geoscience, 3*(2), 100-104.

Clark, I., & Fritz, P. (1997). Environmental Isotopes in Hydrogeology.

Clark, M. P., Fan, Y., Lawrence, D. M., Adam, J. C., Bolster, D., Gochis, D. J., et al. (2015). Improving the representation of hydrologic processes in Earth System Models. *Water Resources Research, 51*(8), 5929-5956.

Dettinger, M. D., Ralph, F. M., Das, T., Neiman, P. J., & Cayan, D. R. (2011). Atmospheric Rivers, Floods and the Water Resources of California. *Water, 3*(2), 445-478.

Dewalle, D. R., Edwards, P. J., Swistock, B. R., Aravena, R., & Drimmie, R. J. (1997). Seasonal isotope hydrology of three Appalachian forest catchments. *Hydrological Processes, 11*(15), 1895-1906.

Evaristo, J., Jasechko, S., & McDonnell, J. J. (2015). Global separation of plant transpiration from groundwater and streamflow. *Nature, 525*(7567), 91-+.

Friedman, I., & Smith, G. I. (1970). Deuterium content of snow cores from Sierra Nevada area. *Science, 169*(3944), 467-&.

Gat, J. R. (1996). Oxygen and hydrogen isotopes in the hydrologic cycle. *Annual Review of Earth and Planetary Sciences, 24*, 225-262.

Goulden, M. L., & Bales, R. C. (2014). Mountain runoff vulnerability to increased evapotranspiration with vegetation expansion. *Proceedings of the National Academy of Sciences of the United States of America, 111*(39), 14071-14075.

Gustafson, J. R., Brooks, P. D., Molotch, N. P., & Veatch, W. C. (2010). Estimating snow sublimation using natural chemical and isotopic tracers across a gradient of solar radiation. *Water Resources Research, 46*.

Ingraham, N. L., & Taylor, B. E. (1991). Light stable isotope systematics of large-scale hydrologic regimes in California and Nevada. *Water Resources Research, 27*(1), 77-90.

Jasechko, S., Birks, S. J., Gleeson, T., Wada, Y., Fawcett, P. J., Sharp, Z. D., et al. (2014). The pronounced seasonality of global groundwater recharge. *Water Resources Research, 50*(11), 8845-8867.

Jodar, J., Custodio, E., Liotta, M., Lamban, L. J., Herrera, C., Martos-Rosillo, S., et al. (2016). Correlation of the seasonal isotopic amplitude of precipitation with annual evaporation and altitude in alpine regions. *Science of the Total Environment, 550*, 27-37.

Kendall, C., & Coplen, T. B. (2001). Distribution of oxygen-18 and deuterium in river waters across the United States. *Hydrological Processes, 15*(7), 1363-1393.

Landwehr, J. M., Coplen, T.B. (2006). *Line-conditioned excess: a new method for characterizing stable hydrogen and oxygen isotoperatios in hydrologic systems*. Paper presented at the Isotopes in Environmental Studies, Aquatic Forum 2004.

O'Geen, A., Safeeq, M., Wagenbrenner, J., Stacy, E., Hartsough, P., Devine, S., et al. (2018). Southern Sierra Critical Zone Observatory and Kings River Experimental Watersheds: A Synthesis of Measurements, New Insights, and Future Directions. *Vadose Zone Journal, 17*(1).

Poage, M. A., & Chamberlain, C. P. (2002). Stable isotopic evidence for a Pre-Middle Miocene rain shadow in the western Basin and Range: Implications for the paleotopography of the Sierra Nevada. *Tectonics, 21*(4).

Roche, J. W., Goulden, M. L., & Bales, R. C. (2018). Estimating evapotranspiration change due to forest treatment and fire at the basin scale in the Sierra Nevada, California. *Ecohydrology, 11*(7).

Rose, K. L., Graham, R. C., & Parker, D. R. (2003). Water source utilization by Pinus jeffreyi and Arctostaphylos patula on thin soils over bedrock. *Oecologia, 134*(1), 46-54.

Rungee, J. (2019). Estimating plant-accessible water storage through evaluating evapotranspiration in the semi-arid western United States using eddy-covariance, remote sensing, and spatially distributed data. PhD Dissertation, University of California, Merced: eScholarship.

Saksa, P. C., Conklin, M. H., Battles, J. J., Tague, C. L., & Bales, R. C. (2017). Forest thinning impacts on the water balance of Sierra Nevada mixed-conifer headwater basins. *Water Resources Research, 53*(7), 5364-5381.

Sprenger, M., Leistert, H., Gimbel, K., & Weiler, M. (2016). Illuminating hydrological processes at the soil-vegetation-atmosphere interface with water stable isotopes. [Review]. *Reviews of Geophysics, 54*(3), 674-704.

Tsujimura, M., Abe, Y., Tanaka, T., Shimada, J., Higuchi, S., Yamanaka, T., et al. (2007). Stable isotopic and geochemical characteristics of groundwater in Kherlen River basin, a semi-arid region in eastern Mongolia. *Journal of Hydrology, 333*(1), 47-57.

Unnikrishna, P. V., McDonnell, J. J., & Kendall, C. (2002). Isotope variations in a Sierra Nevada snowpack and their relation to meltwater. *Journal of Hydrology, 260*(1-4), 38-57.

Visser, A., Thaw, M., Deinhart, A., Bibby, R., Safeeq, M., Conklin, M., et al. (2019). Cosmogenic Isotopes Unravel the Hydrochronology and Water Storage Dynamics of the Southern Sierra Critical Zone. *Water Resources Research, 55*(2), 1429-1450.

von Freyberg, J., Bjarnadottir, T. R., & Allen, S. T. (2019). Influences of forest canopy on snowpack accumulation and isotope ratios. *Hydrological Processes*.

Winograd, I. J., & Friedman, I. (1972). Deuterium as a tracer of regional groundwater flow, Southern Great Basin, Nevada and California. *Geological Society of America Bulletin, 83*(12), 3691-3708.

Zhu, L., Fan, M. J., Hough, B., & Li, L. (2018). Spatiotemporal distribution of river water stable isotope compositions and variability of lapse rate in the central Rocky Mountains: Controlling factors and implications for paleoelevation reconstruction. *Earth and Planetary Science Letters, 496*, 215-226.

Chapter 2

Altitude effect, seasonality and sub-canopy fractionation in Sierra Nevada precipitation and snowmelt stable isotope signatures

Melissa Thaw[1,2], Ate Visser[2], Martha Conklin[1]

[1]University of California, Merced

[2]Lawrence Livermore National Laboratory

Abstract

The purpose of this study is to establish the reference input signatures of precipitation, including isotopic lapse rates, Local Meteoric Water Lines (LMWL) and seasonality for the Sierra Nevada, California through measuring snowmelt and precipitation on expanded temporal and spatial scales (multiple seasons, ~ every 10 days; from 3 meters to >200 km). For two elevational transects in the Central and Southern Sierra Nevada, we found that isotopic lapse rates varied considerably over a precipitation season. Calculated amount weighted mean isotopic lapse rates were -3.3 (± 1.8) and -2.8 (± 1.8) ‰/km for $\delta^{18}O$, for the two different Sierra Nevada locations. Combining all our measurements (259), the Meteoric Water Line for the entire Sierra Nevada was $\delta^{2}H = 7.20 (\pm 0.12) \times \delta^{18}O + 3.13 (\pm 1.24)$ and the amount weighted Meteoric Water Line for the mid-elevation Southern Sierra Critical Observatory (CZO) P301 site was $\delta^{2}H = 6.54 (\pm 0.39) \times \delta^{18}O - 9.08 (\pm 4.91)$, which was composed of seasonally variable isotopic signatures. Seasonally, meteoric water lines varied in slope from 4.7 (± 0.2) in summer to 9.0 (± 0.1) in winter. Meanwhile, there was little inter-annual variation in the Meteoric Water Line from 2016 to 2017, with slopes of 7.5 (± 0.5) and 7.7 (± 0.4), respectively. Seasonal isotopic variation in precipitation fit a sinusoidal model for $\delta^{18}O$ for 2016-2017 at the CZO P301 with an amplitude of 3.4 (± 0.7). Isotopic lapse rates can be utilized to determine recharge elevation. The Meteoric Water Line and seasonal patterns can be used to determine the line-conditioned excess and seasonal contributions to runoff, groundwater and xylem water. These can serve as the foundation for cross-discipline tracer studies in isotope hydrology and ecohydrology.

2.1 Introduction

California's Sierra Nevada provides the majority of the water supply to this state, which is the fifth largest economy in the world (Highlights, 2013). Understanding water fluxes through this highly heterogeneous mountain system has significance to both ecosystem services and the global economy. Tracking water through the Sierra Nevada using stable isotopes can provide information about the source components, timing of release from storage through different flowpaths and ecohydrologic connectivity to forest evapotranspiration by crossing disciplines through the physical and biological systems that are coupled in the critical zone. However, the use of stable isotopes in hydrology and ecohydrology depend heavily on measurements of precipitation and snowmelt stable isotope signatures. Precipitation input stable isotope signatures represent the starting point to track water through the critical zone's atmosphere - vegetation – soil – vadose zone – groundwater – stream continuum and allow interpretation of streams, groundwater, soil water and xylem water signatures (Allen et al., 2019; Evaristo et al., 2016; Jasechko, 2016; Jasechko & Taylor, 2015; Kendall & McDonnell; Sprenger et al., 2016).

Montane critical zone structure, including elevation, canopy cover, as well as seasonality, influence the isotopic signatures of water, providing "fingerprints" to track water from this initial point through the critical zone (Figure 2-1). Elevation also has a strong effect on precipitation type and amount in the Sierra Nevada (Dettinger et al., 2004). The elevation gradient is an important variable in plant available water (Goulden & Bales, 2019). The relationship between elevation and stable isotopes of precipitation (altitude effect) can be used to determine river source and groundwater recharge elevations (Clark & Fritz, 1997; Zhu et al., 2018).

It is well known that precipitation stable isotope values decrease with elevation, as temperature decreases with elevation (Dansgaard, 1954, 1964; Gat & Dansgaard, 1972; Ingraham & Taylor, 1991), which has been termed, the altitude effect. Globally isotopic lapse rates vary from location to location, with a global average of -2.8‰ $\delta^{18}O$/km (Poage & Chamberlain, 2002). Variability in isotopic lapse rates in mountainous regions such as the Alps, has been observed and reported from

-5.0 ‰/km to -3.2 ‰/km for $\delta^{18}O$ (Bortolami, 1978; Clark & Fritz, 1997). Individual isotopic lapse rates cited for the Sierra Nevada vary from -3.1 to -2.1 $\delta^{18}O$/km, but in some cases few data points were used (n=2) (Poage & Chamberlain, 2002). In the Sierra Nevada, some researchers have reported isotopic lapse rates in $\delta^{2}H$ only, limiting the utility and comparability of the data; nevertheless, variability from storm to storm was measured from -36 to -130 ‰/km for $\delta^{2}H$ (n= 20) (Smith et al., 1979). In California isotopic lapse rates have been used to understand recharge (Visser et al., 2018; Visser et al., 2019) and to examine paleo-water signals (Lechler & Niemi, 2012) but were based on limited data. However, differences in storm source water temperatures and atmospheric condensation temperatures, mixing with isotopically different water, and isotopic enrichment due to evaporation as rain drops fall through dry atmosphere, also influence precipitation signatures (Friedman et al., 1992; Smith et al., 1979), which mean that isotopic signatures cannot always serve as direct proxies for condensation temperature (Siegenthaler & Oeschger, 1980).

A second major factor influencing the flux of water and energy in the critical zone, and especially in the Mediterranean climate that characterizes the Southern Sierra Critical Zone, is seasonality. Precipitation stable isotope signatures are useful in determining seasonal source water of plants and streams (Allen et al., 2019; Jasechko et al., 2016). By determining the wave function for seasonality in precipitation stable isotopes, new water portions of streams can be calculated (Jasechko et al., 2016), but this analyses requires measured precipitation input signals at high temporal resolution, beyond what has been previously been measured in the Sierra Nevada (Friedman & Smith, 1970; Ingraham & Taylor, 1991).

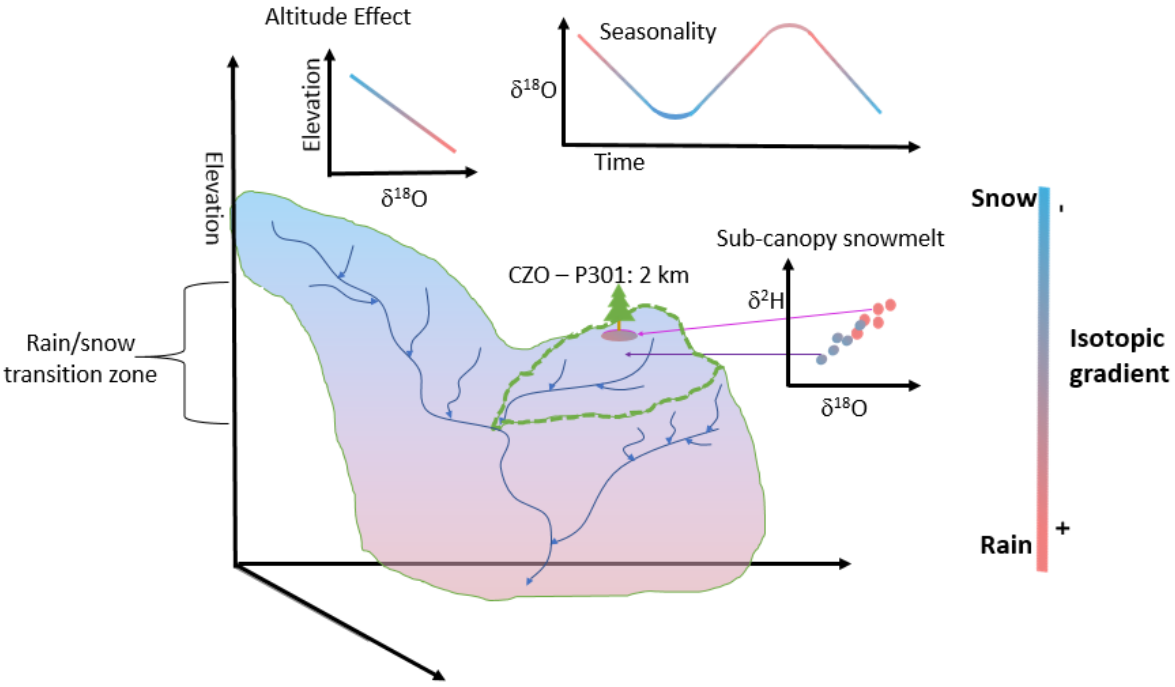

Figure 2-1. Conceptual diagram of critical zone heterogeneities, altitude, season and canopy cover, which impart gradients affecting the input of water stable isotope signatures. These input signatures are the starting point to track water through the critical zone's atmosphere – soil – vadose zone – groundwater – stream continuum.

The Local Meteoric Water Line (LMWL) and dual isotope analyses are fundamental to calculate line conditioned excess (lc-excess) in order to understand storage, mixing and fluxes of water in the critical zone on a finer scale (Sprenger et al., 2015). Within the critical zone soil – plant – atmosphere continuum, the LMWL is used as a reference for plant water source studies and understanding ecohydrologic connectivity (Brooks et al., 2010; Ehleringer et al., 2016; McCutcheon et al., 2017; Moreno-Gutierrez et al., 2012). Stable isotope analyses provide a complementary method to hydrologic models and to study the fluxes of water in the critical zone. This is especially true when hydrometeorological data are limited, for example, in the Sierra Nevada, where precipitation data are one of the largest uncertainties in closing the water balance (Rungee, 2019). Furthermore, isotopic tracers provide a method to track water through the critical zone, despite the lack of information about subsurface structure.

Comprehensive Sierra Nevada meteoric $\delta^{18}O$ and $\delta^{2}H$ data are limited, therefore a well-established Sierra Nevada LMWL is currently lacking. In 1969 researchers measured $\delta^{2}H$ in integrated snow cores across the Sierra Nevada but did not include $\delta^{18}O$ signatures needed to construct a meteoric water line (Friedman & Smith, 1972). Others have combined meteoric signatures with post-meteoric water signatures (surface water and/or groundwater) (Ingraham & Taylor, 1991; Kendall & Coplen, 2001; Rose et al., 2003) to construct LMWLs in the Sierra Nevada, but these can be affected by post-meteoric evaporation, mixing and storage selection (Machavaram & Krishnamurthy, 1995; Visser et al., 2019). The lack of meteoric water stable isotope data limits the ability to construct a reliable LMWL for the Sierra Nevada that encompasses multiple seasons, elevations and latitudes.

On a finer spatial scale, heterogeneous forest canopy influences fluxes of water and energy through biological and physical feedbacks in the critical zone and the Sierra Nevada. Canopy interception has been found to influence snowpack accumulation in the Sierra Nevada (Zheng et al., 2016), and in the Cascades significant differences in snow accumulation and melt were observed with respect to canopy (Storck et al., 2002). Meanwhile, others have found that canopy interception and shading affected snow chemistry and $\delta^{18}O$ signatures through sublimation (Gustafson et al., 2010). Measured differences have been found in adjacent precipitation and throughfall stable isotope signatures in both deciduous and evergreen forests (Kendall & McDonnell; Saxena, 1986; von Freyberg, 2019). Since canopy influences snow in the Sierra Nevada and interception has been observed to affect throughfall signatures in other areas, our final research question is how does forest canopy affect snowmelt signals?

To summarize the objectives of this study, we seek to answer the following research questions through measurements of water stable isotopes in snow, rain and snowmelt in the Sierra Nevada from 2015 to 2017: 1) how do isotopic lapse rates in the Sierra Nevada vary over time and at different locations and what are mean amount weighted isotopic lapse rates? 2) what is the seasonality of precipitation stable isotopes in the Sierra Nevada? 3) what is the LMWL for a central Sierra headwater catchment, how does it change seasonally and interannually and what is the LMWL for the entire Sierra incorporating new data from a range of elevations and latitudes? 4) how does forest canopy affect snowmelt signals?

2.2 Methods and Site Description

Four types of samples were collected using field methods specifically for each sample type, including rain samples, grab samples of snow, snow pit samples, and snowmelt using P-Caps (Frisbee, et al., 2010 (a) and (b); Penna et al., 2014). Rain samples were collected using a funnel connected to a 1 or 2 - liter sample bottle. Each sample bottle contained mineral oil to prevent evaporation and mineral oil was replaced each time samples were collected. On occasions where samplers went missing, were disturbed, inaccessible due to conditions, overflowed or partially frozen,

samples were not collected and data are missing. Grab samples of fresh snow were also collected when snow was present. At the CZO site, several snow pits were dug, individual layers were identified and sampled. Snow pits were dug in open areas on five dates. Only fresh snow layers were included in the Local Meteoric Water Line.

Precipitation amounts during the study period included extreme drought conditions in 2015 and extremely wet conditions in water year (WY) 2017. The drought period from 2012-2014 was the most severe drought in 1200 years due to the combination of the lack of precipitation and high temperatures (Griffin & Anchukaitis, 2014). High temperatures exacerbated the 2012-2014 drought, decreasing snow water equivalent and soil moisture by increasing evaporative demand (Shukla et al., 2015). During the 2012-2015 period, California experienced a severe snowpack deficit, leading to a similarly significant runoff deficit (He et al., 2017). In the opposite extreme, 2017 experienced extreme precipitation as 42 atmospheric rivers made landfall with northern California, many of which were particularly intense and long lasting (Guirguis et al., 2019). Total precipitation at the Providence site in the Critical Zone Observatory (CZO) was approximately 430 mm in WY 2015, 910 mm in WY 2016 and 1770 mm in WY 2017 based on Parameter-elevation Relationships on Independent Slopes Model (PRISM) data.

The Sierra Nevada experiences a Mediterranean climate receiving most of its precipitation in winter. Winter precipitation depends on major storms from the Pacific Ocean and multi-year snow droughts are common (Griffin & Anchukaitis, 2014). The Sierra Nevada extends from near sea level to elevations above 4000 m. Ecotones across this elevation range include chaparral, pine oak woodland, subalpine mixed conifer forest and alpine meadows. The Providence Creek Sub-catchment is located in the Kings River Experimental Watershed in Sierra National Forest at an elevation range of 1.80 to 2.1 km. This site is a mixed conifer forest within the rain-snow transition zone, described in more detail in previous studies (Safeeq & Hunsaker, 2016). The Shorthair flux tower site is located at an elevation of 2.7 km in a pine forest within the snow dominated subalpine zone.

Precipitation and snowmelt samples were collected from 12 locations in the Sierra Nevada, California, USA. Samples were collected in the Southern Sierra Critical Zone (CZO) P301 site (elevation 2.1 km) within the Kings River Experimental Watershed and the nearby Shorthair site (2.7 km). The Southern Sierra Critical Zone Observatory and the Kings River Experimental Watershed has been described by others (Bales et al., 2011; Liu et al., 2013). To understand higher elevation precipitation stable isotope signals, snow grab samples were collected from Mt. Whitney (elevation range 2.69 km to 4.3 km) (Tables A6). Sampling location elevations were determined using Google Earth and identifying landmarks.

Precipitation samples for isotopic lapse rates were collected on the west side of the Sierra Nevada along the "American Transect", along US Route 50 and along the "Kings Transect" along California State Route 168. The American Transect consisted of five elevations between 5.4 and 1.3 km; three additional high elevation snow grab samples were collected from nearby summits of three peaks: Mt. Tallac, 2.96 km, Powderhouse Peak, 2.85 km, and Rubicon Peak, 2.77 m and were included in this dataset. Sampling location coordinates are provided in Table A2-1. In the Kings Transect, precipitation samples were collected at five elevations between 5.6 and 2.3 km and the Southern Sierra Critical Zone Observatory P301 tower (2.1 km). Precipitation samples were collected on 14 days in the American Transect and 18 days on the Kings Transect in 2016 and 2017, integrating precipitation over collection times ranging from one day to several weeks. American and Kings Transect sampling dates are listed in Tables A2-2 and A2-3. American and Kings precipitation collection storm intervals are listed in Tables A2-4 and A2-5.

An amount weighted LMWL was constructed and compared using continuously collected rain and snow samples from the Southern Sierra Critical Zone Observatory P301 site. Rain, snow grab samples and snow layer samples were collected for the LMWL from 3/1/2015 through 8/4/2017 (Table A2-8). A Sierra Nevada wide LMWL was also created that included snow samples collected

from layers in snow pits from the Southern Sierra Critical Zone Observatory Shorthair site collected on March 1, 2016 and February 16, 2017 (Table A2-7).

Snowmelt was sampled from clusters of passive capillary samplers (P-Caps) (Frisbee, et al., 2010 (a) and (b); Penna et al., 2014) in the forested area next to the P301 flux tower (Goulden et al., 2012) within 70 m of each other and the tower. P-Caps were located under forest canopy in three locations under different tree types, White Fir (WF), Incense Cedar (IC) and Jeffrey Pine (JP), and in open areas in two locations (near an Incense Cedar and near a White Fir). Multiple (1-3) P-Caps were installed at each location and sampled throughout the winter and spring seasons (Tables A2-9 and A2-10).

P-Caps (Frisbee, et al., 2010 (a) and (b); Penna et al., 2014) were used to minimize the effects of sampling on signatures of the collected snowmelt (Earman et al., 2006). Passive capillary samplers were modified by adding access tubes to sample snowmelt throughout the winter and spring seasons using a peristaltic pump. Mineral oil was used in the subterranean sample bottles and was replaced after each sample was taken using the peristaltic pump.

Water stable isotopes $\delta^{18}O$ and $\delta^{2}H$ were measured using a Los Gatos Research DLT-100 Liquid-Water Isotope Analyzer at the University of California, Merced Environmental Analytical Laboratory. Hydrogen and oxygen stable isotope values are reported in δ notation: $\delta = (R_{sample} / R_{standard} - 1)$, where R_{sample} and $R_{standard}$ are the $^{2}H/^{1}H$ or $^{18}O/^{16}O$ ratios for the sample and standard, respectively, and referenced to the Vienna Standard Mean Ocean Water (VSMOW) standard.

When a field replicate was taken, the mean of the replicates was calculated and reported. Field precision calculated as the standard error of the mean from field replicates ranged from 0.07 to 2.74‰ for $\delta^{2}H$ and 0.02‰ to 1.15‰ for $\delta^{18}O$.

Parameter-elevation Regressions on Independent Slopes Model (PRISM) precipitation, dew point temperature, temperature and vapor pressure deficit values were downloaded from locations corresponding to sampling locations and dates (PRISM, 2004). PRISM data were used to determine additional meteorological conditions during each sampling period. The mean dew point temperature, mean temperature and total precipitation were calculated. Mean values for temperature and vapor pressure deficit in which PRISM provides minimum and maximum values are listed as "mean min" and "mean max". Linear regression was performed on isotopic lapse rates and the corresponding meteorological conditions.

Mean lapse rates were calculated in two ways, resulting in amount weighted mean slopes and intercepts and non-weighted slopes and intercepts. Non-weighted mean lapse rates were calculated by first removing lapse rates with p-values > 0.05 (95% confidence interval), then calculating the mean slope and mean offset. The amount weighted isotopic lapse rate for each transect was calculated in three steps (Figure 2-2). First, a lapse rate was calculated for each precipitation collection period (set of samples collected on the same date and transect) by fitting a linear function to $\delta^{18}O$ - elevation data. Second, daily 800 m PRISM data were used to calculate the amount of precipitation that fell during each individual sample collection (Figures A2-1 and A2-2, Tables A2-11 and A2-12). Third, the weighted mean of the slope and offset were calculated through direct multiplication of the precipitation portion and slope and offset. The amount weighted standard deviation (σ) was calculated for both slope and offset. Equations for weighted and non-weighted standard deviation are shown as A2-E1 and A2-E2. Mean weighted lapse rates were calculated by weighting the slope and offset by the amount of precipitation through equations 1 through 3:

$$Slope = \sum P_{rain} * slope_n \tag{2-1}$$

$$Offset = \sum P_{rain} * offset_n \tag{2-2}$$

$$P_{rain} = \frac{rain\ amount\ during\ n\ sampling\ period}{total\ rain\ sampled} \tag{2-3}$$

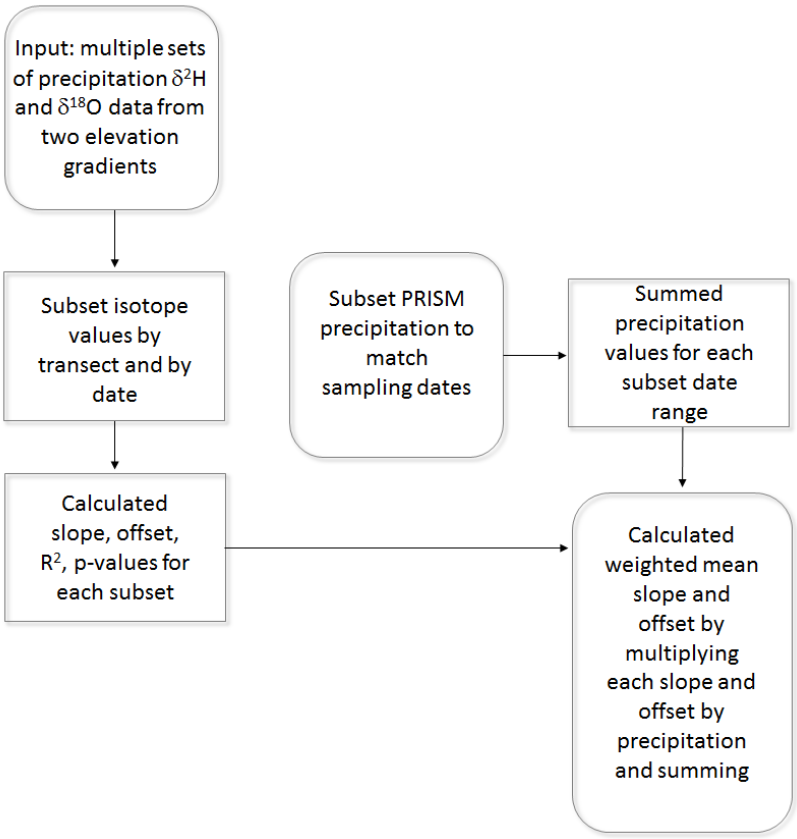

Figure 2-2. Flow chart of analytical methods used to calculate mean amount weighted stable isotope lapse rates.

Temperature lapse rates were also compared to isotopic lapse rates by pairing temperature lapse rates with isotopic lapse rates by date. On days that rained, daily temperature lapse rates were calculated. The mean of those daily rates was calculated and paired with each sampling period. Linear regression was performed on the isotopic lapse rates versus temperature lapse rates to determine the relationship between the two. For the American Transect, temperature data from the American River Wireless Sensor Network was used from the Alpha (2.29 km), Dolly Rice (1.98 km), Echo Peak (2.38 km), Onion (1.85 km), Owens (1.57 km) and Robbs Saddle (1.80 km) sites (Cui, 2020). These sites were selected due to their proximity to precipitation sample collection sites. For each of these sites, the mean daily temperature was calculated from ten individual nodes. Lower elevation temperature data from PFH (Pacific House), elevation 1.1 m and PWS (Placerville), elevation 5.7 km were obtained from the California Data Exchange Center. For the Kings Transect, temperature data were obtained from the California Data Exchange Center from the following sites: BDM (Bald Mountain), elevation 1.44 m, DKY (Dinky), elevation 1.73 m, MTF (Mountain Rest), elevation 1.25 m, and TMR (Tamarack Summit) 2.30 m. Temperature lapse rates corresponding to sampling periods and locations are provided in Tables A2-13 and A2-14.

To understand the spatial variation in precipitation, individual LMWLs were constructed for the CZO P301, CZO Shorthair, the American Transect, the Kings Transect plus Mt. Whitney. A LMWL was constructed comprising of all precipitation data from all sites. LMWLs were constructed using linear regression of precipitation δ^{18}O and δ^{2}H signatures in dual-isotope space, with standard deviation (σ) calculated for respective slopes and offsets. These were not amount weighted.

Seasonality was analyzed by fitting sinusoidal functions to precipitation isotopic signatures over time and seasonal LMWLs were constructed separately for each season at the CZO P301 site. Sinusoidal functions were fitted to precipitation δ^{18}O and δ^{2}H values using Excel. Date values were converted to fractional year values by dividing each date by 365.25. An additive model of sine and cosine functions was fitted to the data with amplitude coefficients and offset parameters following Allen et al. (2018):

$$Precipitation\ \delta^{18}O\ (t) = a_1 cos(2\pi t) + a_2 sin(2\pi t) + offset. \quad (2\text{-}4)$$

Solving for a_1 and a_2 using the LINEST function in Excel, these parameters were used to estimate a new sine function:

$$Precipitation\ \delta^{18}O\ (t) = (amplitude) sin(2\pi t - \varphi); \quad (2\text{-}5)$$

where:

$$amplitude = \sqrt{a_1 + a_2}; \quad (2\text{-}6)$$

and φ was calculated:

$$\varphi = \arctan(a_1, a_2). \quad (2\text{-}7)$$

Uncertainty for each term was calculated in Excel using the LINEST function. R^2 was calculated applying the Excel function CORREL to the modeled δ^{18}O values and empirical δ^{18}O values. Root Mean Square Error (RMSE) was calculated as:

$$RMSE = \sqrt{\sum\left(\delta_{modeled} - \delta_{empirical}\right)^2} \quad (2\text{-}8)$$

The above process was repeated separately for precipitation δ^2H.

Seasonal LMWLs were constructed by separating precipitation data into seasons from March 1, 2015 through August 4, 2017. Deuterium-excess (d-excess) was computed as d= δ^2H - 8(δ^{18}O) (Dansgaard, 1964) to compare seasonal evaporative signals. To determine inter-annual variation of precipitation input, LMWL's were constructed separately for CZO P301 for Water Year (WY) 2016 and WY 2017. Water lines that were compared for statistical difference were compared by calculating the z-score, Equation 2-9 (Clogg et al., 1995). The z-scored was calculated as follows:

$$Z = \frac{\hat{\beta}_v - \hat{\beta}_{nv}}{\left[s^2(\hat{\beta}_v) + s^2(\hat{\beta}_{nv}) \right]^{0.5}}; \quad (2\text{-}9)$$

where, $\hat{\beta}_v$ is the slope of the amount-weighted LMWL and $\hat{\beta}_{nv}$ is the slope of the non-volume weighted LMWL; $s^2(\hat{\beta}_v)$ is the standard error of $\hat{\beta}_v$ and $s^2\hat{\beta}_{nv}$ is the standard error of $\hat{\beta}_{nv}$ (Clogg et al., 1995).

An amount weighted LMWL was constructed from the CZO P301 stable isotope data and precipitation amounts obtained from PRISM according to methods by Hughes and Crawford (2012). The isotopic signature of the precipitation sample was paired with the sum of precipitation during each sampling period. The mean weighted average input signatures for δ^{18}O and δ^2H were calculated based on the precipitation amount that had accumulated for each corresponding stable isotope signature. The amount weighted and the non-amount weighted P301 Local Meteoric Water Lines were compared for statistical difference by calculating the z-score (Equation 2-1).

To determine if there was a significant difference in snowmelt signatures between snowmelt under forest canopy and snowmelt in open areas, snowmelt samplers were classified as open or closed canopy. These two data sets were subjected to a two-tailed T-test. Tests were performed separately for each water year, 2016 and 2017. These data were combined in a dual isotope plot.

Soil moisture and snow depth data beneath forest canopy and in open areas were downloaded from the Southern Sierra Critical Zone Observatory website and compared (*Southern Sierra Critical Zone Observatory website*, 2019). Sensor data from the Southern Sierra Critical Zone Observatory Upper Met Flat site (37.061041°, -119.182416°) were selected due to similarity in aspect, elevation and availability of continuous data for the duration of sampling. Snow depth data from open areas were compared to the mean snow depth data from two sensors located beneath canopy cover, Ponderosa Pine Under Canopy (PPUC) Abies concolor Under Canopy (ACUC). Soil moisture at a 10 cm depth from the open area ("Open10_VWC") was compared to mean soil moisture of two sensors located beneath canopy ("ACUC_10_VWC" and "PPUC_10_VWC"). Soil volumetric water content and soil temperature were measured using Decagon Devices ECHO-TM. Snow depth was measured using Judd Communications ultrasonic depth sensors.

2.3 Results

2.3.1 Isotopic Lapse Rates

Lapse rates constructed from samples collected along the two elevational transects showed considerable variability, yet amount-weighted mean lapse rates for the two transects were similar (Figure 2-3, Tables 2-1, 2-2 and 2-3). For the American Transect, the amount weighted δ^{18}O lapse rate had a slope of -3.3 (± 1.8) and an intercept -6.2 (± 1.8) (Table 2-3).The Kings Transect had an amount weighted δ^{18}O lapse rate slope of -2.8 (± 1.8) and intercept -6.6 (± 3.3) (Table 2-3). In the American Transect four out of eight of the lapse rates showed little elevational dependence with p-values above 0.05 (not significant within the 95% confidence interval) for both δ^{18}O and δ^2H. In

the Kings Transect seven out of twelve of the lapse rates showed little elevational dependence with p-values above 0.05 (95% confidence interval) (Tables 2-1 and 2-2). Weighted and non-weighted stable isotope lapse rates for $\delta^{18}O$ are listed in Table 2-3. Mean amount weighted and non-weighted stable isotope lapse rates for $\delta^{2}H$ are provided in Table 2-A15. Individual lapse rates in the American Transect, ranged from -6.3 (± 1.9) to 0.3 (± 1.0) ‰/km, with one extreme slope value of 9.1 (± 2.9) that occurred during a summer thunderstorm (excluded from Figure 2-3). In the Kings Transect, $\delta^{18}O$ slopes ranged from -5.2 (± 0.6) to 0.5 (± 1.0) ‰/km.

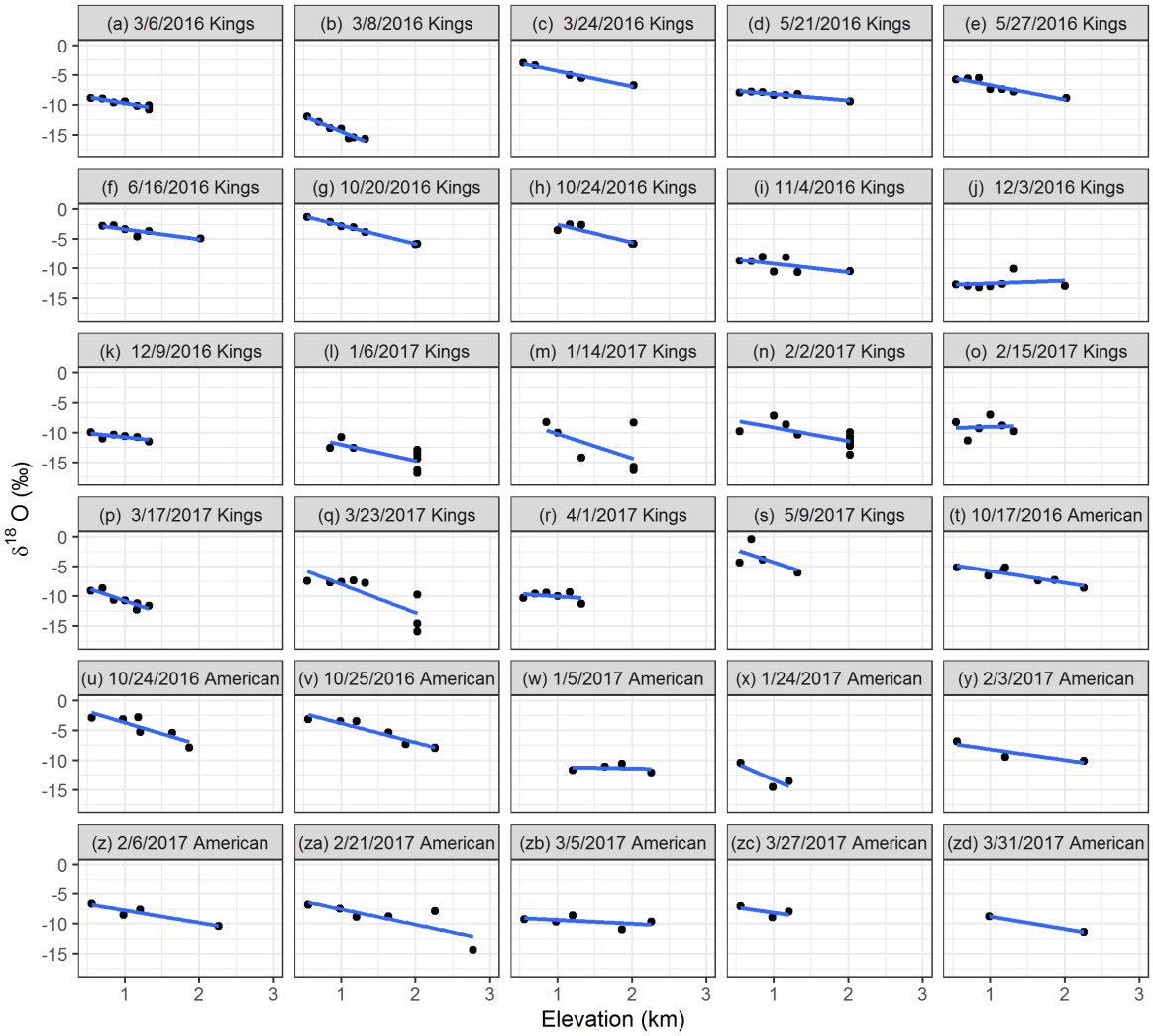

Figure 2-3. Isotopic lapse rates from Kings and American Transects on different dates. Labels indicate sampling date and transect. Blue lines represent linear relationships between elevation and $\delta^{18}O$ for individual lapse rates.

Table 2-1. Individual $\delta^{18}O$ isotopic lapse rates for the Kings Transect.

Sample Date	Slope	Slope Std error	Intercept	Intercept std error	R^2	p-value[1]
3/6/2016	-2.4	0.4	-7.5	0.4	0.90	0.0036
3/8/2016	-5.2	0.6	-9.3	0.6	0.94	0.0004
3/24/2016	-2.6	0.3	-1.7	0.4	0.97	0.0026
5/21/2016	-1.1	0.2	-7.2	0.2	0.87	0.0022
5/27/2016	-2.4	0.5	-4.3	0.6	0.83	0.0042
6/16/2016	-1.7	0.5	-1.7	0.6	0.74	0.0286
10/20/2016	-3.1	0.1	0.4	0.1	0.99	< 0.0001
10/24/2016	-3.1	0.9	0.5	1.4	0.80	0.0399
11/4/2016	-1.4	0.9	-7.8	1.1	0.34	0.1676
12/3/2016	0.5	1.0	-13.0	1.2	0.04	0.6500
12/9/2016	-1.3	0.6	-9.5	0.6	0.54	0.0970
1/6/2017	-2.7	1.1	-9.3	1.9	0.50	0.0494
1/14/2017	-4.1	2.5	-6.1	4.3	0.34	0.1669
2/2/2017	-2.3	0.8	-6.9	1.4	0.48	0.0184
2/15/2017	0.4	2.5	-9.4	2.4	0.00	0.8800
3/17/2017	-4.3	0.9	-6.5	0.9	0.80	0.0062
3/23/2017	-4.8	1.4	-3.2	2.1	0.65	0.0160
4/1/2017	-0.9	1.2	-9.2	1.2	0.11	0.5129
5/9/2017	-4.2	4.0	-0.1	3.6	0.35	0.4062

[1.] A confidence interval of 95% used for calculating non-weighted mean lapse rates.

Table 2-2. Individual $\delta^{18}O$ isotopic lapse rates for the American Transect.

Sample Date	Slope	Slope Std error	Intercept	Intercept std error	R^2	p-value
10/17/2016	-2.0	0.5	-3.7	0.7	0.78	0.0084
10/24/2016	-3.6	0.7	-0.1	1.1	0.82	0.0048
10/25/2016	-3.2	0.6	-0.6	0.9	0.89	0.0049
1/5/2017[1]	-0.3	1.0	-10.9	1.8	0.03	0.8296
1/24/2017	-5.5	3.4	-7.8	3.2	0.72	0.3514
2/3/2017	-6.3	1.9	-1.8	4.1	0.79	0.0452
2/6/2017	-2.1	0.6	-5.6	0.8	0.88	0.0646
2/21/2017	-2.6	1.0	-4.9	1.8	0.61	0.0661
3/5/2017	-0.6	0.7	-8.7	1.0	0.24	0.4044
3/27/2017[2]	-1.8	2.3	-6.3	2.2	0.38	0.5778
3/31/2017	-2.1	NA	-6.7	NA	NA	NA
8/22/2017[1]	9.1	2.9	-16.2	3.8	0.91	0.1952

[1] A confidence interval of 95% used for calculating non-weighted mean lapse rates. [2] Summer thunderstorm; not included in amount weighted mean isotopic lapse rate.[3] Aggregated many storms; not included in amount weighted mean isotope lapse rate. [4] Samples collected over less than 1 km elevation; not included in amount weighted mean isotopic lapse rate.

Table 2-3. Amount weighted (W) and non-weighted (NW) mean $\delta^{18}O$ isotopic lapse rates for the American and Kings Transects. Non-weighted values included only values within a confidence interval of 95%, while amount weighted values include all lapse rates, with the exception of the 8/22/2016 thunderstorm.

Transect	Slope	σ^1	Intercept	σ^1
Kings (W)	-2.8	1.8	-6.6	3.2
Kings (NW)	-3.0	1.2	-4.7	3.5
American (W)	-3.3	1.8	-6.2	1.8
American (NW)	-3.7	1.8	-1.6	1.6

[1] Equations for weighted and non-weighted standard deviation AE1 and AE2.

Through comparison of temperature lapse rates with isotopic lapse rates, ground temperature was not significantly correlated to isotopic lapse rate slopes (Figure 2-A3). In the American Transect temperature lapse rates and isotopic lapse rates resulted in an R^2 of 0.20 (p-value: 0.1773) and in the Kings Transect the R^2 was 0.03 (p-value: 0.4951), which do not indicate significant relationships within a confidence interval of 95%. Individual stable isotope lapse rates, dual isotope plots, and mean data temperature for corresponding sampling periods of rain are listed for the American Transect (Figure 2-A4) and the Kings Transect (Figure 2-A5). The linear relationships between temperature lapse rates and isotopic lapse rates were nearly flat with linear functions, $y = -0.88 (\pm 0.60) x - 8.08 (\pm 3.70)$ and $y = -0.26 (\pm 0.37) x - 4.08 (\pm 2.36)$ for the American and Kings Transect, respectively. Isotopic lapse rates were also compared to mean temperatures during each sampling period of collection through linear analysis, which resulted in R^2 values of 0.43 and 0.02, for the American and Kings Transects, respectively (Table 2-A16). When isotopic lapse rates were compared to mean minimum temperatures during sampling periods of collection, R^2 values were 0.32 and 0.06, for the American and Kings Transects, respectively. Similarly, when comparing isotopic lapse rates to mean maximum temperatures, R^2 values also did not result in a significant relationship, with R^2 values of 0.47 and 0.00 for the American and Kings Transects respectively. Weaker relationships were observed from comparing isotopic lapse rates and vapor pressure deficits, dew point temperatures and precipitation totals (Table 2-A16).

Sampling duration and continuity of storms sampled was qualitatively examined and quantitatively tested by performing linear regression on lapse rates with the number of days sampled, the number of breaks in precipitation, number of partial storms sampled and number of complete storms sampled and no significant relationships resulted (Table 2-A17). Two isotopic lapse rates constructed from continuous rainfall from 3/6/2016 to 3/8/2016 showed evidence of within storm variability (Table 2-1; Figure 2-3 (a) and (b)). The second half of the storm had a steeper isotopic lapse rate, but had a steeper temperature lapse rate in the first part of the storm. The mean temperature lapse rate was -6.5 °C/km in the first part of the storm and -4.2 °C/km in the second part of the storm (Table 2-A14). Many samples were composed of multiple storms, but the samples containing the longest aggregated time period of storm samples had isotopic lapse rates that were less steep, for example, in the American Transect 01/05/2017 contained several storms and had a lapse rate of -0.3 $\delta^{18}O$ (‰/km); all other lapse rates were steeper (Table 2-2).

Although the isotopic lapse rates were different between the American and Kings Transects, located at different latitudes, these two sets of data are not enough to determine if latitude has a significant relationship with the isotopic lapse rates. Other location-related variables that could affect differences in the isotopic lapse rates, such as elevation gradient, topographic complexity (i.e. canyons perpendicular to the elevation gradient) are examples of differences between the two transects that would require additional sampling and analysis at several additional locations to isolate these variables as factors affecting the isotopic lapse rates.

No pattern was apparent between lapse rates that contained snow samples compared to those containing only rain in the American and Kings Transects. In addition, fresh snow $\delta^{18}O$ signatures collected from the Southern Sierra Critical Zone Observatory P301 and Shorthair sites were analyzed using linear regression with their respective elevations, 2 km and 2.7 km, with a resulting slope of -1.4 (± 1.2) ‰/km (p-value = 0.22; adjusted $R^2 = 0.01$). Linear regression performed on Mt. Whitney fresh snow $\delta^{18}O$ signatures and sampling elevation resulted in a slope of -3.6 (± 0.3) ‰/km (p-value = 0.0002; $R^2 = 0.97$). Individual isotopic lapse rates for each transect were paired with respective dual isotope plots and temperature gradient plots over time in Figures 2-A4 and 2-A5 for each transect. Statistical results for linear regression performed on isotopic lapse rates and PRISM meteorological data are provided in Table 2-A5.

2.3.2 Local Meteoric Water Lines

Local Meteoric water lines were constructed to develop both a LMWL for the Sierra Nevada and to test whether they vary as a function of elevation and seasonality. The Local Meteoric Water Lines varied by location with slopes ranging from 5.93 (± 0.35) ‰ to 8.20 (± 0.33) ‰ (Table 2-4), with precipitation signatures generally lower at higher elevation sites. Mean $\delta^{18}O$ signatures ranged from -18.81 (± 2.17) ‰ on Mt. Whitney, to -8.33 (± 3.97) ‰ in the American Transect (Table 2-4). Within each of these groups, most signatures lie near the Global Meteoric Water Line (Figure 2-4) with the exception of summer rain during severe drought (Figure 2-4 (d)), which had d-excess values as low as -43 ‰. Higher elevation meteoric water lines for Shorthair and Mt. Whitney were composed completely of snow samples and these lines were closest to the GMWL.

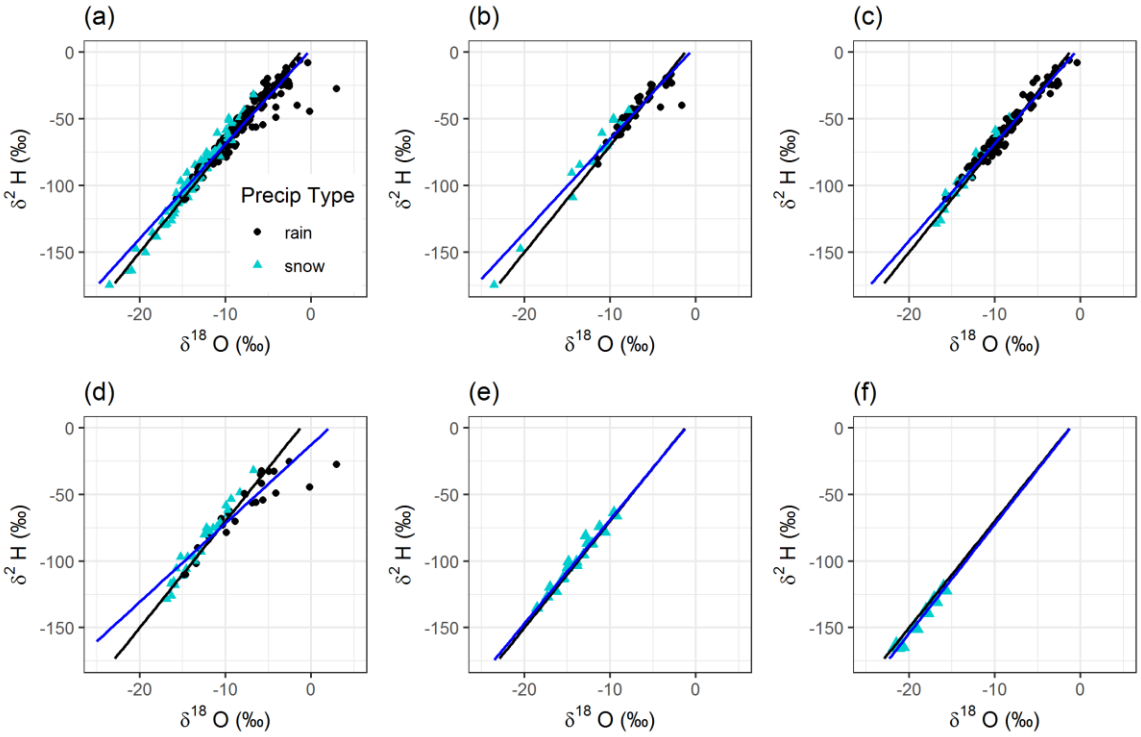

Figure 2-4. Local Meteoric Water Lines (blue) for (a) the entire Sierra Nevada (all meteoric water), (b) the American Transect, (c) the Kings Transect, (d) the Southern Sierra Critical Zone Observatory P301 site, (e) the Southern Sierra Critical Zone Observatory Shorthair site and (f) Mt. Whitney. Marker shape and color indicates precipitation type, either snow or rain. Black lines are the Global Meteoric Water Lines for reference.

Table 2-4. Sierra Nevada Local Meteoric Water Lines, including rain and snow.

Location	Slope	σ^1	Offset	σ^1	R^2
All	7.20	0.12	3.13	1.24	0.93
American Transect	7.04	0.27	4.74	2.45	0.93
Kings Transect	7.27	0.12	4.47	1.23	0.96
CZO P301	5.93	0.35	-12.64	3.87	0.86
CZO P301 amount weighted	6.54	0.39	-9.08	4.91	0.96
CZO Shorthair	7.79	0.36	9.32	5.07	0.96
Whitney	8.20	0.33	9.67	6.18	0.99

[1] Standard deviation of the mean.

Table 2-5. Sierra Nevada Local mean $\delta^{18}O$ and $\delta^{2}H$ input values.

Location	Mean $\delta^{18}O$	σ^{1}	Mean $\delta^{2}H$	σ^{1}
All	-9.80	4.25	-67.39	31.63
American Transect	-8.33	3.97	-53.90	28.93
Kings Transect	-9.20	3.70	-62.39	27.37
CZO P301	-10.31	4.40	-73.83	28.22
CZO P301 amount weighted	-11.94	4.05	-84.71	28.22
CZO Shorthair	-13.77	2.60	-97.85	20.65
Whitney	-18.81	2.17	-144.50	17.83

[1] Standard deviation of the mean.

2.3.3 Seasonality

Although the LMWLs were dominated by winter precipitation, seasonal variability can be seen in the differences in seasonal meteoric water lines (Figure 2-5). Seasonal precipitation water line slopes and offsets reflected seasonal variability (Table 2-6). Mean d-excess was the lowest in summer (-1.3 (± 4.7) ‰) and the highest in winter (15.2 (± 1.1) ‰). Seasonal patterns in precipitation can be seen in more negative winter precipitation signatures and more positive summer precipitation signatures (Figure 2-5). The winter water line slope was steeper than the fall, spring and summer water lines (Table 2-6).

Seasonal variability in the P301 LMWLs was larger than inter-annual variability. Seasonal LMWL slopes ranged from 4.7 (± 0.2) to 9.0 (± 0.1), meanwhile the WY 2016 LMWL slope was 7.5 (± 0.5) and the WY 2017 LMWL slope was 7.7 (± 0.4) and were not significantly different (p-value: 0.49).

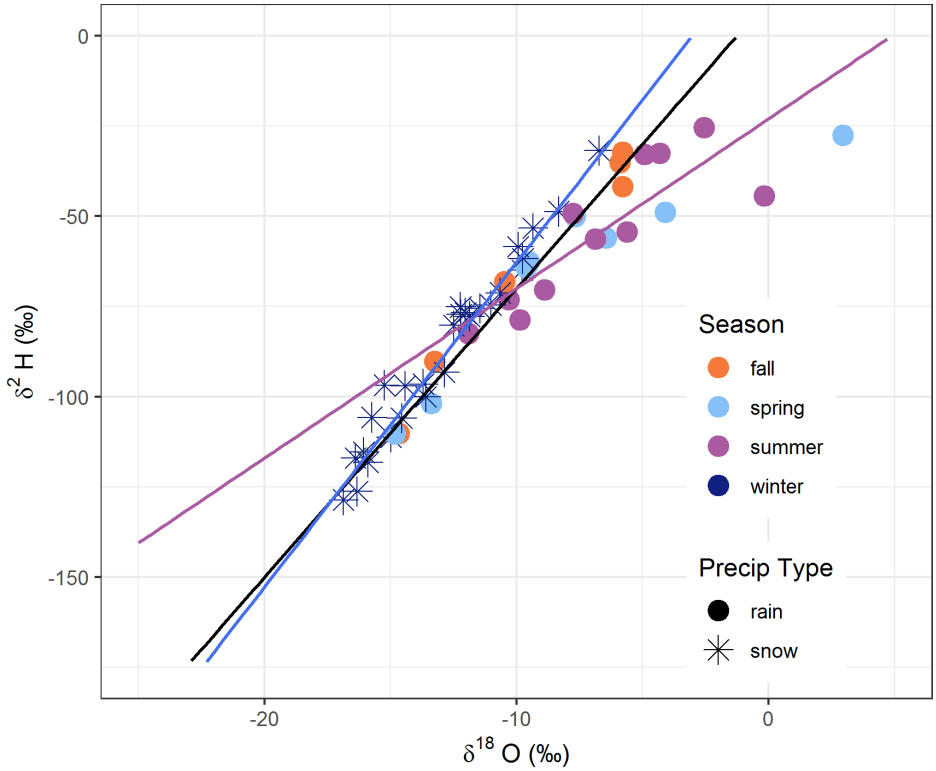

Figure 2-5. Dual-isotope plot of P301 precipitation classified by color representing season. Magenta line is the summer meteoric water line and the blue line is the winter meteoric water line. The black line is the Global Meteoric Water Line, for reference. Precipitation type is shown as snow or rain by marker shape.

Table 2-6. Seasonal and annual meteoric water lines for P301 and corresponding mean d-excess. Summer, fall, winter and spring water lines were composed of precipitation collected from 2015 through 2017.

Location	Slope	σ[1]	Offset	σ[1]	R^2	Mean d-excess (‰)	σ[1]
Summer	4.7	0.2	-23.0	1.5	0.73	-1.3	4.7
Fall	7.9	0.1	10.2	0.7	0.98	11.5	4.9
Winter	9.0	0.1	27.3	0.7	0.96	15.2	1.1
Spring	4.7	0.2	-25.3	2.1	0.76	0.1	7.4
WY2016	7.5	0.5	8.1	5.9	0.93	13.4	1.7
WY2017	7.7	0.4	9.5	4.3	0.95	12.7	1.3

[1] Standard error.

Using data from a single site, the Southern Sierra CZO P301 site, seasonality is investigated, and using the Kings Transect, elevation dependence of the seasonality is investigated. Seasonality can also be seen in the sinusoidal function of $\delta^{18}O$ over the time period that samples were collected for the LMWL at P301 (Figure 2-6). The sinusoidal function had an amplitude of 3.40 (± 0.7) and an offset of -9.5 (± 6) (RMSE = 2.56). The amplitude of the sinusoidal seasonality function increased with elevation (Figure 2-7 and Table 2-7); however, the linear relationship resulted in a slope of 0.83, offset of 3.1, adjusted R^2 is 0.76 and a p-value of 0.08, which is not significant within a 95% confidence interval. The amplitudes at different elevations ranged from 3.4 (± 1.3) to 4.6 (± 0.7) (Table 2-7).

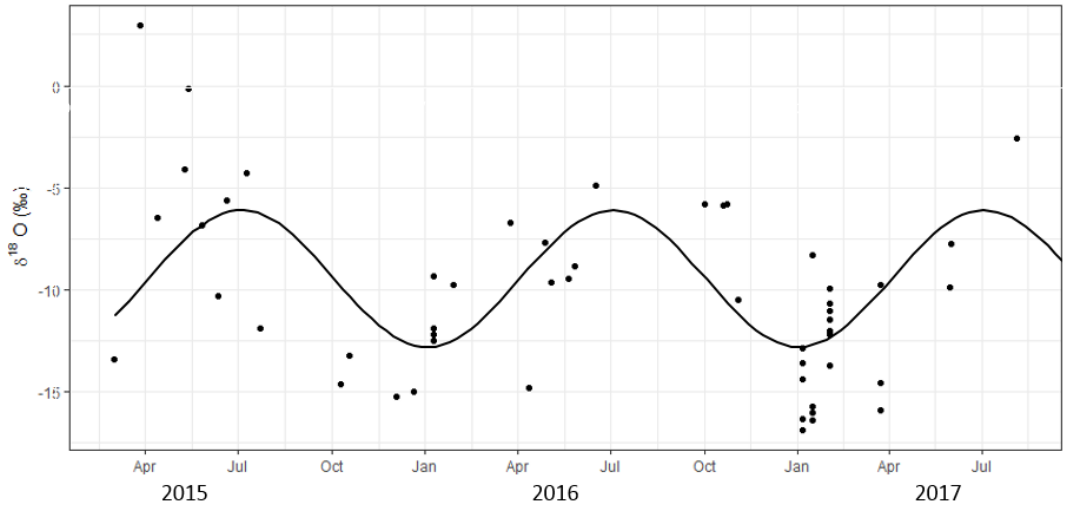

Figure 2-6. Sinusoidal seasonality (black line) fitted to P301 precipitation $\delta^{18}O$ over time.

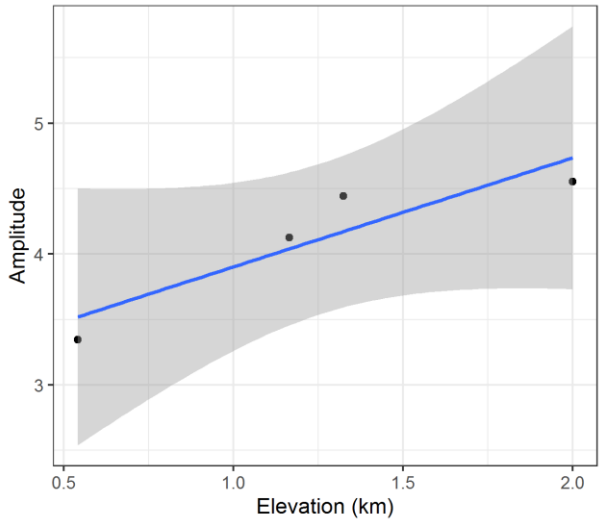

Figure 2-7. Sinusoidal seasonality amplitude values for three elevations in the Kings Transect with blue line representing the linear relationship between seasonal sinusoidal amplitude and elevation. Gray ribbon represents confidence interval of 95%.

Table 2-7. Kings Transect seasonal sinusoidal amplitudes along elevational gradient for $\delta^{18}O$ from March 2016 through March 2017.

Elevation (km)	Amplitude	ϕ	Offset	RMSE[1]
0.5	3.4 (± 1.3)	2.7	-6.7 (± 1.0)	2.55
1.2	4.1 (± 1.1)	2.5	-7.1 (± 0.9)	2.60
1.3	4.4 (± 1.0)	2.5	-7.3 (±0.8)	2.45
2.0[2]	4.6 (± 0.7)	2.5	-9.0 (± 0.6)	2.56

[1] Root mean square error of regression. [2] P301 precipitation limited to same dates as other sites in this table.

2.3.3 Snowmelt interception

Snowmelt under forest canopy and in forest gaps was significantly different (95% confidence interval) in both WY 2016 ($p < 0.001$) and WY 2017 ($p < 0.001$), but the overall variability was higher in WY 2017 (Figure 2-8 (a) through (f)). The snowmelt d-excess mean values for WY 2016 and WY 2017 were the same (within standard error) (Tables 2-A9 and 2-A10). Although the range in snowmelt signatures was larger during WY 2017 than WY 2016, the WY 2016 mean snowmelt signatures were the same, within standard error: -11.0 (± 1.4) ‰ and -12.1 (± 3.1) ‰, respectively. In both 2016 and 2017 snow depth was greater in canopy gaps compared to the area beneath canopy (Figure 2-A6 (a) and (b)). Soil moisture at 10 cm depths under canopy and in open areas were similar in both 2016 and 2017 (Figure 2-A6 (e) and (f)). The variability of soil temperature was low when snow is present and increases in spring once snow depth decreases to zero (Figure 2-A6 (c) and (d)). Isotopically, the lowest values of snowmelt occurred in January in the open areas in 2016 and 2017 (Figure 8 (a), (b), (d) and (e)). The slope of the snow melt water lines for WY 2016 and 2017 are presented in Table 2-8.

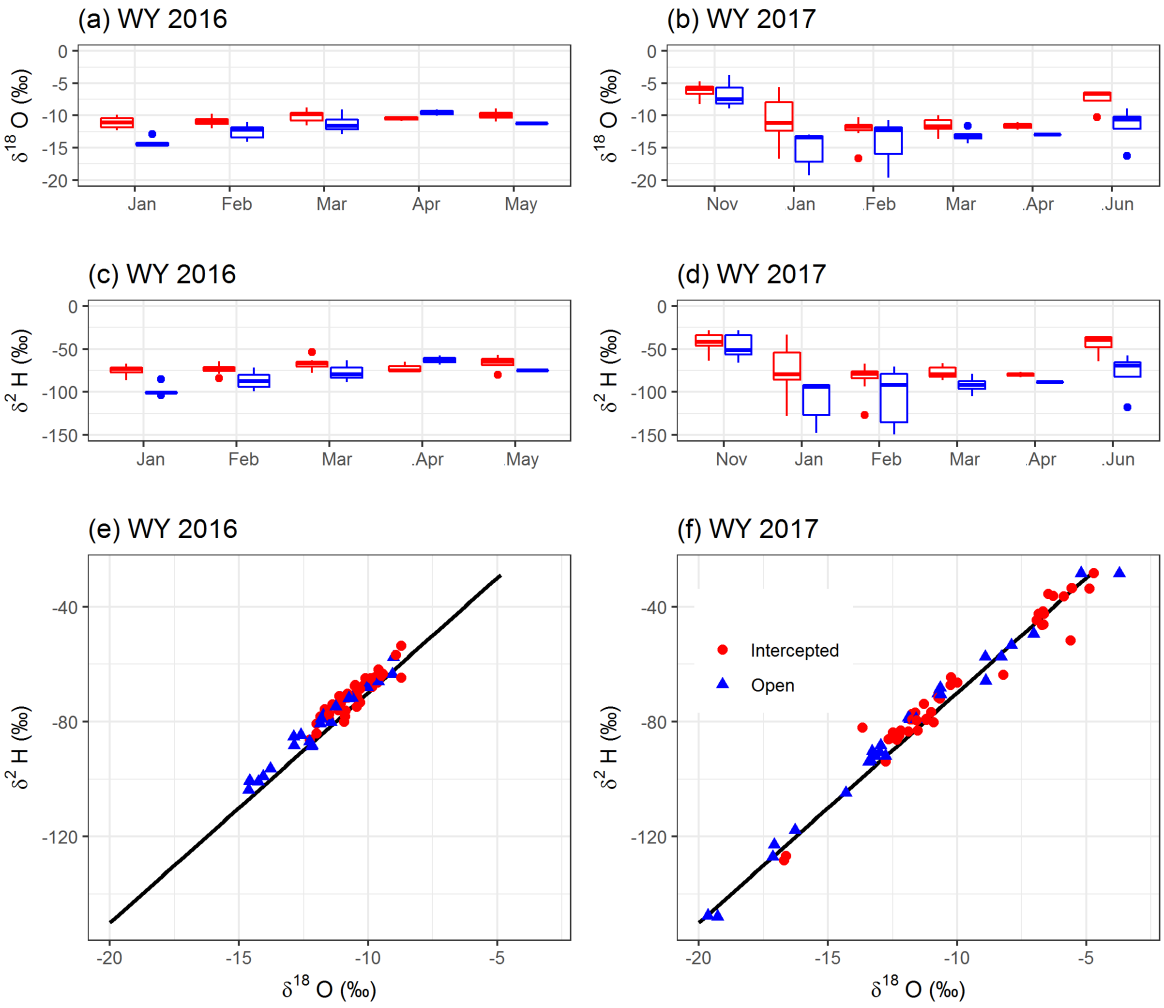

Figure 2-8. Stable isotope signatures of snowmelt over time in water years 2016 and 2017 from Upper P301, with snowmelt sampled from open areas indicated by the color blue and snowmelt sampled beneath the canopy indicated by red. (a) and (b) show $\delta^{18}O$ over time during water years 2016 and 2017, respectively and (c) and (d) show $\delta^{2}H$ over time for water years 2016 and water years 2017, respectively. (e) and (f) are dual-isotope plots of the same snowmelt signatures from water year 2016 and 2017, respectively. Black lines represent the GMWL.

Table 2-8. Snowmelt water lines from Southern Sierra Critical Zone Observatory P301 P-Caps during water years 2016 and 2017.

Water year	Slope	σ^1	Offset	σ^1	R^2
2016	7.05	0.22	8.07	2.48	0.94
2017	7.71	0.14	8.75	1.69	0.97

[1] Standard error.

2.4. Discussion

Individual isotopic lapse rates measured over the short term varied as much as 8.4 ‰/km in $\delta^{18}O$ and were not representative of an annual mean isotopic lapse rate, indicating that a single storm event is not representative of the isotopic lapse rate of the overall input into the system. The variability of the lapse rate can only be measured over time. Furthermore, variation in isotopic lapse rates were not dominated by any single variable, including temperature lapse rate, therefore mean amount weighted lapse rates derived by isotopic measurements cannot be represented by proxies such as temperature lapse rates. Isotopic lapse rates varied within storms (Figure 2-3 (a) and (b) and Table 2-2) and varied across different storms (Figure 2-3 and Table 2-2). Others have measured variability within storms as high as 51‰ in a 60 minute period, explained by precipitation originating in different cloud layers within the same storm (Coplen et al., 2008). The relationship between temperature lapse rate and isotopic lapse rate was weaker than expected, but can be explained by the interaction of source water and variability in condensation temperatures (Friedman & Smith, 1972; Friedman et al., 1992). The Sierra Nevada receives most precipitation in the wet season and little precipitation in the dry season. The single summer (dry) season isotopic lapse rate measured was very different from wet season isotopic lapse rates, with a positive lapse rate of 9.1 (± 2.9) ‰/km. This was the only summer thunderstorm sampled and the reverse isotopic lapse rate may be explained by variables such as elevation differences in recycled evapotranspiration, humidity, convection intensity and cloud height (Rozanski et al., 1993).

The mean weighted isotopic lapse rates of -3.3 (± 1.3) and -2.8 (± 1.8) ‰/km for the American and Kings Transects, respectively, can provide utility for applications in isotope hydrology, however, the standard error reflects the range of precision at which isotopic lapse rates can be measured, applied and compared. Our mean amount weighted lapse rates agree with isotopic lapse rates constructed from literature values, which were calculated as isotopic lapse rates of -2.5 ‰/km (rain) and -3.2 ‰/km (late season snow) in the Central and Northern Sierra and -2.7 ‰/km in the Southern Sierra (Lechler & Niemi, 2012). These values were a combination of integrated precipitation samples collected in the 1980's (Friedman et al., 1992), and precipitation collected from a single storm (Ingraham & Taylor, 1991), but based on the variability over time observed in our data, we can conclude that integrated samples collected over time are more representative than sampling from a single storm. Literature values containing late season snow may have been affected by fractionation during melt and aging, however, our isotopic lapse rates consisted of recent layers of fresh snow. Compared to the global mean isotopic lapse rate of -2.8 ‰/km, Sierra Nevada isotopic lapse rates were similar (Poage & Chamberlain, 2002). Other previous measurements in the Sierra Nevada of aged integrated snow cores from 1969, -40 ‰/km for $\delta^{2}H$ (Friedman & Smith, 1970), is out of the range of isotopic lapse rates for $\delta^{2}H$ of -26.7 (± 14.9) and -19.4 (± 13.9) ‰/km that we measured (Table 2-A15). Inclusion of a larger portion of samples from higher elevations, with more than half of the samples from above 2 km in elevation and many samples collected on the leeward side of the Sierra crest may have led to this difference (Friedman & Smith, 1970), and warrants further research. Measurements compiled from mountains around the world provide evidence of spatial variability from -18.3 to -0.4‰/km for $\delta^{18}O$ (Poage & Chamberlain, 2002). Our results show that if samples are only collected over a short amount of time, isotopic lapse rates can deviate far from an amount weighted mean. In a review of isotopic lapse rates, about half of the studies cited (over 30) were based on less than 10 data points, which may not represent a mean isotopic lapse rate for that region, unless they are integrated over a representative season of precipitation (Poage & Chamberlain, 2002). Nineteen of the other studies cited had between 10 and 20 data points and 13 studies had between 21 and 58 data points (Poage & Chamberlain, 2002).

Stable isotope signatures in the Sierra Nevada are not reliable proxies for paleo-temperature lapse rates because neither the American nor the Kings Transect individual lapse rates were found

to be significantly related to temperature. A stronger relationship between isotopic lapse rates was found with maximum and minimum vapor pressure deficits (Table 2-A16), but only in the American Transect where the R^2 value for linear regression between isotopic lapse rates and maximum and minimum vapor pressure deficits was 0.56 and 0.64. Vapor pressure deficit is the difference between the amount of moisture in the air and how much moisture the air can hold when saturated. Vapor pressure deficit affects condensation and evaporation processes, which are fundamentally important to changes in isotopic values (Gat, 1996). Furthermore, vapor pressure deficit can affect isotopic values as storms move, precipitate and evaporation occurs, especially falling rain drops. Meanwhile R^2 values in the Kings Transect were less than 0.01 for isotopic lapse rates and maximum and minimum vapor pressure deficits (Table 2-A16). The inconsistency in these results may be due to the spatial precision of the vapor pressure deficit values from PRISM output.

The LMWL in the Sierra Nevada is affected by season, drought and elevation. Seasonal variation in the mid-elevation mid-latitude P301 site was observed with lower summer LMWL slopes compared to winter LMWL slopes (Figure 2-5 and Table 2-6). The highest $\delta^{18}O$ and $\delta^{2}H$ values occurred during extreme drought conditions in 2015, when humidity was low, temperatures high and rain could experience more evaporation as it falls through warm, dry air (Gat & Dansgaard, 1972).

LMWL's were steepest for samples collected at the higher elevation sites, including Mt. Whitney (elevation range: 2.8 to 4.3 km) and Shorthair (elevation, 2.7 km), which can be explained by the composition of snow samples as opposed to rain. Raindrops falling through the atmosphere can experience evaporation which is less likely in snow (Gat & Dansgaard, 1972; Rozanski et al., 1993). Since some of our samples were composed of several storms, some composed of partial storms and some composed of single storms, we cannot determine how storm size affects stable isotope lapse rates; this is an area that warrants further research as California receives most of its precipitation through large storms such as atmospheric rivers (Dettinger et al., 2011). Previously measured snowpack stable isotope signatures in the Sierra Nevada at an elevation range of 2.6 km to 3.2 km in Tokopah Valley ranged from $\delta^{18}O$ signatures approximately -16‰ to -11‰ (Huth et al., 2004). This range is similar to the signatures measured at the CZO Shorthair (2.7 m) site, with snow signatures, ranging from -18.5 to -9.31‰ (mean: -13.8 (± 2.6)) (Table 2-A7). The Tokopah Valley is similar in elevation but approximately 60 km south of the Shorthair site. The Mt. Whitney samples were collected at a similar latitude, but higher elevation (2.8 km to 4.3 km) and ranged from -21.5‰ to -16.0‰ (mean: -18.81 (± 2.17)) (Table 2-A6). Temperatures on the leeward side of the Sierra Nevada (eastern side) are cooler than temperatures on the west side; temperature lapse rates were found to vary over time due to changes in weather systems and topographical effects such as cool air drainage in meadows (Lundquist & Cayan, 2007). Snow pit $\delta^{18}O$ signatures collected from the Central Sierra Snow Lab, located approximately 60 km north of the American Transect and at 2.1 km in elevation were reported from -18.3 to -10.9‰ (Taylor et al., 2001). The Central Sierra Snow Lab is closer in latitude to the American Transect than the CZO; American Transect sampling sites located above 1.8 km had $\delta^{18}O$ signatures ranging from –23.52 to -7.25‰. In the early 1990's snowpack signatures from the Central Sierra Snow Laboratory ranged from -21.35 to -4.25‰ in $\delta^{18}O$ (Unnikrishna et al., 2002). Microclimate, specific storm trajectory, interannual variation and a small sample size from the American Transect sites may explain the differences when comparing to the snow samples collected by others.

Seasonality had a strong effect on the precipitation stable isotope signatures in the mid-elevation, mid-latitude Sierra Nevada and the sinusoidal amplitude for the entire duration of measurements at the Southern Sierra Critical Zone Observatory was 3.4‰ (± 0.7). Of mountainous catchments, this amplitude is similar to that of other locations, such as in the Fernow Watershed in the Appalachian Mountains, West Virginia where a sinusoidal seasonal amplitude of 3.15‰ fit precipitation (Dewalle et al., 1997). In the Swiss Alps sinusoidal amplitudes fitted to precipitation

ranged from 2.6 to 6.4‰ (Allen et al., 2018). Additionally, we found that the amplitude of the seasonal signal increased with elevation, which agrees with previous analysis (Jodar et al., 2016).

In a previous study in Southeastern California, seasonal differences in precipitation signatures were a result of storm origin and trajectory and there was no evidence of a correlation between precipitation signatures and seasonal wetness or dryness (Friedman et al., 1992). Storm trajectory likely plays a role in the variation of storms and seasonal differences found here. Winter storms originating in the Pacific Ocean and summer storms originated in the Gulf of Mexico or subtropical Pacific Ocean, can result in more positive isotopic signatures in the Southeastern part of California (Friedman et al., 1992). This resulted in a summer average δ^2H signature of -56‰ and winter average of -78‰ (Friedman et al., 1992), which are similar to our average summer δ^2H signature, -55‰ and the average winter δ^2H signature, -89‰ at the CZO P301 site. The differences in signatures between seasons can be attributed to both source water and evaporation as the rain fell through dry summer air. Some summer precipitation signatures had very low d-excess, which could be attributed to evaporation of falling rain drops or the incorporation and recycled evapotranspiration. The Sierra Nevada forests are actively transpiring during summer (Ingraham & Taylor, 1991; Rozanski et al., 1993). We found that seasonal variability exceeded interannual variability and similar seasonal differences have been observed in the Sierra Nevada, with rain resulting in a meteoric water line with a slope of 6.5 and a snow meteoric water line with a slope of 9.2 (Friedman et al., 1992). Although summer precipitation experienced the most evaporation, which can be seen in the d-excess values, the spring water line reflected the most enrichment, which indicates that summer signatures were influenced by evaporation as rain fell and spring signatures were influenced by storm origin.

Interannual variation in the LMWL was small, except when rain during severe drought conditions was included, as discussed above. Water year 2016 and water year 2017 LMWL slopes were not significantly different 7.5 (± 0.5) and 7.7 (± 0.4) respectively). The LMWL constructed from Sierra Nevada river data was δ^2H = 7.06 (δ^{18}O) - 3.76 (Kendall & Coplen, 2001), which aggregated precipitation over entire basins from the Kern, Kings, Merced, San Joaquin and Mokelumne rivers. The river-derived LMWL has a steeper slope than the volume weighted LMWL (slope: 6.54 ± 0.39) (Table 2-4), and the river-derived LMWL slope was close to the P301 WY 2016 and WY 2017 LMWL slopes (7.5 (± 0.5) and 7.7 (± 0.4), respectively). The river derived water line can be biased towards winter precipitation while summer precipitation is transpired or evaporated.

Seasonal variation expressed by sinusoidal amplitude was related to elevation, with greater amplitudes at higher elevations. Similarly, others have found that lower elevation sites generally yielded lower amplitudes (Allen et al., 2018). The peak day of the month for P301 was day 272, which was later than the range found in Switzerland of 186 and 211 (Allen et al., 2018).

Drought affected the fit of the sinusoidal function due to high isotope values in precipitation during extremely dry conditions in 2015 (Figure 2-6). When precipitation stable isotope data was subset by dates for comparison with lower elevation sites, from March 2016 to March 2017, the amplitude was 4.6 (RMSE = 2.56) and when 2015 drought precipitation data was included, the amplitude was 3.4 (RMSE = 3.56) for δ^{18}O.

Snowmelt signatures beneath canopy were significantly higher than snowmelt in open areas and the difference was more distinct in early season (Figure 2-8 (a), (b), (d), (e)). Enhanced evaporation of the intercepted snow due to differences in temperature, humidity, air flow, albedo and surface area of snow was likely the cause of the difference. Throughfall in coniferous forests have been reported to have isotopically higher signatures caused by evaporation or exchange with ambient vapor (Kendall, 1993). In our case, ambient water vapor would likely be more depleted rather than enriched and intercepted snow would be more likely to interact with ambient vapor than non-intercepted snow, in which case, we would expect intercepted snowmelt to have lower isotope

values than non-intercepted snowmelt. Our results show the opposite. Longwave radiation has been found to provide a significant energy component in winter in forested snow dominated elevations of the Cascades and increases snow melt (Roth & Nolin, 2017). Higher isotopic signatures in snowmelt beneath canopy are most likely caused by proximate longwave radiation from tree trunks and branches.

Snowmelt signatures from open areas dominate the input signatures of snowmelt into the critical zone because there is a greater amount of snow in forest gaps than beneath canopy. In addition, forest gaps appear to consist of a greater area than the area beneath canopy at the P301 site, which can be seen in Lidar images of canopy (Oroza et al., 2018). Greater snow depths in forest gaps compared to beneath canopy were observed during the sampling periods (Figure 2-A6 (a) and (b)). Furthermore, Sierra Nevada snow accumulation has been found to be significantly affected by canopy at P301 and similar sites and the correlation is stronger at sites at this elevation compared to higher elevation sites due to higher vegetation density (Zheng et al., 2016). In the Sierra Nevada, snow accumulation has a stronger relationship with surrounding canopies than the canopy directly above and multi-layer canopy reduces snow accumulation on the ground (Zheng et al., 2016). Although canopy affects snow accumulation and ablation, canopy has not been found to affect soil moisture at the P301 site (Bales et al., 2011; Oroza et al., 2018). Likewise, comparing soil moisture at 10 cm depths in forest gaps and beneath forest canopy during snowmelt isotope sampling in 2016 and 2017, yields no clear difference.

References

Allen, S. T., Kirchner, J. W., Braun, S., Siegwolf, R. T. W., & Goldsmith, G. R. (2019). Seasonal origins of soil water used by trees. *Hydrology and Earth System Sciences, 23*(2), 1199-1210.

Allen, S. T., Kirchner, J. W., & Goldsmith, G. R. (2018). Predicting Spatial Patterns in Precipitation Isotope (delta H-2 and delta O-18) Seasonality Using Sinusoidal Isoscapes. *Geophysical Research Letters, 45*(10), 4859-4868.

Bales, R. C., Hopmans, J. W., O'Geen, A. T., Meadows, M., Hartsough, P. C., Kirchner, P., et al. (2011). Soil Moisture Response to Snowmelt and Rainfall in a Sierra Nevada Mixed-Conifer Forest. *Vadose Zone Journal, 10*(3), 786-799.

Bortolami, G. (1978). *Isotope hydrology of the Val Corsaglia, Maritime Alps, Piedmont, Italy* (Vol. 1). Isotope Hydrology: International Atomic Energy Agency

Brooks, J. R., Barnard, H. R., Coulombe, R., & McDonnell, J. J. (2010). Ecohydrologic separation of water between trees and streams in a Mediterranean climate. *Nature Geoscience, 3*(2), 100-104.

Clark, I., & Fritz, P. (1997). Environmental Isotopes in Hydrogeology.

Clogg, C. C., Petkova, E., & Haritou, A. (1995). Statistical-methods for comparing regression-coefficients between models. *American Journal of Sociology, 100*(5), 1261-1293.

Coplen, T. B., Neiman, P. J., White, A. B., Landwehr, J. M., Ralph, F. M., & Dettinger, M. D. (2008). Extreme changes in stable hydrogen isotopes and precipitation characteristics in a landfalling Pacific storm. *Geophysical Research Letters, 35*(21).

Cui, G. (2020). Mountain precipitation pattern in mixed rain-snow areas from a distributed wireless-sensor network. In R. Bales (Ed.). In Review.

Dansgaard, W. (1954). Oxygen-18 abundance in fresh water. *Nature, 174*(4422), 234-235.

Dansgaard, W. (1964). Stable isotopes in precipitation. *Tellus, 16*(4), 436-468.

Dettinger, M., Redmond, K., & Cayan, D. (2004). Winter orographic precipitation ratios in the Sierra Nevada - Large-scale atmospheric circulations and hydrologic consequences. *Journal of Hydrometeorology, 5*(6), 1102-1116.

Dettinger, M. D., Ralph, F. M., Das, T., Neiman, P. J., & Cayan, D. R. (2011). Atmospheric Rivers, Floods and the Water Resources of California. *Water, 3*(2), 445-478.

Dewalle, D. R., Edwards, P. J., Swistock, B. R., Aravena, R., & Drimmie, R. J. (1997). Seasonal isotope hydrology of three Appalachian forest catchments. *Hydrological Processes, 11*(15), 1895-1906.

Earman, S., Campbell, A. R., Phillips, F. M., & Newman, B. D. (2006). Isotopic exchange between snow and atmospheric water vapor: Estimation of the snowmelt component of groundwater recharge in the southwestern United States. *Journal of Geophysical Research-Atmospheres, 111*(D9).

Ehleringer, J. R., Barnette, J. E., Jameel, Y., Tipple, B. J., & Bowen, G. J. (2016). Urban water - a new frontier in isotope hydrology. *Isotopes in Environmental and Health Studies, 52*(4-5), 477-486.

Evaristo, J., McDonnell, J. J., Scholl, M. A., Bruijnzeel, L. A., & Chun, K. P. (2016). Insights into plant water uptake from xylem-water isotope measurements in two tropical catchments with contrasting moisture conditions. [Article]. *Hydrological Processes, 30*(18), 3210-3227.

Friedman, I., & Smith, G. I. (1970). Deuterium content of snow cores from Sierra Nevada area. *Science, 169*(3944), 467-&.

Friedman, I., & Smith, G. I. (1972). Deuterium content of snow as an index to winter climate in Sierra-Nevada area. *Science, 176*(4036), 790-&.

Friedman, I., Smith, G. I., Gleason, J. D., Warden, A., & Harris, J. M. (1992). Stable isotope composition of waters in southeastern california. 1. modern precipitation. *Journal of Geophysical Research-Atmospheres, 97*(D5), 5795-5812.

Frisbee, M. D., Phillips, F. M., Campbell, A. R., & Hendrickx, J. M. H. (2010). Modified passive capillary samplers for collecting samples of snowmelt infiltration for stable isotope analysis in remote, seasonally inaccessible watersheds 1: laboratory evaluation. *Hydrological Processes, 24*(7), 825-833.

Frisbee, M. D., Phillips, F. M., Campbell, A. R., Hendrickx, J. M. H., & Engle, E. M. (2010). Modified passive capillary samplers for collecting samples of snowmelt infiltration for stable isotope analysis in remote, seasonally inaccessible watersheds 2: field evaluation. *Hydrological Processes, 24*(7), 834-849.

Gat, J., & Dansgaard, W. (1972). Stable isotope survey of the fresh water occurrences in Israel and the northern Jordan Rift Valley (Vol. 16, pp. 177-211). Journal of Hydrology.

Gat, J. R. (1996). Oxygen and hydrogen isotopes in the hydrologic cycle. *Annual Review of Earth and Planetary Sciences, 24*, 225-262.

Goulden, M. L., Anderson, R. G., Bales, R. C., Kelly, A. E., Meadows, M., & Winston, G. C. (2012). Evapotranspiration along an elevation gradient in California's Sierra Nevada. *Journal of Geophysical Research-Biogeosciences, 117*.

Goulden, M. L., & Bales, R. C. (2019). California forest die-off linked to multi-year deep soil drying in 2012-2015 drought. *Nature Geoscience, 12*(8), 632-+.

Griffin, D., & Anchukaitis, K. J. (2014). How unusual is the 2012-2014 California drought? *Geophysical Research Letters, 41*(24), 9017-9023.

PRISM (2004). Parameter-elevation Regressions on Independent Slopes Model (PRISM). Oregon State University.

Guirguis, K., Gershunov, A., Shulgina, T., Clemesha, R. E. S., & Ralph, F. M. (2019). Atmospheric rivers impacting Northern California and their modulation by a variable climate. *Climate Dynamics, 52*(11), 6569-6583.

Gustafson, J. R., Brooks, P. D., Molotch, N. P., & Veatch, W. C. (2010). Estimating snow sublimation using natural chemical and isotopic tracers across a gradient of solar radiation. *Water Resources Research, 46*.

He, M. X., Russo, M., & Anderson, M. (2017). Hydroclimatic Characteristics of the 2012-2015 California Drought from an Operational Perspective. *Climate, 5*(1).

Heckert, A. (2016). Dataplot reference manual, Volume 2: Subcommands and library. 2, from https://www.itl.nist.gov/div898/software/dataplot/refman2/ch2/weightsd.pdf

Highlights, C. W. P. U. (2013). Sacramento, California: Department of Water Resources, State of California.

Huth, A. K., Leydecker, A., Sickman, J. O., & Bales, R. C. (2004). A two-component hydrograph separation for three high-elevation catchments in the Sierra Nevada, California. *Hydrological Processes, 18*(9), 1721-1733.

Ingraham, N. L., & Taylor, B. E. (1991). Light stable isotope systematics of large-scale hydrologic regimes in California and Nevada. *Water Resources Research, 27*(1), 77-90.

Jasechko, S. (2016). Partitioning young and old groundwater with geochemical tracers. *Chemical Geology, 427*, 35-42.

Jasechko, S., Kirchner, J. W., Welker, J. M., & McDonnell, J. J. (2016). Substantial proportion of global streamflow less than three months old. *Nature Geoscience, 9*(2), 126-+.

Jasechko, S., & Taylor, R. G. (2015). Intensive rainfall recharges tropical groundwaters. [Article]. *Environmental Research Letters, 10*(12), 7.

Jodar, J., Custodio, E., Liotta, M., Lamban, L. J., Herrera, C., Martos-Rosillo, S., et al. (2016). Correlation of the seasonal isotopic amplitude of precipitation with annual evaporation and altitude in alpine regions. *Science of the Total Environment, 550*, 27-37.

Kendall, C. (1993). *Impact of isotopic heterogeneity in shallow systems on modeling of stormflow generation*. University of Maryland University of Maryland.

Kendall, C., & Coplen, T. B. (2001). Distribution of oxygen-18 and deuterium in river waters across the United States. *Hydrological Processes, 15*(7), 1363-1393.

Kendall, C., & McDonnell, J. *Isotope tracers in catchment hydrology*.

Lechler, A. R., & Niemi, N. A. (2012). The influence of snow sublimation on the isotopic composition of spring and surface waters in the southwestern United States: Implications for stable isotope-based paleoaltimetry and hydrologic studies. *Geological Society of America Bulletin, 124*(3-4), 318-334.

Liu, F. J., Hunsaker, C., & Bales, R. C. (2013). Controls of streamflow generation in small catchments across the snow-rain transition in the Southern Sierra Nevada, California. *Hydrological Processes, 27*(14), 1959-1972.

Lundquist, J. D., & Cayan, D. R. (2007). Surface temperature patterns in complex terrain: Daily variations and long-term change in the central Sierra Nevada, California. *Journal of Geophysical Research-Atmospheres, 112*(D11).

Machavaram, M. V., & Krishnamurthy, R. V. (1995). Earth surface evaporative process - a case-study from the Great-Lakes region of the united-states based on deuterium excess in precipitation. *Geochimica Et Cosmochimica Acta, 59*(20), 4279-4283.

McCutcheon, R. J., McNamara, J. P., Kohn, M. J., & Evans, S. L. (2017). An evaluation of the ecohydrological separation hypothesis in a semiarid catchment. *Hydrological Processes, 31*(4), 783-799.

Moreno-Gutierrez, C., Dawson, T. E., Nicolas, E., & Querejeta, J. I. (2012). Isotopes reveal contrasting water use strategies among coexisting plant species in a Mediterranean ecosystem. *New Phytologist, 196*(2), 489-496.

Oroza, C. A., Bales, R. C., Stacy, E. M., Zheng, Z. S., & Glaser, S. D. (2018). Long-Term Variability of Soil Moisture in the Southern Sierra: Measurement and Prediction. *Vadose Zone Journal, 17*(1).

Penna, D., Ahmad, M., Birks, S. J., Bouchaou, L., Brencic, M., Butt, S., et al. (2014). A new method of snowmelt sampling for water stable isotopes. *Hydrological Processes, 28*(22), 5637-5644.

Poage, M. A., & Chamberlain, C. P. (2002). Stable isotopic evidence for a Pre-Middle Miocene rain shadow in the western Basin and Range: Implications for the paleotopography of the Sierra Nevada. *Tectonics, 21*(4).

Rose, K. L., Graham, R. C., & Parker, D. R. (2003). Water source utilization by Pinus jeffreyi and Arctostaphylos patula on thin soils over bedrock. *Oecologia, 134*(1), 46-54.

Roth, T. R., & Nolin, A. W. (2017). Forest impacts on snow accumulation and ablation across an elevation gradient in a temperate montane environment. *Hydrology and Earth System Sciences, 21*(11), 5427-5442.

Rozanski, K., Araguas-Araguas, L., & Gonfiantini, R. (1993). Isotopic patterns in modern global precipitation (Vol. 78, pp. 1-36). *Climate change in continental isotopic records*.

Rungee, J. (2019). Estimating plant-accessible water storage through evaluating evapotranspiration in the semi-arid western United States using eddy-covariance, remote sensing, and spatially distributed data. University of California, Merced: eScholarship.

Safeeq, M., & Hunsaker, C. T. (2016). Characterizing runoff and water yield for headwater catchments in the Southern Sierra Nevada. *Journal of the American Water Resources Association, 52*(6), 1327-1346.

Saxena, R. K. (1986). Estimation of canopy reservoir capacity and O-18 fractionation in throughfall in a pine forest. *Nordic Hydrology, 17*(4-5), 251-260.

Shukla, S., Safeeq, M., AghaKouchak, A., Guan, K., & Funk, C. (2015). Temperature impacts on the water year 2014 drought in California. *Geophysical Research Letters, 42*(11), 4384-4393.

Siegenthaler, U., & Oeschger, H. (1980). Correlation of O-18 in precipitation with temperature and altitude. *Nature, 285*(5763), 314-317.

Smith, G. I., Friedman, I., Klieforth, H., & Hardcastle, K. (1979). Areal distribution of deuterium in Eastern California precipitation, 1968-1969. *Journal of Applied Meteorology, 18*(2), 172-188.

Southern Sierra Critical Zone Observatory website. (2019). Retrieved November 1, 2017, from http://criticalzone.org/sierra/data/

Sprenger, M., Herbstritt, B., & Weiler, M. (2015). Established methods and new opportunities for pore water stable isotope analysis. *Hydrological Processes, 29*(25), 5174-5192.

Sprenger, M., Leistert, H., Gimbel, K., & Weiler, M. (2016). Illuminating hydrological processes at the soil-vegetation-atmosphere interface with water stable isotopes. [Review]. *Reviews of Geophysics, 54*(3), 674-704.

Storck, P., Lettenmaier, D. P., & Bolton, S. M. (2002). Measurement of snow interception and canopy effects on snow accumulation and melt in a mountainous maritime climate, Oregon, United States. *Water Resources Research, 38*(11).

Taylor, S., Feng, X. H., Kirchner, J. W., Osterhuber, R., Klaue, B., & Renshaw, C. E. (2001). Isotopic evolution of a seasonal snowpack and its melt. *Water Resources Research, 37*(3), 759-769.

Unnikrishna, P. V., McDonnell, J. J., & Kendall, C. (2002). Isotope variations in a Sierra Nevada snowpack and their relation to meltwater. *Journal of Hydrology, 260*(1-4), 38-57.

Visser, A., Moran, J. E., Singleton, M. J., & Esser, B. K. (2018). Importance of river water recharge to the San Joaquin Valley groundwater system. *Hydrological Processes, 32*(9), 1202-1213.

Visser, A., Thaw, M., Deinhart, A., Bibby, R., Safeeq, M., Conklin, M., et al. (2019). Cosmogenic Isotopes Unravel the Hydrochronology and Water Storage Dynamics of the Southern Sierra Critical Zone. *Water Resources Research, 55*(2), 1429-1450.

von Freyberg, J. (2019). Influences of forest canopy on snowpack accumulation and isotope ratios. In T. Bjarnadóttir (Ed.). Hydrological Processes.

Zheng, Z., Kirchner, P. B., & Bales, R. C. (2016). Topographic and vegetation effects on snow accumulation in the southern Sierra Nevada: a statistical summary from lidar data. *Cryosphere, 10*(1), 257-269.

Zhu, L., Fan, M. J., Hough, B., & Li, L. (2018). Spatiotemporal distribution of river water stable isotope compositions and variability of lapse rate in the central Rocky Mountains: Controlling factors and implications for paleoelevation reconstruction. *Earth and Planetary Science Letters, 496*, 215-226.

Appendix to Chapter 2

This is the equation used to calculate non-weighted standard deviation of slope and offset:

$$s = \sqrt{\frac{\sum_{i=1}^{N}(x_i - \bar{x})^2}{N-1}}, \quad \text{(AE1)}$$

This is the equation used to calculate amount-weighted standard deviation of slope and offset:

$$s_w = \sqrt{\frac{\sum_{i=1}^{N} w_i(x_i - \bar{x})^2}{\frac{N'-1}{N'}\sum_{i=1}^{N} w_i}}, \quad \text{(AE2)}$$

where the standard deviation is s and weighted standard deviation s_w, $\bar{x}$ is the weighted mean and N' is the number of weights (Heckert, 2016).

Table A2-1. All sampling locations and elevations for rain, snow and snowmelt.

Location	Latitude	Longitude	Elevation (km)	Precipitation Type
American Transect	38.76064	-120.575692	1.20	Rain and snow
American Transect	38.78574	-120.215179	1.64	Rain and snow
American Transect	38.77080	-120.448779	0.98	Rain and snow
American Transect	38.80880	-120.134667	1.86	Rain and snow
American Transect	38.81482	-120.03401	2.26	Rain and snow
American Transect	38.72772	-120.80639	0.56	Rain and snow
Kings Transect	37.04415	-119.473282	0.54	Rain and snow
Kings Transect	37.06054	-119.449317	0.70	Rain and snow
Kings Transect	37.04799	-119.432286	0.85	Rain and snow
Kings Transect	37.03895	-119.408118	1.00	Rain and snow
Kings Transect	37.05169	-119.40088	1.17	Rain and snow
Kings Transect	37.05801	-119.371882	1.32	Rain and snow
P301	37.06737	-119.195066	2.00	Rain, snow and snowmelt
Shorthair	37.06765	-118.986524	2.70	Snow
Whitney	36.57949	-118.293286	4.30	Snow
Whitney	36.57946	-118.291653	4.21	Snow
Whitney	36.58097	-118.285946	3.85	Snow
Whitney	36.58095	-118.274227	3.46	Snow
Whitney	36.58422	-118.259745	3.15	Snow
Whitney	36.58635	-118.249597	2.81	Snow
Whitney	36.58599	-118.24188	2.50	Snow
Mt Tallac	38.90590	-120.10000	2.95	Snow
Rubicon Peak	38.98917	-120.133506	2.76	Snow
Powderhouse Peak	38.77602	-119.965459	2.88	Snow

Table A2-2. American Transect stable isotope values for each corresponding sampling date and elevation.

Date	$\delta^{18}O$ (‰)	$\delta^{2}H$ (‰)	Elevation (km)	Precipitation Type
10/17/2016	-5.10	-24.46	0.56	rain
10/17/2016	-6.50	-33.30	0.97	rain
10/17/2016	-5.64	-35.64	1.18	rain
10/17/2016	-5.12	-28.04	1.20	rain
10/17/2016	-7.32	-42.79	1.64	rain
10/17/2016	-7.25	-45.59	1.86	rain
10/17/2016	-8.57	-58.00	2.26	rain
10/24/2016	-2.86	-16.74	0.56	rain
10/24/2016	-3.13	-20.54	0.97	rain
10/24/2016	-2.82	-23.34	1.18	rain
10/24/2016	-5.23	-24.08	1.20	rain
10/24/2016	-5.43	-30.83	1.64	rain
10/24/2016	-7.92	-46.18	1.86	rain
10/24/2016	-7.98	-47.51	2.26	rain
10/25/2016	-3.15	-21.91	0.56	rain
10/25/2016	-3.48	-24.84	0.99	rain
10/25/2016	-3.49	-19.28	1.20	rain
10/25/2016	-5.38	-33.46	1.64	rain
10/25/2016	-7.35	-44.95	1.86	rain
10/25/2016	-7.86	-49.16	2.26	rain
1/5/2017	-11.63	-79.52	1.20	rain
1/5/2017	-11.12	-73.21	1.64	snow
1/5/2017	-10.58	-71.39	1.86	snow
1/5/2017	-12.06	-82.41	2.26	snow
1/24/2017	-10.43	-67.82	0.56	rain
1/24/2017	-14.50	-90.39	0.99	snow
1/24/2017	-13.56	-84.68	1.20	snow
2/3/2017	-6.80	-42.51	0.56	rain
2/3/2017	-9.44	-62.33	1.20	rain
2/3/2017	-10.08	-67.40	2.26	snow
1/29/2017	-20.46	-147.49	2.85[1]	snow
1/28/2017	-23.52	-174.50	2.96[2]	snow
2/6/2017	-6.58	-37.11	0.56	rain
2/6/2017	-8.46	-54.64	0.98	rain
2/6/2017	-7.56	-43.44	1.20	rain
2/6/2017	-10.38	-70.43	2.26	snow
2/21/2017	-6.74	-34.44	0.56	rain
2/21/2017	-7.47	-42.46	0.98	rain
2/21/2017	-8.81	-52.32	1.20	rain
2/21/2017	-8.70	-53.11	1.64	snow
2/21/2017	-7.85	-43.68	2.26	snow
2/19/2017	-14.35	-108.98	2.77[3]	snow
3/5/2017	-9.21	-56.12	0.56	rain
3/5/2017	-9.64	-51.02	0.98	graupel
3/5/2017	-8.56	-49.38	1.20	rain
3/5/2017	-10.98	-60.62	1.86	snow
3/5/2017	-9.63	-49.34	2.26	snow
3/27/2017	-8.94	-61.94	0.98	rain
3/27/2017	-7.03	-47.76	0.56	rain
3/27/2017	-7.92	-50.89	1.20	rain
3/31/2017	-8.73	-61.67	0.98	rain

3/31/2017	-11.41	-83.82	2.26	rain
8/22/2017	-7.93	-56.30	0.98	rain
8/22/2017	-4.12	-41.09	1.20	rain
8/22/2017	-1.62	-39.75	1.64	rain

[1] Snow grab sample collected from summit of Powderhouse Peak.
[2] Snow grab sample collected from summit of Mt. Tallac.
[3] Snow grab sample collected from summit of Rubicon Peak.

Table A2-3. Kings Transect stable isotope values for each corresponding sampling date and elevation.

Date	$\delta^{18}O$ (‰)	$\delta^{2}H$ (‰)	Elevation (km)	Precipitation Type
3/6/2016	-8.91	-57.03	0.54	rain
3/6/2016	-8.96	-57.81	0.70	rain
3/6/2016	-9.63	-61.06	0.85	rain
3/6/2016	-9.45	-58.58	1.00	rain
3/6/2016	-10.19	-64.38	1.17	rain
3/6/2016	-10.77	-69.59	1.32	snow
3/8/2016	-11.95	-83.08	0.54	rain
3/8/2016	-12.83	-87.71	0.70	rain
3/8/2016	-13.85	-93.65	0.85	rain
3/8/2016	-14.00	-96.53	1.00	rain
3/8/2016	-15.58	-108.02	1.10	rain
3/8/2016	-15.47	-108.11	1.17	rain
3/8/2016	-15.71	-109.94	1.32	rain
3/24/2016	-2.95	-11.85	0.54	rain
3/24/2016	-3.42	-18.33	0.70	rain
3/24/2016	-5.06	-19.79	1.17	rain
3/24/2016	-5.50	-22.93	1.32	rain
3/24/2016	-6.73	-31.76	2.02	rain
5/21/2016	-7.99	-50.93	0.54	rain
5/21/2016	-7.84	-52.62	0.70	rain
5/21/2016	-7.91	-57.41	0.85	rain
5/21/2016	-8.39	-55.96	1.00	rain
5/21/2016	-8.40	-57.91	1.17	rain
5/21/2016	-8.26	-53.82	1.32	rain
5/21/2016	-9.49	-62.65	2.02	rain
5/27/2016	-5.77	-41.94	0.54	rain
5/27/2016	-5.63	-40.53	0.70	rain
5/27/2016	-5.49	-40.00	0.85	rain
5/27/2016	-7.43	-52.19	1.00	rain
5/27/2016	-7.43	-52.20	1.17	rain
5/27/2016	-7.84	-54.83	1.32	rain
5/27/2016	-8.88	-70.36	2.02	rain
6/16/2016	-2.78	-25.28	0.70	rain
6/16/2016	-2.65	-21.79	0.85	rain
6/16/2016	-3.33	-24.61	1.00	rain
6/16/2016	-4.55	-28.92	1.17	rain
6/16/2016	-3.69	-24.08	1.32	rain
6/16/2016	-4.92	-32.91	2.02	rain
10/20/2016	-5.89	-35.15	2.00	rain
10/20/2016	-3.83	-18.69	1.32	rain
10/20/2016	-3.02	-15.03	1.17	rain
10/20/2016	-2.82	-12.74	1.00	rain
10/20/2016	-2.10	-9.79	0.85	rain
10/20/2016	-1.31	-6.21	0.54	rain
10/20/2016	-5.80	-41.83	2.02	rain
10/24/2016	-3.53	-31.13	1.00	rain
10/24/2016	-2.55	-24.00	1.17	rain
10/24/2016	-2.62	-23.65	1.32	rain
10/24/2016	-5.79	-32.30	2.00	rain
10/24/2016	-5.79	-32.30	2.02	rain
11/4/2016	-8.68	-60.53	0.54	rain

11/4/2016	-8.75	-61.26	0.70	rain
11/4/2016	-8.04	-56.62	0.85	rain
11/4/2016	-10.56	-70.74	1.00	rain
11/4/2016	-8.06	-58.51	1.17	rain
11/4/2016	-10.67	-69.97	1.32	rain
11/4/2016	-10.48	-68.19	2.02	rain
12/3/2016	-12.69	-85.17	0.54	rain
12/3/2016	-12.93	-87.01	0.70	rain
12/3/2016	-13.16	-87.02	0.85	rain
12/3/2016	-13.04	-85.87	1.00	rain
12/3/2016	-12.62	-85.05	1.17	rain
12/3/2016	-10.07	-66.57	1.32	rain
12/3/2016	-12.91	-90.08	2.00	snow
12/9/2016	-9.97	-71.60	0.54	rain
12/9/2016	-10.98	-74.93	0.70	rain
12/9/2016	-10.36	-76.69	0.85	rain
12/9/2016	-10.59	-76.13	1.00	rain
12/9/2016	-10.73	-76.01	1.17	rain
12/9/2016	-11.52	-80.43	1.32	rain
1/6/2017	-12.61	-94.16	0.85	rain
1/6/2017	-10.79	-82.36	1.00	rain
1/6/2017	-12.59	-87.85	1.17	rain
1/6/2017	-12.86	-93.25	2.02	snow pit (0-5)
1/6/2017	-16.32	-126.23	2.02	Snow pit (5-23)
1/6/2017	-14.42	-97.04	2.02	Snow pit rain crust (23-25)
1/6/2017	-16.87	-128.61	2.02	Snow pit light powder (25-48)
1/6/2017	-13.60	-100.05	2.02	Snow pit (48-55 cm)
1/14/2017	-8.20	-49.23	0.85	rain
1/14/2017	-9.98	-64.91	1.00	rain
1/14/2017	-14.24	-99.08	1.32	rain
1/14/2017	-8.33	-48.67	2.02	snow pit rain crust (50-54)
1/14/2017	-16.06	-115.38	2.02	snow pit (57-73)
1/14/2017	-16.39	-117.02	2.02	snow pit rain/sun crust (72-75)
1/14/2017	-15.74	-105.76	2.02	snow pit (75-78)
2/2/2017	-9.74	-70.76	0.54	rain
2/2/2017	-7.16	-50.51	1.00	rain
2/2/2017	-8.62	-50.03	1.17	rain
2/2/2017	-10.39	-68.05	1.32	rain
2/1/2017	-13.70	-96.52	2.02	snow pit crust (70-85)
2/1/2017	-11.02	-74.66	2.02	snow pit (85-115)
2/1/2017	-11.46	-75.50	2.02	snow pit (116-117)
2/1/2017	-12.03	-76.82	2.02	snow pit (120 - 130)
2/1/2017	-10.65	-71.22	2.02	several crust layers (130-140)
2/1/2017	-9.94	-58.43	2.02	snow pit crust (140-141)
2/1/2017	-12.22	-75.13	2.02	snow pit (143-156)
2/15/2017	-8.26	-52.60	0.54	rain
2/15/2017	-11.34	-81.89	0.70	rain
2/15/2017	-9.29	-69.39	0.85	rain
2/15/2017	-7.02	-45.90	1.00	rain
2/15/2017	-8.75	-68.98	1.17	rain
2/15/2017	-9.77	-62.81	1.32	rain
3/17/2017	-9.05	-57.73	0.54	rain
3/17/2017	-8.63	-57.15	0.70	rain
3/17/2017	-10.60	-67.46	0.85	rain

3/17/2017	-10.69	-68.97	1.00	rain
3/17/2017	-12.31	-81.24	1.16	rain
3/17/2017	-11.22	-72.22	1.17	rain
3/17/2017	-11.64	-77.35	1.32	rain
3/23/2017	-7.40	-45.02	0.54	rain
3/23/2017	-7.69	-47.55	0.85	rain
3/23/2017	-7.60	-47.05	1.00	rain
3/23/2017	-7.32	-47.35	1.17	rain
3/23/2017	-7.74	-47.18	1.32	rain
3/23/2017	-9.75	-61.77	2.02	snow pit (153-155)
3/23/2017	-15.90	-118.24	2.02	snow pit (125-140)
3/23/2017	-14.56	-105.97	2.02	snow pit (123-125)
4/1/2017	-10.33	-77.94	0.54	rain
4/1/2017	-9.56	-75.22	0.70	rain
4/1/2017	-9.38	-69.12	0.85	rain
4/1/2017	-10.01	-74.82	1.00	rain
4/1/2017	-9.32	-65.09	1.17	rain
4/1/2017	-11.28	-79.15	1.32	rain
5/9/2017	-4.31	-25.06	0.54	rain
5/9/2017	-0.42	-8.02	0.70	rain
5/9/2017	-3.84	-22.37	0.85	rain
5/9/2017	-6.06	-33.69	1.32	rain

[1] Snow grab sample collected from summit of Powderhouse Peak.
[2] Snow grab sample collected from summit of Mt. Tallac.
[3] Snow grab sample collected from summit of Rubicon Peak.

Table A2-4. American Transect precipitation collection storm intervals.

Date	No. days collecting	No. breaks between precipitation	No. partial storms collected	No. complete storms collected
10/17/2016	14	1	1	2
10/24/2016	7	2	2	1
10/25/2016	1	0	1	0
1/5/2017	72	6	2	5
1/24/2017	24	1	0	2
2/3/2017	2	1	1	0
2/6/2017	3	0	1	0
2/21/2017	15	1	2	0
3/5/2017	12	1	2	0
3/27/2017	22	3	2	2
3/31/2017	4	0	1	0
8/22/2017	22	2	0	2

Table A2-5. Kings Transect precipitation collection storm intervals.

Date	No. days collecting	No. breaks between precipitation	No. partial storms collected	No. complete storms collected
3/6/2016	2	0	1	0
3/8/2016	2	0	1	0
3/24/2016	16	2	1	1
5/21/2016	58	8	0	9
5/27/2016	6	0	1	0
6/6/2016	10	1	1	1
10/20/2016	2	0	0	1
10/24/2016	4	0	1	0
11/4/2016	11	3	1	3
12/3/2016	29	2	0	3
12/9/2016	6	0	1	0
1/6/2017	28	4	2	3
1/14/2017	8	0	1	0
2/2/2017	19	0	0	1
2/15/2017	13	0	0	1
3/17/2017	30	2	0	3
3/23/2017	6	0	0	1
4/1/2017	9	1	0	2
5/9/2017	38	3	0	4

Table A2-6. Mt. Whitney snow stable isotope values. All samples were collected on April 2, 2016 and were surface layer grab samples following recent storm.

Elevation (km)	$\delta^{18}O$ (‰)	$\delta^{2}H$ (‰)
2.81	-15.98	-121.09
3.15	-17.07	-129.70
3.46	-18.06	-138.32
3.85	-19.34	-150.07
4.21	-21.48	-164.14
4.30	-20.93	-163.65

Table A2-7. Southern Sierra Critical Zone Observatory Shorthair site (2.7 km) snow stable isotope values. Snow layers were measured from the ground surface to the top of the snowpack.

Date	Snow Layer Depth (cm)	$\delta^{18}O$ (‰)	$\delta^{2}H$ (‰)
3/1/2016	surface	-10.62	-78.10
3/1/2016	0-50	-15.55	-113.46
3/1/2016	98	-15.45	-112.75
3/1/2016	60-98	-14.83	-100.56
3/1/2016	98-115	-16.31	-122.87
3/1/2016	115-130	-12.11	-87.03
3/1/2016	135-155	-13.12	-95.16
3/1/2016	155-162	-13.91	-103.30
2/16/2017	205-262	-11.25	-74.18
2/16/2017	262-263	-14.96	-104.82
2/16/2017	263-288	-12.88	-81.14
2/16/2017	288-292	-17.03	-119.51
2/16/2017	292-300	-9.55	-63.55
2/16/2017	300 crust	-12.65	-86.53
2/16/2017	305-315	-13.95	-100.69
2/16/2017	315-335	-9.31	-66.12
2/16/2017	335-360	-18.50	-135.15
2/16/2017	360-365	-17.31	-126.99
2/16/2017	365-375	-12.25	-87.29

Table A2-8. Precipitation samples used to construct the LMWL and the amount-weighted LMWL. Samples were collected from the Southern Sierra Critical Zone Observatory P301 tower. Snow layers were measured from the ground surface to the top of the snowpack.

Date	$\delta^{18}O$ (‰)	$\delta^{2}H$ (‰)	Sample Type /Snow Layer Depth (cm)
3/1/2015	-13.39	-101.84	Rain
3/26/2015	2.95	-27.50	Rain
4/13/2015	-6.45	-56.03	Rain
5/9/2015	-4.10	-48.95	Rain
5/13/2015	-0.17	-44.42	Rain
5/27/2015	-6.87	-56.36	Rain
6/11/2015	-10.31	-73.09	Rain
6/20/2015	-5.62	-54.29	Rain
7/9/2015	-4.31	-32.62	Rain
7/22/2015	-11.91	-82.56	Rain
10/10/2015	-14.65	-110.22	Rain
10/18/2015	-13.25	-90.16	Rain
12/4/2015	-15.25	-96.82	snow grab sample
12/21/2015	-14.99	-111.19	snow grab sample
1/9/2016	-12.49	-80.29	snow pit (10-30)
1/9/2016	-9.35	-53.31	snow pit (30-40)
1/9/2016	-11.87	-77.75	snow pit (40-55)
1/9/2016	-12.20	-77.17	snow pit (55-100)
1/28/2016	-9.78	-64.91	snow grab sample
3/24/2016	-6.73	-31.76	snow grab sample
4/12/2016	-14.82	-110.33	Rain
4/27/2016	-7.68	-50.15	Rain
5/4/2016	-9.62	-64.18	Rain
5/21/2016	-9.49	-62.65	Rain
5/27/2016	-8.88	-70.36	Rain
6/16/2016	-4.92	-32.91	Rain
10/2/2016	-5.80	-41.83	Rain
10/20/2016	-5.89	-35.15	Rain
10/24/2016	-5.79	-32.30	Rain
11/4/2016	-10.48	-68.19	Rain
1/6/2017	-12.86	-93.25	snow pit (0-5)
1/6/2017	-16.32	-126.23	Snow pit (5-23)
1/6/2017	-14.42	-97.04	Snow pit rain crust (23-25)
1/6/2017	-16.87	-128.61	Snow pit light powder (25-48)
1/6/2017	-13.60	-100.05	Snow pit (48-55 cm)
1/15/2017	-8.33	-48.67	snow pit rain crust (50-54)
1/15/2017	-16.06	-115.38	snow pit (57-73)
1/15/2017	-16.39	-117.02	snow pit rain/sun crust (72-75)
1/15/2017	-15.74	-105.76	snow pit (75-78)
2/1/2017	-13.70	-96.52	snow pit crust (70-85)
2/1/2017	-11.02	-74.66	snow pit (85-115)
2/1/2017	-11.46	-75.50	snow pit (116-117)
2/1/2017	-12.03	-76.82	snow pit (120 - 130)
2/1/2017	-10.65	-71.22	snow pit several crust layers (130-140)
2/1/2017	-9.94	-58.43	snow pit crust (140-141)
2/1/2017	-12.22	-75.13	snow pit (143-156)
3/23/2017	-9.75	-61.77	snow pit (153-155)
3/23/2017	-15.90	-118.24	snow pit (125-140)
3/23/2017	-14.56	-105.97	snow pit (123-125)
5/31/2017	-9.87	-78.65	Rain

6/1/2017	-7.76	-49.26	Rain
8/4/2017	-2.56	-25.47	Rain

Table A2-9. Water year 2016 snowmelt stable isotope data collected from P-Caps located at the Southern Sierra Critical Zone Observatory P301 tower. The first two letters in sampler ID indicate nearest tree species (white fir, WF, incense cedar, IC, Jeffrey pine (JP), 3rd and 4th letters indicate location either Under Canopy (UC) or Gap (G) and numbers differentiate P-Caps within clusters. Samplers located within 70 m of the P301 flux tower.

Date	Sampler ID	$\delta^{18}O$ (‰)	$\delta^{2}H$ (‰)	d-excess (‰)
1/12/2016	WFUC1	-12.26	-86.24	11.84
1/12/2016	ICUC1	-11.07	-73.56	15.00
1/12/2016	ICUC2	-9.89	-67.22	11.90
1/12/2016	ICUC3	-10.31	-73.27	9.21
1/28/2016	ICUC1	-11.69	-75.55	17.97
1/28/2016	ICUC3	-11.05	-72.54	15.86
1/28/2016	JPUC2	-10.43	-71.23	12.21
1/28/2016	ICUC2	-11.85	-78.13	16.67
1/28/2016	JPUC1	-12.00	-80.61	15.39
1/28/2016	WFUC1	-10.51	-67.14	16.94
2/11/2016	WFUC1	-10.52	-70.65	13.51
2/11/2016	JPUC2	-11.02	-72.63	15.53
2/11/2016	JPUC1	-11.39	-73.95	17.17
2/11/2016	JPUC3	-10.79	-71.64	14.68
2/24/2016	WFUC1	-12.00	-84.05	11.95
2/24/2016	ICUC1	-11.51	-79.14	12.94
2/24/2016	ICUC3	-11.16	-76.04	13.24
2/24/2016	ICUC2	-11.08	-71.96	16.68
2/24/2016	JPUC2	-10.19	-67.38	14.14
2/24/2016	JPUC1	-9.73	-64.55	13.29
3/2/2016	JPUC2	-9.84	-67.93	10.79
3/2/2016	JPUC1	-9.61	-65.82	11.06
3/8/2016	JPUC1	-9.65	-66.35	10.85
3/8/2016	JPUC2	-9.76	-66.58	11.50
3/8/2016	ICUC1	-9.66	-64.06	13.22
3/8/2016	ICUC2	-9.79	-65.07	13.25
3/8/2016	ICUC3	-9.43	-63.28	12.16
3/8/2016	WFUC1	-9.90	-66.37	12.83
3/17/2016	JPUC2	-9.49	-63.98	11.94
3/17/2016	JPUC 1	-10.81	-70.27	16.21
3/17/2016	WFUC1	-11.51	-77.35	14.73
3/17/2016	ICUC 1	-8.73	-53.62	16.22
3/17/2016	ICUC3	-10.53	-67.61	16.63
3/17/2016	ICUC2	-11.13	-71.08	17.96
3/24/2016	WFUC1	-10.90	-78.08	9.12
3/24/2016	ICUC3	-8.73	-64.75	5.09
3/24/2016	JPUC1	-11.15	-74.07	15.13
4/7/2016	WFUC1	-10.88	-76.20	10.84
4/7/2016	ICUC1	-10.11	-64.86	16.02
4/7/2016	JPUC1	-10.44	-74.79	8.73
5/4/2016	WFUC1	-8.92	-56.80	14.56
5/4/2016	ICUC2	-10.32	-68.55	14.01
5/4/2016	ICUC1	-9.91	-64.77	14.51
5/4/2016	ICUC3	-9.60	-61.76	15.04
5/4/2016	JPUC1	-10.94	-80.00	7.52
1/12/2016	WFG1	-14.63	-103.73	13.31
1/12/2016	WFG2	-14.25	-100.96	13.04
1/28/2016	WFG1	-14.59	-100.54	16.18

1/28/2016	WFG2	-12.89	-85.20	17.92
1/28/2016	ICG1	-14.57	-100.77	15.79
2/11/2016	WFG1	-11.02	-71.89	16.27
2/11/2016	WFG2	-11.74	-77.78	16.14
2/11/2016	ICG1	-13.78	-96.35	13.89
2/23/2016	WFG2	-14.07	-99.06	13.50
2/24/2016	ICG1	-12.27	-86.92	11.24
2/24/2016	WFG1	-12.18	-88.29	9.15
3/2/2016	ICG1	-11.44	-80.20	11.32
3/2/2016	WFG1	-12.61	-84.66	16.22
3/2/2016	WFG2	-9.06	-63.44	9.04
3/8/2016	WFG1	-11.82	-78.98	15.58
3/8/2016	ICG1	-9.60	-66.10	10.70
3/9/2016	WFG2	-10.61	-71.73	13.15
3/17/2016	ICG1	-12.87	-88.32	14.64
3/17/2016	WFG1	-11.86	-80.74	14.14
3/24/2016	ICG1	-12.19	-88.51	9.01
3/24/2016	WFG1	-10.75	-71.86	14.14
4/7/2016	WFG1	-9.03	-57.60	14.64
4/7/2016	ICG1	-10.03	-68.06	12.18
5/4/2016	WFG1	-11.25	-74.79	15.21

Table A2-10. Water year 2017 snowmelt stable isotope data collected from P-Caps located at the Southern Sierra Critical Zone Observatory P301 tower. The first two letters in sampler ID indicate nearest tree species (white fir, WF, incense cedar, IC, Jeffrey pine (JP), 3rd and 4th letters indicate location either Under Canopy (UC) or Gap (G) and numbers differentiate P-Caps within clusters. Samplers located within 70 m of the P301 flux tower.

Date	Sampler ID	$\delta^{18}O$ (‰)	$\delta^{2}H$ (‰)	d-excess (‰)
11/4/2016	17WFUC1	-6.68	-41.58	11.86
11/10/2016	17WFUC1	-4.71	-28.21	9.47
11/10/2016	17ICUC2	-5.62	-51.68	-6.72
11/10/2016	17ICUC1	-8.22	-63.74	2.02
11/10/2016	17ICUC3	-6.65	-42.37	10.83
11/10/2016	17JPUC1	-6.72	-46.24	7.52
11/10/2016	17JPUC2	-5.88	-36.32	10.72
11/10/2016	17JPUC3	-5.55	-33.45	10.95
11/10/2016	17WFUC2	-4.88	-33.62	5.42
1/14/2017	17ICUC2	-12.58	-85.76	14.88
1/14/2017	17JPUC3	-11.20	-79.27	10.33
1/15/2017	17ICUC1	-12.35	-86.33	12.47
1/15/2017	17ICuC1	-12.33	-85.93	12.71
1/15/2017	17ICUC2	-11.20	-79.07	10.53
1/15/2017	17WFUC2	-16.72	-128.18	5.58
1/15/2017	17WFUC1	-10.92	-80.17	7.19
2/1/2017	17JPUC3	-12.49	-83.67	16.25
2/1/2017	17JPUC2	-11.76	-77.33	16.75
2/1/2017	17WFUC1	-11.81	-79.11	15.37
2/1/2017	17JPUC3	-12.77	-93.78	8.38
2/1/2017	17WFUC2	-16.64	-126.76	6.36
2/15/2017	17WFUC2	-11.29	-73.75	16.57
2/15/2017	17ICUC1	-11.54	-82.97	9.35
2/15/2017	17JPUC2	-11.78	-78.35	15.89
2/15/2017	17ICUC2	-10.25	-67.23	14.77
2/15/2017	17JPUC3	-12.25	-84.74	13.26
2/15/2017	17ICUC3	-10.74	-70.28	15.64
2/15/2017	17WFUC2	-11.63	-76.87	16.17
3/1/2017	17JPUC3	-12.66	-86.04	15.24
3/1/2017	17ICUC2	-11.74	-79.11	14.81
3/1/2017	17JPUC3	-11.89	-83.30	11.82
3/23/2017	17WFUC1	-11.58	-79.50	13.14
3/23/2017	17JPUC3	-9.99	-66.43	13.49
3/23/2017	17ICUC1	-10.73	-71.63	14.21
3/23/2017	17JPUC3	-10.67	-71.88	13.48
3/23/2017	17WFUC2	-13.67	-82.00	27.36
4/1/2017	17WFUC1	-11.02	-76.62	11.54
4/1/2017	17ICUC1	-12.19	-83.08	14.44
1/6/2017	17CZTUC1	-5.57	-33.51	11.05
1/6/2017	17CZTUC2	-6.92	-44.57	10.79
1/6/2017	17CZTUC3	-6.66	-46.10	7.18
6/1/2017	17JPUC3	-6.85	-42.52	12.28
6/1/2017	17WFUC2	-6.29	-36.24	14.08
6/1/2017	17WFUC1	-6.47	-35.60	16.16
6/1/2017	17ICUC2	-10.24	-64.55	17.37
11/4/2016	17WFG1	-7.91	-53.35	9.93
11/10/2016	17WFG2	-8.29	-57.37	8.95
11/10/2016	17WFG1	-5.20	-28.37	13.23

11/10/2016	17ICG1	-8.88	-65.77	5.27
11/10/2016	17ICG4	-3.71	-28.44	1.24
11/10/2016	17ICG2	-7.04	-49.45	6.87
1/14/2017	17ICG1	-17.15	-127.07	10.13
1/14/2017	17ICG2	-13.43	-94.04	13.40
1/15/2017	17WFG2	-13.00	-90.68	13.32
1/15/2017	17WFG1	-19.28	-147.82	6.42
1/15/2017	17WFG3	-13.17	-91.89	13.47
2/1/2017	17ICG3	-19.65	-147.49	9.71
2/1/2017	17WFG2	-12.76	-91.90	10.18
2/15/2017	17WFG1	-11.83	-79.10	15.54
2/15/2017	17WFG2	-11.89	-78.67	16.45
2/15/2017	17WFG3	-10.74	-70.27	15.65
2/15/2017	17WFG1	-17.09	-122.77	13.95
2/15/2017	17ICG1	-20.00	-149.65	10.35
3/1/2017	17WFG2	-13.29	-90.32	16.00
3/1/2017	17ICG3	-11.60	-79.09	13.71
3/1/2017	17ICG2	-14.30	-104.83	9.57
3/23/2017	17ICG1	-13.35	-93.29	13.51
4/1/2017	17ICG1	-12.96	-88.30	15.38
6/1/2017	17WFG1	-16.27	-117.71	12.45
6/1/2017	17WFG2	-10.66	-68.29	16.99
6/1/2017	17WFG3	-8.91	-57.39	13.89
6/1/2017	17ICG2	-10.63	-70.50	14.54

Table A2-11. Precipitation amount corresponding to sampling periods for the American Transect.

Date	Precipitation (mm)
10/17/2016	190.01
10/24/2016	3.53
10/25/2016	4.09
1/5/2017	478.38
1/24/2017	544.12
2/3/2017	11.52
2/6/2017	262.07
2/21/2017	372.09
3/5/2017	126.61
3/31/2017	66.05
3/27/2017	21.97
8/22/2017	8.31
Total	2088.75

Table A2-12. Precipitation amount corresponding to sampling periods for the Kings Transect.

Date	Precipitation (mm)
3/6/2016	78.81
3/8/2016	103.08
3/24/2016	7.97
5/21/2016	83.36
5/27/2016	18.33
6/16/2016	11.34
10/20/2016	31.2
10/24/2016	21.5
11/4/2016	50.74
12/3/2016	59.09
12/9/2016	21.74
1/6/2017	310.24
1/14/2017	345.1
2/2/2017	223.54
2/15/2017	235.81
3/17/2017	51.07
3/23/2017	214.9
4/1/2017	43.42
5/9/2017	167.97
total	2079.21

Table A2-13. Isotopic lapse rates with corresponding temperature lapse rates for the American Transect.

Elevation (km)	Temperature Lapse Rate (°C/km)	Isotopic Lapse Rate $\delta^{18}O$ (‰/km)
10/17/2016	-6.6	-2.0
10/24/2016	-4.5	-3.6
10/25/2016	-5.8	-3.2
1/5/2017	-5.4	-0.3
1/24/2017	-6.2	-5.5
2/3/2017	-5.1	-6.3
2/6/2017	-6.0	-2.1
2/21/2017	-5.9	-2.6
3/5/2017	-7.3	-0.6
3/27/2017	-6.7	-1.8
3/31/2017	-7.6	-2.1

Table A2-14. Isotopic lapse rates with corresponding temperature lapse rates for the Kings Transect.

Elevation (km)	Temperature Lapse Rate (°C/km)	Isotopic Lapse Rate $\delta^{18}O$ (‰/km)
3/6/2016	-6.5	-2.4
3/8/2016	-4.2	-5.2
3/24/2016	-4.9	-2.6
5/21/2016	-6.9	-1.1
5/27/2016	-7.9	-2.4
6/16/2016	-8.5	-1.7
10/20/2016	-6.5	-3.1
10/24/2016	-7.5	-3.1
11/4/2016	-6.4	-1.4
12/3/2016	-5.7	0.5
12/9/2016	-5.8	-1.3
1/6/2017	-6.0	-2.7
1/14/2017	-6.2	-4.1
2/2/2017	-6.4	-2.3
2/15/2017	-6.4	0.4
3/17/2017	-6.5	-4.3
3/23/2017	-5.9	-4.8
4/1/2017	-4.7	-0.9
5/9/2017	-5.7	-4.2

Table A2-15. Amount weighted (W) and non-weighted (NW) mean δ^2H isotopic lapse rates for the American and Kings Transects. Non-weighted values included only values within a confidence interval of 95%, while amount weighted values include all lapse rates, with the exception of the 8/22/2016 thunderstorm.

Transect	Slope	σ[1]	Intercept	σ[1]
Kings (W)	-19.4	13.9	-43.3	24.8
Kings (NW)	-21.6	12.3	-30.1	26.2
American (W)	-22.3	5.9	-30.4	17.9
American (NW)	-26.7	14.9	-5.7	4.7

[1] Weighted and non-weighted standard deviation equations listed Equations A1 and A2.

Table A2-16. Results of linear analysis of isotopic lapse rates (slopes and offsets) with corresponding meteorological characteristics during sampling collection periods, including dew point temperature, total precipitation and vapor pressure deficit. Meteorological characteristics are listed as independent variables and were derived from PRISM data and subset by date for corresponding stable isotope sampling periods, in which precipitation occurred.

Dependent Variable ($\delta^{18}O$)	**Independent variable**	**American Transect R^2**	**Kings Transect R^2**
Slope	Mean Dew Point Temperature (°C)	0.35	0.09
Slope	Mean Temperature (°C)	0.43	0.02
Slope	Mean Min. Temperature (°C)	0.32	0.06
Slope	Mean Max Temperature (°C)	0.47	0.00
Slope	Total Precipitation (mm)	0.04	0.08
Slope	Mean Max. Vapor Pressure Deficit (HPa)	0.56	0.00
Slope	Mean Min. Vapor Pressure Deficit (HPa)	0.64	0.00
Offset	Mean Dew Point Temperature (°C)	0.02	0.34
Offset	Mean Temperature (°C)	0.04	0.24
Offset	Mean Min. Temperature (°C)	0.01	0.31
Offset	Mean Max Temperature (°C)	0.08	0.18
Offset	Total Precipitation (mm)	0.05	0.00
Offset	Mean Max. Vapor Pressure Deficit (HPa)	0.20	0.09
Offset	Mean Min. Vapor Pressure Deficit (HPa)	0.27	0.08

Table A2-17. Results to linear regression performed on isotopic lapse rates (slopes and offsets) and sampling characteristics, including the number of days samples were collected, the number of breaks between periods of precipitation, the number of partial storms collected and the number of complete storms collected.

Independent Variable	Dependent variable	R^2	p-value
No. of days precipitation was collected	Slope	0.06	0.2000
No. breaks between precipitation	Slope	0.04	0.2598
No. partial storms collected	Slope	0.01	0.5653
No. complete storms collected	Slope	0.04	0.2778
No. of days precipitation was collected	Offset	0.12	0.0589
No. breaks between precipitation	Offset	0.05	0.2174
No. partial storms collected	Offset	0.00	0.6047
No. complete storms collected	Offset	0.06	0.1905

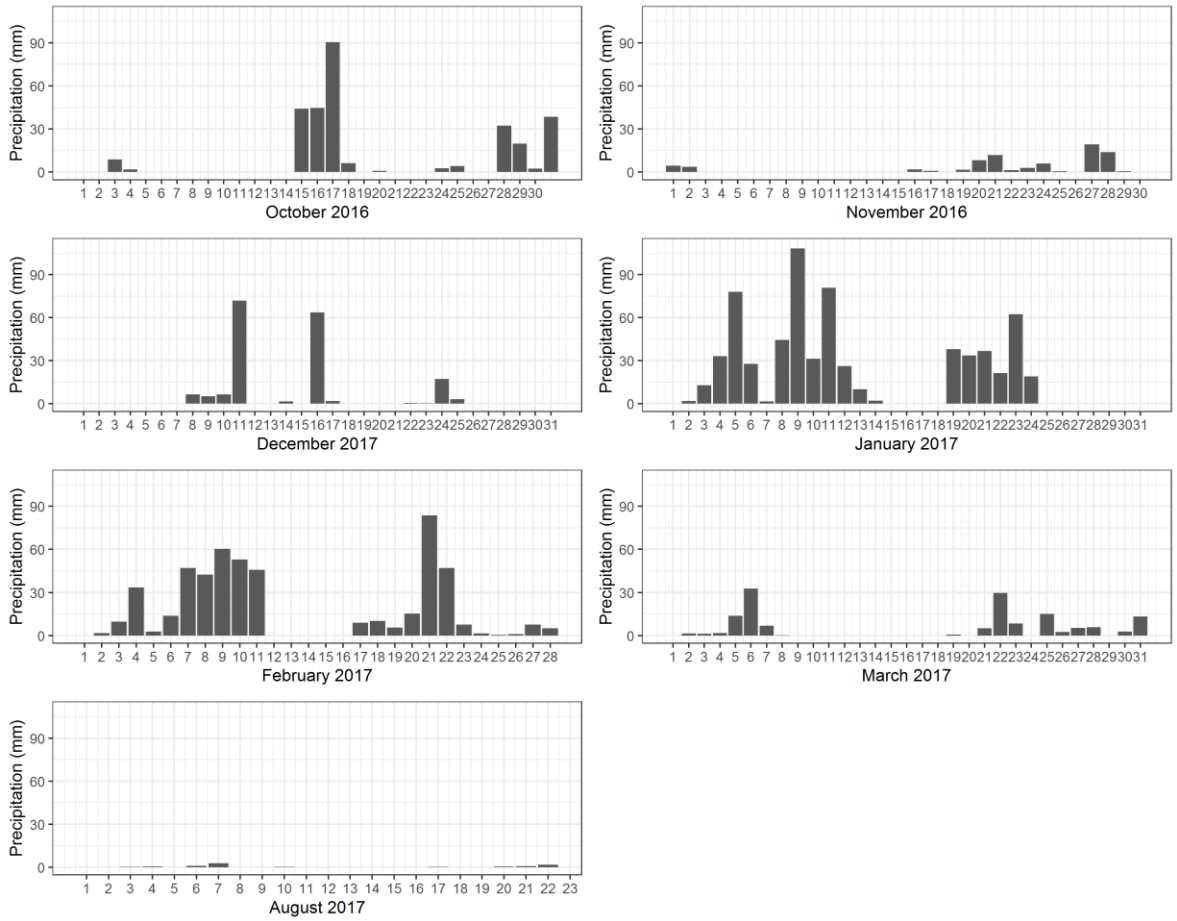

Figure A2-1. American Transect daily PRISM precipitation amounts for the time period that the American Transect was sampled for precipitation stable isotopes.

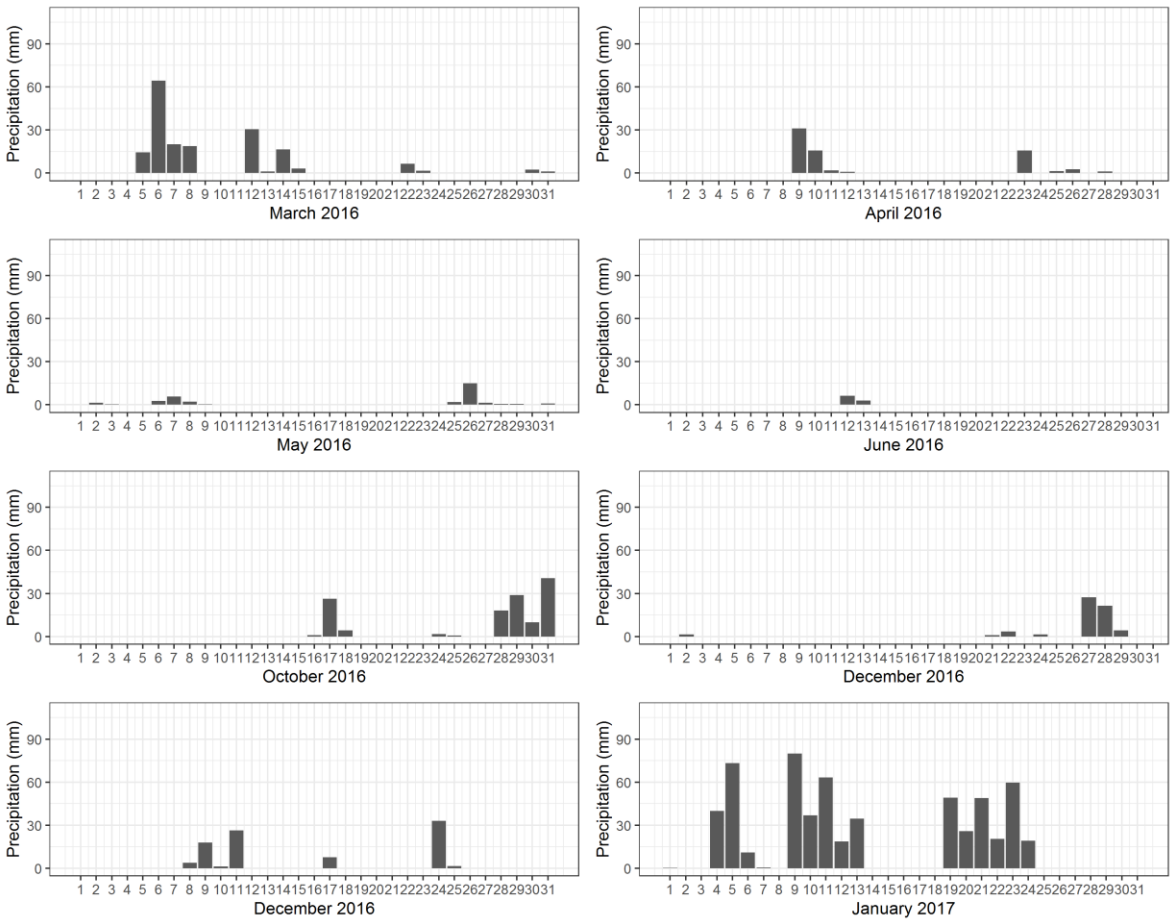

Figure A2-2. Kings Transect daily PRISM precipitation amounts for the time period that the American Transect was sampled for precipitation stable isotopes.

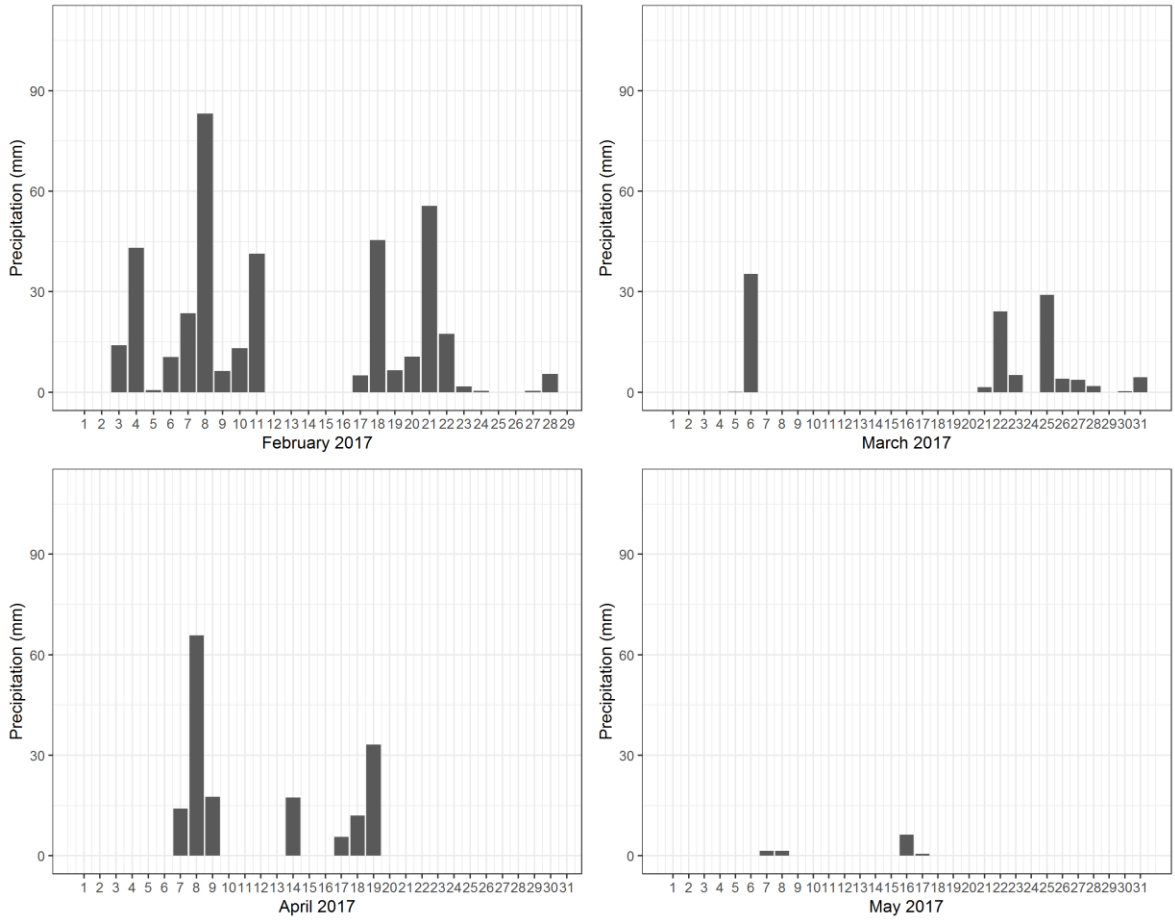

Figure A2-2. continued.

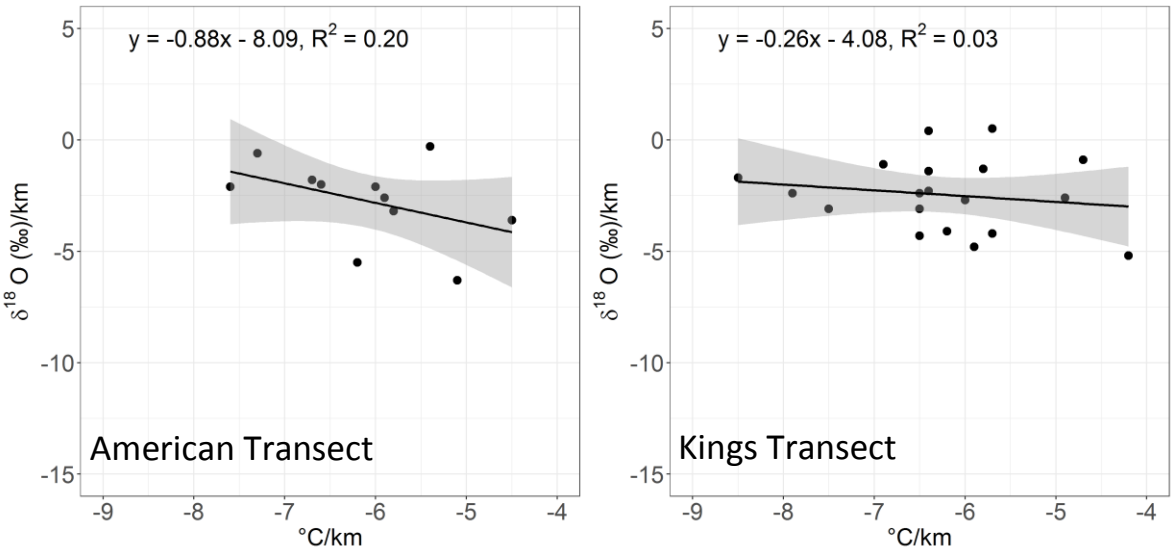

Figure A2-3. a) American Transect and b) Kings Transect isotopic lapse rates and temperature lapse rates for corresponding sampling dates. Data presented in Tables A13 and A14.

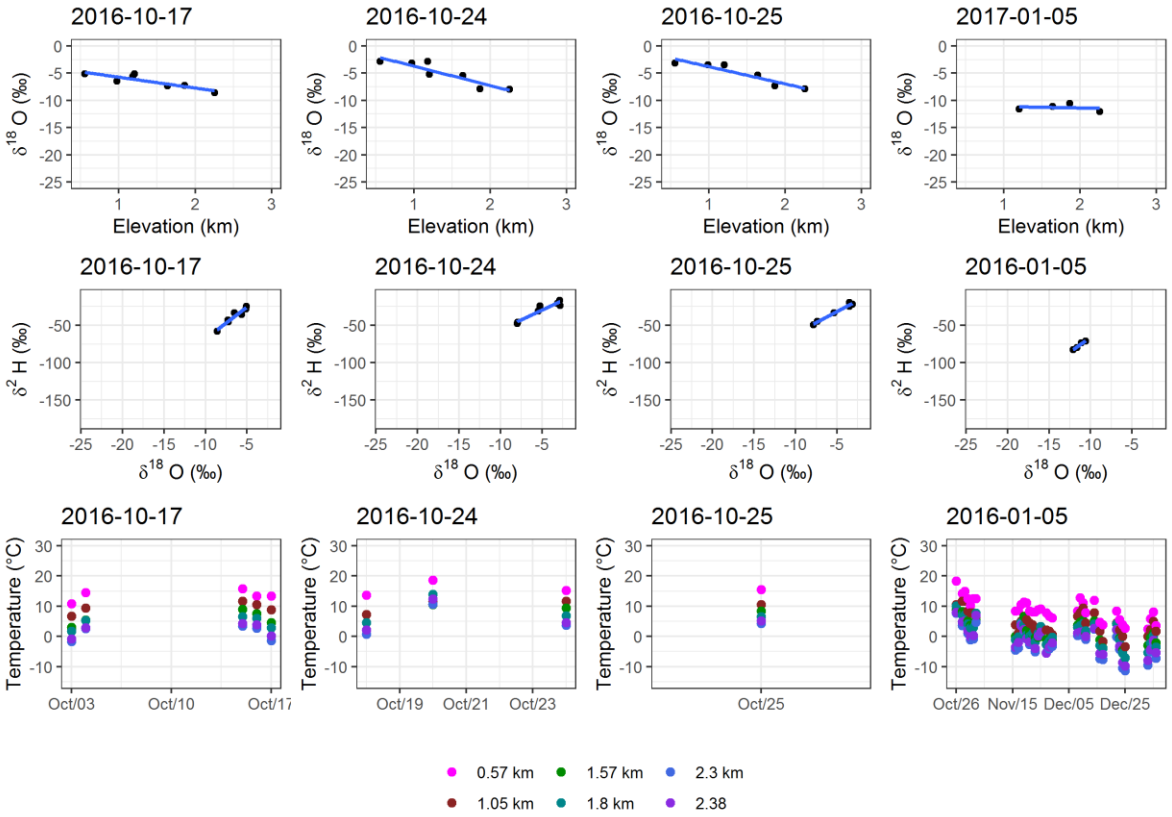

Figure A2-4. American Transect stable isotope lapse rates, dual-isotope plots and mean daily temperature data for corresponding sampling periods.

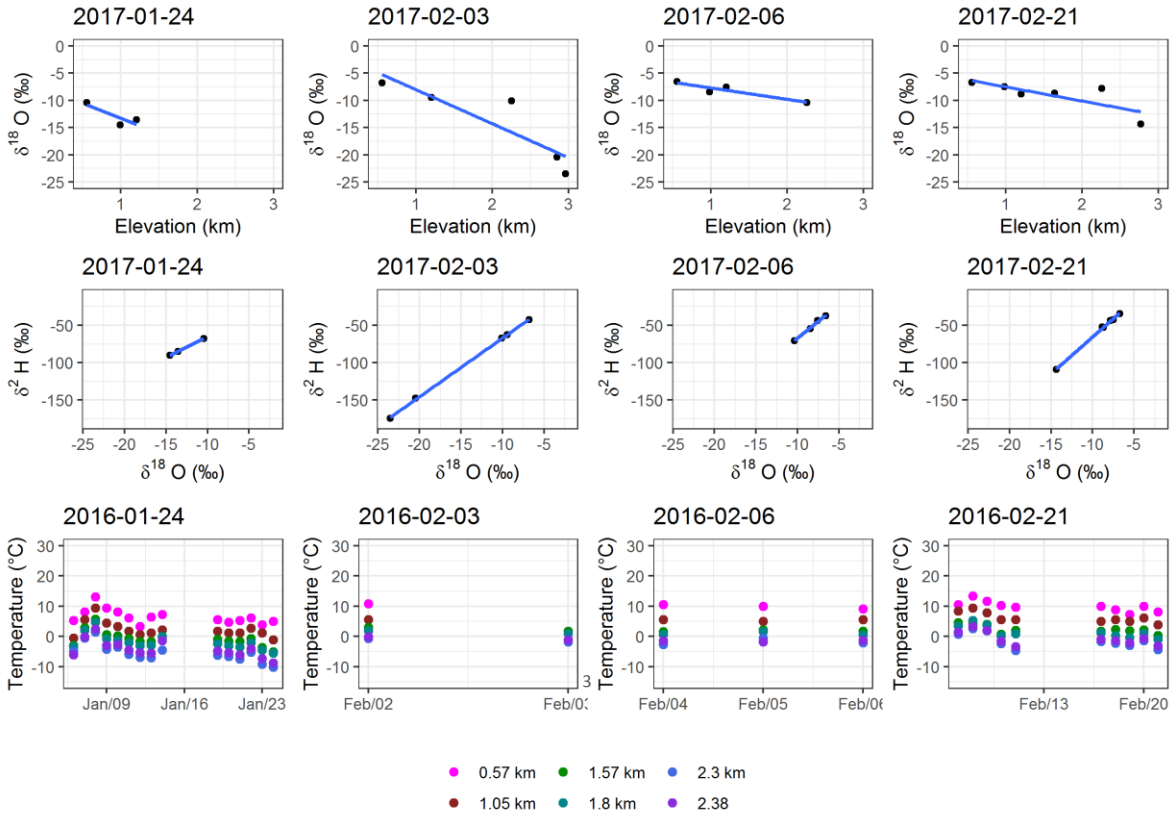

Figure A2-4. (continued)

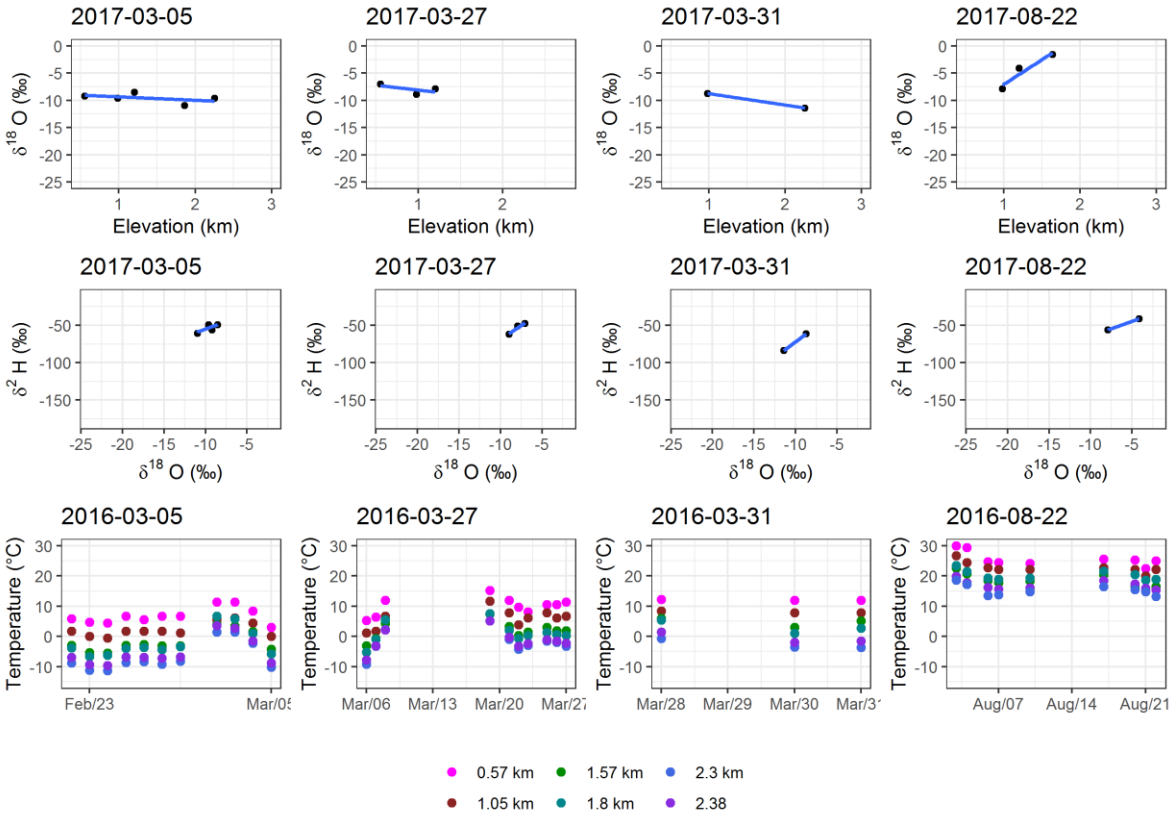

Figure A2-4. (continued)

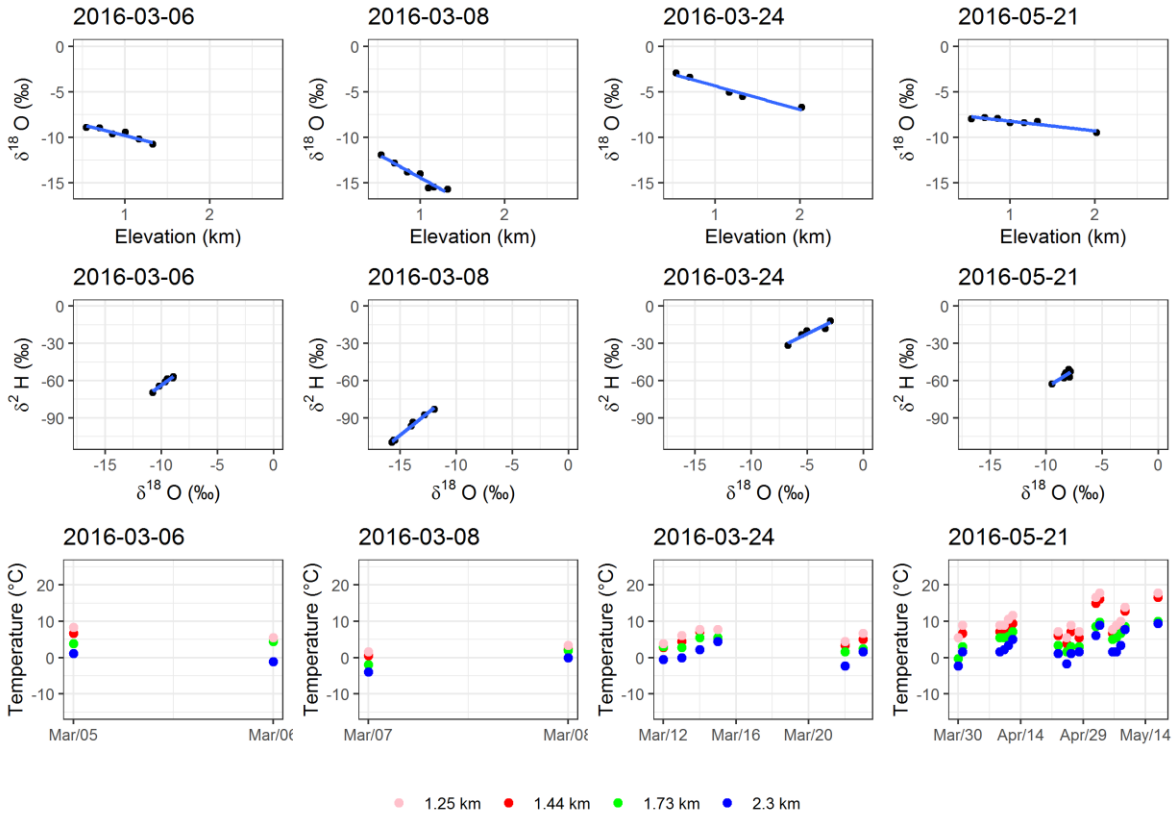

Figure A2-5. Kings Transect stable isotope lapse rates, dual-isotope plots and mean daily temperature data for corresponding sampling periods.

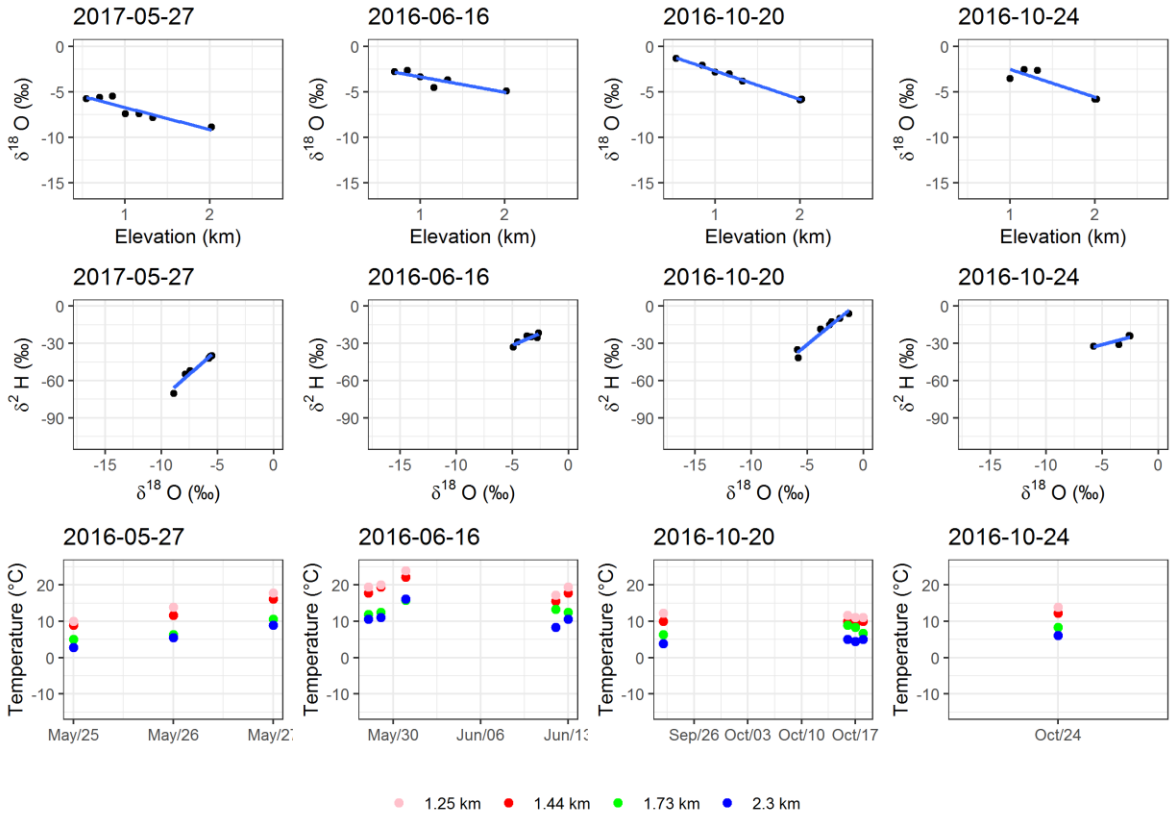

Figure A2-5. (continued)

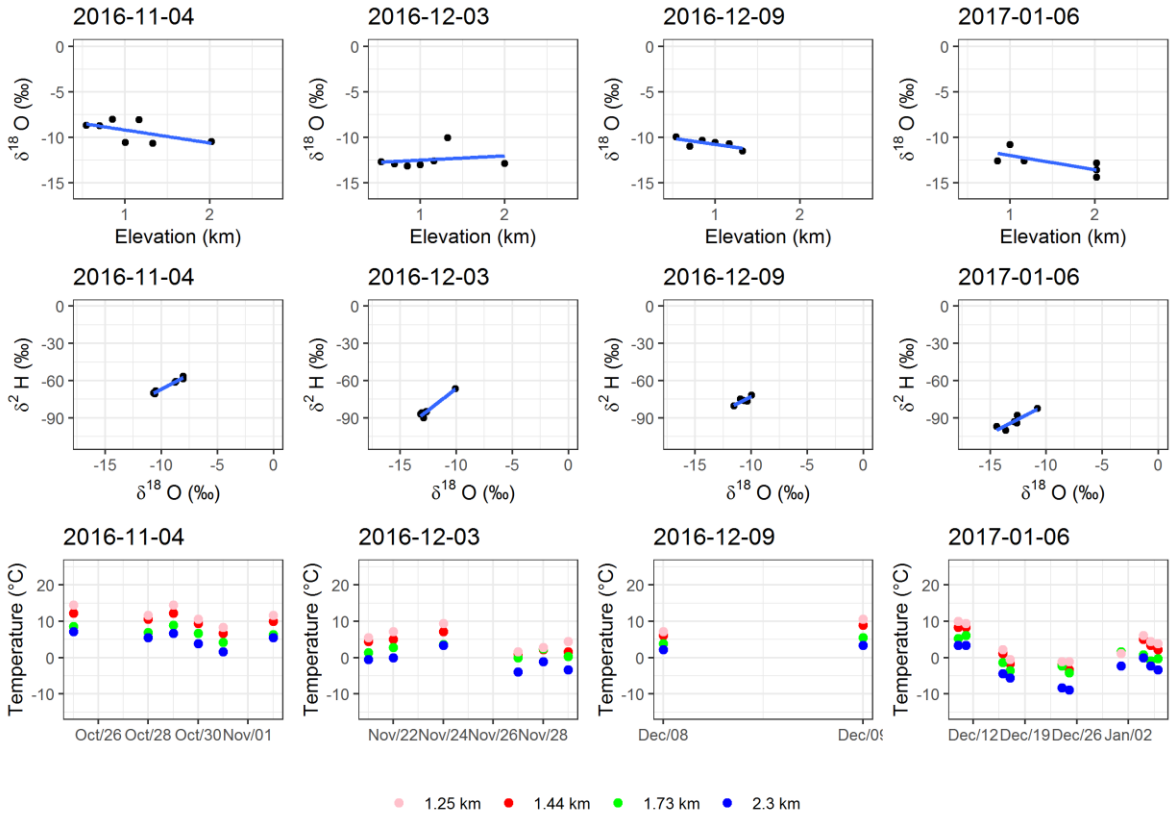

Figure A2-5. (continued)

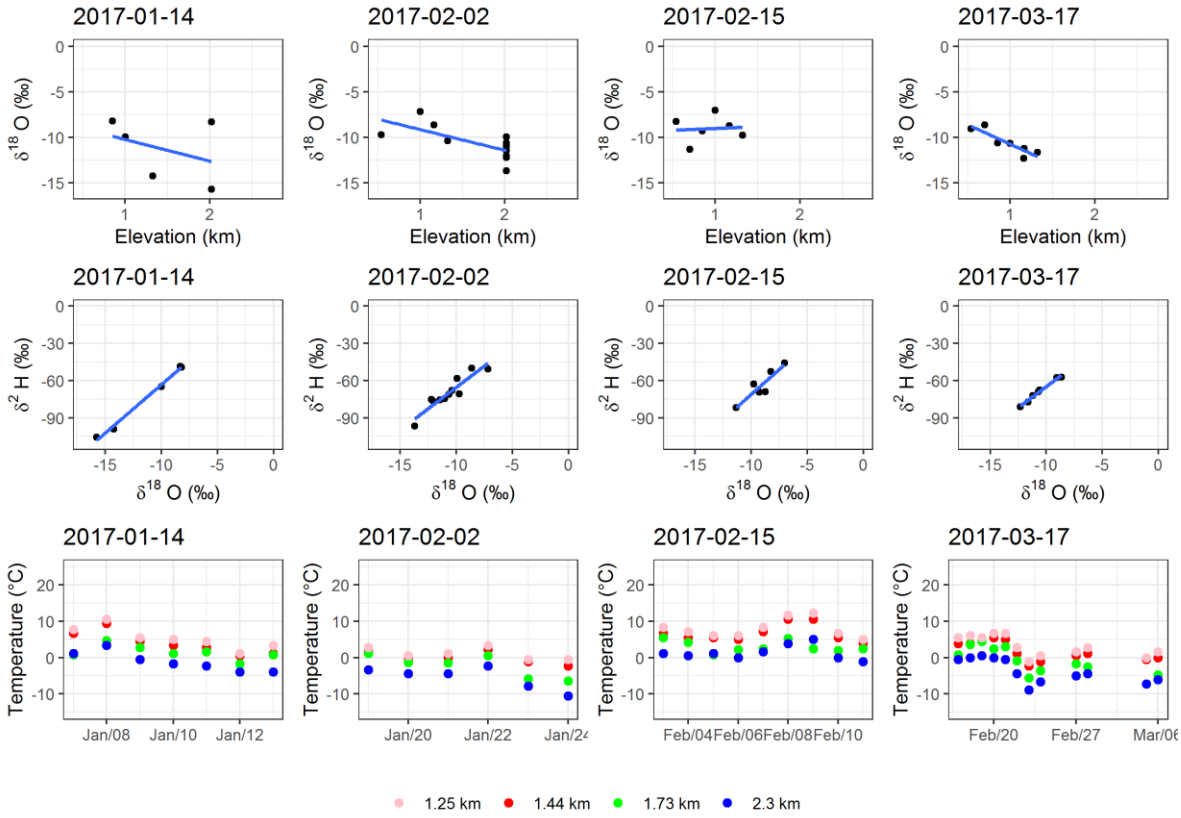

Figure A2-5. (continued)

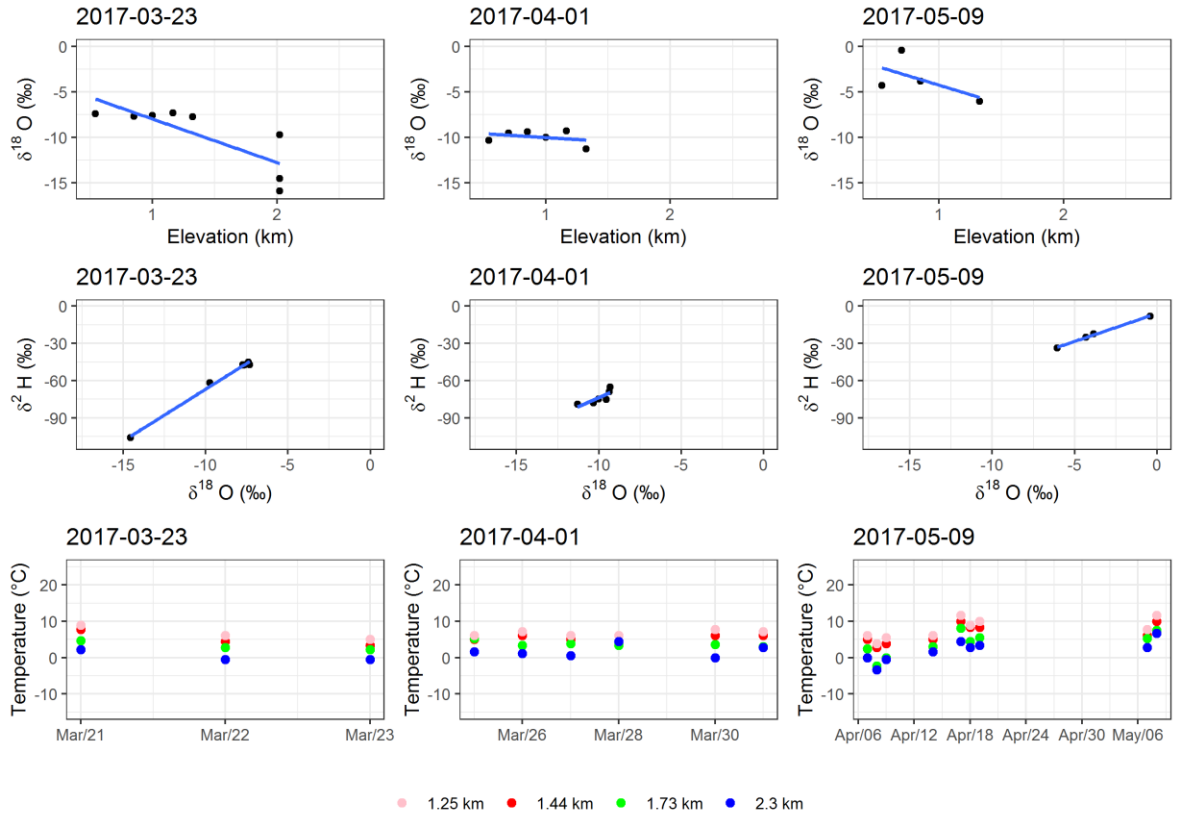

Figure A2-5. (continued)

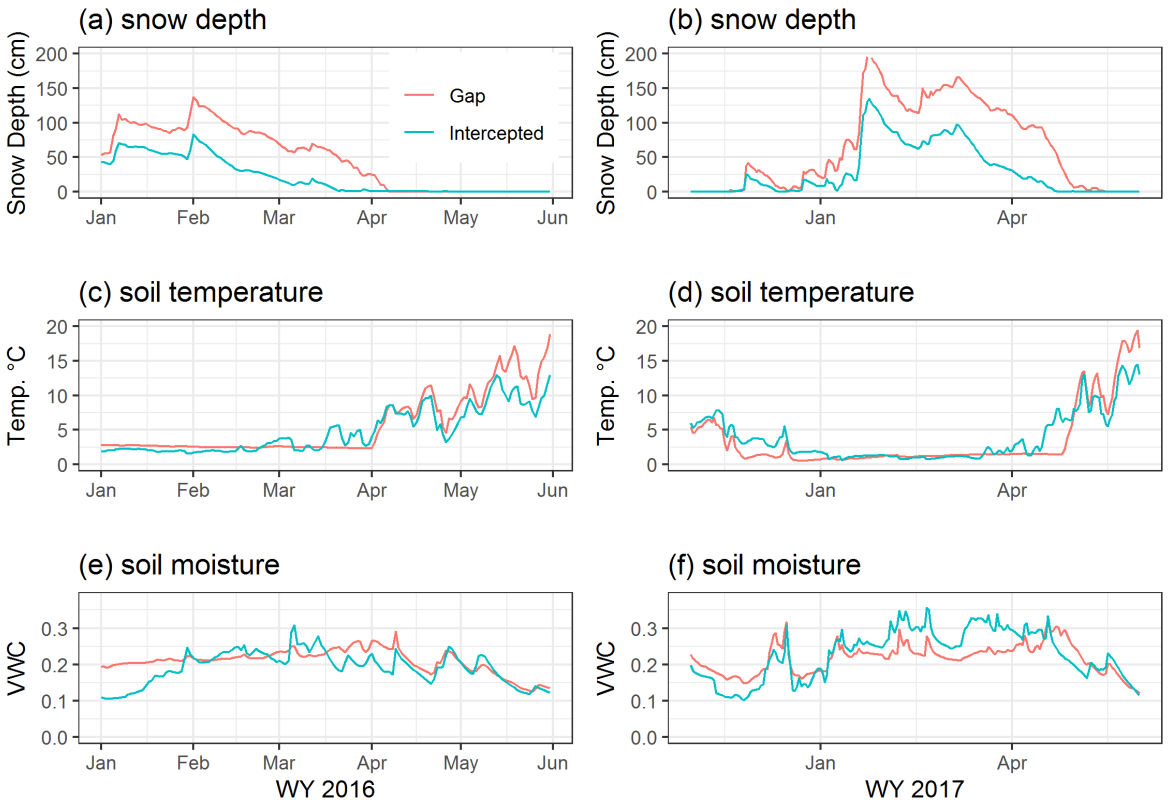

Figure A2-6. Comparison of snow depth, soil temperature and soil moisture in flat terrain sensors located in Upper Met site during sampling period within WY 2016 and WY 2017. Red line indicates sensor location in open canopy gap and blue line indicates sensor location beneath canopy cover, resulting in intercepted snow and snowmelt. Soil temperature and snowmelt were measured at 10 cm depths.

Chapter 3

A multi-tracer ($\delta^{18}O$, $\delta^{2}H$, ^{3}H) approach reveals temporal ecohydrologic connectivity in the Southern Sierra Critical Zone

Melissa Thaw [1], Ate Visser [2], Amanda Deinhart[2], Richard Bibby[2], Erik Oerter[2], Martha Conklin[1]

[1]University of California, Merced

[2]Lawrence Livermore National Laboratory

Abstract

How plant water sources are linked to subsurface storage and runoff is an important question in critical zone science and, particularly in the Sierra Nevada, California, where evapotranspiration uses the majority of precipitation that falls there. Through the use of ^{3}H, combined with water stable isotopes, $\delta^{18}O$ and $\delta^{2}H$, we found that forest vegetation accessed young water and switched sources depending on availability. By sampling precipitation stable isotope signatures at sub-seasonal temporal resolution, we observed xylem signatures respond to new water input. New $\delta^{18}O$, $\delta^{2}H$ and ^{3}H data were used to track each component of the hydrologic cycle (precipitation, runoff, evapotranspiration and storage) through the critical zone seasonally, including seasons where evapotranspiration and snowmelt input were in phase (winter snowmelt) and out of phase (seasonally dry summer). Snowmelt dominated saturated zone meadow water contributing to runoff in all seasons. Water that originated as snowmelt contributed to transpiration, unless other sources, such as recent rain, became available. In cases where xylem $\delta^{18}O$ and $\delta^{2}H$ signatures matched those of deeper saturated zone water, ^{3}H data showed that xylem water was actually distinctly younger than the deep saturated zone water. For example, during 2016, which experienced relatively normal snowpack in winter and seasonally dry summer conditions, mean summer saturated zone water and xylem water were similar in $\delta^{18}O$ -12.4 (± 0.04) ‰ and -12.5 (± 0.3), respectively), but mean saturated zone water and xylem water were distinctly different in ^{3}H (5.54 (± 0.24) pCi/L and 13.74 (± 1.11) pCi/L, respectively). Measuring ^{3}H as an additional tracer through vegetation provides insight into the time scale that vegetation water sources are linked to headwater catchment saturated zone meadow water and subsequent runoff. Thus, we provide a new perspective from a new combination of tracers, examining the fluxes of water through the critical zone on different temporal and spatial scales.

3.1 Introduction

Hydrologic connectivity among components of the hydrologic cycle (precipitation, runoff, evapotranspiration, storage) determine opportunities for water and forest resource optimization in California's Sierra Nevada, which provides the majority of water resources to the state (DWR, 2014). Likewise, mountains provide the majority of water resources to many regions globally (Messerli et al., 2004), and are important to ecosystem and economic health. For example, water from the Sierra Nevada supports California's large economy, the fifth largest in the world. The Sierra Nevada's snowpack is seen as the largest water reservoir in the state, which results from optimal orographic effects, attributed to the orientation of the mountain range, perpendicular to oncoming Pacific storms (Dettinger et al., 2004). The Sierra Nevada's strong elevation gradient and resulting temperature gradient results in diverse ecotones and forest types. Water fluxes are affected by interaction and feedbacks between components of the critical zone, including elevation, climate, geology and forest heterogeneities.

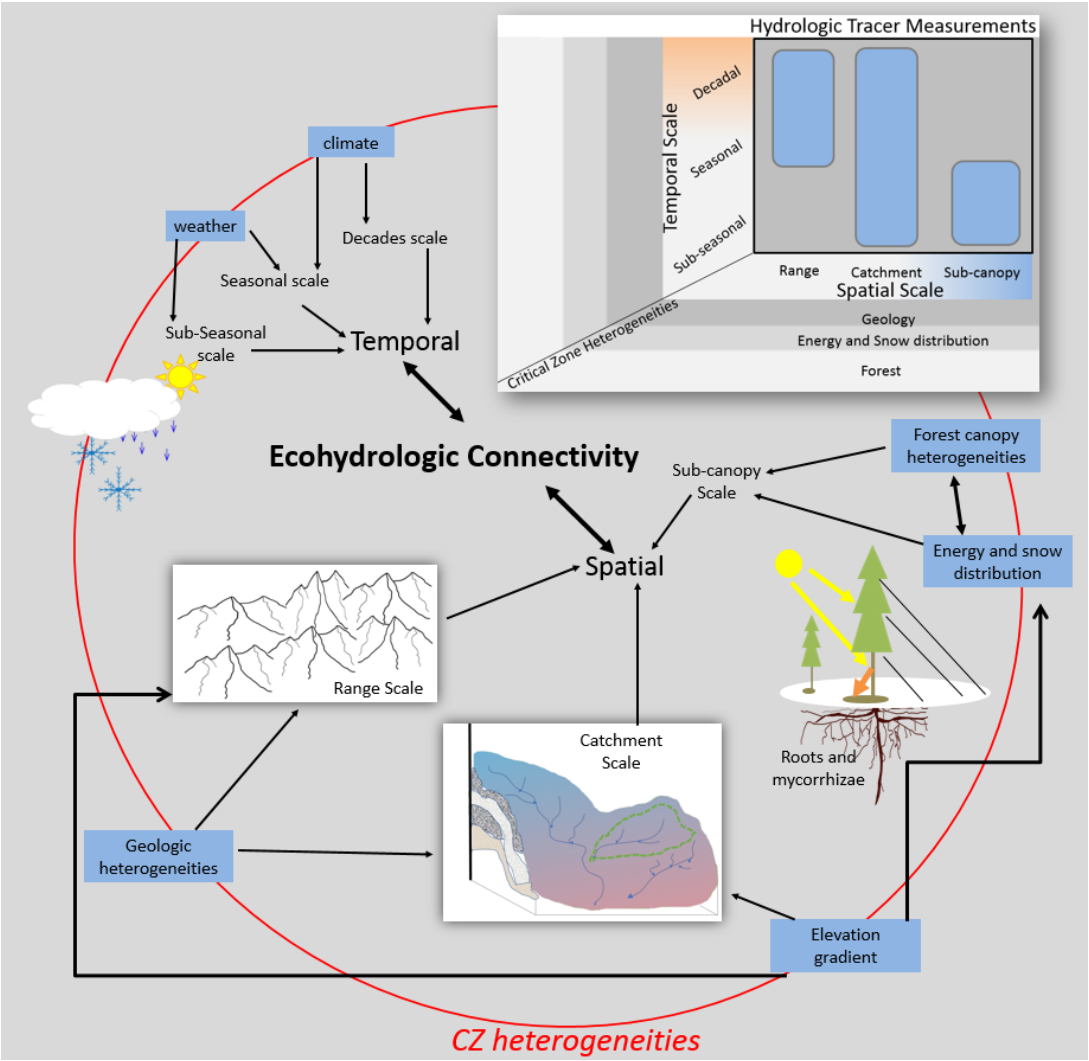

Figure 3-1. Conceptual diagram showing scales and processes investigated. Within the Critical Zone, in which heterogeneities in geology, energy, water and biota influence feedbacks in the flux of energy and water, we collected hydrologic tracer data across different spatial and temporal scales. Ecohydrologic connectivity, how water is linked through the runoff – saturated zone – plant – atmosphere continuum, exists on different spatial and temporal scales. In the Southern Sierra Critical Zone, spatial scales can be classified as mountain range, catchment and sub-canopy and temporal scales can be classified as decadal, seasonal and sub-seasonal. Heterogeneities in geology, energy/water input and forest type/structure/distribution have a strong influence on the flux of water through the Southern Sierra Critical Zone. Isotopic tracer data collected at different scales, provides insight into ecohydrologic connectivity within both spatial and temporal dimensions. The unique combination of three isotopic tracers, $\delta^{18}O$, $\delta^{2}H$ and ^{3}H, used to track water through vegetation, the saturated zone and runoff, provide a comprehensive, cross-disciplinary understanding of water fluxes through the critical zone.

Ecohydrologic connectivity is influenced by the heterogeneities within the critical zone. Large heterogeneities in the Sierra Nevada critical zone are climate, weather, geology and forest canopy (Figure 3-1). The elevation at which forest types occur is also related to hydrologic feedbacks; for example, the highest evapotranspiration occurs within the rain-snow transition zone at 1 km and 2 km, with less evapotranspiration occurring at low and high elevations, where forests are water limited and temperature limited, respectively (Goulden et al., 2012; Goulden & Bales, 2014). Of the fluxes in the hydrologic cycle, forest evapotranspiration can be manipulated by forest management practices, theoretically increasing runoff with a reduction in evapotranspiration. For example, in subalpine Central Sierra forests, (Saksa et al., 2017), found that runoff increased up to 14% through thinning in a non-water stressed forest in a headwater catchment. On the plot scale, (Ziemer, 1964) found that within a decade following tree thinning in a sub-alpine Sierra Nevada forest, soil moisture losses were related to the distance to trees and to the time since thinning. In addition, (Roche et al., 2018) found that a 21% reduction in evapotranspiration resulted following a 45% reduction basal-area due to wildfire. (Bales et al., 2018) found that drought- and fire- induced tree mortality led to a 15% increase in precipitation minus evapotranspiration in the Kings River Basin during a year with normal snowpack. Using a mass balance approach, researchers have inferred that evapotranspiration potentially reduces runoff that could otherwise be used downstream. Through the mass balance approach researchers have provided evidence that reductions in evapotranspiration may lead to increases in runoff, but how those components are linked and on what time scale has not been addressed.

Sierra Nevada vegetation accesses water from soil, weathered bedrock and even tens of meters deep into the subsurface, through bedrock fractures (Hubbert et al., 2001; Rose et al., 2003; Stone & Kalisz, 1991). Variation in root structure, synergy with mycorrhizae, species composition and competition can affect where vegetation access water (Davis, 1986; Royce & Barbour, 2001; Bornyasz et al., 2005; Shainsky & Radosevich, 1986). The water storage capacity of weathered bedrock in the Sierra Nevada is high, 32-58% (Holbrook et al., 2014; Hubbert et al., 2001) and during Sierra Nevada summers, weathered bedrock, found below approximately 75 cm depth, has been found to constitute most of the plant-available water storage, as opposed to soil (Holbrook et al., 2014; Hubbert et al., 2001; Rose et al., 2003).

Plant water sources may be distinct from groundwater and runoff, evidenced by distinct stable isotope signatures in xylem water when compared to stream water and groundwater, (Bowling et al., 2017; Brooks et al., 2010; McCutcheon et al., 2017). Furthermore, (Evaristo et al., 2015) compiled a large set of global data and determined a widespread pattern of vegetation with distinct isotopic signatures from groundwater and runoff in many climates. However, these studies sampled vegetation during the growing season, which was out of phase with major precipitation input. (Herve-Fernandez et al., 2016) sampled xylem water throughout different seasons in a climate with distinctly wet and dry seasons and found vegetation using both mobile (water that infiltrates and recharges groundwater and contributes to streamflow) and immobile (tightly-bound water within unsaturated soil) water, demonstrating connectedness between plant water sources and sources of groundwater and streamflow. Hence, this leads to the question of how connectedness among vegetation water sources, saturated zone meadow water and runoff may change when transpiration is in- or out- of- phase with precipitation input in the Sierra Nevada.

Many studies, including those mentioned above, have effectively used stable isotopes to understand plant water sources and connections to groundwater and runoff, however, hydrology research has benefited from employing multiple tracers to understanding hydrologic processes

(Dincer et al., 1974; Plummer et al., 2001; Stewart et al., 2010; Visser et al., 2019; Widory et al., 2004), therefore, employing multiple tracers to understand plant-water sources can inform water use and storage across time scales in the critical zone. The utility of using additional tracers, such as tritium (^{3}H), to track water through plants adds information about the "age" of plant water sources (Zhang et al., 2017), while acting as a tool that is not subject to the same methodological challenges of water extraction for stable isotope analysis (M. Meissner et al., 2014; Oerter et al., 2014; Orlowski, Pratt, et al., 2016; Orlowski et al., 2018; Oshun et al., 2016; Sprenger et al., 2015), thus the addition of ^{3}H as a tracer to track water through vegetation provides an opportunity to compare findings drawn from ^{3}H and stable isotope results.

In the mid-elevation (~2 km) "happy zone" of the snow-dominated Sierra Nevada, snowmelt and evapotranspiration are in phase, evapotranspiration is high most of the year and increases with length of day, which coincides with snowmelt in spring. In other snow dominated forested areas, canopy interception has been found to affect isotopic signatures of throughfall (Gustafson et al., 2010; Kendall, 1993; Saxena, 1986), hence utilizing the isotopically distinct signatures of snowmelt resulting from forest interception can shed light on the ecohydrologic connectivity between interception and runoff. In the past, when deciduous trees were replaced with conifers during forest hydrology experiments, transpiration and interception increased and streamflow decreased (Swank, 1968). Thus understanding the effects of interception on runoff is particularly relevant in the Sierra Nevada, where resource optimization is sought through forest management. In the Sierra Nevada evapotranspiration has been measured using flux towers to measure eddy covariance (Fisher et al., 2005; Goulden et al., 2012) and transpiration has been measured using sap flux measurements (Fisher et al., 2007; Kurpius et al., 2003), however, these studies measured the rate of evapotranspiration, and few studies have examined how streamflow and subsurface storage is linked to sources of evapotranspiration (Rose et al., 2003). When snowmelt and transpiration are in phase, our approach was to (a) determine vegetation water sources using snowmelt signatures, thereby determining how the forest intercepts snowmelt from infiltrating through the subsurface through transpiration and determine the timescale that the snowmelt is connected to the saturated zone and runoff. Prior plant-water source investigations in the Sierra Nevada have taken place during summer when precipitation is out of phase with evapotranspiration (Rose et al., 2003; Smith et al., 1991), meanwhile, similar investigations taking place throughout different seasons, in turn, have yielded nuanced results (Herve-Fernandez et al., 2016).

While the theory of ecohydrological separation suggests that vegetation accesses a separate pool of water than that contributing to recharge and runoff (Brooks et al., 2010; Evaristo et al., 2015) mass balance approaches provide evidence that evapotranspiration, including canopy interception, can reduce streamflow (Roche et al., 2018; Swank, 1968). Consequently, understanding temporal connectivity among components of the hydrologic cycle in the Sierra Nevada (Figure 3-1) is relevant to understanding drought resilience of both vegetation and water resources derived from deeply stored water and runoff and has practical importance to forest management for resource optimization.

3.2 Materials and Methods

Our approach was to measure δ^{18}O, δ^{2}H and ^{3}H in each component of the hydrologic cycle at different spatial and temporal scales within the critical zone setting (Figures 3-1 and 3-2). Using seasonal and sub-seasonal precipitation and snowmelt input δ^{18}O and δ^{2}H for reference, we compared the input signals to xylem and saturated zone water δ^{18}O and δ^{2}H values. Complementing this analysis, we compared xylem ^{3}H concentrations with that of saturated zone meadow water to determine the relative "age" of water composed of each component, which bridged the decadal

scale, at which ^{3}H is an effective tracer, to the sub-seasonal scale that precipitation signatures changed. Mountain range scale river runoff ^{3}H measurements up-scaled the perspective on the relative mean age of runoff. On the opposite end of the spatial scale, sub-canopy $\delta^{18}O$ and $\delta^{2}H$ snowmelt signatures, soil moisture and snow depth were compared to understand how intercepted snowmelt contributed to runoff and evapotranspiration (xylem signals).

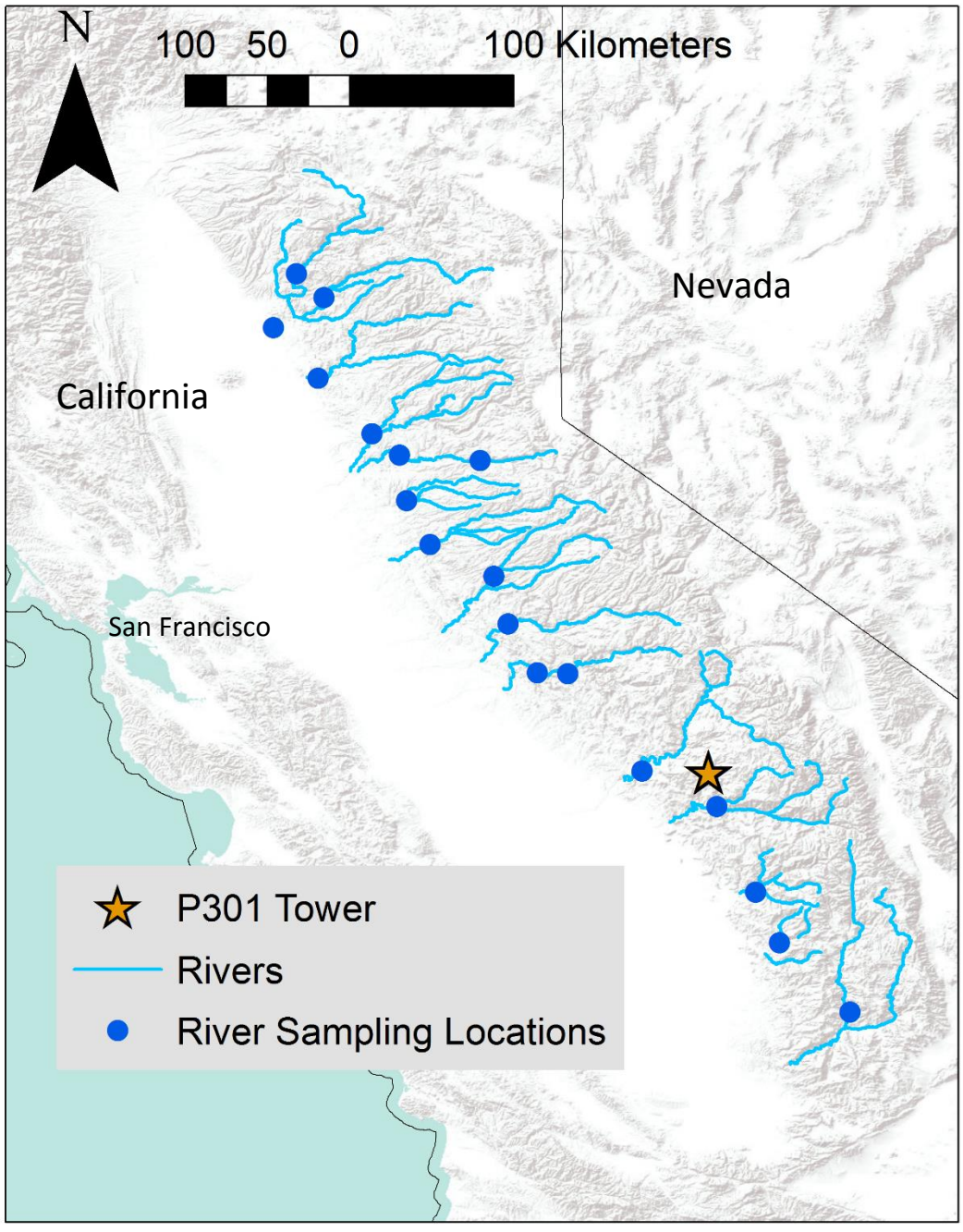

Figure 3-2. Sampling locations of major Sierra Nevada rivers and location of the P301 Tower, within the Southern Sierra Critical Zone Observatory. To capture the majority of catchment water without complications of reservoir residence time, rivers were sampled above major reservoirs and below most of each catchment. Only relevant sections of major rivers are shown.

The Southern Sierra Critical Zone Observatory Providence Creek P301 headwater catchment is located in the Central Sierra Nevada, CA, USA, where the P301 Tower is located (Figure 3-2). This site is within the rain-snow transition zone, with a mean annual temperature of 8 °C and mean annual precipitation of 1015 mm/year (Safeeq and Hunsaker, 2016). Vegetation, soil, precipitation and snowmelt were collected within 65 meters of the eddy covariance flux tower (Goulden et al., 2012), located at 37 ° 04' 02.66; 119 ° 11' 42".27 within the sub-catchment referred to as, "P301" (Figure 3-3). P301 has an area of 0.992 km^2 and an elevation range of 1.8 to 2.1 km. The vegetation is comprised of subalpine mixed conifer forest. Saturated zone meadow water was sampled 32 meters in elevation below and 319 meters northwest of the flux tower in the P301 Middle Meadow (Figure 3-3).

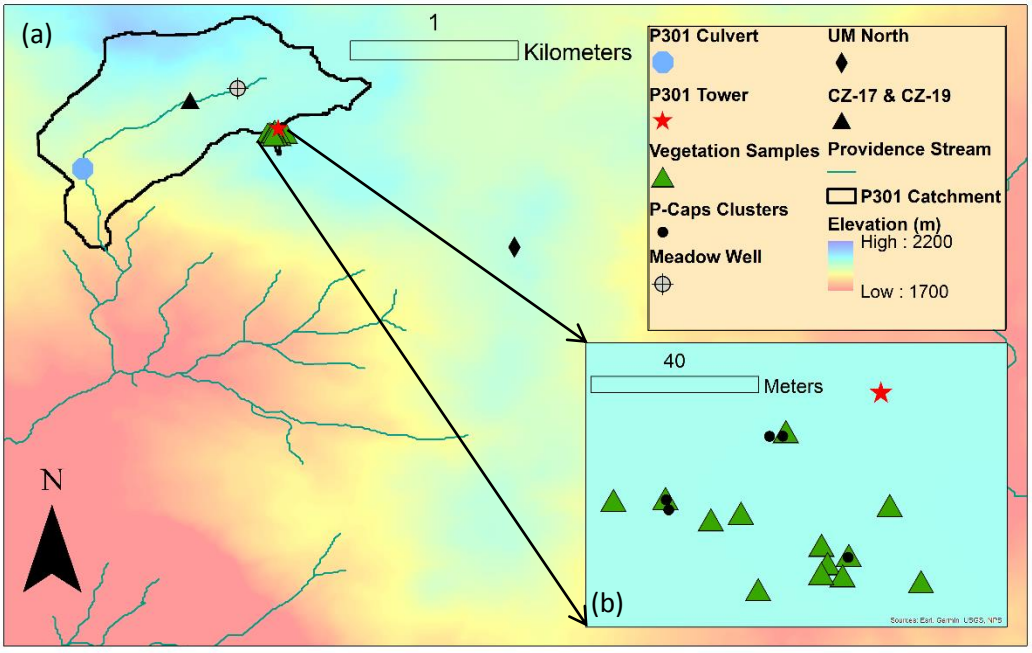

Figure 3-3. Site location map showing (a) P301 catchment with meadow sampling well near headwater of the P301 stream. Vegetation sampling locations and P-Caps (snowmelt samplers) are clustered near the P301 tower. Elevation is shown as color gradient. Stream water was sampled from the P301 culvert. Soil moisture and snow depth sensors located at Upper Met (UM) North and CZ-17 and CZ-19 were used to compare soil moisture and snow depth beneath canopy and in forest gaps. Inset (b) shows enlarged area of P-Caps and vegetation sampling locations.

Four types of precipitation input samples were collected: rain samples, grab samples of snow, snow pit samples, and snowmelt using passive capillary samplers (Frisbee, et al., 2010 (a) and (b); Penna et al., 2014) in 2015, 2016 and 2017. Rain samples were collected using a funnel connected to a 1-liter sample bottle, located at the P301 tower, which contained mineral oil to prevent evaporation. On occasions where samplers went missing, were disturbed, inaccessible due to conditions, overflowed or partially frozen, samples were not collected and data are missing. Grab samples of fresh snow were also collected when snow was present. Snow pits were dug in open areas on five dates and individual layers were identified and sampled (Chapter 2). Only fresh snow was used for the Local Meteoric Water Line. Snow and rain stable isotope signatures were used for the Local Meteoric Water Line. Precipitation samples were collected for the LMWL at the CZO P301 site from 3/1/2015 through 8/4/2017.

Passive capillary samplers (Frisbee, et al., 2010 (a) and (b); Penna et al., 2014) were used to minimize the effects of snowmelt sampling on signatures of the collected snowmelt (Earman et al., 2006). Passive capillary samplers consisted of fiberglass wick with one end tied in a spiral at the snow/soil interface and the other end passing through a tube to a glass sample bottle buried beneath the soil surface. The sample bottle contained mineral oil, which was replaced with fresh mineral oil each time a sample was taken. A peristaltic pump was used to collect samples and refresh mineral oil through the access tube. Passive capillary samplers were installed in clusters in the forested area around the Providence CZO Eddy Covariance flux tower (Goulden et al., 2012) within 70 meters of each other on a knoll in which aspect was not a variable. Passive capillary samplers were located under forest canopy in three locations under different tree types (White Fir, Incense Cedar and Jeffrey Pine) and in open areas in two locations (near an Incense Cedar and near a White Fir). Multiple (1-3) Passive capillary samplers were installed at each location and sampled throughout the winter and spring seasons (Chapter 1). Snowmelt was sampled throughout Water Year (WY) 2016 and Water Year 2017, approximately every 10 days at the CZO P301 site (Chapter 2).

Vegetation samples (n=76) were collected as tree cores from trees and as branches from shrubs (barked peeled off). White fir (*Abies concolor*), incense cedar (*Calocedrus decurrens*), Jeffrey Pine (*Pinus jeffreyi*) trees were sampled. Mountain whitethorn (*Ceanothus cordulatus*) and Greenleaf manzanita (*Arctostaphylos patula*) shrubs were sampled (Table A3-1). Soil samples were collected using a hand augur from the P301 site on four occasions, July 2015, August 2015, February 2016 and August 2016. Soils were sampled every ten cm in the top 100 cm, and every 25 cm down to 3 meters or until the augur was rejected on bedrock. The soil at this site has a uniform texture composed of sandy and loamy sand, with the majority of the soil composed of sand and about 2% silt and about 1% clay (Bales et al., 2011). The soil contains weakly developed entisols and inceptisols with granite, granodiorite and quartz diorite the parent material (Bales et al., 2011).

Saturated zone water was collected from a monitoring well (MMW4, described by (Lucas, 2016)) in the center of "Middle Meadow" located 32 meters lower in elevation and 319 meters northwest of the P301 flux tower (Figure 3-3) The total depth of the well was 272 cm with a casing above ground surface of 40 cm and a surface elevation of 1985 m above sea level (lower in elevation to the P301 tower located to the south at an elevation of 2015 m above sea level). This well was located within the wet meadow at the headwaters of the P301 catchment, also described by (Lucas, 2016). Additionally, water samples were collected downstream of the meadow at the "P301 culvert" on a monthly basis.

One to two gallons of soil and branches approximately 10 cm in diameter and 2 to 4 meters long were collected from P301 site on 8/19/2015 and 8/9/2016 for ^{3}H analysis. Precipitation was collected in plastic bins over time in the P301 site and saturated zone meadow water was also collected from P301 meadow for ^{3}H analysis. Major rivers originating in the Sierra Nevada were

sampled in the spring and late summer of 2017 for ^{3}H, including the Kern, Tule, Kaweah, Kings, San Joaquin, Merced, Tuolumne, Stanislaus, Mokelumne, Cosumnes, South Fork of the American (two locations), North Fork of the American, Yuba, Feather (below Oroville dam), Middle Fork of the Feather, and North Fork of the Feather (Figure 3-3 and Table 3-A2).

Cryogenic vacuum distillation was used to extract water from vegetation and soil samples before analysis of $\delta^{18}O$ and $\delta^{2}H$. Samples were kept frozen until extraction. Vegetation and soil masses were recorded before and after extraction. We used the Environmental Radiochemistry Freeze Dry system at Lawrence Livermore National Laboratory to extract sample water. The system consisted of 30 identical glass receptacles attached to a vacuum pump through individual valves that can be opened manually or through the system computer. Each receptacle is connected to an individual cold-trap to collected extracted water cooled with a slurry of dry ice and ethylene glycol. Vegetation and soil samples within their receptacles are supported by individual electric heating mantles; the temperature can be controlled individually. After samples were loaded and cold traps prepared, vacuum pressure was reduced to ~ 30 millitorr (~4 Pa). Samples remained in the system for approximately 90 hours; dry ice was added every 6 hours to maintain the cold trap. For the August 2016 soil samples, the heating mantles were heated to 100 °C; all other samples remained at room temperature during extraction. Preliminary tests were conducted in which water of known isotopic value was added to oven dried soil, extracted using this system and measured for $\delta^{2}H$, which resulted in extracted water within -8.03 ± 3.27‰ of known isotopic value for $\delta^{2}H$. In these trials, 100 mL of soil was dried for 24 hours in a drying oven at 105 °C and either 10 grams or 5 grams of deionized water with known isotopic composition was added (Table A3-3). Various methods have been used to extract water from soil for stable isotope analysis with vacuum pressure ranging from 0.3 Pa to 13 Pa, extraction times ranging from 15 min to 180 min and temperatures ranging from 35 °C to greater than 100 °C, outlined by (Orlowski, 2013), and reviewed by Sprenger et al. (2016). The cryogenic vacuum distillation system's variables used for this study fell within the range of these previous methods, with the exception of the longer extraction time.

Water was extracted from soil and vegetation samples separately for ^{3}H using a vacuum pump attached to a drying oven and ice water cold trap. Sample masses were recorded before and after extraction. Samples were placed in the drying oven which was heated to temperature of 105 °C and evacuated to approximately 0.6 bar. A diaphragm vacuum pump (Pfeiffer MVP015) attached to the drying oven circulated water vapor and atmospheric gases through coiled copper tubing submerged in ice water to deposit the condensed sample water into a sample bottle. Residual water vapor was trapped in a second dry ice water trap and the remaining dry air was returned to the oven in a closed system.

Precipitation, snowmelt, saturated zone meadow water and river water were analyzed using the Los Gatos Research DLT-1000 isotope analyzer at the University of California, Merced Environmental Analytical Laboratory. Cryogenic vacuum distillation was used to extract water from vegetation and soil samples, which were then analyzed for $\delta^{18}O$ and $\delta^{2}H$ on an Isoprime (now Elementar) isotope ratio mass spectrometer at Lawrence Livermore National Laboratory. Hydrogen and oxygen stable isotope values are reported in δ notation: $\delta = (R_{sample} / R_{standard} - 1)$, where R_{sample} and $R_{standard}$ are the $^{2}H/^{1}H$ or $^{18}O/^{16}O$ ratios for the sample and standard, respectively, and referenced to the Vienna Standard Mean Ocean Water (VSMOW) standard. Saturated zone meadow water, surface water, precipitation and water extracted from soil and vegetation were analyzed for ^{3}H using helium-3 ingrowth and noble gas mass spectrometry (Surano et al., 1992) at Lawrence Livermore National Laboratory.

Snow depth was measured using Judd Communications ultrasonic depth sensors and volumetric water content (VWC) was measured using Decagon Devices ECHO-TM volumetric water content (VWC); soil sensors were co-located with snow depth sensors. Sensor data presented

here share the most similar microclimate and hydrologic characteristics and provide continuous measurement to show the effects of variability in precipitation and drought. The sensor cluster CZ-19, located in a forest gap, and CZ-17 cluster, located beneath canopy were used to compare soil moisture under different canopy conditions. Soil moisture was analyzed at depths of 10, 30, 60 90 cm. Similarly, additional soil moisture data from sensors located at the Southern Sierra Critical Zone Observatory P301 Upper Met North site were analyzed (Figure 3-3). Mean values were calculated for each depth of VWC measured beneath forest canopy and compared with single sensor VWC in open areas (forest gaps). For example, the Under Canopy (UC) Average 10 cm VWC was calculated from sensors CDUC- 10 cm, ACUC-10 cm and PLUC-10 cm, which was compared to the Open-10 cm VWC values. UC Average-30 cm VWC was the mean calculated form CDUC-30 cm, ACUC-30 cm, PLUC-cm and was compared to Open-30 cm VWC. UC Average-60 cm VWC was calculated from ACUC-60 cm and PLUC-60 cm and compared to Open-60 cm VWC. UC Average-90 cm VWC was calculated from CDUC-90 cm and PLUC-90 cm VWC and compared to Open-90 cm VWC. Large data gaps in CDUC-60 cm and ACUC-90 cm VWC data precluded inclusion of data from these sensors. Snow depth data from sensors located were also compared for differences beneath canopy and in open areas.

Parameter-elevation Regressions on Independent Slopes Model (PRISM) precipitation values were used to represent precipitation amounts. PRISM precipitation values are produced from an analytical model incorporating statistical methods with existing climatological data to distribute the point measurements over regularly spaced grid cells in spatial format. We downloaded precipitation values on February 23, 2019 using the location 37.0668, -119.1848, elevation 1.9681 km (covering the P301 site) at a 4 km spatial resolution for dates 2015-03-01 to 2016-11-11.

We performed analysis on vegetation stable isotope data grouped by sampling date to determine fractionation compensation values for δ^2H and δ^{18}O. Fractionation compensation values were calculated by projecting the measured vegetation δ^{18}O and δ^2H in dual isotope space to the volume weighted LMWL using the slope calculated from mean monthly temperature and relative humidity based on methods presented in (Benettin et al., 2018). See Table A3-3 for original δ^{18}O and δ^2H values and fractionation-compensated values, with slopes used for fractionation compensation. See Table A3-4 for mean monthly relative humidity and temperature values used to calculate respective slopes for fractionation compensation. The LMWL was volume weighted using methods from (Hughes & Crawford, 2012). Temperature and relative humidity from the Southern Sierra Critical Zone Observatory P301 eddy covariance flux tower were used (Goulden, 2018). Xylem signatures and saturated zone meadow water δ^{18}O were plotted over time against precipitation δ^{18}O values, which were fitted to a sinusoidal function (Chapter 2).

We performed t-tests to determine if there was a difference between saturated zone meadow water δ^{18}O signatures and snowmelt δ^{18}O signatures under canopy or in open areas. Soil signatures and the volume weighted LMWL were used to calculate the line conditioned excess: lc-excess = δ^2H - (6.54) * δ^{18}O – (-9.08)(Landwehr, 2006).

^{3}H values for precipitation, soil, vegetation, major rivers, and saturated zone meadow water were grouped by sample type and then were analyzed for statistical difference using the Wilcoxon ranks sum test in order to determine if the ^{3}H concentrations of each component were distinct in age.

3.3 Results

We compared the δ^{18}O signatures of vegetation to new precipitation, snowmelt and saturated zone meadow water to study the response of vegetation sources to changes in hydrologic conditions (Figure 3-4). The volume weighted LMWL had a slope of 6.45 ± 4.05 and an offset of -9.03 ±

28.22 (weighted standard deviation). Seasonality of precipitation was reflected in the sinusoidal function with an amplitude of 3.40 and an offset of -9.50 (Chapter 2). Mean fractionation-compensated xylem signatures over time are listed in Table 3-1. Raw xylem $\delta^{18}O$ and $\delta^{2}H$ values, together with fractionation-compensated values are listed in Table A3-4, mean monthly temperature, relative humidity and slopes used to calculate fractionation compensation are listed in Table A3-5. Mean saturated zone meadow water had a signature of -12.4 ± 0.01‰ in $\delta^{18}O$ (Table 3-2), volume weighted precipitation has a $\delta^{18}O$ signature -11.9‰. Steam water downstream of meadow water had similar stable isotopic values (Table 3-2). All saturated zone meadow and stream $\delta^{18}O$ and $\delta^{2}H$ values are listed in Table A3-6. T-test results showed there was very little variation in saturated zone meadow water signatures, so mean and standard error were computed from all saturated zone meadow water values and this mean was compared to each snowmelt group. In summer 2015, following summer rain with a signature of -4.3‰, the mean fractionation-compensated vegetation signature was -11.6 ± 0.3 ‰. Next, summer rain with a $\delta^{18}O$ signature of -11.9‰ fell and was followed by a shift in vegetation to a mean value of -11.8 ± 0.4 ‰. Summer 2015 followed a severe snow drought but experienced summer rain (Figure 3-4). On the other hand, summer 2016 followed slightly below average winter precipitation but no summer rain (Figure 3-4). Summer 2016 mean vegetation signatures shifted to -12.5 ± 0.3‰, matching mean saturated zone meadow water -12.4 ± 0.04‰. Furthermore, vegetation shifted again in fall 2016. Following October rain with a signature of -8.9‰ the mean vegetation $\delta^{18}O$ signature shifted to -9.8 ± 0.6 ‰. November rain with a signature of -10.48‰, the mean vegetation signature that followed was -9.6 ± 0.3 ‰. Trees had significantly more positive $\delta^{18}O$ and $\delta^{2}H$ signatures than shrubs after fractionation compensation with p-values for both 0.03.

Forest vegetation xylem water consistently had higher and more variable ^{3}H concentrations compared to saturated zone meadow water, in summer 2015, winter 2016 and again in summer 2016 (Figure 3-4 (b). During August 2016, which experienced normal seasonal summer drought, following a relatively normal winter, while $\delta^{18}O$ values for vegetation xylem and saturated zone meadow water were similar (Figure 3-4 (a)), vegetation xylem ^{3}H concentrations were distinctly higher than saturated zone meadow water ^{3}H (Figure 3-4 (b)). Both vegetation xylem water and precipitation ^{3}H values vary more over time than saturated zone meadow water ^{3}H (Figure 3-4 (b)).

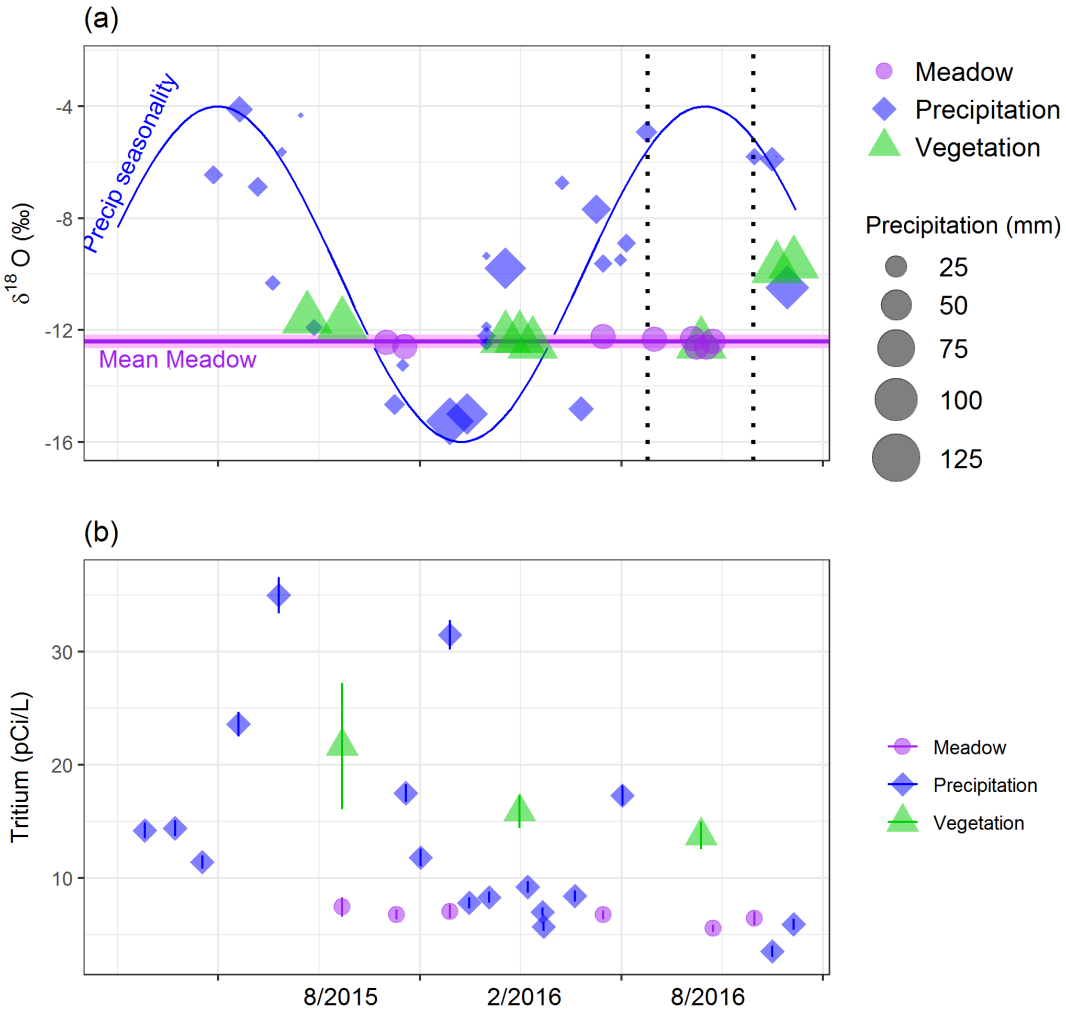

Figure 3-4. Southern Sierra Critical Zone Observatory vegetation, groundwater and precipitation ^{3}H and $\delta^{18}O$ patterns over time. Although vegetation xylem $\delta^{18}O$ during normal summer conditions match saturated zone meadow water, distinctly high and variable ^{3}H concentrations suggest that xylem accessed shallower flow paths consisting of younger water. (a) Forest vegetation xylem water $\delta^{18}O$ are shown as triangles. Precipitation $\delta^{18}O$ is shown with diamonds, with amount indicated by relative size and seasonal sinusoidal pattern. Saturated zone meadow water $\delta^{18}O$ is represented by circles, with the mean plotted as a horizontal line and ribbon represents the standard error. Dotted vertical lines bound normal seasonal precipitation conditions characteristic of the Mediterranean climate, in which snowmelt input is followed by a rainless, dry summer; xylem water at this time plots on top of the meadow water (saturated zone) mean signature in $\delta^{18}O$. Fall rain immediately after the summer dry season in 2016 corresponds with xylem water $\delta^{18}O$ increases.

Table 3-1. Mean vegetation xylem $\delta^{18}O$ and $\delta^{2}H$ for each sampling date, sampled from the Southern Sierra Critical Zone Observatory, P301 site.

Sampling Date	**Mean $\delta^{18}O$ (‰)**	**± σ^{1}**	**Mean $\delta^{2}H$ (‰)**	**± σ^{1}**
7/15/2015	-11.6	0.3	-84.6	2.1

8/19/2015	-11.8	0.4	-86.4	2.6
1/28/2016	-12.3	0. 9	-89.7	5.8
2/11/2016	-12.3	0.9	-89.3	5.8
2/24/2016	-12.5	0.5	-90.4	3.4
8/9/2016	-12.5	0. 3	-90.3	1.8
10/24/2016	-9.8	0. 6	-73.8	3.7
11/10/2016	-9.6	0.3	-72.1	2.1

[1] σ is standard error.

Table 3-2. Comparison of mean snowmelt signatures measured beneath forest canopy and in forest gaps, vegetation and the saturated zone in the meadow.

Water Year	Under Canopy Snowmelt	Open Canopy Snowmelt	Vegetation	Meadow Saturated Zone	P301 Stream
2016	-10.5 ± 0.1	-12.0 ± 0.4	-12.4 ± 0.5	-12.4 ± 0.1	-11.9 ± 0.0
2017	-11.4 ± 0.4	-12.3 ± 0.8	-	-12.4 ± 0.1	-12.2 ± 0.2

Dual-isotope plots in Figure 3-5 shows that vegetation signatures clustered near saturated zone meadow water signatures in most instances, with the exception of October and November when vegetation signatures were shifted higher. When aggregating all vegetation data, according to Welch Two Sample T-test results, saturated zone meadow water and vegetation $\delta^{18}O$ signatures were significantly different (p-value: 0.002, confidence interval 95%) but, on the other hand, saturated zone meadow water and vegetation $\delta^{2}H$ signatures were not significantly different (p-value: 0.46). Soil signatures plotted to the left of the LMWL in July and August 2015 and plotted near the LMWL during winter 2016 and August 2016. Categorized by species, vegetation $\delta^{18}O$ and $\delta^{2}H$ raw values in dual-isotope space did not show any distinct patterns, nor did individual trees and shrubs reflect patterns plotted over time (Figure 3-A1). When August 2016 soil signatures are compared to vegetation, soil, intercepted snowmelt and open area snowmelt, soil signatures plot near snowmelt in open areas and vegetation signatures (raw values) plot between meadow saturated zone water and soil signatures (Figure 3-6 (a)).

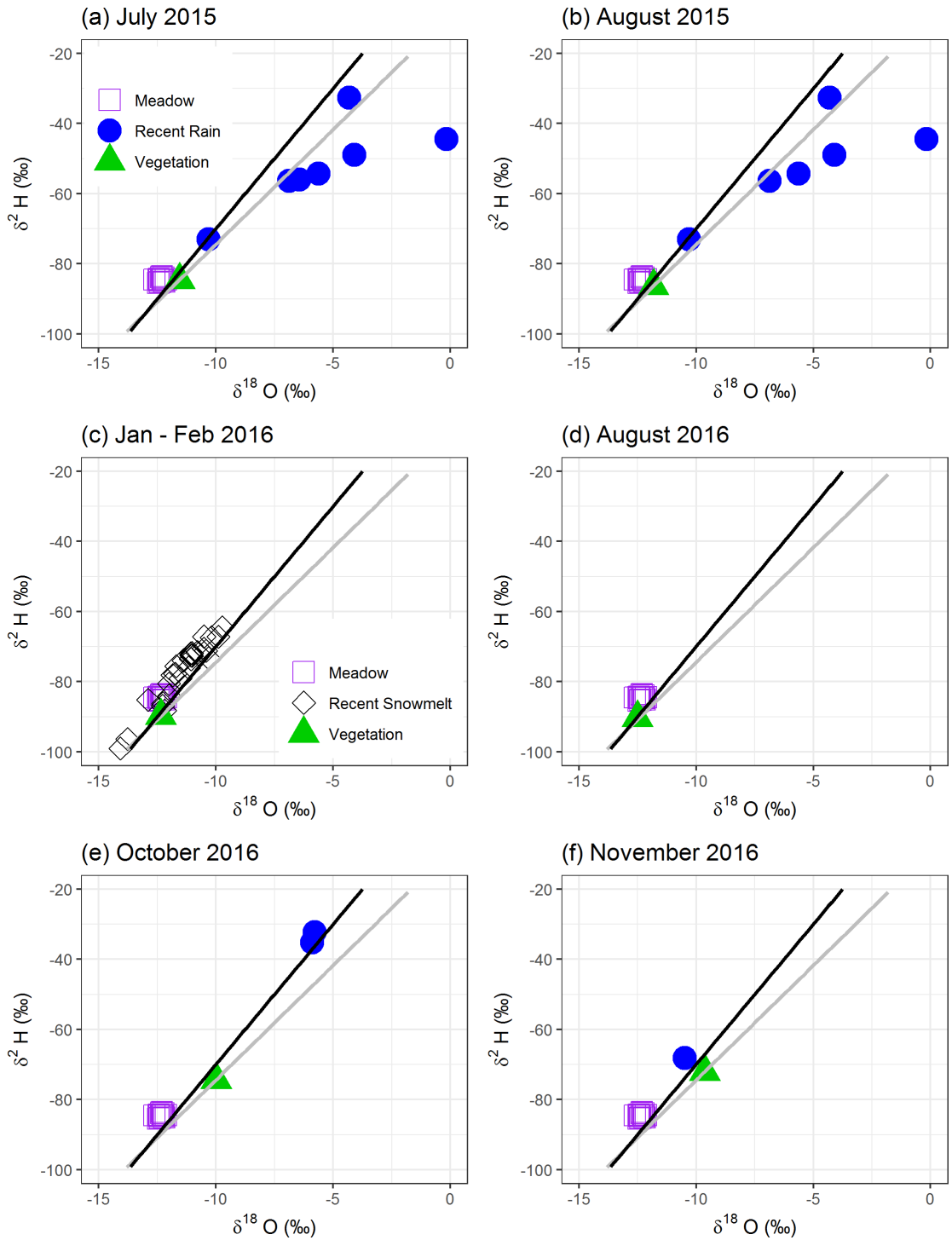

Figure 3-5. Dual-isotope plots showing mean xylem signatures for each sampling date, saturated zone meadow water and recent input signatures at the Southern Sierra Critical Zone Observatory, P301 site. (a) July 2015 and (b) August 2015 show recent summer rain, following severe snow drought (c) winter 2016 includes recent snowmelt input, (d) August 2016, which followed a normal snow year, but did not experience rain. (e) October 2016 and (f) November 2016 show recent autumn rain.

Soil water $\delta^{18}O$ and $\delta^{2}H$ results were limited to samples collected in August 2016, which were heated during cryogenic vacuum distillation; however analysis of August 2016 soil profiles of both $\delta^{18}O$ and ^{3}H did not reflect distinct endmembers (Figure 3-6 (b) and (c)). Soil moisture within the soil profile was highest at a depth of 200 and 250 cm (Figure 3-6 (d). In dual-isotope space, vegetation signatures cluster near saturated zone meadow water, but do not overlap (Figure 3-6 (a)); however, the saturated zone meadow water is distinct from xylem and soil water ^{3}H.

Soil water stable isotope data that experienced incomplete extraction were not compared to vegetation signatures; however, it was determined that regardless of the long duration of extraction (90 hours), extraction efficiency depended on heating soil samples during extraction. In dual-isotope space (Figure A3-2 (a)) soil water signatures from extraction without heat clustered to the left of the LMWL, slightly outside the reasonable range of precipitation input. Samples with low extraction efficiencies had lower isotopic values in both $\delta^{18}O$ (Figure A3-2 (c)) and $\delta^{2}H$ (Figure A3-2 (d)). However, the vertical soil profiles all show a recognizable pattern (Figure A3-3(a)). The difference in mean $\delta^{18}O$ from July 2015 (not heated) and August 2016 (heated) and August 2015 (not heated) and August 2016 soil water was 4.9‰ and 4.5‰ respectively. When the rough "corrections" of 4.9 and 4.5‰ are applied, the vertical profiles of all three soil sample sets are very similar (Figure A3-3 (b)). This organized vertical pattern in the soil profile should not be used to suggest that the soil signatures are accurate. The estimated systematic error that we calculated has no applicability to other studies because the soil samples were collected at different times; this value only demonstrates that additional rigorous testing is needed to determine how temperature can cause a systematic error. The samples that experienced incomplete extraction had extraction efficiencies (water extracted during cryogenic vacuum distillation divided by the total soil moisture mass) ranging from 71% to 80%. All values are listed in Table A3-6.

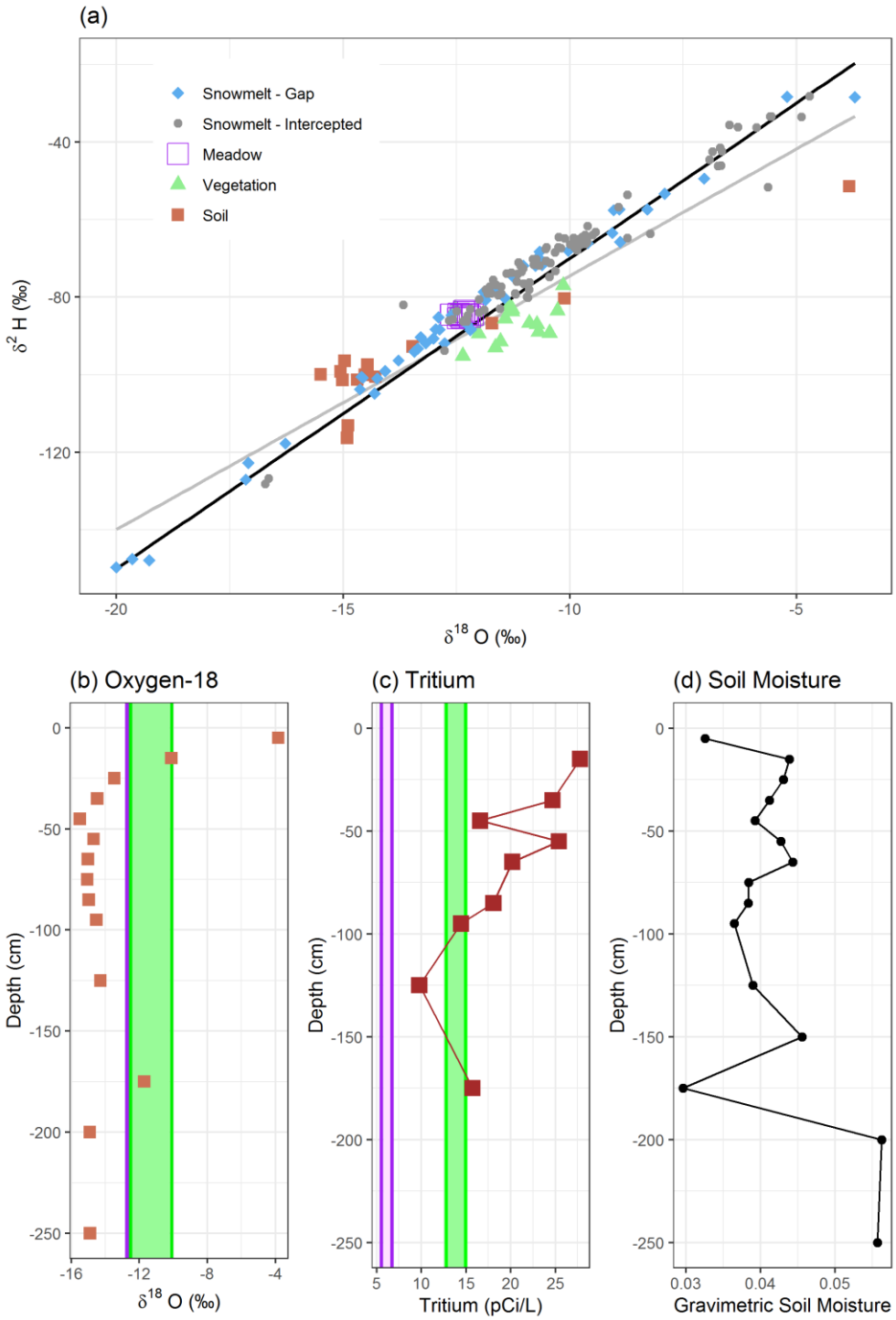

Figure 3-6. (a) Dual-isotope plot showing August 2016 soil signatures (solid brown squares) with respect to 2016 snowmelt from forest gaps (blue diamonds), 2016 intercepted snowmelt (small hollow black squares), meadow saturated zone water (large, purple hollow squares) and August 2016 vegetation signatures (raw values, not fractionation-compensated). (b) The same uncorrected soil water $\delta^{18}O$ values plotted with depth green band indicates range of xylem water $\delta^{18}O$ and purple band indicating the meadow saturated zone range of $\delta^{18}O$. Meadow saturated zone $\delta^{18}O$ range includes values from October 2015 through October 2017. (c) Tritium soil profile with soil

shown by brown squares, green band indicates the range of vegetation xylem tritium concentrations and the purple band indicates saturated zone meadow water tritium concentrations from May 2016 to October 2016. All vegetation and soil samples were collected from the Southern Sierra Critical Zone Observatory P301 data on August 9, 2016 and are raw, uncorrected values.

Open canopy snowmelt matched both mean winter vegetation signatures and saturated zone meadow water stable isotope signatures. Mean xylem water values during the three winter sampling events were the same, within standard error Table 3-1. Aggregated winter vegetation signatures were not significantly different than saturated zone meadow water signatures; p-values = 0.95 and 0.10 for $\delta^{18}O$ and $\delta^{2}H$, respectively. Mean snowmelt $\delta^{18}O$ values collected from under canopy areas were -11.1 ± 0.3 ‰, -10.9 ± 0.2 ‰, -10.9 ± 0.3 ‰ and in open areas were -14.2 ± 0.3 ‰, -12.2 ± 0.8 ‰, -12.8 ± 0.2 ‰ for January, mid-February, and late February, respectively. When snowmelt signatures from the entire 2016 water year were classified into under canopy or open area snowmelt and compared to winter vegetation signatures, winter vegetation $\delta^{18}O$ and $\delta^{2}H$ were significantly different than under canopy snowmelt signatures (p-value < 0.001 for both $\delta^{18}O$ and $\delta^{2}H$) (Table 3-2).

Mean snowmelt signatures from open areas (un-intercepted snowmelt), vegetation xylem signatures during winter and saturated zone meadow water signatures were similar. To determine how snowmelt and vegetation signatures changed during winter 2016, mean values were calculated for vegetation sampled on each of three days: 1/28/2016, 2/11/2016 and 2/24/2016. Snowmelt was grouped by canopy (under canopy or open) and mean values were calculated for each group from snowmelt signatures from three groups: (1) 1/12/2016 and 1/28/2016, (2) 2/11/2016 and (3) 2/24/2016. To compare winter vegetation signatures with snowmelt signatures, we used a t-test. For example, during WY 2016, open canopy snowmelt $\delta^{18}O$ was -12.0 ± 0.4 ‰, xylem was -12.4 ± 0.5 ‰ and saturated zone meadow water was -12.4 ± 0.04 ‰, on the other hand, canopy intercepted snowmelt had a mean $\delta^{18}O$ signature of -10.5 ± 0.1 ‰. Likewise, snowmelt from open areas (un-intercepted snowmelt) and saturated zone meadow water, in both years, 2016 (p-value: 0.35) and 2017 (p-value 0.95) were not statistically significantly different. In WY 2017, snowmelt signatures from open areas (un-intercepted snowmelt), were, again, similar to saturated zone meadow water signatures. Furthermore, saturated zone meadow water was statistically significantly different than snowmelt under forest canopy (intercepted snowmelt) in both water years, 2016 (p-value < 0.001) and in 2017 (p-value: 0.02). Saturated zone meadow water stable isotope signatures were similar to those of the P301 stream water, sampled downstream (Table 3-2; see Figure 3-3 for sampling locations).

Comparing soil moisture at different depths in water year 2016 provided a range of wet and dry conditions and generally reflected a pattern of higher soil moisture at shallow depths in open areas compared to beneath canopy during winter and spring (Figure 3-7). At deeper depths, the opposite pattern occurred, and higher soil moisture can be found beneath the forest canopy (Figure 3-7). Similar patterns are seen in soil moisture in water years from 2010 to 2014 (Figures A3-4 through A3-6, A3-8). Generally, open areas had deeper snow than beneath forest canopy, which was more apparent in wet years (Figure A3-7, (b)) compared to dry years (Figure A3-7 (d) and (e)).

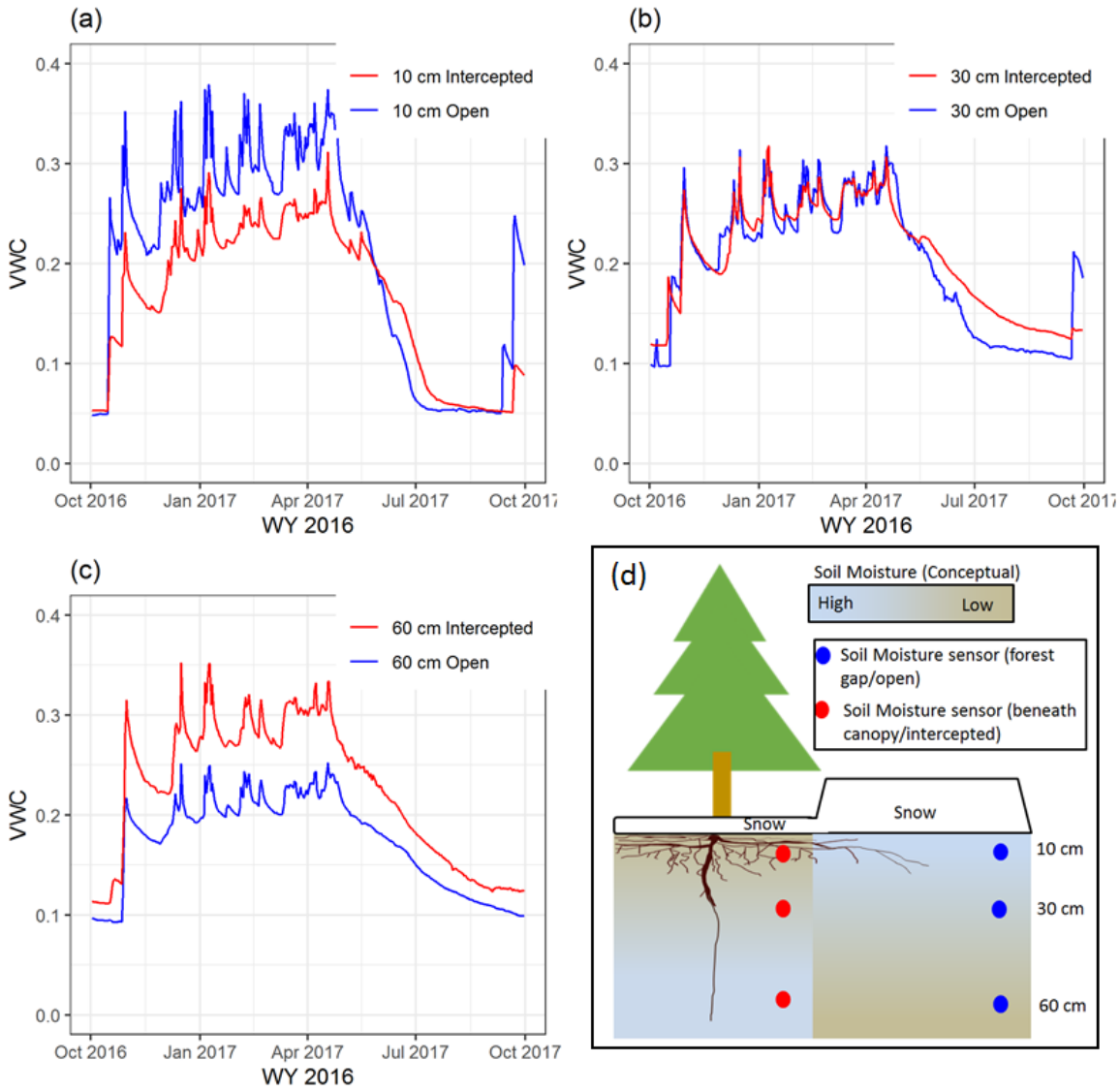

Figure 3-7. Soil volumetric water content (VWC) measured by sensors located at the Southern Sierra Critical Zone Observatory Upper Met North aspect site beneath forest canopy (red) and in open areas (blue) at (a) 10 cm depth, (b) 30 cm depth and (c) 60 cm depth. (d) A conceptual diagram showing the general pattern of lower volumetric water content directly beneath forest canopy compared to open areas at shallow depths during snow melt season. The reverse is observed at deeper depths (60 cm) where volumetric water content is higher beneath forest canopy and lower in open areas. Figure 3-A8 shows a similar pattern from sensors CZ-17 and CZ-19; see Figures 3-A4 through 3-A7 for additional supporting soil moisture data and analysis. Tree root density is shown as higher in shallow depths, but additional roots extending deeper, beyond surface soil layers (Klos et al., 2018). Snow is generally deeper in forest gaps, and comprises the majority of snow at this elevation (Zheng et al., 2016).

The variability of ^{3}H concentrations in vegetation, soil and precipitation was higher than that of major rivers and saturated zone meadow water (Figure 3-8). The mean precipitation input value was 12.6 ± 1.6 pCi/L. Saturated zone meadow water and vegetation ^{3}H concentrations were statistically significantly different (p-value < 0.001). The mean and standard deviation of ^{3}H in P301 saturated zone meadow water was 6.8 ± 0.7 pCi/L, meanwhile soil water and vegetation water had a high mean (and standard deviation) tritium concentration, 21.6 ± 8.2 pCi/L and 22.3 ± 5.9 pCi/L, respectively. ^{3}H concentrations in the P301 saturated zone meadow water were similar to those of major California rivers, meanwhile, ^{3}H concentrations in vegetation, soil and precipitation were higher and had higher variability (Figure 3-8). During 2016, which experienced normal snowpack and summer seasonal drought, saturated zone water and xylem water were distinctly different in ^{3}H: 5.54 (± 0.24) pCi/L and 13.74 (± 1.11) pCi/L, respectively (Figure 3-4 (b)). Individual ^{3}H values are listed in Table 3-A6.

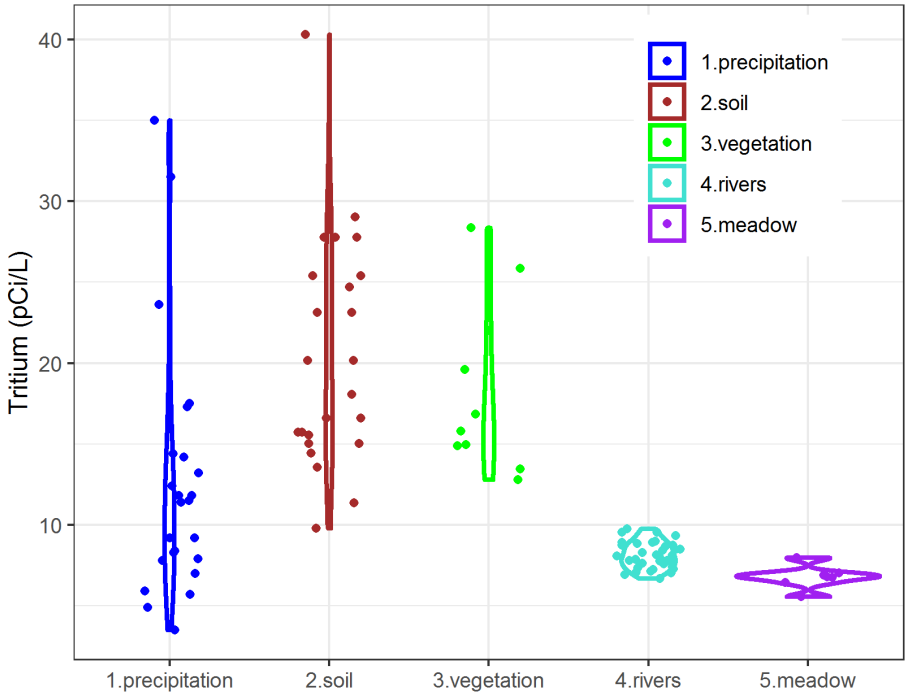

Figure 3-8. Violin plot showing ^{3}H concentrations for precipitation, soil, vegetation and meadow saturated zone water in the Southern Sierra Critical Zone Observatory, and tritium concentrations from major rivers originating in the Sierra Nevada. Precipitation was collected from February 2015 through June 2017, saturated zone meadow water was collected from August 2015 through October 2016, soil water was collected during four sampling events, August 2015, February 2016, August 2016 and October 2015, vegetation was collected in August 2015, February 2016 and August 2016; river samples were collected twice in 2017, once during spring runoff in late March and early April and once in late Auguste, early September. Points are jittered, a small amount of random variation was added to the location of each point on the x-axis, to avoid over-plotting points.

3.3 Discussion

Both ^{3}H and stable isotope results show that xylem water was composed of young water compared to saturated zone meadow water and runoff (Figure 3-4 and Figure 3-8). ^{3}H concentrations in xylem water were significantly higher and had more variability than deep saturated zone meadow water and runoff. Saturated zone meadow water was composed of water up to 20 years old (Visser et al., 2019) and river runoff had similar tritium concentrations to that of saturated zone meadow water. On the other hand, vegetation and soil water ^{3}H concentrations were similar in range to precipitation and could not be used to quantitatively calculate a mean age Figure 8. Saturated zone meadow water ^{3}H measured at the P301 site was in the same range as groundwater that has been previously measured in the Sierra Nevada, with previous measurements slightly lower (Table 3-3). Our results confirm previous findings (Visser et al., 2019) which showed evapotranspiration uses mostly the youngest water from the range of ages of water in storage. On the other hand, P301 water age distribution of streamflow varies with streamflow rate, preferring older water during dry periods and younger water during wet periods (Visser et al., 2019). This can be explained by saturated zone meadow water and rivers aggregating flowpaths driven by gravity, including deep and long flow paths. Previous research has shown that other Sierra Nevada meadows have localized groundwater inputs (Lucas et al., 2016). Presumably, trees and shrubs have access to dominantly more shallow compartments and have roots that are physically close to the surface and the trees sampled here were located at a higher elevation, on top of a knoll near, but above the meadow. Water accessed by vegetation intercepts water along shorter, near-surface flow paths because that is where at least some portion of roots exist.

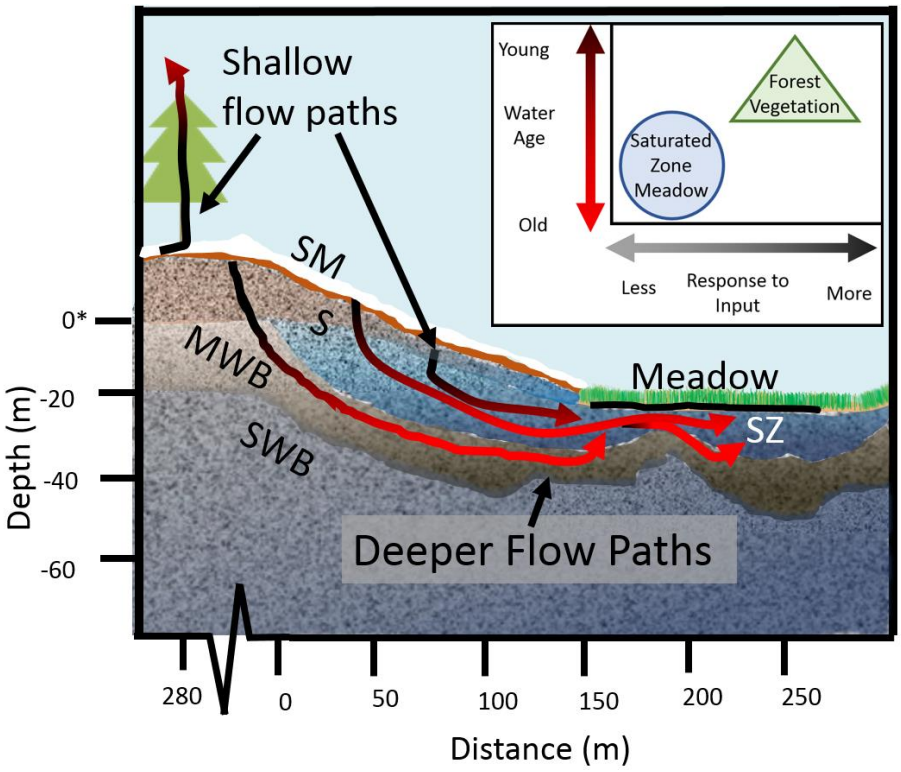

Figure 3-9. Interpretive cross section adapted from Holbrook et al. (2014) with conceptual flow paths to vegetation and the saturated zone at the Southern Sierra Critical Zone Observatory, P301 headwater catchment. Tree cores were sampled from trees located ~30 meters higher and 280 meters from the "0" m reference distance and represented by Holbrook et al. (2014). Snowmelt input (SM) follows shallow, deep/long and mixed flow paths. Vegetation accessed shallow flow paths containing relatively young water compared to older water which composed the saturated zone (SZ). Deep flow paths can travel through moderately weathered bedrock (MWB) and saprolite (S) (Holbrook et al., 2014) and shallow snowmelt can travel through and near the surface mineral soil (unlabeled brown line beneath snow) (Lucas, 2016). Somewhat weathered bedrock (SWB) bounds MWB and influences subsurface connectivity, for example, at the 200 m distance (~ -30 m depth). Inset: Saturated zone water is composed of older water compared to forest vegetation (xylem water); likewise, vegetation responds to new inputs of precipitation due to its proximity to shallow flow paths. Saturated zone water is less responsive to new input as it is composed of a mix of older and younger water, including a larger amount of water that has traveled through longer, deeper flow paths.

Table 3-3. Tritium concentrations in the CZO P301 saturated zone meadow water and groundwater in the Sierra Nevada measured by others.

Location	Range (pCi/L)	Mean (pCi/L)
CZO P301[1]	5.54 to 10.41	8.03 (± 0.30)
Northern Sierra Nevada[2]	-0.5 to 11.92	3.76
Central Sierra Nevada[3]	1.60 and 4.31	NA

[1] Measured here. [2] Segal et al. (2014). [3] Moore et al. (2017).

Previous studies using ^{3}H to determine water use by trees have shown varying results. (Zhang et al., 2017) found apple trees in the southern Loess Plateau of China were using water several decades old. Unlike our southern Sierra Nevada site, the Loess Plateau site is drier, has summer rains, and the apple trees were planted, rather than native species adapted to the site. Additionally, (Zhang et al., 2017) suggest that the old water being used by vegetation is also the less mobile water, and not deep water because the tree root depths were not observed to reach the depth of deeper groundwater. Therefore, the trees were found accessing the water that was available in this relatively dry climate. On the other hand, (Lewis & Burgy, 1964) used ^{3}H to observe trees using very deep water when they injected saturated zone meadow water with ^{3}H in the foothills of the Sierra Nevada and found that oak trees utilized water from fractured bedrock groundwater deeper than 21 meters during dry seasons.

By sampling stable isotope signatures in vegetation over time, we found that vegetation responded to new rain when it became available (Figure 3-4). In summer, 2015 and fall 2016, vegetation signatures responded to summer rain with more positive signatures. We can discount the more positive signatures being a result of evaporation through the bark of the tree, since the vegetation signatures in mid-summer, 2016, following weeks of warm, dry weather would also be more positive, if that were the mechanism. On the contrary, these mid-summer vegetation signatures match previous winter snowmelt and mean saturated zone meadow water stable isotope signatures. Furthermore, by performing fractionation compensation the possible effects of evaporation through the bark are compensated for to eliminate that factor in determining source water. Rose et al. (2003) also observed Sierra Nevada vegetation responded to new rain, specifically greenleaf manzanita (*Arctostaphylos patula*). This leads to the question, what explains vegetation shifting water sources? (Dawson & Pate, 1996) found plant species with dimorphic rooting systems utilized different water sources in different seasons and conditions, which agrees with the shifts in water sources we observed here.

Rose et al. (2003) also found that xylem water signatures indicated that vegetation was utilizing weathered bedrock water several meters deep during the summer season, which is considered an important pool of water sustaining vegetation through dry seasons. Additionally, shrubs similar to those studied here (*Arctostaphylos grandulosa* and *Ceanothus greggii*) have been observed to utilize water stored in weathered bedrock with roots deeper than 4 meters (Sternberg et al., 1996). White fir trees have been observed to have deep tap roots to survive dry summers, and Jeffrey pine roots have been observed in the Southern Sierra to extend deep roots, beyond soil and weathered bedrock into bedrock fractures (Hubbert et al., 2001). Roots have been found to grow along the bedrock-soil interface and enter fractures encountered along the way (Hubbert et al., 2001). The portion of shallow and deep roots and rooting depths of similar tree species have been found to vary with soil type and thickness (Berndt, 1958; Herman, 1969). To summarize what is known about the root systems of the vegetation species sampled here, roots extend from the soil surface, laterally and downward, with roots extending deep beyond bedrock into bedrock fractures to unknown depths. This allows vegetation to access water sources in different compartments, from recent rain to more deeply stored water. When rain is not available and vegetation is accessing more deeply stored water, our ^{3}H data show that the deeply stored water is still younger than saturated zone meadow water and river runoff. It is possible that by extracting water from deep bedrock fractures, trees facilitate and accelerate downward flow paths resulting in younger ages than found in saturated zone meadow water or the P301 stream.

Soil water stable isotope data were limited due to problems with extraction methods. We found that, although preliminary test results (Table A3-3) and organized vertical soil profiles (Figure A3-3 and A3-9) suggested that our methods sufficiently extracted soil water, further analysis of extraction efficiency determined that low sample temperatures during extraction led to a systematic

error in the isotopic values. Although we were able to rewet soil with water of a known isotopic value and sufficiently recover that water, we found that this preliminary test was misleading and may not be sufficient to test the efficacy of extraction methods. (Sprenger et al., 2015) also questions the efficacy of spiking soil with water of a known isotopic content and our data contributes evidence to this finding. (Orlowski, 2013) suggest that extending the time during cryogenic vacuum distillation can improve extraction efficiency of cryogenic vacuum distillation. Common extraction times range from 30 minutes to 180 minutes (Orlowski, Breuer, et al., 2016; West et al., 2006). However, we found that even when we extended cryogenic vacuum distillation to more than 96 hours, heat was necessary to increase the saturated vapor pressure within the vessel to allow for complete extraction. The organized vertical profiles (Figure A3-3 (a)) suggest that a systematic error occurred, and a rough correction of the shift leads to vertical profiles that are very similar between summer profiles in 2015 and 2016 (Figure A3-3 (b)). A similar vertical curving pattern indicating evaporation near the surface of the soil has been documented by (Barnes & Allison, 1983, 1988). Surface soil water that has experienced evaporation has higher isotopic signatures than deeper soil water layers (Barnes & Allison, 1983, 1988). This organized vertical pattern in the soil profile should not be used to suggest that the soil signatures are accurate. The estimated systematic error that we calculated has no applicability to other studies because the soil samples were collected at different times; this value only demonstrates that additional rigorous testing is needed to determine how temperature can cause a systematic error. We calculated a rough estimate based on mean values of the entire soil profile, but the error may be larger or smaller depending on soil type, soil moisture and the amount of hygroscopic and biologically bound water in the soil (Sprenger et al., 2015).

Snowmelt from forest gaps largely made up saturated zone meadow water and subsequent stream runoff based on stable isotope data. Snowmelt that had experienced canopy interception did not contribute to saturated zone water. It is known that canopy interception and shading effects snow depth, distribution and ablation (Gustafson et al., 2010; Kattelmann et al., 1983; Varhola et al., 2010; Zheng et al., 2016). The absence of canopy-intercepted snowmelt signatures in saturated zone meadow water indicates that intercepted snowmelt represents a very small flux of water entering the subsurface, compared to the open-area snowmelt. Intercepted snowmelt may be accessed quickly by forest vegetation due to its proximity to tree roots, supported by our finding that trees access water that is most readily available. Nevertheless, vegetation xylem water stable isotope signatures are similar to the signatures measured in the open areas, attributed to the deeper snow in forest gaps (Figure 3-9 and Figure A3-7). On the larger scale, deeper snow in open areas, and lower snow depths beneath forest canopy, minimally affects the overall amount of snow in the Sierra Nevada at this elevation (Zheng et al., 2018). The extension of roots beyond the horizontal boundary of canopy allowed trees to access water from different locations in the subsurface and use non-intercepted snowmelt in winter. Indeed, Jeffrey Pine roots have been observed to extend over 10 to 20 meters from the trees laterally (Burns, 1990; Hubbert et al., 2001) and incense cedar drought resistance is due to "a complete occupancy of the soil mass" (Burns, 1990).

Previous work found that canopy interception did not have an effect on the depth integrated soil moisture at the Southern Sierra Critical Zone Observatory P301 site (Oroza et al., 2018) and no pattern in volumetric water content was observed in 2008 and 2009 with canopy interception (Bales et al., 2011). By examining soil moisture at individual depths, data suggest that soil moisture is lower directly beneath forest canopy at shallow depths and higher at deeper depths, compared to canopy gap areas during snow melt season (Figure 3-7). Several explanations could possibly account for this pattern, for example, shallow roots beneath forest canopy using soil moisture most easily accessible, directly within the trees' immediate footprint, at shallow depths, where most roots are located. On the other hand, preferential flow along roots beneath the tree canopy could route

water more quickly to depth compared to open forest gaps where fewer vertically oriented roots exist (Figure 3-8 (d)). Roots are known to form macropores which channel water to depth, creating preferential flow paths (Angers and Caron, 1998; Johnson and Lehmann, 2006). However, (Bales et al., 2011) previously found that soil moisture at this location was not affected by canopy interception (Bales et al., 2011), suggesting that the pattern seen in these sets of sensors is coincidental. The difference in soil moisture at 10 cm beneath the canopy and in the open areas starts with the onset of winter precipitation, in which there is more snow in open areas than beneath forest canopy. There was a delayed response for the deeper sensors. Differences in soil moisture near the surface are a reflection of snow melt input, whereas some preferential flow can affect deeper soil moisture. Soil moisture during the summer was higher beneath the canopy compared to the open area at all depths (Figure 3-7) at the Upper Met North site, which could reflect hydraulic redistribution by trees. Hydraulic lift has been observed in similar species of pine and fir during dry seasons, in which tree roots redistributed water to upper layers of soil that experienced daytime evaporation (Brooks et al., 2002; Domec et al., 2004). During spring the 10 cm open area soil dried faster than soil beneath the forest canopy, possibly due to differences in shading, indicating that evaporation had a larger influence on surface soil compared to transpiration.

This study was limited by methods and assumptions that are worth further investigation, including assumptions about fractionation after water is taken up by the plant and questions about cryogenic vacuum distillation of dry soils. Many isotope ecohydrology studies have made the assumption that the stable isotope signature in vegetation xylem water represents source water (Dawson, 1991; Rose et al., 2003), but when plotted in dual-isotope form, vegetation signatures plot to the right of source waters (Bowling et al., 2017; Evaristo et al., 2015; Gierke et al., 2016; McCutcheon et al., 2017; Newberry et al., 2017). To explain why vegetation plots to the right of source water signatures, some have proposed an un-sampled water source, possibly tightly bound water within the soil (Bowling et al., 2017; Brooks et al., 2010) and others have used techniques to project the vegetation signatures back to the source water (Allen et al., 2019; Benettin et al., 2018; Evaristo et al., 2015). This second method assumes that some evaporation occurs between uptake and xylem sampling. Further research is needed to definitively determine why vegetation often plots to the right of source water, which may be specific to plant species and plant physiology.

The use of $\delta^{18}O$ and $\delta^{2}H$ to understand hydrological processes in the vadose zone can be improved by answering questions that relate to both measurement methods and soil processes, including: 1) what is the total force required to extract water from different soil types/moisture levels and is that force equal to that of plants? 2) Does hygroscopic water retain a unique isotopic signature, should this be considered plant-available water, how easily does this water mix with new precipitation and what methods should be employed to extract it? Firstly, numerous methods have been used to measure water stable isotopes in soil, yet, these methods have been found to lead to inconsistent results, some of which is due to inconsistent forces applied to separate the water from the soil (Orlowski, Pratt, et al., 2016). Secondly, while water is extracted from soil, it is not known if that is the same water that is available to plants, which may vary among plant species. Thirdly, the role of hygroscopic water in isotope ecohydrology may complicate research methods, but also may play a role in what is accessible to plants and when plants access it. Answering these questions is beyond the scope of this study, but pose important challenges in critical zone science, as stable isotopes $\delta^{18}O$ and $\delta^{2}H$ are important tracers used to understand vadose zone water movement. In this study we found that isotopic temporal variability in water available to plants is important to understand where trees get their water. Meanwhile, new methods to collect high temporal resolution soil water data promise to further improve our understanding of vadose zone processes (Orlowski, Pratt, et al., 2016), for example use of membrane inlet laser spectroscopy with high sample throughput (Oerter et al., 2014).

Further research is also needed to characterize the subsurface structure, the role of bedrock fractures in storing and routing water to both roots and subsurface stores, and to determine species differences in water use strategy. Sampling water within bedrock fractures is logistically difficult, but our results point to vegetation accessing a pool of water that has a stable isotope signature similar to deeper saturated zone meadow water , but younger, according to ^{3}H data, which indicates water at an intermediate point along a flow path leading to the deeper subsurface. Furthermore, WE know that roots extend into bedrock fractures therefore vegetation likely uses this water source. Differences among tree and shrub species in terms of water sources, shifts in water sources and competition strategies is an area of further research needed to inform forest management; although this study provides data from several different species, the sample size is still too limited to perform statistical analysis to fully understand vegetation species differences.

3.4 Conclusions

We used both stable isotopes and ^{3}H to track water through a Sierra Nevada headwater catchment and found that vegetation accesses younger water compared to saturated zone meadow water and runoff, which provides a new way to work across time scales to predict subsurface storage and water use by forest vegetation, an important knowledge gap in critical zone science (Klos et al., 2018). Secondly, we observed vegetation accessing new sources of water (precipitation, snowmelt) when they became available. By observing patterns in snowmelt isotopic signatures we determined that saturated zone meadow water was composed of snowmelt that had not experienced canopy interception. The new approach of tracking water through each component of the hydrologic cycle with both ^{3}H and water stable isotopes provides unique insight on both temporal and spatial dynamics and links between forest water use, storage and runoff. Additionally, by providing new data from this snow dominated mountain system in which snowmelt input and transpiration occur simultaneously throughout winter and spring, this study adds a new setting to existing literature, which have mostly been conducted in rain-dominated climates, by providing new data from this snow dominated mountain systems.

Sierra Nevada forests transpire a significant amount of California's water resources, which has sparked interest in applying forest management to improve California's water supply. A significant interest in critical zone science is to develop new methods "to work across time scales to predict subsurface water storage and use,"(Klos et al., 2018) which we provide through the unique application of a combination of hydrologic tracers, $\delta^{18}O$, $\delta^{2}H$ and ^{3}H, to track water from through the critical zone continuum from the atmosphere, vegetation and subsurface. Determining the source water composition of evapotranspiration is informative for forest managers. We found, based on ^{3}H data, that saturated zone meadow water is older than water taken up by vegetation but both pools are similar, in stable isotope signatures, to un-intercepted snowmelt. By constraining the isotopic signatures of precipitation continuously for multiple seasons and measuring precipitation signatures immediately before sampling vegetation signatures, we observed vegetation changed water sources depending on availability. Using both ^{3}H with stable isotopes provides new insights into ecohydrological water sources in the critical zone. We determined changes in connectivity among vegetation source water, runoff and saturated zone meadow water by sampling throughout different seasons in the Sierra Nevada, a snow dominated system, when evapotranspiration were both in- and out- of phase with precipitation input. Our findings that vegetation consistently used younger water compared to the saturated zone meadow water, have implications for drought resilience and vulnerability. As climate perturbations occur, the response of baseflow runoff and saturated zone water to drought may lag, compared to the response of forest vegetation, which accesses younger water, even during summer. On the other hand, by being able to access new

sources of water as they become available, such as summer rain, forest vegetation is more adaptable on a shorter time scale, within the critical zone, compared to runoff and saturated zone water. We found that runoff and saturated zone meadow water was largely composed of snowmelt from forest gaps, rather than snowmelt that had been intercepted by canopy cover. Perturbations in climate causing a longer growing season, or expansion of forest vegetation upward in elevation (Goulden & Bales, 2014), then would mean that more vegetation would access this snowmelt that may otherwise infiltrate to recharge the saturated zone.

References

Allen, S. T., Kirchner, J. W., Braun, S., Siegwolf, R. T. W., & Goldsmith, G. R. (2019). Seasonal origins of soil water used by trees. *Hydrology and Earth System Sciences, 23*(2), 1199-1210.

Angers, D. A., & Caron, J. (1998). Plant-induced changes in soil structure: processes and feedbacks. Biogeochemistry, 42(1-2), 55-72.

Bales, R. C., Goulden, M. L., Hunsaker, C. T., Conklin, M. H., Hartsough, P. C., O'Geen, A. T., et al. (2018). Mechanisms controlling the impact of multi-year drought on mountain hydrology. *Scientific Reports, 8*.

Bales, R. C., Hopmans, J. W., O'Geen, A. T., Meadows, M., Hartsough, P. C., Kirchner, P., et al. (2011). Soil Moisture Response to Snowmelt and Rainfall in a Sierra Nevada Mixed-Conifer Forest. *Vadose Zone Journal, 10*(3), 786-799.

Barnes, C. J., & Allison, G. B. (1983). The distribution of deuterium and o-18 in dry soils .1. Theory. *Journal of Hydrology, 60*(1-4), 141-156.

Barnes, C. J., & Allison, G. B. (1988). Tracing of water-movement in the unsaturated zone using stable isotopes of hydrogen and oxygen. *Journal of Hydrology, 100*(1-3), 143-176.

Benettin, P., Volkmann, T. H. M., von Freyberg, J., Frentress, J., Penna, D., Dawson, T. E., et al. (2018). Effects of climatic seasonality on the isotopic composition of evaporating soil waters. *Hydrology and Earth System Sciences, 22*(5), 2881-2890.

Berndt, H. W., Gibbons, R.D. (1958). *Root distribution of some native trees and understory plants growing in three sites within Ponderosa pine watersheds in Colorado*: US Department of Agriculture, Forest Service.

Bornyasz, M. A., Graham, R. C., & Allen, M. F. (2005). Ectomycorrhizae in a soil-weathered granitic bedrock regolith: Linking matrix resources to plants. *Geoderma, 126*(1-2), 141-160.

Bowling, D. R., Schulze, E. S., & Hall, S. J. (2017). Revisiting streamside trees that do not use stream water: can the two water worlds hypothesis and snowpack isotopic effects explain a missing water source? *Ecohydrology, 10*(1).

Brooks, J. R., Meinzer, F. C., Coulombe, R. O. B., & Gregg, J. (2002). Hydraulic redistribution of soil water during summer drought in two contrasting Pacific Northwest coniferous forests. Tree physiology, 22(15-16), 1107-1117.

Brooks, J. R., Barnard, H. R., Coulombe, R., & McDonnell, J. J. (2010). Ecohydrologic separation of water between trees and streams in a Mediterranean climate. *Nature Geoscience, 3*(2), 100-104.

Burns, R., Honkala, B. (1990). *Silvics of North America*. Agriculture Handbook 654: US Department of Agriculture Forest Service.

Davis, S. (1986). Water use patterns of four co-occurring chaparral shrubs. In H. Mooney (Ed.) (Vol. 70, pp. 172-177). *Oecologia*.

Dawson, T. (1991). Streamside trees that do not use stream water. In J. Ehleringer (Ed.) (Vol. 350, pp. 335). Nature.

Dawson, T. E., & Pate, J. S. (1996). Seasonal water uptake and movement in root systems of Australian phraeatophytic plants of dimorphic root morphology: A stable isotope investigation. *Oecologia, 107*(1), 13-20.

Dettinger, M., Redmond, K., & Cayan, D. (2004). Winter orographic precipitation ratios in the Sierra Nevada - Large-scale atmospheric circulations and hydrologic consequences. *Journal of Hydrometeorology, 5*(6), 1102-1116.

Dincer, T., Mugrin, A. A., & Zimmermann, U. (1974). Study of infiltration and recharge through sand dunes in arid zones with special reference to stable isotopes and thermonuclear tritium. *Journal of Hydrology, 23*(1-2), 79-109.

Domec, J. C., Warren, J. M., Meinzer, F. C., Brooks, J. R., & Coulombe, R. (2004). Native root xylem embolism and stomatal closure in stands of Douglas-fir and ponderosa pine: mitigation by hydraulic redistribution. Oecologia, 141(1), 7-16.

DWR. (2014). *California Water Plan 2013: Strategic Plan*. California Department of Water Resources.

Earman, S., Campbell, A. R., Phillips, F. M., & Newman, B. D. (2006). Isotopic exchange between snow and atmospheric water vapor: Estimation of the snowmelt component of groundwater recharge in the southwestern United States. *Journal of Geophysical Research-Atmospheres, 111*(D9).

Evaristo, J., Jasechko, S., & McDonnell, J. J. (2015). Global separation of plant transpiration from groundwater and streamflow. *Nature, 525*(7567), 91-+.

Fisher, J. B., Baldocchi, D. D., Misson, L., Dawson, T. E., & Goldstein, A. H. (2007). What the towers don't see at night: nocturnal sap flow in trees and shrubs at two AmeriFlux sites in California. *Tree Physiology, 27*(4), 597-610.

Fisher, J. B., DeBiase, T. A., Qi, Y., Xu, M., & Goldstein, A. H. (2005). Evapotranspiration models compared on a Sierra Nevada forest ecosystem. *Environmental Modelling & Software, 20*(6), 783-796.

Frisbee, M. D., Phillips, F. M., Campbell, A. R., & Hendrickx, J. M. H. (2010). Modified passive capillary samplers for collecting samples of snowmelt infiltration for stable isotope analysis in remote, seasonally inaccessible watersheds 1: laboratory evaluation. *Hydrological Processes, 24*(7), 825-833.

Frisbee, M. D., Phillips, F. M., Campbell, A. R., Hendrickx, J. M. H., & Engle, E. M. (2010). Modified passive capillary samplers for collecting samples of snowmelt infiltration for stable isotope analysis in remote, seasonally inaccessible watersheds 2: field evaluation. *Hydrological Processes, 24*(7), 834-849.

Gierke, C., Newton, B. T., & Phillips, F. M. (2016). Soil-water dynamics and tree water uptake in the Sacramento Mountains of New Mexico (USA): a stable isotope study. *Hydrogeology Journal, 24*(4), 805-818.

Goulden, M. (2018). Goulden Lab California Data - UCI ESS. from https://www.ess.uci.edu/~california/

Goulden, M. L., Anderson, R. G., Bales, R. C., Kelly, A. E., Meadows, M., & Winston, G. C. (2012). Evapotranspiration along an elevation gradient in California's Sierra Nevada. *Journal of Geophysical Research-Biogeosciences, 117*.

Goulden, M. L., & Bales, R. C. (2014). Mountain runoff vulnerability to increased evapotranspiration with vegetation expansion. *Proceedings of the National Academy of Sciences of the United States of America, 111*(39), 14071-14075.

Gustafson, J. R., Brooks, P. D., Molotch, N. P., & Veatch, W. C. (2010). Estimating snow sublimation using natural chemical and isotopic tracers across a gradient of solar radiation. *Water Resources Research, 46*.

Herman, R. (1969). Root development and height increment of Ponderosa pines in pumice soils of central Oregon (Vol. 15, pp. 226-237). Forest Science: Society of American Foresters.

Herve-Fernandez, P., Oyarzun, C., Brumbt, C., Huygens, D., Bode, S., Verhoest, N. E. C., et al. (2016). Assessing the "two water worlds' hypothesis and water sources for native and exotic evergreen species in south-central Chile. *Hydrological Processes, 30*(23), 4227-4241.

Holbrook, W. S., Riebe, C. S., Elwaseif, M., Hayes, J. L., Basler-Reeder, K., Harry, D. L., et al. (2014). Geophysical constraints on deep weathering and water storage potential in the Southern Sierra Critical Zone Observatory. *Earth Surface Processes and Landforms, 39*(3), 366-380.

Hubbert, K. R., Graham, R. C., & Anderson, M. A. (2001). Soil and weathered bedrock: Components of a Jeffrey pine plantation substrate. *Soil Science Society of America Journal, 65*(4), 1255-1262.

Hughes, C. E., & Crawford, J. (2012). A new precipitation weighted method for determining the meteoric water line for hydrological applications demonstrated using Australian and global GNIP data. *Journal of Hydrology, 464*, 344-351.

Johnson, M. S., & Lehmann, J. (2006). Double-funneling of trees: Stemflow and root-induced preferential flow. Ecoscience, 13(3), 324-333.

Kattelmann, R. C., Berg, N. H., & Rector, J. (1983). The potential for increasing streamflow from sierra-nevada watersheds. *Water Resources Bulletin, 19*(3), 395-402.

Kendall, C. (1993). *Impact of isotopic heterogeneity in shallow systems on modeling of stormflow generation*. University of Maryland University of Maryland.

Klos, P. Z., Goulden, M. L., Riebe, C. S., Tague, C. L., O'Geen, A. T., Flinchum, B. A., et al. (2018). Subsurface plant-accessible water in mountain ecosystems with a Mediterranean climate. *Wiley Interdisciplinary Reviews-Water, 5*(3).

Kurpius, M. R., Panek, J. A., Nikolov, N. T., McKay, M., & Goldstein, A. H. (2003). Partitioning of water flux in a Sierra Nevada ponderosa pine plantation. *Agricultural and Forest Meteorology, 117*(3-4), 173-192.

Landwehr, J. M., Coplen, T.B. (2006). *Line-conditioned excess: a new method for characterizing stable hydrogen and oxygen isotoperatios in hydrologic systems*. Paper presented at the Isotopes in Environmental Studies, Aquatic Forum 2004.

Lewis, D. C., & Burgy, R. H. (1964). Relationship between oak tree roots + groundwater in fractured rock as determined by tritium tracing. *Journal of Geophysical Research, 69*(12), 2579-&.

Lucas, R. G., Suárez, F., Tyler, S. W., Moran, J. E., & Conklin, M. H. (2016). Polymictic pool behaviour in a montane meadow, Sierra Nevada, CA. Hydrological Processes, 30(18), 3274-3288.

Lucas, R. (2016). *Evapotranspiration and groundwater patterns in montane meadows of the Sierra Nevada, CA*. University of California, Merced, eScholarship.

McCutcheon, R. J., McNamara, J. P., Kohn, M. J., & Evans, S. L. (2017). An evaluation of the ecohydrological separation hypothesis in a semiarid catchment. *Hydrological Processes, 31*(4), 783-799.

Meissner, M., Kohler, M., Schwendenmann, L., Holscher, D., & Dyckmans, J. (2014). Soil water uptake by trees using water stable isotopes (delta H-2 and delta O-18)-a method test regarding soil moisture, texture and carbonate. *Plant and Soil, 376*(1-2), 327-335.

Messerli, B., Viviroli, D., & Weingartner, R. (2004). Mountains of the world: Vulnerable Water Towers for the 21(st) century. *Ambio*, 29-34.

Newberry, S. L., Nelson, D. B., & Kahmen, A. (2017). Cryogenic vacuum artifacts do not affect plant water-uptake studies using stable isotope analysis. *Ecohydrology, 10*(8).

Oerter, E., Finstad, K., Schaefer, J., Goldsmith, G. R., Dawson, T., & Amundson, R. (2014). Oxygen isotope fractionation effects in soil water via interaction with cations (Mg, Ca, K, Na) adsorbed to phyllosilicate clay minerals. *Journal of Hydrology, 515*, 1-9.

Orlowski, N. (2013). Validation and application of a cryogenic vacuum extraction system for soil and plant water extraction for isotope analysis. In H. G. Frede (Ed.) (Vol. 2, pp. 179-193). *Journal of Sensors and Sensor Systems*.

Orlowski, N., Breuer, L., & McDonnell, J. J. (2016). Critical issues with cryogenic extraction of soil water for stable isotope analysis. *Ecohydrology, 9*(1), 3-10.

Orlowski, N., Pratt, D. L., & McDonnell, J. J. (2016). Intercomparison of soil pore water extraction methods for stable isotope analysis. *Hydrological Processes, 30*(19), 3434-3449.

Orlowski, N., Winkler, A., McDonnell, J. J., & Breuer, L. (2018). A simple greenhouse experiment to explore the effect of cryogenic water extraction for tracing plant source water. *Ecohydrology, 11*(5).

Oroza, C. A., Bales, R. C., Stacy, E. M., Zheng, Z. S., & Glaser, S. D. (2018). Long-Term Variability of Soil Moisture in the Southern Sierra: Measurement and Prediction. *Vadose Zone Journal, 17*(1).

Oshun, J., Dietrich, W. E., Dawson, T. E., & Fung, I. (2016). Dynamic, structured heterogeneity of water isotopes inside hillslopes. *Water Resources Research, 52*(1), 164-189.

Penna, D., Ahmad, M., Birks, S. J., Bouchaou, L., Brencic, M., Butt, S., et al. (2014). A new method of snowmelt sampling for water stable isotopes. *Hydrological Processes, 28*(22), 5637-5644.

Plummer, L. N., Busenberg, E., Bohlke, J. K., Nelms, D. L., Michel, R. L., & Schlosser, P. (2001). Groundwater residence times in Shenandoah National Park, Blue Ridge Mountains, Virginia, USA: a multi-tracer approach. *Chemical Geology, 179*(1-4), 93-111.

Roche, J. W., Goulden, M. L., & Bales, R. C. (2018). Estimating evapotranspiration change due to forest treatment and fire at the basin scale in the Sierra Nevada, California. *Ecohydrology, 11*(7).

Rose, K. L., Graham, R. C., & Parker, D. R. (2003). Water source utilization by Pinus jeffreyi and Arctostaphylos patula on thin soils over bedrock. *Oecologia, 134*(1), 46-54.

Royce, E. B., & Barbour, M. G. (2001). Mediterranean climate effects. I. Conifer water use across a Sierra Nevada ecotone. *American Journal of Botany, 88*(5), 911-918.

Saksa, P. C., Conklin, M. H., Battles, J. J., Tague, C. L., & Bales, R. C. (2017). Forest thinning impacts on the water balance of Sierra Nevada mixed-conifer headwater basins. *Water Resources Research, 53*(7), 5364-5381.

Saxena, R. K. (1986). Estimation of canopy reservoir capacity and o-18 fractionation in throughfall in a pine forest. *Nordic Hydrology, 17*(4-5), 251-260.

Shainsky, L. J., & Radosevich, S. R. (1986). Growth and water relations of pinus-ponderosa seedlings in competitive regimes with arctostaphylos-patula seedlings. *Journal of Applied Ecology, 23*(3), 957-966.

Smith, S. D., Wellington, A. B., Nachlinger, J. L., & Fox, C. A. (1991). Functional-responses of riparian vegetation to streamflow diversion in the eastern Sierra-Nevada. *Ecological Applications, 1*(1), 89-97.

Sprenger, M., Herbstritt, B., & Weiler, M. (2015). Established methods and new opportunities for pore water stable isotope analysis. *Hydrological Processes, 29*(25), 5174-5192.

Sternberg, P. D., Anderson, M. A., Graham, R. C., Beyers, J. L., & Tice, K. R. (1996). Root distribution and seasonal water status in weathered granitic bedrock under chaparral. *Geoderma, 72*(1-2), 89-98.

Stewart, M. K., Morgenstern, U., & McDonnell, J. J. (2010). Truncation of stream residence time: how the use of stable isotopes has skewed our concept of streamwater age and origin. *Hydrological Processes, 24*(12), 1646-1659.

Stone, E. L., & Kalisz, P. J. (1991). On the maximum extent of tree roots. *Forest Ecology and Management, 46*(1-2), 59-102.

Surano, K. A., Hudson, G. B., Failor, R. A., Sims, J. M., Holland, R. C., Maclean, S. C., et al. (1992). Heliuim-3 mass-spectrometry for low-level tritium analysis of environmental-samples. *Journal of Radioanalytical and Nuclear Chemistry-Articles, 161*(2), 443-453.

Swank, W. T. (1968). *The influence of rainfall interception on streamflow*. Southeastern Forest Experiment Station: USDA Forest Service.

Varhola, A., Coops, N. C., Weiler, M., & Moore, R. D. (2010). Forest canopy effects on snow accumulation and ablation: An integrative review of empirical results. *Journal of Hydrology, 392*(3-4), 219-233.

Visser, A., Thaw, M., Deinhart, A., Bibby, R., Safeeq, M., Conklin, M., et al. (2019). Cosmogenic Isotopes Unravel the Hydrochronology and Water Storage Dynamics of the Southern Sierra Critical Zone. *Water Resources Research, 55*(2), 1429-1450.

West, A. G., Patrickson, S. J., & Ehleringer, J. R. (2006). Water extraction times for plant and soil materials used in stable isotope analysis. *Rapid Communications in Mass Spectrometry, 20*(8), 1317-1321.

Widory, D., Kloppmann, W., Chery, L., Bonnin, J., Rochdi, H., & Guinamant, J. L. (2004). Nitrate in groundwater: an isotopic multi-tracer approach. *Journal of Contaminant Hydrology, 72*(1-4), 165-188.

Zhang, Z. Q., Evaristo, J., Li, Z., Si, B. C., & McDonnell, J. J. (2017). Tritium analysis shows apple trees may be transpiring water several decades old. *Hydrological Processes, 31*(5), 1196-1201.

Zheng, Z., Kirchner, P. B., & Bales, R. C. (2016). Topographic and vegetation effects on snow accumulation in the southern Sierra Nevada: a statistical summary from lidar data. *Cryosphere, 10*(1), 257-269.

Ziemer, R. R. (1964). Summer evapotranspiration trends as related to time after logging of forests in sierra nevada. *Journal of Geophysical Research, 69*(4), 615-&.

Appendix to Chapter 3

Table A3-1. Vegetation - species and sample dates.

Sample Date	Sample ID	Species
7/15/2015	IC11	(*Calocedrus decurrens*) Incense cedar
7/15/2015	IC12	(*Calocedrus decurrens*) Incense cedar
7/15/2015	IC14	(*Calocedrus decurrens*) Incense cedar
7/15/2015	IC16	(*Calocedrus decurrens*) Incense cedar
7/15/2015	IC17	(*Calocedrus decurrens*) Incense cedar
7/15/2015	JP	(*Pinus jeffreyi*) Jeffrey Pine
7/15/2015	Man1	(*Arctostaphylos patula*) Greenleaf manzanita
7/15/2015	Man2	(*Arctostaphylos patula*) Greenleaf manzanita
7/15/2015	SWT1	(*Ceanothus cordulatus*) Mountain whitethorn
7/15/2015	SWT2	(*Ceanothus cordulatus*) Mountain whitethorn
7/15/2015	WF13	(*Abies concolor*) White fir
7/15/2015	WF18	(*Abies concolor*) White fir
7/15/2015	WF19	(*Abies concolor*) White fir
8/19/2015	IC11	(*Calocedrus decurrens*) Incense cedar
8/19/2015	IC12	(*Calocedrus decurrens*) Incense cedar
8/19/2015	IC16	(*Calocedrus decurrens*) Incense cedar
8/19/2015	IC17	(*Calocedrus decurrens*) Incense cedar
8/19/2015	JP	(*Pinus jeffreyi*) Jeffrey Pine
8/19/2015	Manz1	(*Arctostaphylos patula*) Greenleaf manzanita
8/19/2015	SWT1	(*Ceanothus cordulatus*) Mountain whitethorn
8/19/2015	SWT2	(*Ceanothus cordulatus*) Mountain whitethorn
8/19/2015	WF13	(*Abies concolor*) White fir
8/19/2015	WF14	(*Abies concolor*) White fir
8/19/2015	WF18	(*Abies concolor*) White fir
8/19/2015	WF19	(*Abies concolor*) White fir
1/28/2016	IC11	(*Calocedrus decurrens*) Incense cedar
1/28/2016	JP	(*Pinus jeffreyi*) Jeffrey Pine
1/28/2016	Man	(*Arctostaphylos patula*) Greenleaf manzanita
1/28/2016	SWT	(*Ceanothus cordulatus*) Mountain whitethorn
1/28/2016	WF13	(*Abies concolor*) White fir
1/28/2016	WF14	(*Abies concolor*) White fir
1/28/2016	WF18	(*Abies concolor*) White fir
1/28/2016	WF19	(*Abies concolor*) White fir
2/11/2016	IC11	(*Calocedrus decurrens*) Incense cedar
2/11/2016	IC77	(*Calocedrus decurrens*) Incense cedar
2/11/2016	JP	(*Pinus jeffreyi*) Jeffrey Pine
2/11/2016	ManSnow	(*Arctostaphylos patula*) Greenleaf manzanita
2/11/2016	ManSun	(*Arctostaphylos patula*) Greenleaf manzanita
2/11/2016	SP	(*Pinus lambertiana*) Sugar pine
2/11/2016	WF13	(*Abies concolor*) White fir
2/11/2016	WF14	(*Abies concolor*) White fir
2/11/2016	WF18	(*Abies concolor*) White fir
2/11/2016	WF19	(*Abies concolor*) White fir
2/24/2016	IC11	(*Calocedrus decurrens*) Incense cedar
2/24/2016	IC17	(*Calocedrus decurrens*) Incense cedar
2/24/2016	JP	(*Pinus jeffreyi*) Jeffrey Pine
2/24/2016	SWT	(*Ceanothus cordulatus*) Mountain whitethorn
2/24/2016	WF13	(*Abies concolor*) White fir
2/24/2016	WF18	(*Abies concolor*) White fir

2/24/2016	WF19	(*Abies concolor*) White fir
8/9/2016	IC11	(*Calocedrus decurrens*) Incense cedar
8/9/2016	IC12	(*Calocedrus decurrens*) Incense cedar
8/9/2016	IC16	(*Calocedrus decurrens*) Incense cedar
8/9/2016	JP	(*Pinus jeffreyi*) Jeffrey Pine
8/9/2016	Man	(*Arctostaphylos patula*) Greenleaf manzanita
8/9/2016	Man	(*Arctostaphylos patula*) Greenleaf manzanita
8/9/2016	Man 3H	(*Arctostaphylos patula*) Greenleaf manzanita
8/9/2016	SWT1	(*Ceanothus cordulatus*) Mountain whitethorn
8/9/2016	SWY2	(*Ceanothus cordulatus*) Mountain whitethorn
8/9/2016	WF13	(*Abies concolor*) White fir
8/9/2016	WF14	(*Abies concolor*) White fir
8/9/2016	WF18	(*Abies concolor*) White fir
8/9/2016	WF19	(*Abies concolor*) White fir
8/9/2016	WF34_10Small	(*Abies concolor*) White fir
8/9/2016	WF3H	(*Abies concolor*) White fir
10/24/2016	IC11	(*Calocedrus decurrens*) Incense cedar
10/24/2016	JP	(*Pinus jeffreyi*) Jeffrey Pine
10/24/2016	Man	(*Arctostaphylos patula*) Greenleaf manzanita
10/24/2016	SWT	(*Ceanothus cordulatus*) Mountain whitethorn
10/24/2016	WF13	(*Abies concolor*) White fir
10/24/2016	WF18	(*Abies concolor*) White fir
11/10/2016	IC11	(*Calocedrus decurrens*) Incense cedar
11/10/2016	IC12	(*Calocedrus decurrens*) Incense cedar
11/10/2016	JP	(*Pinus jeffreyi*) Jeffrey Pine
11/10/2016	WF13	(*Abies concolor*) White fir
11/10/2016	WF18	(*Abies concolor*) White fir

Table A3-2. Sample locations for major California rivers sampled for ^{3}H.

River	Latitude	Longitude
Kings	36.87907011	-119.1514826
Kaweah	36.41164033	-118.9394584
Tule	36.1345304	-118.8104271
San Joaquin	37.072849	-119.562091
Merced	37.605005	-119.967136
Tuolumne	37.87695235	-120.2951532
Stanislaus	38.13673355	-120.3731061
Mokelumne	38.31142667	-120.721651
Kern	35.75448822	-118.4232964
Cosumnes	38.55073476	-120.8499863
Yuba	39.22077275	-121.3343129
SF American	38.77104124	-120.4484441
Merced	37.610651	-120.135162
SF American (Coloma)	38.80057879	-120.8890236
NF Feather	39.79255715	-121.4523101
Feather (Oroville)	39.49752525	-121.579564
MF Feather	39.66097961	-121.3032316
NF American	38.91563683	-121.0402699

Table A3-3. Cryogenic Vacuum Distillation trial results.

Sample Name	average (‰) in δ^2H	Standard deviation	Difference (‰)	Sample Description	Water Recovery
DI soil extraction	-97.52	0.12	-	DI water used to wet soils	100%
soil extraction 1	-102.56	0.16	-5.04	soil + 10g water	100%
soil extraction 2	-103.99	0.11	-6.47	soil + 10g water	95%
soil extraction 3	-110.10	0.47	-12.58	soil + 10g water	100%
soil extraction 4	-98.38	0.12	-0.86	soil + 5g water	100%
soil extraction 5	-96.76	0.51	0.76	soil + 5g water	100%
soil extraction 6	-96.03	0.29	1.49	soil + 5g water	-
soil extraction 7	-96.18	0.04	1.35	10g water only	-
soil extraction 8	-95.95	0.30	1.57	10g water only	-

Table A3-4. Xylem samples $\delta^{18}O$ and $\delta^{2}H$, slope (FC-Slope) used for individual fractionation compensation calculations and resulting fractionation-compensated $\delta^{18}O$ and $\delta^{2}H$ values ($\delta^{18}O$ (FC)) and $\delta^{2}H$ (FC).

Sample Date	Sample ID	$\delta^{18}O$ (‰)	$\delta^{2}H$ (‰)	FC - Slope	$\delta^{18}O$ (FC) (‰)	$\delta^{2}H$ (FC) (‰)
1/28/2016	IC11	-10.4	-77.9	3.3	-10.6	-78.4
1/28/2016	Man	-10.8	-94.0	3.3	-15.2	-108.4
1/28/2016	SWT	-9.7	-74.8	3.3	-10.4	-77.4
1/28/2016	WF14	-11.7	-90.8	3.3	-13.3	-96.1
1/28/2016	WF19	-10.7	-83.8	3.2	-12.1	-88.3
2/11/2016	WF13	-14.2	-107.4	3.2	-15.9	-112.8
2/11/2016	IC11	-10.2	-77.4	3.2	-10.7	-78.9
2/11/2016	JP	-10.6	-78.0	3.2	-10.6	-78.0
2/11/2016	IC77	-11.6	-85.0	3.2	-11.6	-85.2
2/11/2016	Man1	-11.7	-98.0	3.2	-15.5	-110.2
2/11/2016	Man2	-10.8	-81.1	3.2	-11.2	-82.3
2/11/2016	WF14	-9.2	-73.6	3.2	-10.5	-77.7
2/24/2016	JP	-11.7	-86.2	3.2	-11.9	-87.1
2/24/2016	IC11	-11.8	-85.9	3.2	-11.8	-85.9
2/24/2016	IC17	-13.7	-96.9	3.2	-13.7	-96.9
2/24/2016	WF19	-13.3	-98.1	3.2	-13.9	-99.8
2/24/2016	WF18	-10.1	-78.8	3.2	-11.2	-82.1
7/15/2015	WF13	-10.8	-82.6	3.0	-11.6	-85.0
7/15/2015	IC12	-9.1	-75.1	3.0	-10.9	-80.6
7/15/2015	IC17	-10.7	-86.7	3.0	-12.9	-93.2
7/15/2015	WF18	-8.3	-80.1	3.0	-13.0	-94.3
7/15/2015	IC11	-9.1	-71.6	3.0	-9.9	-74.1
7/15/2015	JP15	-10.1	-78.5	3.0	-11.1	-81.4
7/15/2015	IC14	-8.7	-72.8	3.0	-10.6	-78.6
7/15/2015	WF19	-9.7	-83.0	3.0	-12.7	-91.9
7/15/2015	Man1	-6.2	-69.8	3.0	-11.9	-86.9
7/15/2015	Man2	-9.5	-83.5	3.0	-13.0	-93.9
7/15/2015	IC16	-8.6	-68.4	3.0	-9.5	-71.0
7/15/2015	SWT1	-9.2	-78.7	3.0	-11.9	-86.7
7/15/2015	SWT2	-8.3	-73.7	3.0	-11.2	-82.5
8/19/2015	IC11	-11.3	-88.0	3.0	-12.7	-92.2
8/19/2015	IC12	-9.5	-75.3	3.0	-10.7	-78.8
8/19/2015	IC16	-10.5	-78.3	3.0	-10.7	-78.8
8/19/2015	IC17	-10.6	-82.9	3.0	-11.9	-86.6
8/19/2015	Manz1	-11.2	-93.6	3.0	-14.4	-103.1
8/19/2015	JP	-10.2	-76.0	3.0	-10.3	-76.5
8/19/2015	SWT1	-9.7	-75.3	3.0	-10.5	-77.7
8/19/2015	SWT2	-7.2	-72.7	3.0	-11.9	-86.7
8/19/2015	WF13	-11.3	-82.2	3.0	-11.3	-82.2
8/19/2015	WF18	-10.3	-86.5	3.0	-13.1	-95.0
8/19/2015	WF19	-9.6	-83.1	3.0	-12.8	-92.5
8/9/2016	Man	-10.4	-89.3	2.9	-13.7	-98.8
8/9/2016	Man	-10.7	-89.0	2.9	-13.4	-97.0
8/9/2016	SWT1	-11.6	-93.0	2.9	-13.8	-99.2
8/9/2016	WF14	-10.9	-86.7	2.9	-12.6	-91.8
8/9/2016	IC16	-12.4	-95.2	2.9	-13.8	-99.4
8/9/2016	JP	-12.0	-89.4	2.9	-12.5	-90.8
8/9/2016	WF18	-11.4	-85.6	2.9	-11.9	-87.0

8/9/2016	WF13	-11.3	-82.3	2.9	-11.3	-82.3
8/9/2016	IC11	-11.3	-83.7	2.9	-11.5	-84.4
8/9/2016	WF34_10Small	-12.5	-83.0	2.9	-12.5	-83.1
8/9/2016	IC12	-11.3	-83.1	2.9	-11.3	-83.2
8/9/2016	Man 3H	-10.7	-87.0	2.9	-12.9	-93.2
8/9/2016	WF3H	-10.3	-83.5	2.9	-12.3	-89.3
8/9/2016	SWY2	-11.5	-91.5	2.9	-13.4	-97.0
8/9/2016	WF19	-10.1	-77.0	2.9	-10.6	-78.2
10/24/2016	IC11	-10.7	-80.8	3.1	-11.2	-82.2
10/24/2016	WF13	-7.4	-58.1	3.1	-7.5	-58.3
10/24/2016	JP	-10.1	-79.0	3.1	-11.2	-82.4
10/24/2016	SWT	-7.1	-66.2	3.1	-10.3	-76.2
10/24/2016	Man	-4.8	-57.9	3.1	-9.8	-73.4
10/24/2016	WF18	-8.8	-70.4	3.1	-9.9	-73.9
11/10/2016	WF13	-10.1	-76.9	3.3	-10.6	-78.7
11/10/2016	IC11	-8.8	-66.6	3.3	-8.8	-66.5
11/10/2016	IC12	-9.2	-69.4	3.3	-9.3	-69.6
11/10/2016	JP	-9.8	-73.9	3.3	-10.0	-74.4
11/10/2016	WF18	-9.3	-70.4	3.3	-9.5	-71.2

Table A3-5. Monthly mean temperatures and relative humidity values used to calculate slopes for fractionation compensation calculations. Temperature and humidity values from the P301 flux tower were used.

Year	Month	Mean Temperature (Kelvin)	Mean Relative Humidity	Slope
2015	1	281	0.37	3.2
2015	2	281	0.49	3.2
2015	3	282	0.52	3.2
2015	4	280	0.56	3.2
2015	5	282	0.65	3.2
2015	6	291	0.37	3.0
2015	7	290	0.51	3.0
2015	8	292	0.34	3.0
2015	9	290	0.35	3.0
2015	10	287	0.37	3.1
2015	11	282	0.41	3.2
2015	12	278	0.51	3.3
2016	1	277	0.47	3.3
2016	2	282	0.31	3.2
2016	3	279	0.58	3.3
2016	4	280	0.52	3.2
2016	5	283	0.59	3.2
2016	6	291	0.37	3.0
2016	7	293	0.32	2.9
2016	8	292	0.30	2.9
2016	9	288	0.36	3.0
2016	10	286	0.48	3.1
2016	11	278	0.43	3.3
2016	12	276	0.44	3.3

Table A3-6. Southern Sierra P301 stream and meadow saturated zone $\delta^{18}O$ and $\delta^{2}H$ values.

Date	Sampling Location	$\delta^{18}O$ (‰)	$\delta^{2}H$ (‰)
2/4/2015	P301 Culvert	-12.0	-83.2
3/4/2015	P301 Culvert	-12.3	-84.0
4/2/2015	P301 Culvert	-11.8	-82.3
5/8/2015	P301 Culvert	-11.6	-82.5
6/7/2015	P301 Culvert	-11.4	-81.3
7/7/2015	P301 Culvert	-11.8	-83.2
8/7/2015	P301 Culvert	-11.7	-81.3
10/12/2015	P301 Culvert	-11.8	-81.5
10/21/2015	P301 Culvert	-11.7	-82.0
12/4/2015	P301 Culvert	-12.0	-82.9
1/13/2016	P301 Culvert	-12.1	-83.3
2/7/2016	P301 Culvert	-12.2	-83.6
3/2/2016	P301 Culvert	-12.0	-83.5
4/6/2016	P301 Culvert	-11.8	-80.7
5/4/2016	P301 Culvert	-12.1	-81.6
5/21/2016	P301 Culvert	-11.6	-82.2
7/2/2016	P301 Culvert	-12.0	-83.0
8/1/2016	P301 Culvert	-11.9	-81.6
9/8/2016	P301 Culvert	-12.0	-80.9
10/2/2016	P301 Culvert	-12.0	-81.0
11/4/2016	P301 Culvert	-11.8	-80.0
12/3/2016	P301 Culvert	-12.0	-82.1
2/1/2017	P301 Culvert	-13.1	-90.4
3/27/2017	P301 Culvert	-12.9	-93.1
5/9/2017	P301 Culvert	-11.8	-81.5
5/31/2017	P301 Culvert	-11.9	-81.8
7/6/2017	P301 Culvert	-12.0	-82.5
8/3/2017	P301 Culvert	-12.1	-84.0
8/27/2017	P301 Culvert	-12.1	-83.5
10/21/2015	Meadow	-12.1	-84.5
5/4/2016	Meadow	-12.2	-83.9
6/24/2016	Meadow	-12.3	-83.9
8/1/2016	Meadow	-12.6	-84.5
8/5/2016	Meadow	-12.6	-84.5
8/15/2016	Meadow	-12.6	-84.5
8/21/2016	Meadow	-12.4	-84.7
10/2/2016	Meadow	-12.5	-84.4
10/20/2016	Meadow	-12.6	-86.4
3/3/2017	Meadow	-12.3	-84.5
6/1/2017	Meadow	-12.4	-85.2
8/4/2017	Meadow	-12.2	-85.1
8/16/2017	Meadow	-12.5	-85.5
10/12/2017	Meadow	-12.2	-84.7

Table A3-7. Tritium concentrations in CZO P301 precipitation, vegetation and meadow saturated zone.

Collection Date	Sample	^{3}H (pCi/L)	Error (pCi/L)[1]
2/4/2015	P301 Precip	14.20	0.60
3/6/2015	P301 Precip	14.40	0.60
4/2/2015	P301 Precip	11.40	0.50
5/8/2015	P301 Precip	23.60	1.00
6/17/2015	P301 Precip	35.00	1.50
10/21/2015	P301 Precip	17.50	0.70
11/5/2015	P301 Precip	11.80	0.70
12/4/2015	P301 Precip	31.50	1.20
12/23/2015	P301 Precip	7.80	0.40
1/12/2016	P301 Precip	8.30	0.40
2/19/2016	P301 Precip	9.20	0.40
3/5/2016	P301 Precip	7.00	0.30
3/6/2016	P301 Precip	5.70	0.30
4/6/2016	P301 Precip	8.40	0.40
5/23/2016	P301 Precip	17.30	0.80
10/20/2016	P301 Precip	3.50	0.40
11/10/2016	P301 Precip	5.90	0.40
1/6/2017	P301 Precip	9.20	0.50
1/6/2017	P301 Precip	7.90	0.60
2/1/2017	P301 Precip	4.90	0.30
3/2/2017	P301 Precip	11.80	0.60
6/1/2017	P301 Precip	11.50	0.50
6/1/2017	P301 Precip	13.20	0.50
8/19/2015	White Fir	30.06	1.41
8/19/2015	White Fir	15.11	2.41
8/19/2015	Incense Cedar	19.47	0.68
8/19/2015	Sierra White Thorn	23.01	1.15
8/19/2015	Manzanita	20.64	1.01
2/11/2016	White fir	14.88	0.64
2/11/2016	Incense Cedar	16.83	1.18
8/9/2016	White fir	14.96	0.77
8/9/2016	Greenleaf manzanita	12.78	0.58
8/9/2016	Incense Cedar	13.47	0.76
08/19/15	Meadow	7.96	0.41
08/19/15	Meadow	6.89	0.41
10/12/15	Meadow	6.77	0.33
12/04/15	Meadow	7.03	0.50
05/04/16	Meadow	6.73	0.32
08/21/16	Meadow	5.54	0.24
10/02/16	Meadow	6.42	0.52

[1] Instrument error.

Table A3-8. Soil stable isotope values, cryogenic vacuum efficiency, total soil moisture and corrected $\delta^{18}O$ values shown in Figure 7 and Figure A3-3 for three sample dates from soil surface to bedrock. Soil samples were collected from P301 at the Southern Sierra Critical Zone Observatory.

Collection Date	$\delta^{18}O$ (‰)	$\delta^{2}H$ (‰)	**Depth (cm)**	**Gravimetric Soil Moisture**	**Extraction Efficiency**	$\delta^{18}O$ (‰) (corrected)
8/9/2016	-3.8	-51.4	-5	0.033	89	NA
8/9/2016	-10.1	-80.3	-15	0.044	99	NA
8/9/2016	-13.5	-92.8	-25	0.043	99	NA
8/9/2016	-14.5	-97.4	-35	0.041	100	NA
8/9/2016	-15.5	-99.9	-45	0.039	98	NA
8/9/2016	-14.7	-101.3	-55	0.043	98	NA
8/9/2016	-15.0	-101.3	-65	0.044	99	NA
8/9/2016	-15.1	-99.2	-75	0.038	100	NA
8/9/2016	-15.0	-96.4	-85	0.038	99	NA
8/9/2016	-14.5	-100.0	-95	0.037	97	NA
8/9/2016	-14.3	-100.5	-125	0.039	99	NA
8/9/2016	-	-96.4	-150	0.046	100	NA
8/9/2016	-11.7	-86.7	-175	0.030	100	NA
8/9/2016	-14.9	-116.3	-200	0.056	99	NA
8/9/2016	-14.9	-113.1	-250	0.056	99	NA
8/19/2015	-10.6	-79.9	-7.5	-	-	-5.7
8/19/2015	-14.6	-101.7	-18.5	0.091	74	-9.7
8/19/2015	-16.7	-104.8	-27	0.090	71	-11.8
8/19/2015	-19.0	-111.6	-36.5	0.085	73	-14.1
8/19/2015	-18.8	-112.5	-46.5	0.077	74	-13.9
8/19/2015	-18.1	-110.3	-57	0.074	80	-13.2
8/19/2015	-18.4	-120.1	-67	0.074	75	-13.5
8/19/2015	-18.8	-118.9	-77	0.076	77	-13.9
8/19/2015	-18.6	-118.7	-87	0.071	77	-13.7
8/19/2015	-17.6	-116.3	-97	0.068	83	-12.7
8/19/2015	-19.3	-126.0	-100	0.074	86	-14.4
8/19/2015	-17.2	-109.0	-200	0.099	79	-12.3
8/19/2015	-19.9	-124.5	-300	0.053	75	-15.0
8/19/2015	-19.8	-130.2	-400	0.086	74	-14.9
8/19/2015	-20.8	-123.1	-425	0.073	76	-15.9
7/15/2015	-16.4	-104.4	-20	0.096	74	-11.9
7/15/2015	-16.4	-89.2	-25	0.123	72	-11.9
7/15/2015	-17.4	-101.9	-35	0.125	78	-12.9
7/15/2015	-19.0	-111.8	-45	0.091	80	-14.5
7/15/2015	-19.5	-123.0	-55	0.081	84	-15.0
7/15/2015	-19.6	-127.4	-65	-	-	-15.1
7/15/2015	-19.9	-127.8	-75	0.080	81	-15.4
7/15/2015	-19.7	-130.5	-85	0.071	84	-15.2
7/15/2015	-17.1	-112.0	-200	0.107	83	-12.6
7/15/2015	-17.7	-112.4	-247	0.077	81	-13.2

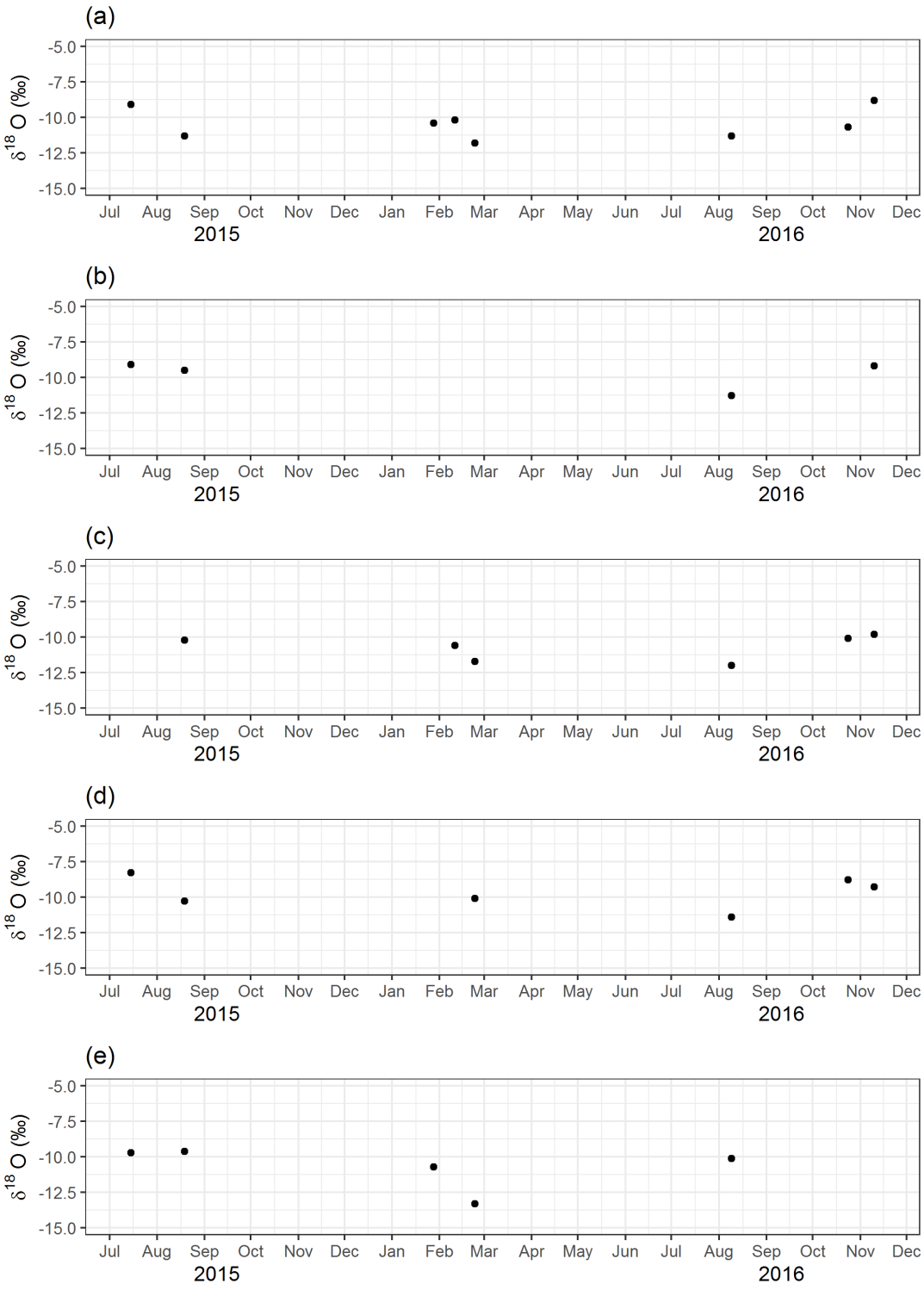

Figure A3-1. Individual shrubs and tree $\delta^{18}O$ values over time, (a) Incense Cedar 11 (IC11), (b), Incense Cedar 12 (IC12), (c) Jeffrey Pin (JP), (d) White fir 18 (WF18), (e) White fir 19 (WF19). Cont. next page.

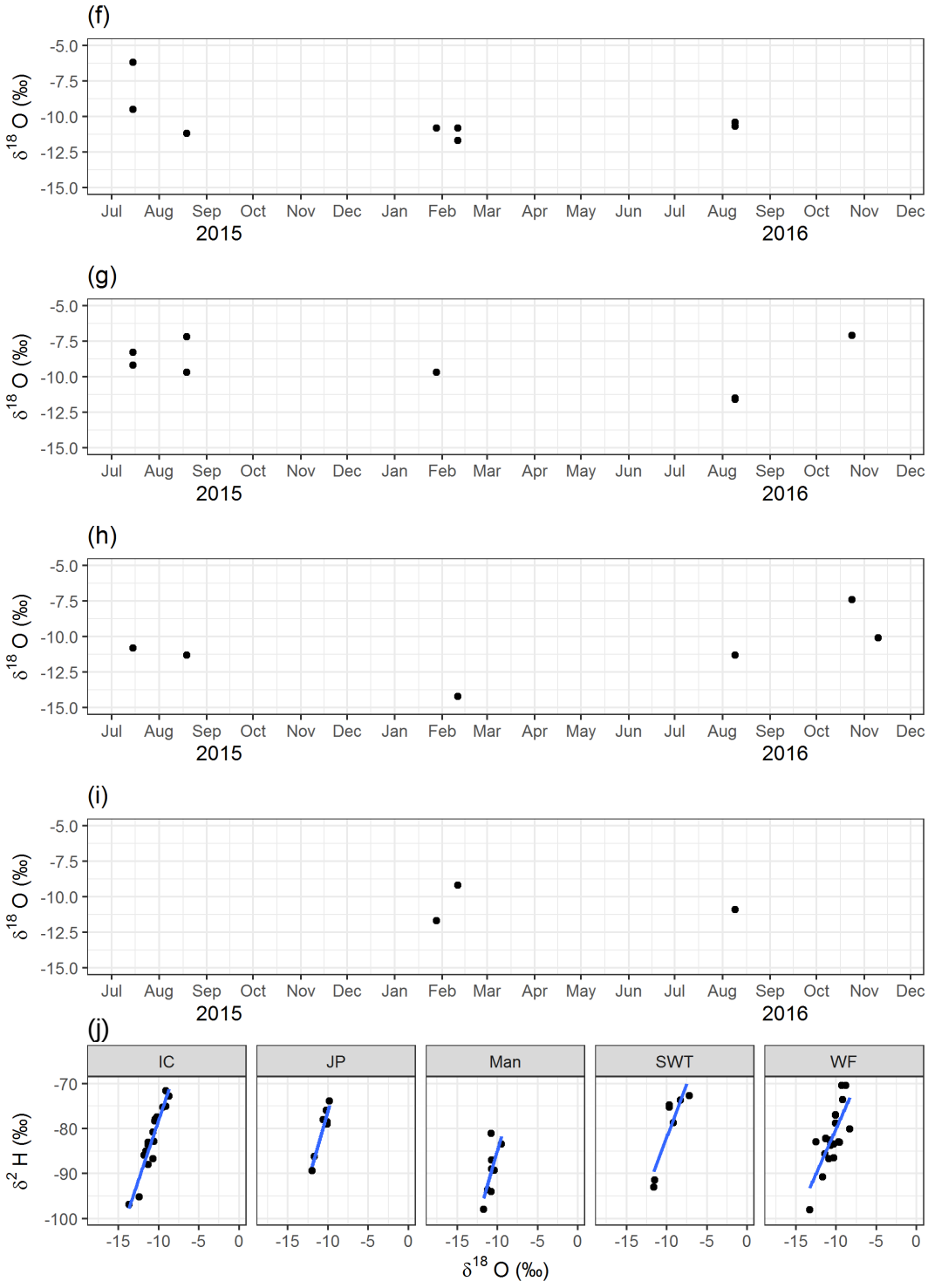

Figure A3-1. cont. Individual shrubs and tree $\delta^{18}O$ values over time (f) Manzanita, (g) Sierra White Thorn (SWT), (h) White fir 13 (WF13), (i) White fir 14 (WF14) and (j) dual-isotope plots of vegetation categorized by species.

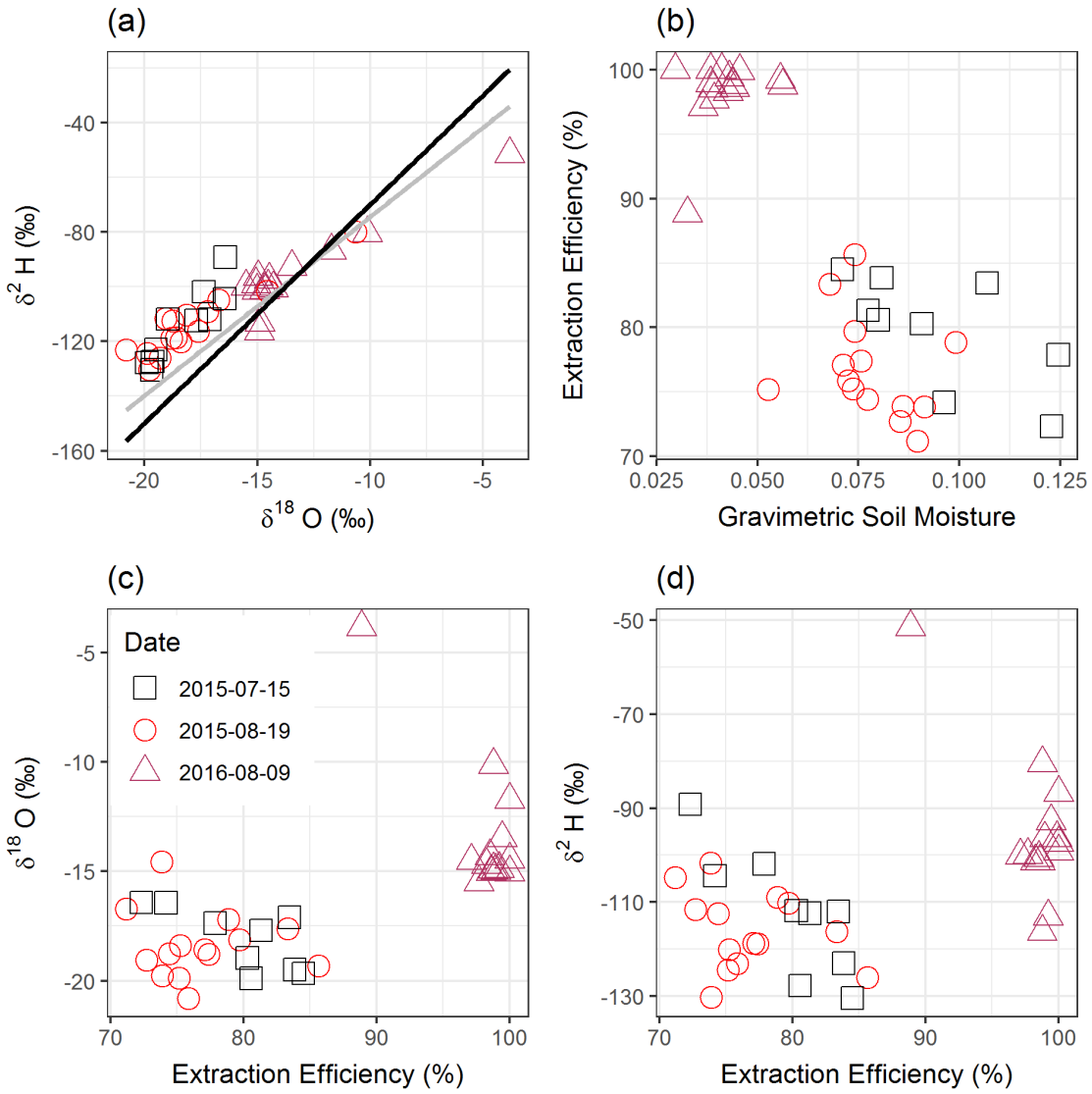

Figure A3-2. Soil water isotopic signatures, gravimetric soil moisture and extraction efficiency represented for each sampling date: soils sampled 2015-07-15 (squares), soils sampled 2015-08-19 (circles) and soils sampled on 2016-08-09 (triangles). Soils sampled on 2016-08-09 were heated to 100 °C during extraction and sampled from 2015-07-15 and 2015-0819 were not heated during extraction. (a) Soil stable isotope signatures in dual-isotope space. Black line is the Global Meteoric Water Line and the grey line is the Local Meteoric Water Line. (b) Gravimetric soil moisture and soil water extraction efficiency (percent of total soil moisture extracted during cryogenic vacuum distillation). (c) Extraction efficiency and $\delta^{18}O$ values and (d) extraction efficiency and $\delta^{2}H$ values. All values are listed in Table A3-7.

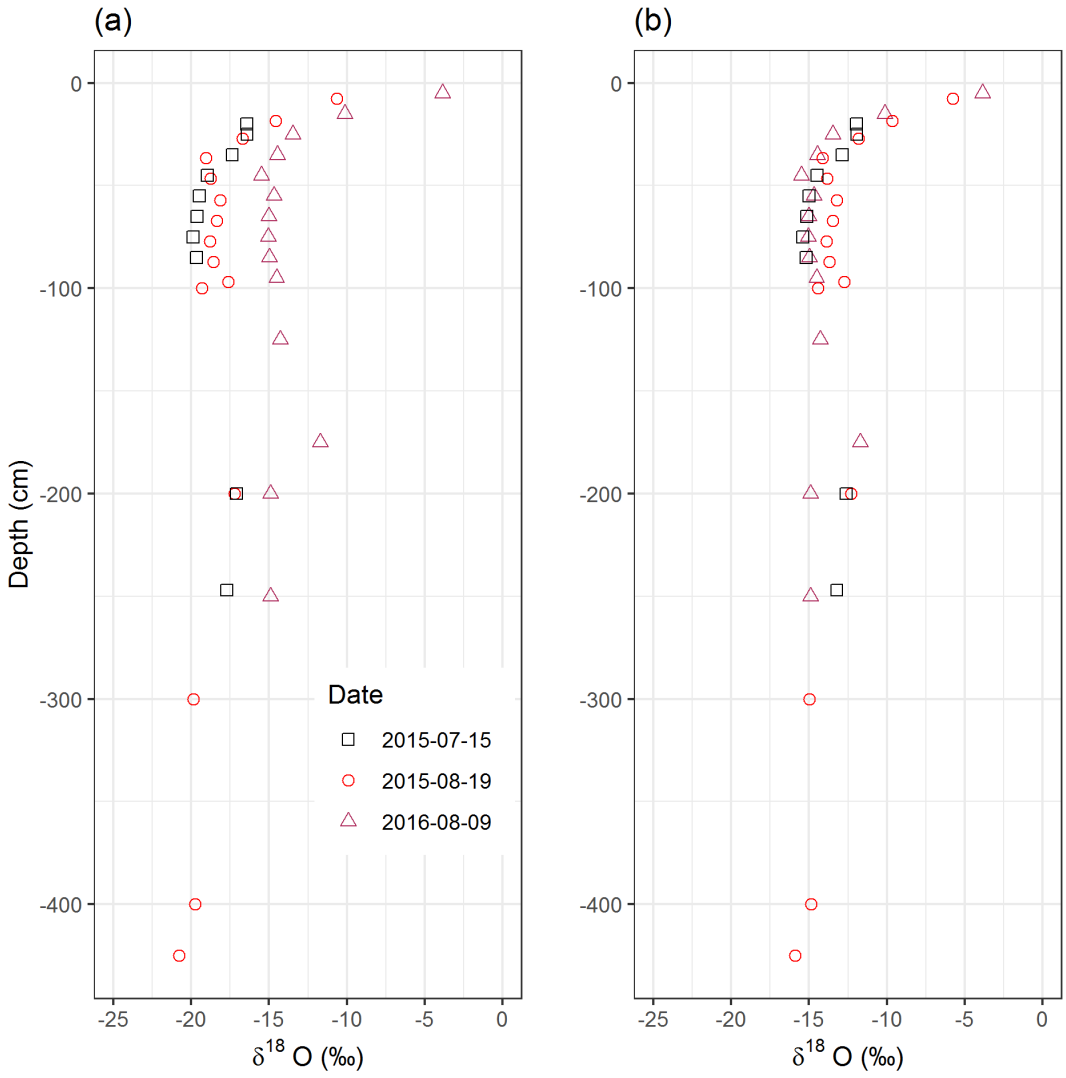

Figure A3-3. Soil water $\delta^{18}O$ values at sampling depth below ground surface from three sampling dates: 2015-07-15 (squares), 2015-08-19 (circles) and 2016-08-09 (triangles); soil samples in 2015 were not heated during cryogenic vacuum distillation and soil samples in 2016 were heated to 100 °C. (a) shows raw $\delta^{18}O$ values and (b) shows corrected 2015 $\delta^{18}O$ values. July 2015 values were shifted by 4.9 ‰ and August 2015 values were shifted by 4.5 ‰. Values are listed in Table A7.

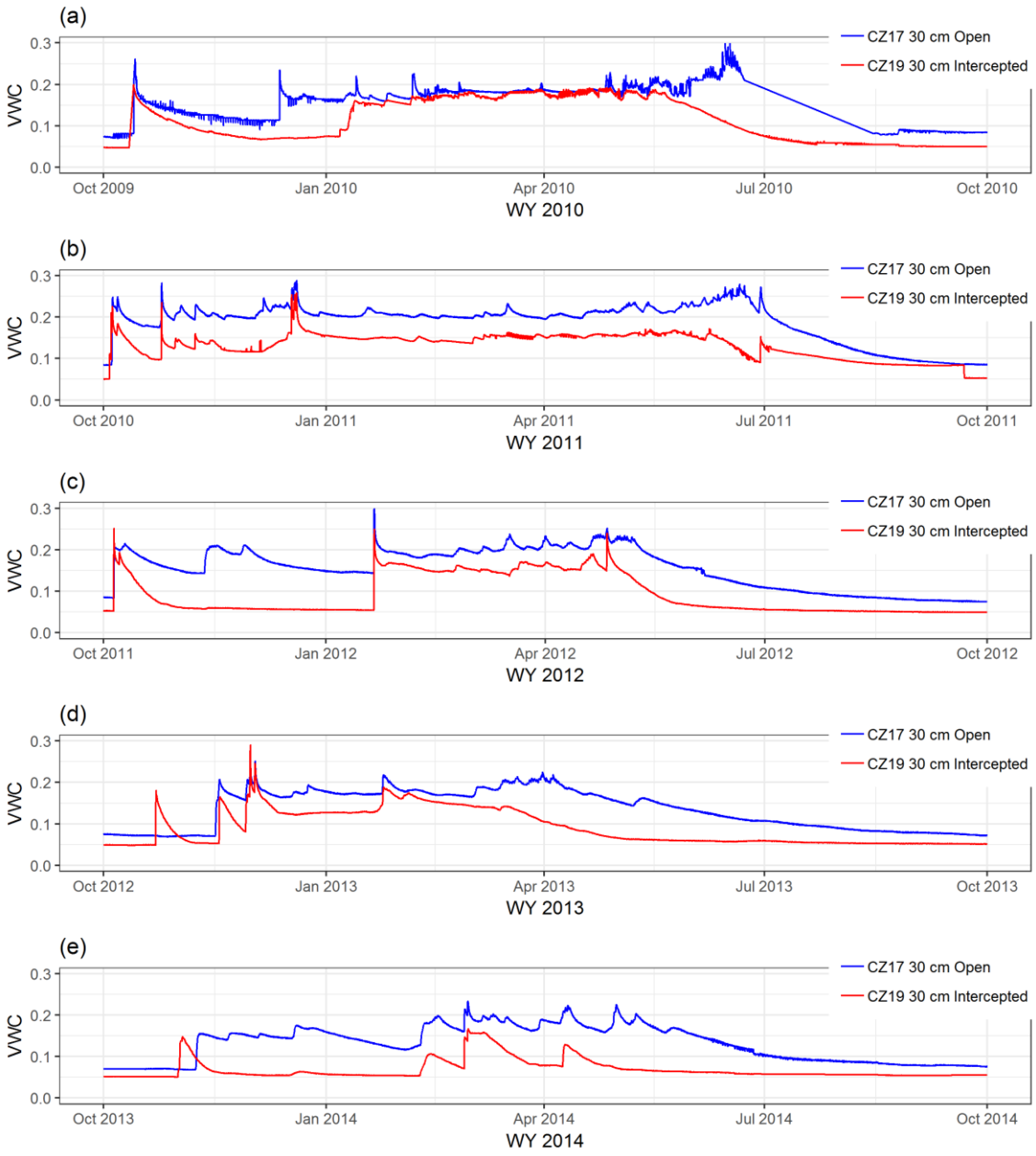

Figure A3-4. Southern Sierra Critical Zone Observatory P301 Volumetric Water Content (VWC) from sensors located in forest gap (CZ-17) and beneath canopy (intercepted) (CZ-19) at 30 cm depth in (a) 2010, (b) 2011, (c) 2012, (d) 2013 and (e) 2014. At 30 cm depth soil moisture is generally higher in forest gaps compared to beneath forest canopy. This pattern was consistent between drought years and years that received heavy snow, for example, WY 2011 received heavy snow and WY 2014 experienced snow drought. During both years, VWC was higher in forest gaps than beneath forest canopy.

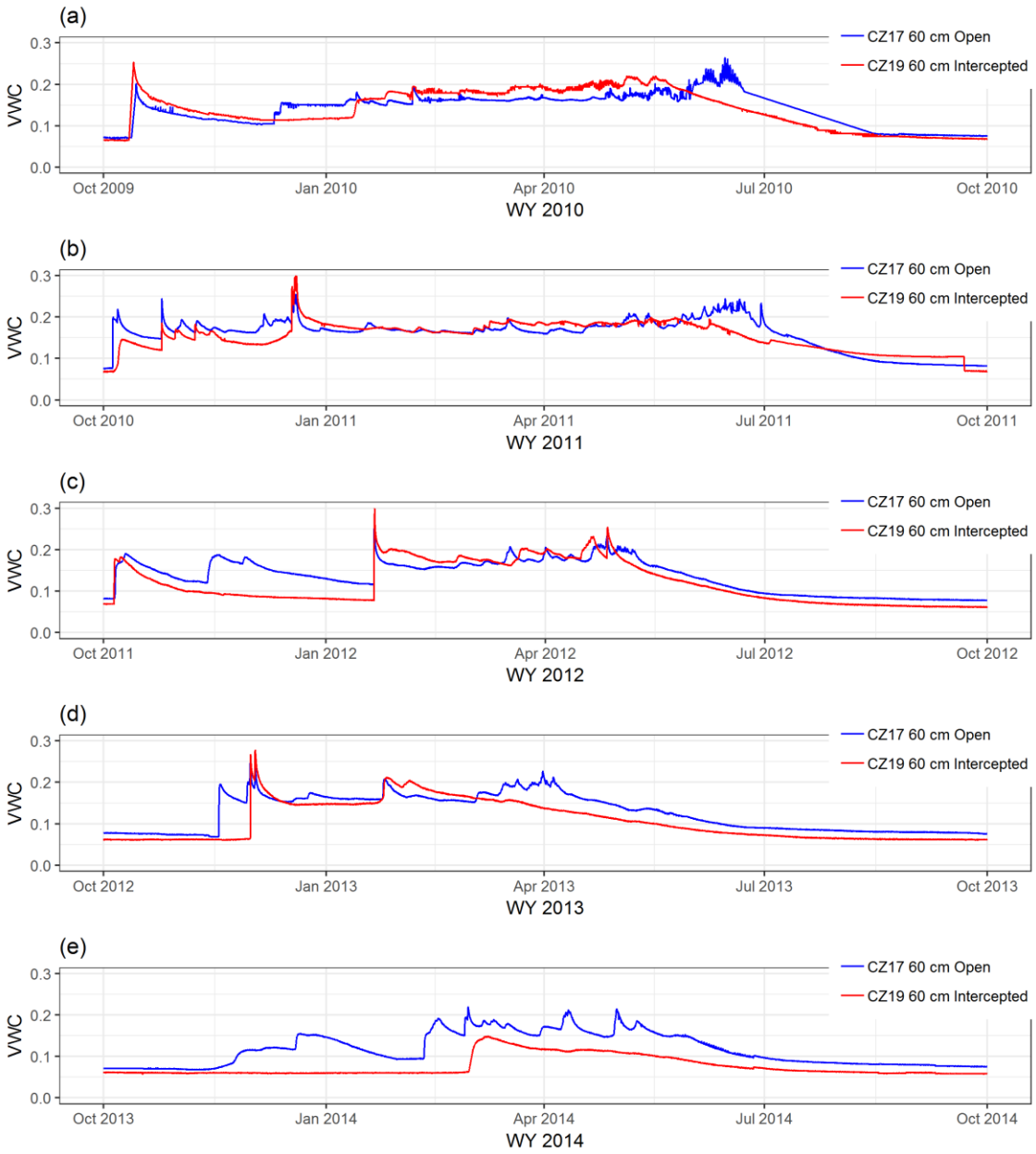

Figure A3-5. Southern Sierra Critical Zone Observatory P301 Volumetric Water Content (VWC) from sensors located in forest gap (CZ17) and beneath canopy (intercepted) (CZ19) at 60 cm depth in (a) 2010, (b) 2011, (c) 2012, (d) 2013 and (e) 2014. At 60 cm soil moisture is similar in forest gaps compared to open areas, but is slightly higher in open areas during spring 2010, 2012, 2013 and 2014. In 2014, which was a snow drought, soil moisture was higher in forest gaps compared to beneath canopy.

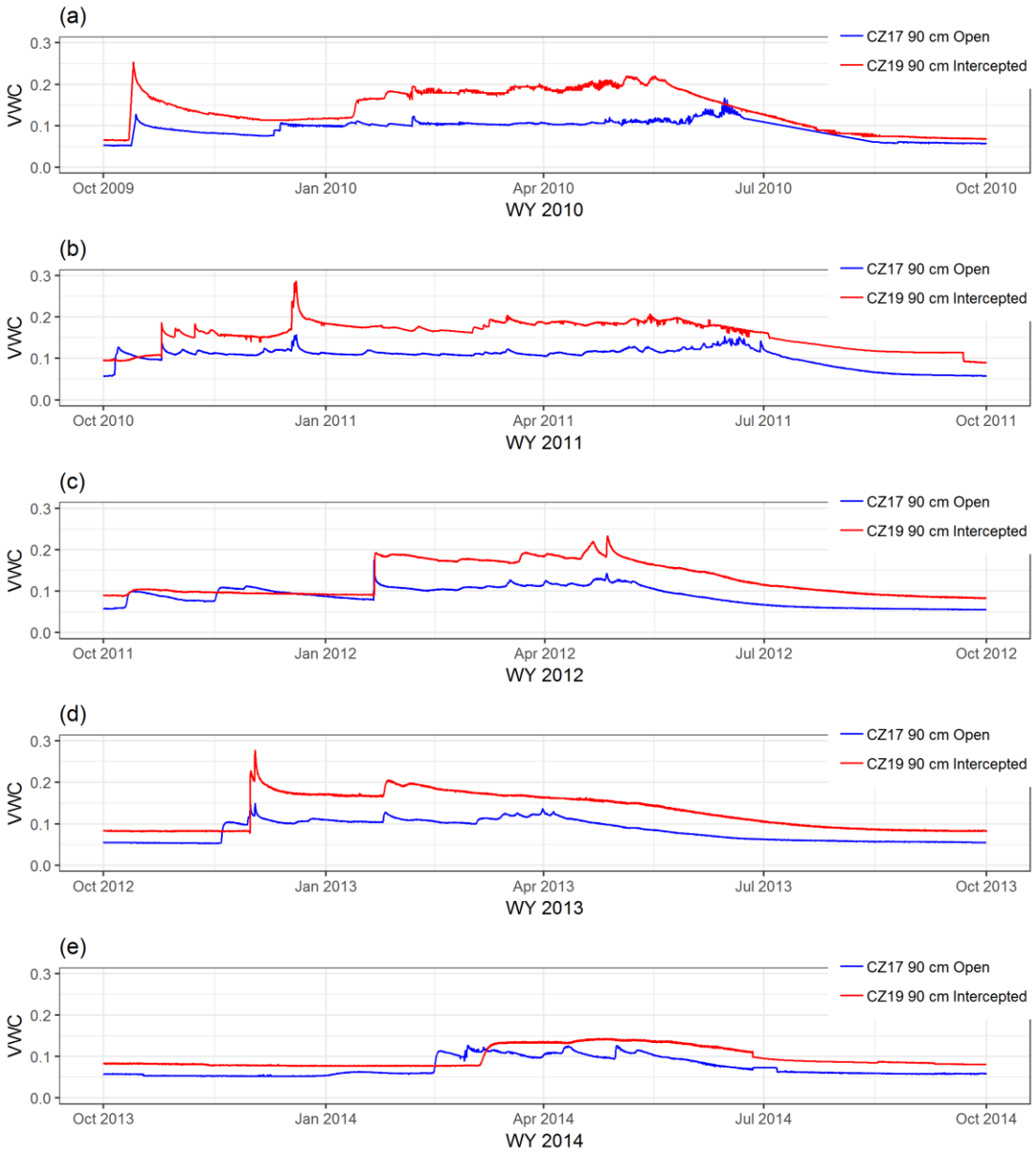

Figure A3-6. Southern Sierra Critical Zone Observatory P301 Volumetric Water Content (VWC) from sensors located in forest gap (CZ-17) and beneath canopy (intercepted) (CZ-19) at 90 cm depth in (a) 2010, (b) 2011, (c) 2012, (d) 2013 and (e) 2014. At 90 cm in all years, soil moisture was generally higher beneath forest canopy compared to forest gaps. This pattern was consistent across very wet years (WY 2011) and dry years (WY 2014).

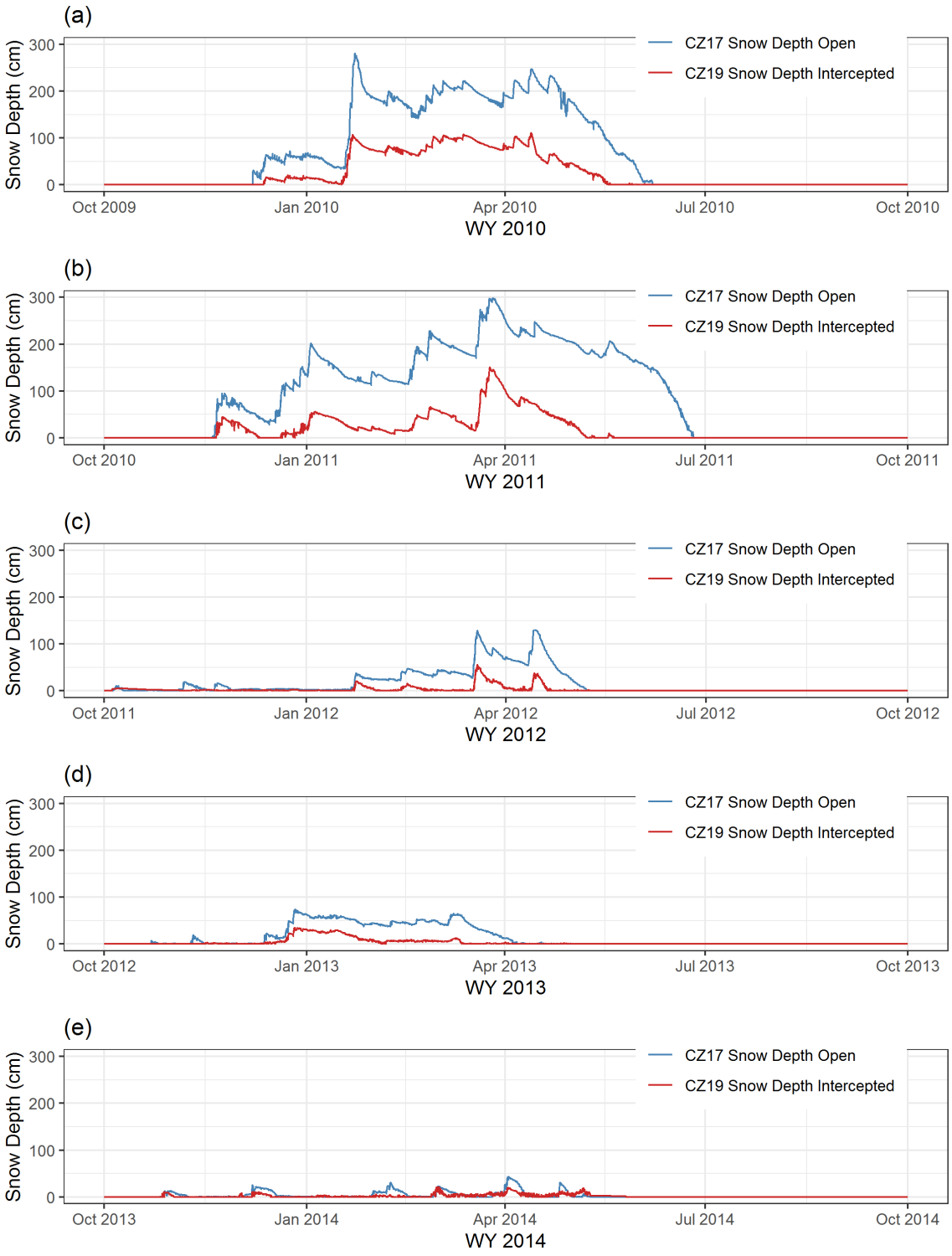

Figure A3-7. Southern Sierra Critical Zone Observatory P301 snow depth from sensors located in forest gap (CZ-17) and beneath canopy (intercepted) (CZ-19) in (a) 2010, (b) 2011, (c) 2012, (d) 2013 and (e) 2014. Snow depth is generally higher in open areas than beneath canopy, with differences increased during years with heavy snow. The snowmelt rate is generally similar in open areas compared to beneath forest canopy.

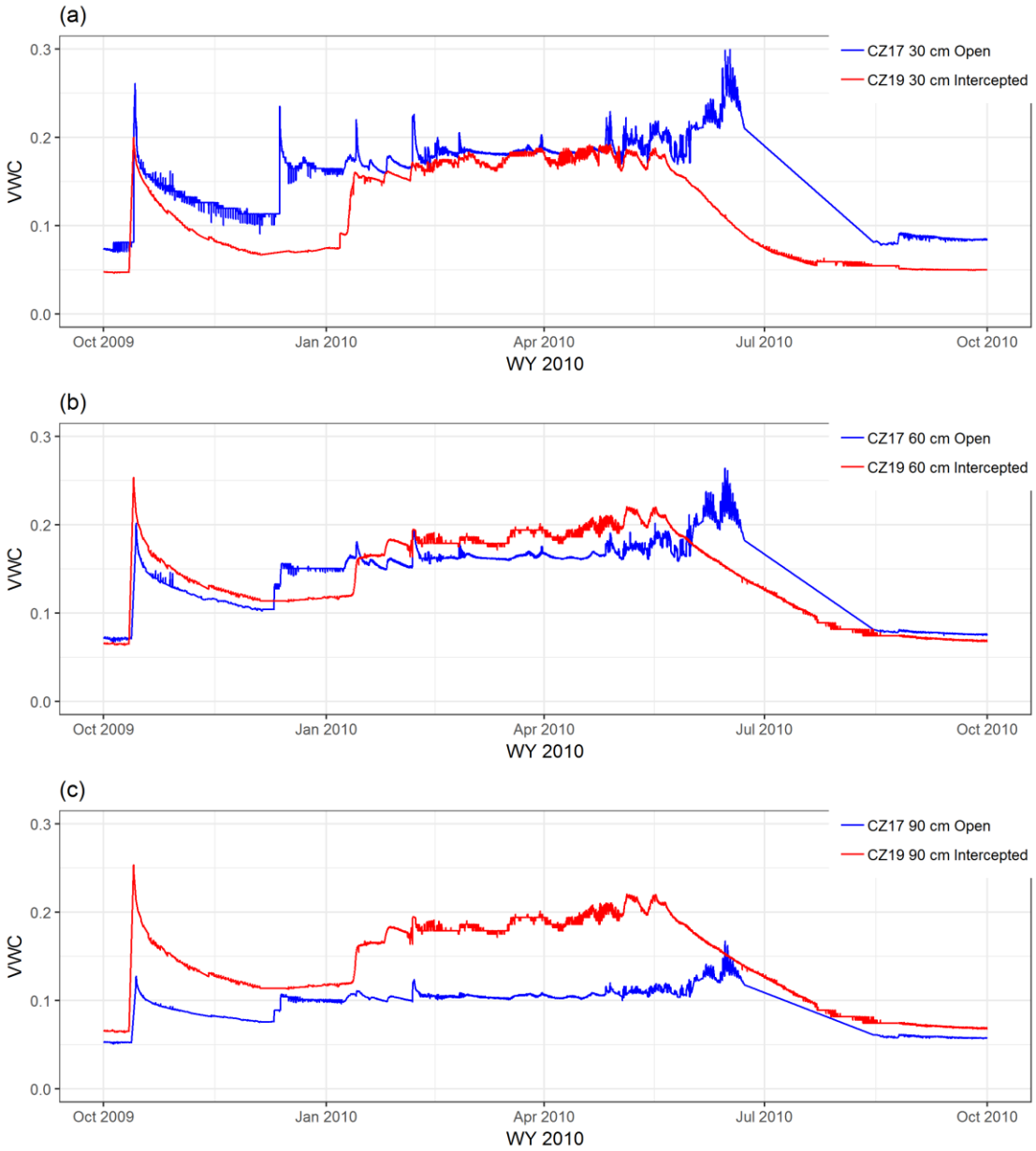

Figure A3-8. Southern Sierra Critical Zone Observatory P301 Volumetric Water Content (VWC) from sensors located in forest gap (CZ-17) and beneath canopy (intercepted) (CZ-19) at (a) 30 cm, (b) 60 cm and (c) 90 cm during WY 2010, which received a similar amount of winter precipitation as WY 2016, when winter vegetation samples were collected. At 30 cm (a) VWC is higher in the forest gap, at 60 cm (b) VWC is slightly lower in the forest gap, and at 90 cm VWC is even lower in the forest gap (c). This figure shows that near the surface open area soil moisture is higher but at deeper depths, soil moisture is higher beneath the canopy.

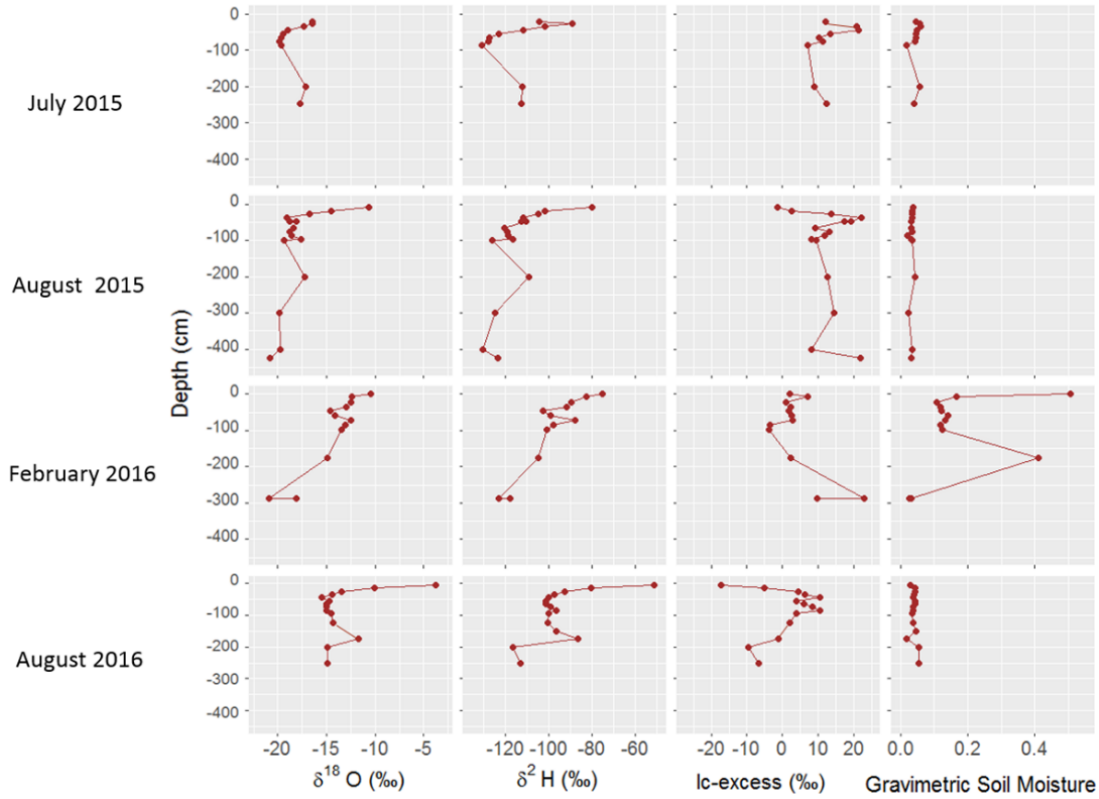

Figure A3-9. Soil $\delta^{18}O$, $\delta^{2}H$, lc-excess and gravimetric soil moisture from July 2015, August 2015, February 2016 and August 2016 are plotted at the mean sample depth for each respective sample. Volume weighted P301 LMWL was used to calculate lc-excess.

Chapter 4

Sierra Nevada river source elevation using stable isotope lapse rates

Melissa Thaw[1,2], Ate Visser[2], Joseph Rungee[1] and Martha Conklin[1]

[1]University of California, Merced; mthaw@ucmerced.edu

[2]Lawrence Livermore National Laboratory

Abstract

Sierra Nevada rivers provide the majority of California water resources, as many montane rivers provide the majority of water resources around the world. Elevational differences in precipitation, evapotranspiration and subsurface storage across the Sierra Nevada cause complex critical zone heterogeneities that can be difficult to untangle on the mountain range scale. We systematically determined Sierra Nevada river source elevations using water stable isotope data and confirmed these results through an independent spatially distributed mass balance approach. Based on water stable isotope data, we found that Sierra Nevada river water originated from a mean source elevation of 2.5 (± 0.7) km in 2017 during spring runoff. Based on the mass balance approach, the mean water source elevation was 2.2 (± 0.5). Individually, river water originated above their mean hypsometric catchment elevation and generally all river water originated above the rain-snow transition zone. Dry season river signatures were affected by evaporation, which was enhanced at low elevations and likely occurred by in-river processes rather than during infiltration.

4.1 Introduction

Understanding the source elevation of California Sierra Nevada rivers is essential for adaptive management of forest and water resources in the context of changing rain-snow transition elevation and elevation gradients in evapotranspiration. Climate change has resulted in a decline in snow water equivalent (SWE) and earlier snowmelt and runoff, leading to lower summer runoff and a shift in peak river runoff (Barnett et al., 2005; Dettinger et al., 2004; Mote et al., 2018). More than 60% of snowmelt occurs above 2.1 km in individual Sierra Nevada river basins, characterized by remotely sensed area snow cover (Rice et al., 2011), but after snow has melted, late season runoff includes a component of water that has been stored in the subsurface, as seen in high elevation meadows, which discharge groundwater in the headwaters of the Sierra Nevada (Liu et al., 2017; Lucas, 2016; Shaw et al., 2014). Evapotranspiration (ET) is predicted to increase as forests expand upslope in areas currently cold-limited, resulting in potentially decreased river flow (Goulden & Bales, 2014). For example, the Sierra Nevada Kings river catchment above 2.4 km provides a disproportionately large volume of the river's discharge because ET is cold limited above that elevation (Goulden & Bales, 2014). In an analysis of individual catchments in the Kings River basin, although all catchments received similar amounts of precipitation, streamflow contributions were higher from higher elevations, attributed to lower ET at those higher elevations (Hunsaker et al., 2012; Safeeq & Hunsaker, 2016).

Upscaling our understanding of elevational contributions of runoff can provide comprehensive understanding of range scale processes across the highly heterogeneous landscape of the Sierra Nevada. Being able to compare elevational contributions among individual rivers can shed light on how differences in subsurface geology and overall elevation distribution affect storage and release of runoff. An analysis of 10 headwater Sierra Nevada rivers, using a spatially distributed evapotranspiration product to partition annual precipitation and runoff into evapotranspiration and runoff found that water available for storage and ET is most vulnerable to drought at low and mid-elevations (Rungee, 2019). Uncertainties and heterogeneities in precipitation and subsurface geology in the Sierra Nevada mean that few have been able to use water balance approaches to determine mountain range-scale elevational contributions to runoff. However, basin-scale analysis has shown that during drought, upper elevations provide runoff when lower elevations dry out (Rungee et al., 2019).

Stable isotopes have been used to determine groundwater recharge elevation and river source elevations without hydrometeorological data (Clark & Fritz, 1997; Tsujimura et al., 2007; Zhu et

al., 2018). While groundwater generally maintains isotopic signatures of input sources, surface water can experience evaporation, in turn affecting isotopic signatures of stream flow. Evaporative fractionation can be detected through calculations of deuterium - excess (d-excess) and line-conditioned excess (lc-excess). As such, stable isotopes are also useful in understanding evaporative processes (Skrzypek et al., 2015). D-excess has long been used as a quantitative measure of evaporative isotope effects (Dansgaard, 1964). Lc-excess expresses the offset between the Local Meteoric Water Line (LMWL) and surface water samples and was developed to understand evaporative processes and contributions of local precipitation to surface waters at varying locations (Landwehr, 2006).

Here, we use Sierra Nevada river stable isotope data to answer the following research questions: What is the source elevation of individual Sierra Nevada rivers and of river runoff on the mountain range scale? How do stable isotopes contribute to an analysis of river source elevation as signals of evaporative processes? How does d-excess/lc-excess change in rivers over time and space and what implications does that have on interpreting stable isotope data? Where does evaporation occur from water's path from precipitation to runoff? How do groundwater isotopic lapse rates compare to precipitation stable isotope lapse rates and what is the range of mean recharge elevations for low-to mid-elevation groundwater? Mountain-range scale analysis supports previous conclusions that high elevations contribute most water to rivers in the Sierra Nevada which is summarized in the graphical abstract, Figure 4-1 (Bales et al., 2018; Goulden & Bales, 2014).

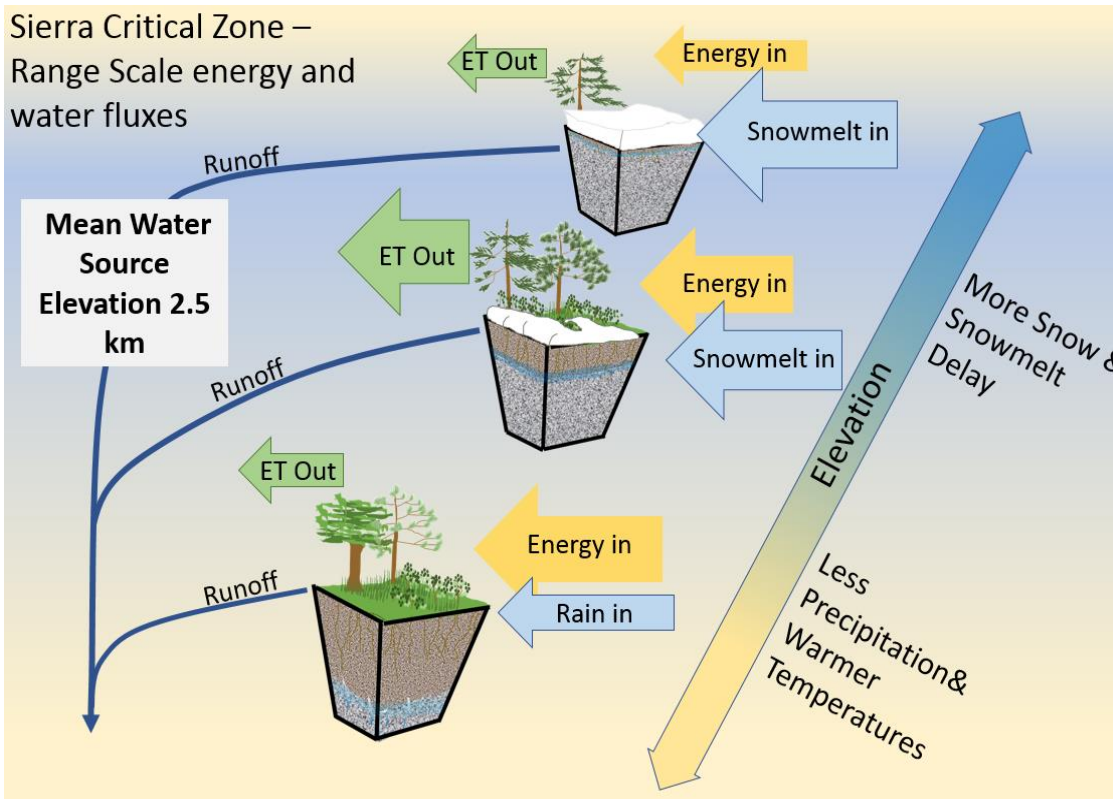

Figure 4-1. Graphical abstract and conceptual diagram of critical zone fluxes of energy and water across the Sierra Nevada with respect to elevation. Three zones are represented by conceptual "pixels". Arrow size represents relative magnitude of energy and precipitation into the critical zone and evapotranspiration (ET) out of the critical zone at different elevations. The low elevation range is rain dominated, warmer, consisting of pine-oak woodland, and ET is water limited; the mid-elevation mixed conifer forest, around 2 km in elevation, is within the rain-snow transition zone and ET is not energy or water limited and has the highest ET, while the upper elevation zone, consisting of subalpine forest, is energy limited, with ET inactive in winter (Goulden & Bales, 2014). This zone is snow dominated. Diagonal arrow represents the primary effects of the elevation gradient on energy and water, in which higher elevations receive more precipitation, and experience a delay to the input of runoff as snow melts. Area decreases with elevation. Lower elevations receive less precipitation, which can more quickly become accessed by active vegetation year-round. Regolith thickness is highest at the lower elevation zone and thinnest at the highest elevation zone (O'Geen et al., 2018).

4.1. Materials and Methods

The Sierra Nevada is the most prominent mountain range in California, located on the eastern side of California and is approximately 600 km long, covering a latitudinal distance from about 36 to 40 degrees N. The highest elevation of the mountain range, 4.4 m is located in the Southern Sierra at approximately 36.5 degrees N. The Sierra Nevada formed during two separate periods of uplift and is composed of Quaternary alluvium, Cenozoic volcanic rocks, granitic rocks, and metamorphic rocks (Wakabayashi & Sawyer, 2001). Most major rivers descend the west side of the Sierra Nevada, which has a less steep elevational gradient than the east side of the Sierra Nevada. Major river catchments and watershed basins on the west side include the Feather, Yuba, American, Cosumnes, Mokelumne, Calaveras, Stanislaus, Tuolumne, Merced, San Joaquin, Kings, Kaweah, Tule, Kern rivers. The deep river canyons of the San Joaquin and Kings rivers formed 70-80 million years ago, earlier than the shallower river canyons of the Tuolumne and Merced rivers (House et al., 1998). These river canyons have become steeper over time due to uplift (Wakabayashi & Sawyer, 2001).

The Sierra Nevada is within 300 km of the Pacific Ocean and its orientation perpendicular to oncoming Pacific storms leads to significant orographic precipitation (Dettinger et al., 2004). With a Mediterranean climate, the Sierra Nevada receives the majority of precipitation during winter. Meanwhile, the Sierra Nevada experiences a high interannual variability in precipitation, with yearly snow water equivalents usually 25% - 60% anomalous of the long-term average (Cayan, 1996). Three-year droughts are a common feature of the Sierra Nevada climate (Griffin & Anchukaitis, 2014).

The Kern, Tule, Kaweah, Kings, San Joaquin, Merced, Tuolumne, Mokelumne, Cosumnes, American, Yuba and Feather were sampled for water stable isotopes during two major field campaigns in spring 2017 and late summer 2017. Rivers were sampled below the majority of the drainage area of each catchment, but above major reservoirs. The location of sampling sites were constrained by road access and accessibility. All 2017 river sampling locations and mean catchment elevations are listed in Table A4-4. In addition, the South Fork of the American river was sampled monthly from March 27, 2017 through August 22, 2017 and the Merced river was sampled monthly February 12, 2017 through August 29, 2017. Samples were collected in May and August 2018 from 23 sites ranging in elevation from 0.039 to 2.2 km within the Cosumnes River catchment, representing the nested watershed scale. See Tables A4-1 – A4-3 for locations and respective mean catchment elevations.

Standard methods were used to collect river water samples for stable isotope analysis. Water samples were collected in French square glass jars without head space. A Los Gatos Research DLT-100 Liquid Water Isotope Analyzer was used to measure water stable isotopes δ^2H and $\delta^{18}O$. Hydrogen and oxygen stable isotope values are reported in δ notation: $\delta = (R_{sample} / R_{standard} - 1)$, where R_{sample} and $R_{standard}$ are the $^2H/^1H$ or $^{18}O/^{16}O$ ratios for the sample and standard, respectively, and referenced to the Vienna Standard Mean Ocean Water (VSMOW) standard.

Sierra Nevada specific isotopic lapse rates (the change of the isotopic signatures of precipitation with altitude) and the (LMWL), constructed from 2015 through 2017 were used for this study. The LMWL was developed from rain and snow samples collected from the Southern Sierra Critical Zone Observatory (CZO) P301 tower site (2.1 km elevation) and the Shorthair site (2.7 km), in addition to two main elevational transects including the American Transect, from elevations 0.56 km to 2.25 km along highway 50 in the northern Sierra Nevada and the Kings Transect from elevations 0.56 km to 2.25 km in the in the Southern Sierra Nevada. Additional snow samples were collected on Mt. Whitney from elevations 2.8 to 4.3 km in elevation (Chapter 1); these are called fractionation-compensated values. The Sierra-wide LMWL had a slope of 7.20 and an offset of 3.13. Isotopic lapse rates used to calculate source elevations were amount weighted. For the American Transect, a slope

of -3.3 (± 1.8) and offset -6.2 (± 1.8) for $\delta^{18}O$ and a slope of -22.3 (± 5.9) and intercept of -30.4 (± 17.9) for $\delta^{2}H$ were used. For the Kings Transect, a slope of -2.8 (± 1.8) and intercept of -6.6 (3.2) for $\delta^{18}O$ and -19.4 (± 13.9) and offset of -43.3 (± 24.8) for $\delta^{2}H$ were used.

Groundwater stable isotope data was obtained from the USGS Groundwater Ambient Monitoring and Assessment (GAMA) program collected from 2006 to 2008 (Belitz et al., 2010; Ferrari, 2008; Shelton, 2010). This groundwater data was filtered to locations on the west slope of the Sierra Nevada (Figure 4-2 (b)) and to samples collected during the dry season, August through October. Spring data was not included because only low elevation groundwater was sampled in the spring.

Tracer predicted source elevation, the elevation at which the isotopic data is used to determine the river source elevation, was calculated using the river $\delta^{18}O$ and $\delta^{2}H$ and the precipitation isotopic lapse rates. Tracer predicted source elevation was calculated through the following steps (Figure 4-2 (a)) 1) River samples were separated into wet (October 1 through June 15) and dry (June 16 through September 30) seasons. 2) River signatures were then corrected for evaporative fractionation using mean monthly temperature and relative humidity for each sampling location following Benettin et al. (Benettin et al., 2018) and the Sierra-wide LMWL (Chapter 1). Relative humidity and temperature values were obtained from PRISM (PRISM, 2004). Groundwater was not corrected for evaporation through fractionation compensation because groundwater d-excess values were above zero indicating no, or very limited, evaporation. 3) The American Transect lapse rate was applied to all data from sampling sites above 37 degrees north and the Kings Transect was applied to sampling sites below 37 degrees north. River source elevations were calculated on $\delta^{18}O$ and $\delta^{2}H$ data separately, and the mean was calculated from the two values.

Mean catchment elevation, above the sampling elevation, was determined using GIS digital elevations models (Archuleta, 2017) or published values (Molotch & Meromy, 2014). Mean catchment elevation was compared to the tracer predicted source elevation for rivers sampled in 2017, separated by collection season (spring and fall seasons). Linear regression was performed on predicted source elevation and mean catchment elevation to determine if higher elevation catchments discharged water from higher elevations compared to catchments with lower mean catchment elevations. Similarly, mean catchment elevations were compared to tracer predicted source elevations for the Cosumnes River, separately for the May 2018 and August 2018 sampling periods.

Rain-snow transition elevations from Rungee (2019) were used to compare with Cosumnes River predicted mean catchment elevation, d-excess at different elevations, precipitation across the entire Sierra Nevada and GAMA groundwater from across the entire Sierra Nevada. Rungee (2019) used snow-covered area developed from Landsat 5-8 data, and snow-covered area maps were averaged by basin and binned into 100 m elevation bands. Rungee (2019) then used linear interpolation between the two elevation bands above and below 50% fractional-snow-covered area to estimate elevational transition from rain to snow. The mean was taken from these basins' rain-snow transition elevations and plotted with Sierra-wide precipitation and groundwater data.

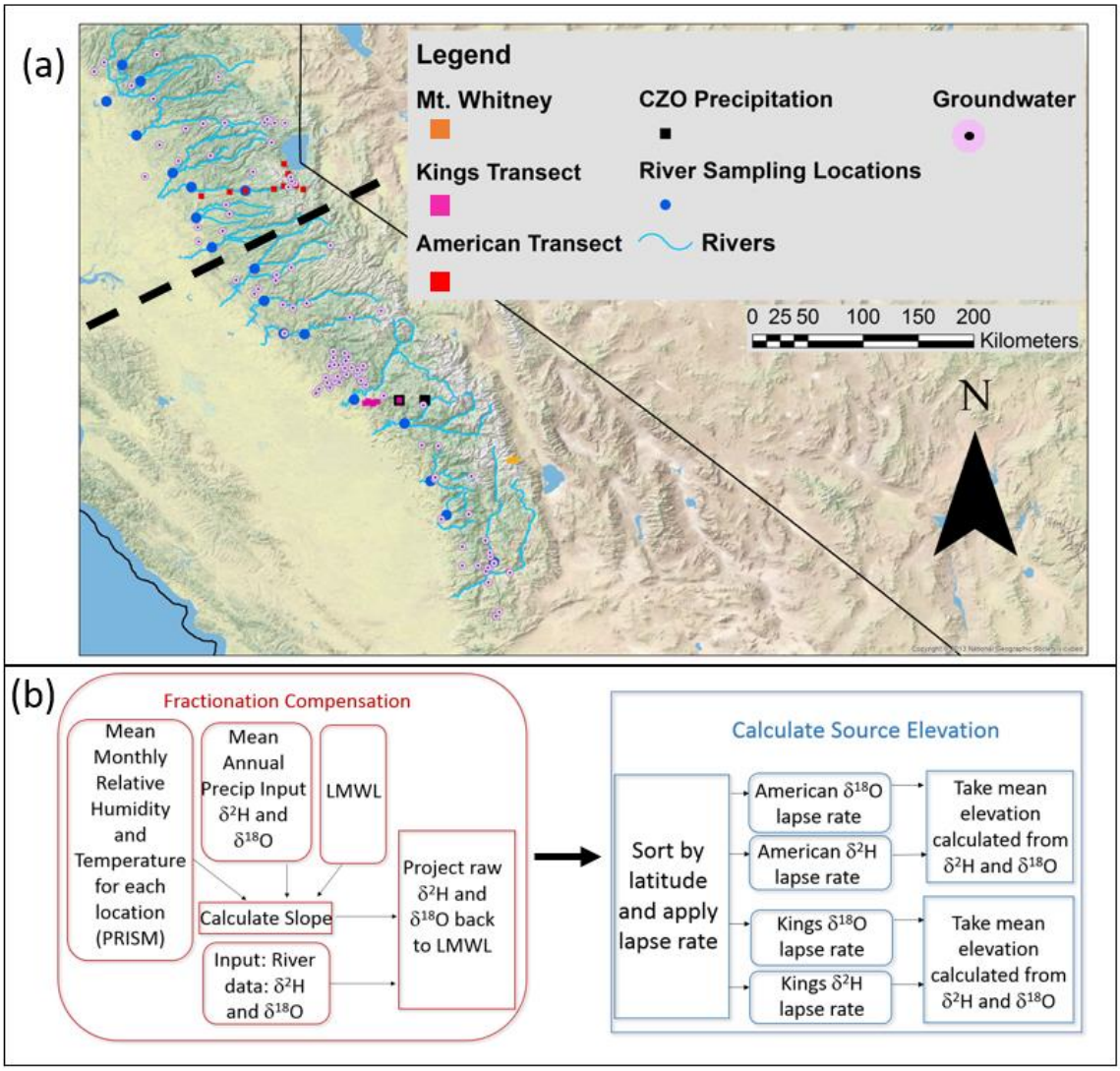

Figure 4-2. Map of precipitation and river sampling locations across the entire Sierra Nevada. (a), and (b) flow chart showing analytical methods to calculate river water source elevation from tracer data. The American and Kings Transects (red and pink squares) were used to collect precipitation δ^2H and $\delta^{18}O$ sample data for isotopic lapse rates (Chapter 1), which were combined with precipitation samples from the Southern Sierra CZO (black squares) and Mt. Whitney (yellow squares) for a LMWL composed of a range of rain and snow from a wide range of elevations and latitudes. Pink circles are groundwater sampling locations.

In addition to estimating river source elevations using tracer data, a spatially distributed mass balance approach was also used (Rungee, 2019). The mass balance approach is based on spatially distributed estimates of precipitation (P) and evapotranspiration (ET) to calculate long term mean runoff (P-ET). The method relies on PRISM (Group, 2004) precipitation product at 800 m resolution. Annual evapotranspiration data is derived from remotely sensed NDVI, calibrated against flux tower stations (Goulden & Bales, 2014; Rungee, 2019). Spatially distributed P-ET was first aggregated over 100m elevation intervals within each river catchment and then the mean source elevation was calculated. Details of the spatially distributed mass balance approach are presented by Rungee (2019).

The variability in isotopic signatures over space and time was examined using violin plots comparing $\delta^{18}O$ values from Sierra – wide precipitation, snowmelt (see chapter 1), rivers sampled in both wet and dry seasons of 2017, the Cosumnes River sampled in both wet and dry seasons of 2018, and the American and Merced rivers sampled through the transition from wet to dry season in 2017. Dual-isotope plots were also created to compare water lines of rivers sampled in both wet and dry seasons of 2017, the Cosumnes River sampled in both wet and dry seasons of 2018 and GAMA groundwater data.

Evaporative signals were determined by calculating d-excess and lc-excess, which represent fractionation processes occurring since precipitation (Dansgaard, 1964; Landwehr, 2006). D-excess was calculated using Equation 4-1 and lc-excess was calculated using equation 2.

$$\text{d-excess} = \delta^{2}H - 8\times\delta^{18}O; \tag{4-1}$$

$$\text{lc-excess} = \delta^{2}H - 7.2\times\delta^{18}O - 3.13. \tag{4-2}$$

When comparing evaporative signals of precipitation, d-excess was used and lc-excess was used for river samples and groundwater.

To understand evaporative processes affecting river stable isotope signatures, we calculated lc-excess and d-excess to examine how elevation and season are related to evaporative signals, compared evaporative signals of the Cosumnes River in wet and dry seasons to evaporative signals of Sierra-wide precipitation and groundwater and, finally, examined seasonal shifts in Cosumnes river stable isotope values in dual-isotope form. Slope and distance of seasonal shifts in dual-isotope space were calculated and compared with sampling location elevation to understand the relationship between seasonal isotopic shift and elevation. To determine how groundwater and precipitation evaporative signals contributed to river water evaporative signals we compared d-excess of precipitation, groundwater, spring Cosumnes river and fall Cosumnes river.

We determined the recharge elevation of Sierra Nevada groundwater and calculated the groundwater isotopic lapse rate, in order to compare it to the precipitation lapse rate using GAMA groundwater data, described above.

4.3 Results

The mean source elevation for all rivers sampled in spring 2017, using the tracer method was 2.5 km, with a pattern showing Southern Sierra river water originating from higher elevations and Northern Sierra river water originating from lower elevations (Figure 4-3 (a)). The mean rain-snow transition elevation based on all basins calculated by Rungee (2019) was 1.8 km. All spring 2017 rivers originated from above their mean catchment elevation, which can be seen in Figure 4-3 (a), in which all points plot above the 1:1 line. The linear relationship between spring predicted source

elevation and mean catchment elevation is significant, with a p-value of 0.0021. Measured and fractionation-compensated stable isotope values for 2017 rivers are provided in Table A4-5.

Fall river predicted source elevations did not show a significant relationship with mean catchment elevation (Figure 4-3 (b)) with a p-value of 0.2674. Additionally, the Kern and Feather rivers had predicted source elevations below their mean catchment elevations. Individual predicted source elevations and mean catchment elevations are provided in Table 4-1.

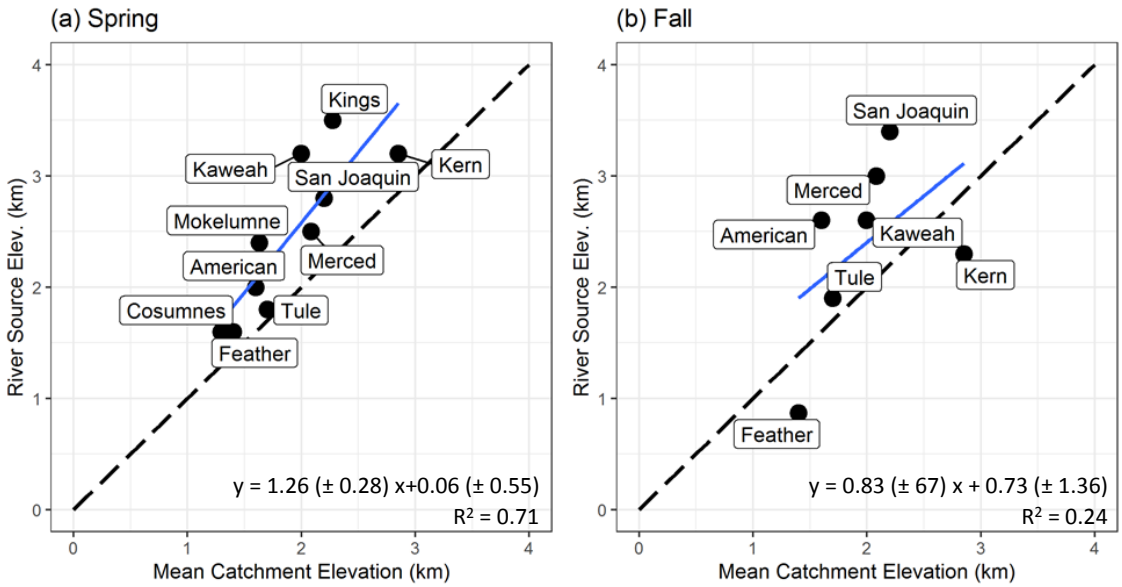

Figure 4-3. Tracer predicted river source elevations versus hypsometric mean catchment elevation using tracer approach for (a) wet season and (b) dry season for major Sierra Nevada rivers. Dashed black line is the 1:1 line for reference. Results indicate that most river water originates above mean catchment elevation on a range scale. In the wet season, (a) tracer results indicate higher elevation source waters in rivers with catchments reaching higher elevations, such as the Kings, Kern and Kaweah rivers. Linear relationship p-value: 0.0021. Dry season tracer data and mean catchment elevations do not yield a significant relationship within a 95% confidence interval, with a p-value of 0.2674 (b), with an R^2 of 0.24, however, most values indicate river sources above their mean catchment elevations. All values have been compensated for evaporative fractionation described above.

Table 4-1. Spring and fall mean catchment elevations and predicted source elevations for the tracer method and mass balance method.

River	WY 2017 Source Elevation (mass balance) (km)	Spring 2017 Source Elevation (tracer) (km)	Fall 2017 Source Elevation (tracer) (km)	Hypsometric Mean Catchment Elevation (km)[1]
Kern	2.5	3.2	2.3	2.9
Tule	2.2	1.8	1.9	1.7
Kaweah	2.6	3.2	2.6	2.0
Kings	2.8	3.5	-	2.3
San Joaquin	2.7	2.8	3.4	2.2
Merced	2.3	2.5	3.0	2.1
Mokelumne	2.0	2.4	-	1.6
Cosumnes	1.2	1.6	-	1.3
Feather	1.5	1.6	0.9	1.4
American	1.7	2.0	2.6	1.6
Mean	2.2	2.5	2.4	-

[1] Hypsometric mean catchment elevations were calculated based on the elevation of area above each sampling site.

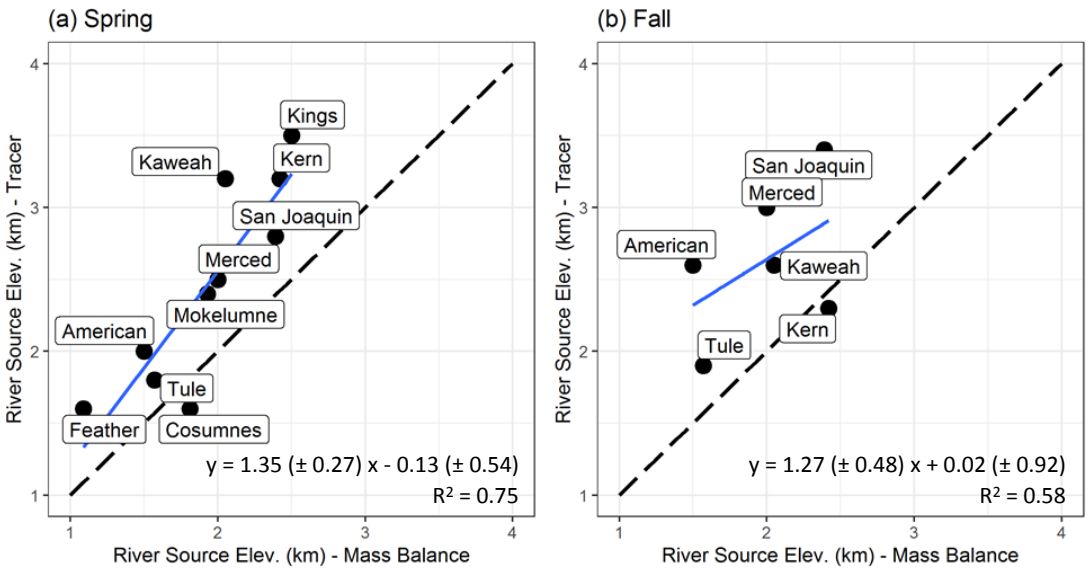

Figure 4-4. Two independent methods used to calculate Sierra Nevada river source elevations, including a spatially distributed mass balance method and tracer method, described here. In both (a) and (b) season specific tracer predicted source elevations are compared to annual average source predictions by the mass balance approach. Tracer data was collected in both spring (a) and fall (b) from major rivers and compared to the mean annual mass balance derived values. Dashed lines are 1:1 lines shown for reference.

The spatially distributed mass balance approach to predicting river source elevations agreed with tracer-based predictions for spring values (Figure 4-4 (a)) but not fall river samples (Figure 4-4 (b)). River source elevations predicted using the tracer method and mass balance method resulted in a significant linear relationship with a p-value of 0.0011 for spring samples, but in fall the relationship was significant within a 95% confidence interval, with a p-value of 0.0467. The mean predicted source elevation using the mass balance method was 2.2 (± 0.5) km compared to 2.5 (± 0.7) km for spring rivers and 2.4 (± 0.8) km for fall rivers using the tracer method. Predicted source elevations by both methods are compared in Table 4-1.

The range of variability across the Sierra Nevada range was greater than what was observed in individual river basins and the precipitation and snowmelt input. For example, variation in monthly $\delta^{18}O$ in the American and Merced rivers from the wet season through the dry season was smaller than the variation in $\delta^{18}O$ across the entire Sierra Nevada (Figure 4-5; see Table A4-5 for values). Cosumnes river $\delta^{18}O$ sampled across the catchment and over time also reflected lower variability than river $\delta^{18}O$ sampled over the entire range. Precipitation $\delta^{18}O$ values collected over a wide range of elevations, seasons and latitudes showed the highest variability. The variability in snowmelt, collected in the central Sierra reflects the seasonal variability in winter precipitation, although most values clustered from -12.5 ‰ to -10‰. River samples collected from across the entire Sierra Nevada in 2017 shows a wider range of $\delta^{18}O$ values compared to the samples collected from individual catchments, including the Cosumnes, American and Merced rivers. From late March, 2017 through August 2017, the American river mean tracer predicted source elevation, based on isotopic data, was 2.5 (± 0.3) km. Similarly, from early February 2017 through late August 2017, the Merced mean tracer predicted source elevation was 2.1 (± 0.4) km. The standard deviation of the mean for Sierra Nevada rivers was higher, in spring the standard deviation was 0.7 km and in fall, it was 0.8, which do not include extreme values. Dual isotope plots and water lines for river, groundwater and precipitation data grouped separately can be found in Figure A4-1 and Table A4-1. Water lines for rivers sampled in spring were steeper and less variable than water lines for rivers sampled in the fall.

Some river $\delta^{18}O$ and $\delta^{2}H$ values did not follow expected patterns (Table A4-5). For example, during spring 2017, the Yuba, Tuolumne and Stanislaus rivers did not follow expected patterns. The Yuba and Tuolumne river values were very high with $\delta^{18}O$ values of -5.83 ‰ and –9.01 ‰. The Stanislaus $\delta^{18}O$ value was very low, -14.81, yet had the very low lc-excess value of -8.37 ‰. During fall, 2017, several rivers had very high $\delta^{18}O$ and $\delta^{2}H$ values, with low lc-excess values, including the Kings, Tuolumne, Stanislaus, Mokelumne, Cosumnes and Yuba rivers, which led to negative values for tracer predicted mean source elevations. These values were not included in calculations for mean source elevation when grouped by season or otherwise. See Table A4-5 for all values.

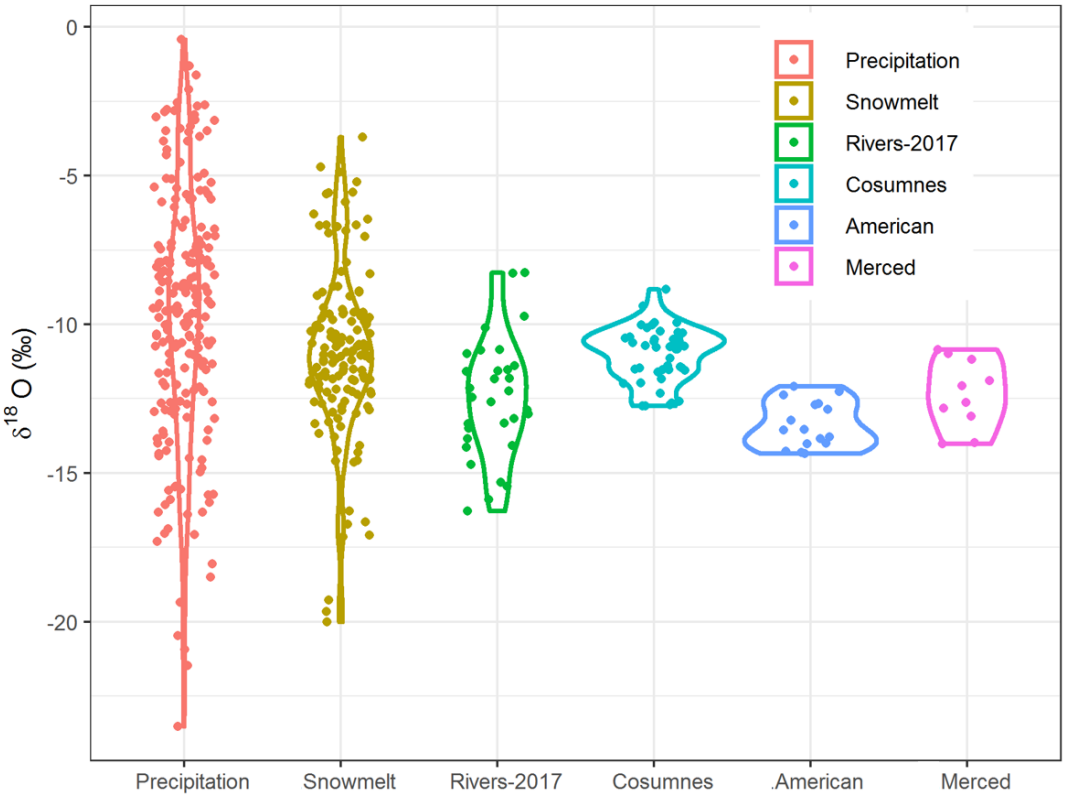

Figure 4-5. Variability in $\delta^{18}O$ in precipitation and snowmelt (temporal and spatial variability) compared to major Sierra Nevada rivers in 2017 (two sampling dates), the Cosumnes river in wet and dry seasons 2018 at several sampling locations (temporal and spatial variability), the American and Merced rivers over time in 2017 (temporal variability). All river values were corrected for evaporative fractionation through fractionation compensation methods described above. Precipitation and snowmelt values are measured, uncorrected values. Data variability is only indicated vertically for $\delta^{18}O$; horizontally, randomly jittered to reduce horizontal over-plotting.

Cosumnes River tracer predicted source elevation was significantly linearly related to mean hypsometric catchment elevation in both May 2018 and August 2018 (Figure 4-6) and most river water originated above the rain-snow transition zone. In May the slope was lower than in August. Cosumnes River sampling locations, measured isotope values, fractionation-compensated values and mean catchment elevations are provided in Tables A4-2 and A4-3.

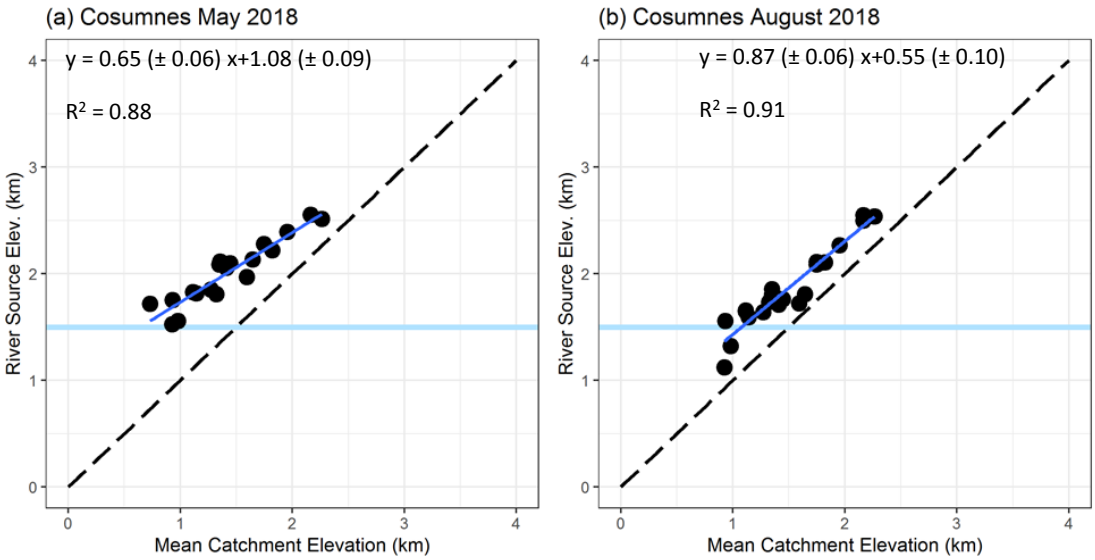

Figure 4-6. Cosumnes river hypsometric mean catchment elevation and tracer predicted river source elevation for (a) wet season and (b) dry season, from river $\delta^{18}O$ and $\delta^{2}H$ data collected at higher spatial resolution, at different elevations in the catchment. Dashed black line is the 1:1 line for reference. Blue line is the rain-snow transition zone in Cosumnes river catchment. All values have been compensated for evaporative fractionation described above.

Measured (uncorrected) stable isotope values of Cosumnes river samples shifted to higher values from May 2018 to August 2018, while at the same time lc-excess decreased (Figure 4-7 (a) and (b)), which was associated with higher temperatures in August than May (Figure 4-7 (c)). Furthermore, the stable isotope lapse rate for measured, uncorrected isotopic values in August was steeper than in May, and slightly steeper than the American Transect precipitation isotopic lapse rate (shown in green in Figure 4-7 (a) and (b)). This shift was caused by evaporative fractionation, as indicated by the shift in lc-excess. Note the seasonal differences in lc-excess and the difference in the ranges of lc-excess in Figure 4-7 (a) and (b). The temperature lapse rate was lower in August compared to May, and temperatures were between 7 and 10 degrees lower in May compared to August 2017 (Figure 4-7 (d).

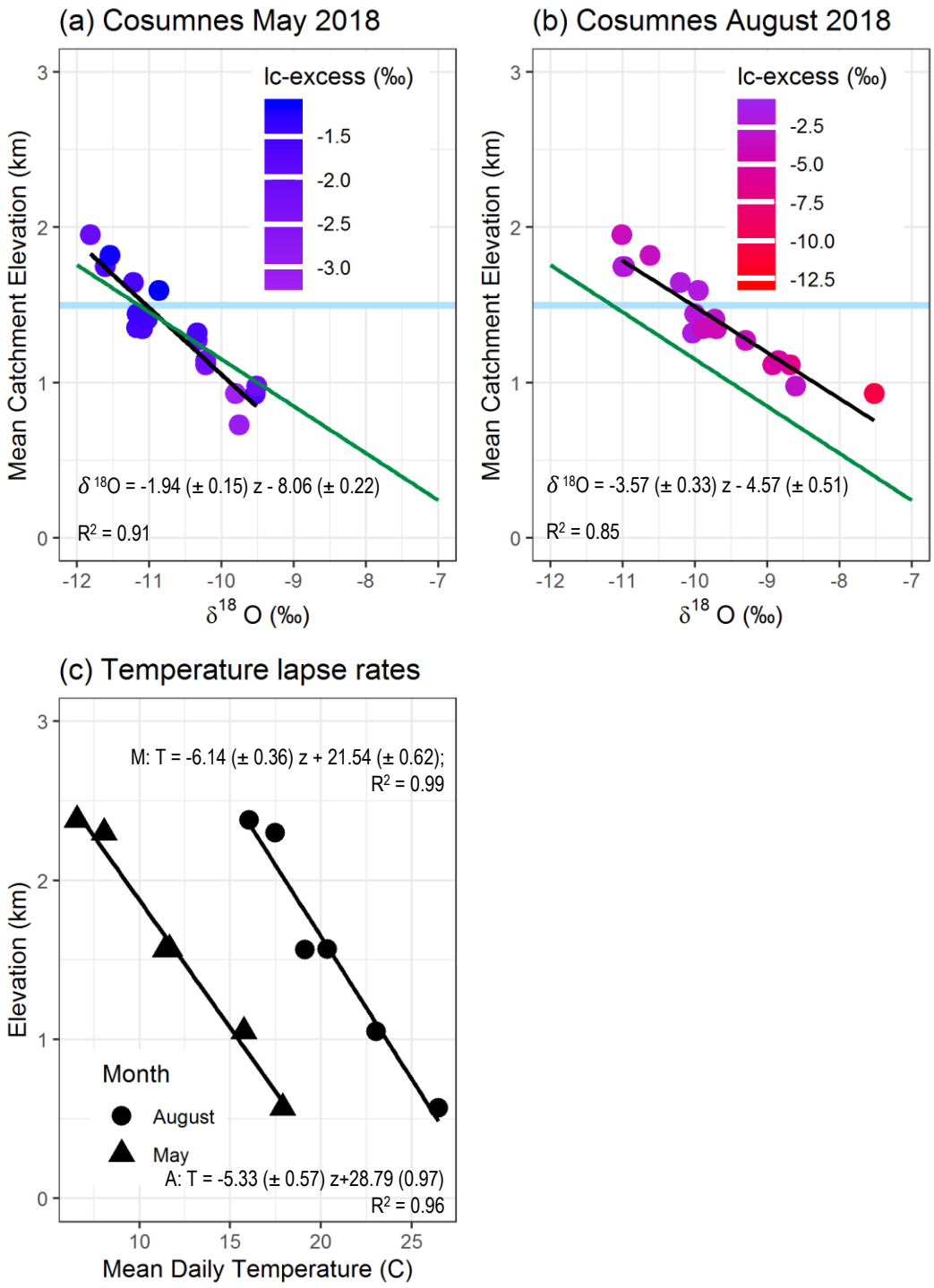

Figure 4-7. Cosumnes river mean catchment elevations for each sampling site versus $\delta^{18}O$ values (uncorrected for evaporative fractionation) for wet season (a) and dry season (b) 2018 and temperature lapse rates for wet and dry seasons (c). Color gradient in (a) and (b) indicates lc-excess calculated from river samples $\delta^{18}O$ and $\delta^{2}H$. Green line indicates American Transect isotopic lapse rate and blue line indicates rain-snow transition zone in the Cosumnes basin.

Equations listed represent results of linear models for mean catchment elevation (independent variable) and $\delta^{18}O$ (dependent variable) (axis switched from what is shown). Axis in (a) and (b) are switched for visualization of elevational effect on $\delta^{18}O$ and lc-excess. Temperature gradients (c) were calculated from data collected by the American River Wireless Sensor Network, including the Alpha site (2.3 km), Echo site (2.38 km) and Owens site (1.57 km), along with data downloaded from the California Data Exchange Center (CDEC) including the Pacific House (1.05 km) site and Placerville Weather Station (0.57 km).

The Cosumnes River isotopic values shifted in dual-isotope space from near the Global Meteoric Water Line (GMWL) to the right from May 2018 to August 2018, with more dramatic shifts at lower elevations, below 1.5 km. (Figure 4-8). The lc-excess and the slope and distance of these seasonal shifts at each sampling elevation were quantified, which varied with elevation (Figure 4-9), especially below 1 km in elevation. August 2018 lc-excess for the Cosumnes river decreased with elevation below 1 km, with lc-excess values below -10 ‰ at the lowest elevation sampling sites and the highest lc-excess value of -1.1 ‰ at the highest sampling elevation (Figure 4-9 (a)). The lowest lc-excess value was observed in the South Fork of the Cosumnes River near 0.5 km elevation (Figure 4-9 (a)), which appears to be an outlier. Two other points had lc-excess values that deviated from the general pattern in Figure 4-9 (a), which were from samples taken from the Camp Creek Headwaters (38.68242, -120.34819) and the Cosumnes River North Fork below Capps Crossing (38.65272, -120.41283). The Camp Creek Headwaters site also had relatively low lc-excess when sampled during spring. However, the North Fork of the Cosumnes River isotopic shifts generally conform to a predictable pattern (Figure 4-8). The seasonal shift in lc-excess, which is the difference between May lc-excess and August lc-excess follows the same pattern (Figure 4-9 (b)), with a larger difference in lc-excess at low elevations. The slope and distance that the $\delta^{18}O$ and $\delta^{2}H$ points shift in dual isotope space also reflect a pattern with elevation, with steeper slopes at higher elevation and greater shifts in distance at low elevation (Figure 4-9 (c) and (d)).

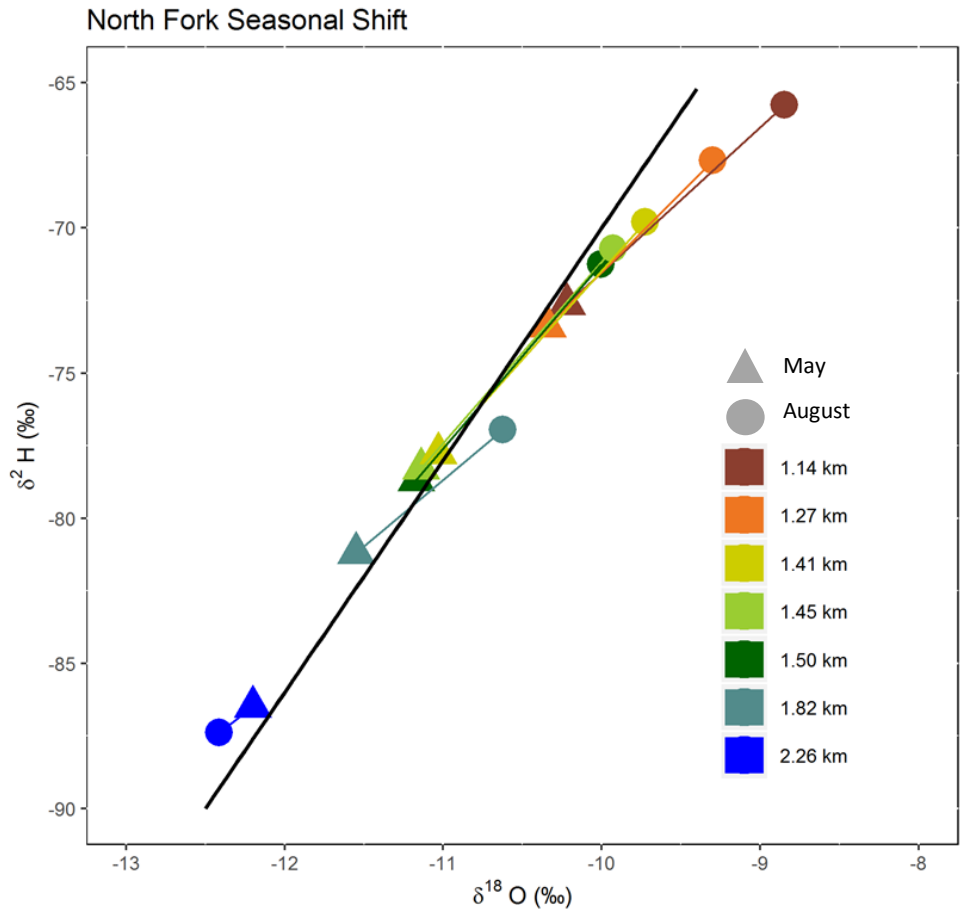

Figure 4-8. North Fork of the Cosumnes River seasonal shift in isotopic values in dual-isotope space. Triangles indicate samples taken in May 2018 and circles indicate samples taken in August 2018. Colors indicate sampling locations and lines connect sampling locations over time. All values are measured, uncorrected $\delta^{18}O$ and $\delta^{2}H$ values. The black line is the Global Meteoric Water Line.

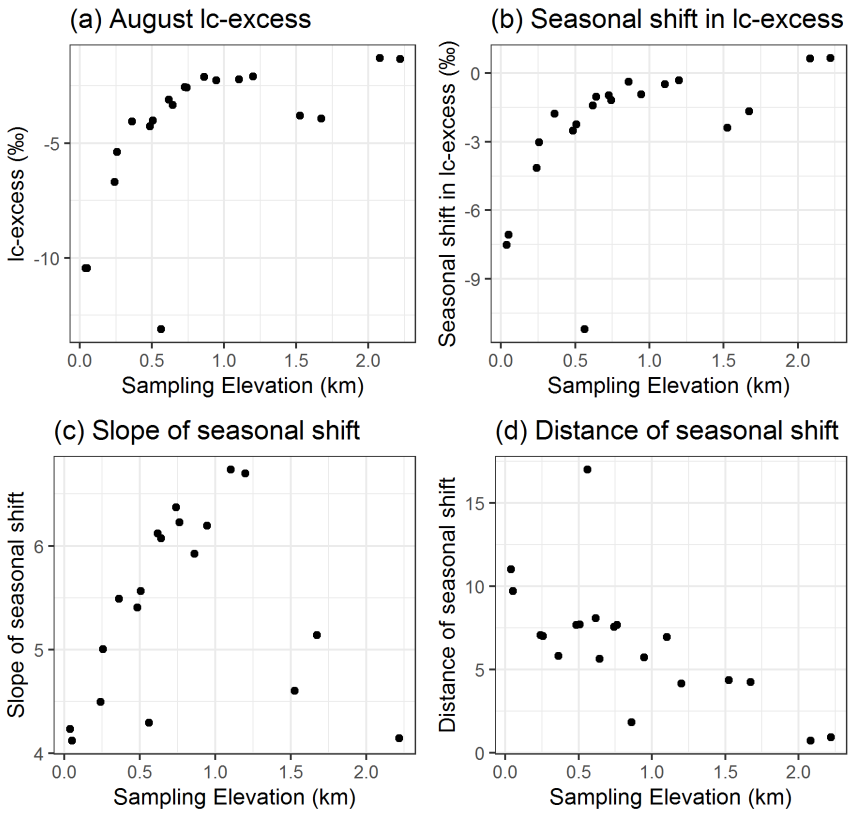

Figure 4-9. Seasonal shifts in isotopic values of the Cosumnes River with elevation from May 2018 to August 2018. (a) shows the increase in lc-excess with elevation, reflecting a decrease in evaporation with elevation during the dry season in August. (b) shows the seasonal change in lc-excess, which is the difference in lc-excess from May to August, which shows that the change in lc-excess is enhanced at low elevations, and near zero at the higher elevations. (c) shows the seasonal shift in slope from dual-isotope space, with steeper slopes (i.e. steeper rates of change in dual-isotope space) from May to August at higher elevations. (d) shows the distance of that seasonal shift of isotopic values in dual-isotope space.

Comparing Cosumnes River elevational evaporative signals with Sierra Nevada-wide precipitation and Sierra Nevada-wide groundwater elevational evaporative signals, it appears that there is a relationship between elevation and evaporation only for in the Cosumnes River water samples. The same pattern does not appear in precipitation or groundwater data (Figure 4-10). In order to compare river evaporative signals with precipitation, we used d-excess, and found that most precipitation, groundwater and May Cosumnes river d-excess values fell above the zero line, and only Cosumnes low elevation d-excess values slope down with elevation (Figure 4-10). August Cosumnes River d-excess values from samples above 1.5 km hover around 10 ‰ in both May and August 2018. Groundwater shows a significant relationship between d-excess and elevation and linear regression resulted in a positive slope of 1.37 (± 0.43) (R^2 of 0.16 and p-value of 0.0024), however, all values are above zero Figure 10 (d).

The recharge elevation for groundwater was generally higher than the sampling location and on average, groundwater was recharged 0.8 km higher than the sampling location (standard deviation: 0.50). Groundwater data sampled in the months of August through October in 2006 through 2008 applied to the isotopic lapse rates developed in Chapter 1, resulted in recharge elevations above sampling elevations (Figure 11 (a)). The groundwater isotopic lapse rate (Figure 4-11 (b)), a result of linear regression performed on measured, uncorrected groundwater $\delta^{18}O$ values with sampling elevation, was $\delta^{18}O = -2.42$ (± 0.12) (elevation) - 8.12 (± 0.18), with an R^2 of 0.88. The groundwater lapse rate was slightly lower than the precipitation lapse rates for the Kings and American Transects, which were -2.8 (± 1.8) and -3.3 (± 1.8), respectively. GAMA groundwater sampling location coordinates, $\delta^{18}O$ and d^2H, and predicted source elevations are listed in Table 4-A6.

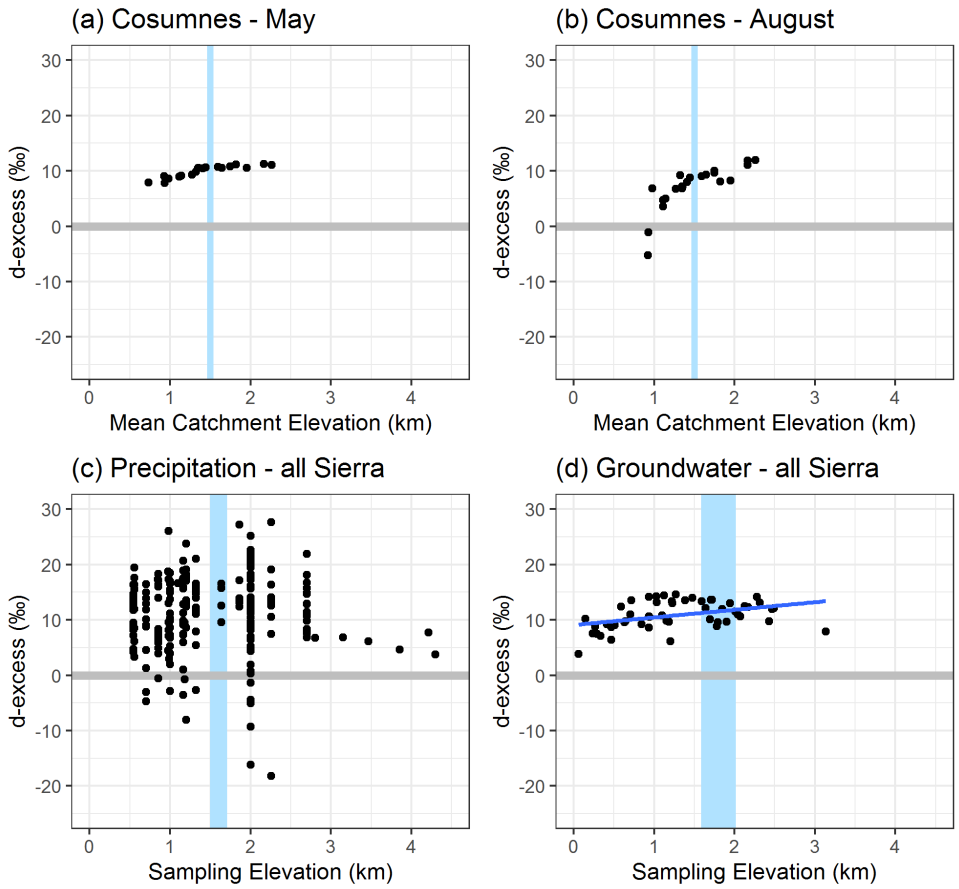

Figure 4-10. D-excess plotted from (a) Cosumnes River samples collected in May 2018, versus mean hypsometric catchment elevation, (b) Cosumnes River samples collected in August 2018, versus mean catchment elevation, and (c), Sierra Nevada precipitation, versus sampling elevation (d) Sierra Nevada groundwater versus sampling elevation. Gray line plotted at y=0 is for reference. Linear regression of groundwater and sampling elevation is represented by the blue line in (d), which is y = 1.37 (± 0.43) x + 9.08 (± 0.63), with an R^2 of 0.16 and p-value of 0.0024, indicating a significant relationship at the 95% confidence interval. Light blue vertical bands represent the mean rain-snow transition zone (Rungee, 2019), for (a) most precipitation samples were collected between 37.0 and 38.8 degrees N latitude, where the rain-snow transition zone ranges from about 1.5 to 2.1 km in elevation, for (c) and (d), in the Cosumnes River catchment the rain-snow transition zone is at about 1.5 km in elevation, and for (d) groundwater samples were collected from August through October 2006 – 2008 from between 35.3 and 39.9 degrees N latitude, where the rain-snow transition zone is located from 1.5 to 2.1 km in elevation.

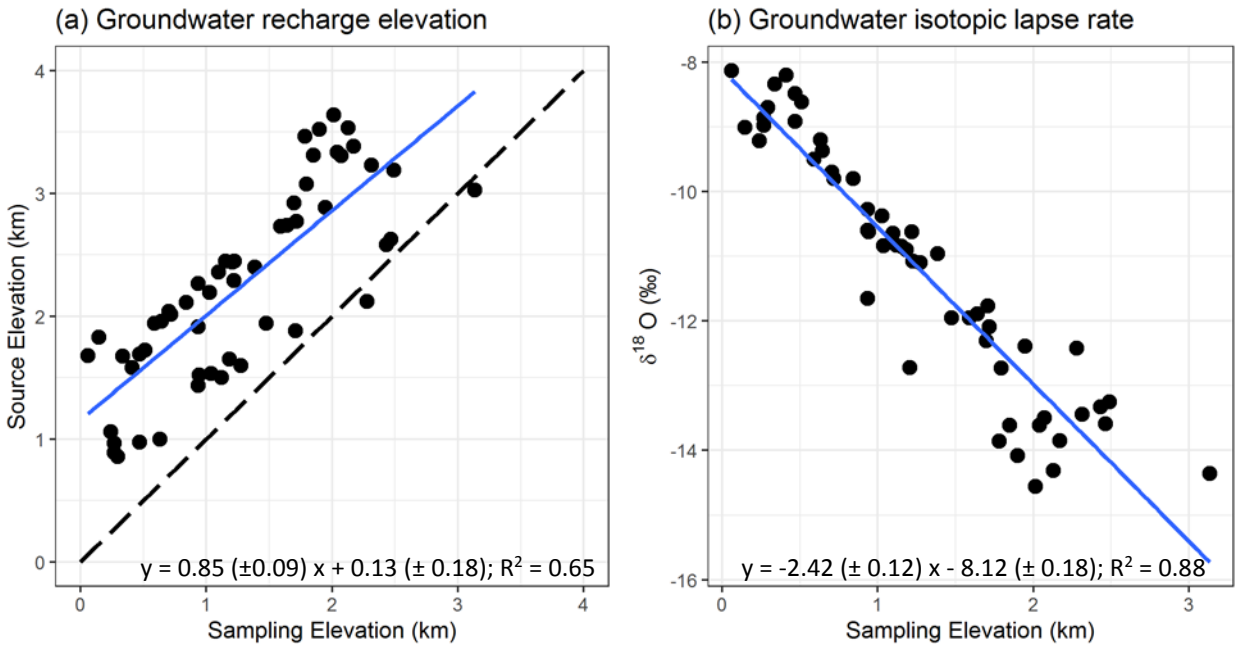

Figure 4-11. Predicted source elevation versus sampling elevation (a) and groundwater $\delta^{18}O$ lapse rate (b) derived from Sierra Nevada groundwater $\delta^{18}O$ and $\delta^{2}H$ data collected through the State of California Groundwater Ambient Monitoring and Assessment (GAMA) program in 2008(Ferrari, 2008; Shelton, 2010). Measured $\delta^{18}O$ and $\delta^{2}H$ values (no fractionation correction) were used. Dashed black line is the 1:1 line for reference.

4.4 Discussion

The tracer predicted source elevations show the importance of mid- and upper- elevations for major rivers. The mean source elevation of major Sierra Nevada rivers was 2.5 (± 0.7) km, and individually, river source elevations correlated with mean catchment elevations and were generally above the mean rain-snow transition zone, 1.8 km. Sierra Nevada precipitation increases with elevation, yet ET is limited at high elevations and, in some basins, it has been shown that sub-catchments above 2 km store more water during droughts due to year to year excesses of water resulting when precipitation exceeds evapotranspiration and are not available at lower elevations in the form of runoff (P-ET) (Bales et al., 2018; Goulden & Bales, 2014; Hunsaker et al., 2012; Safeeq & Hunsaker, 2016). Because water stable isotopes are considered the only conservative tracers, the data we collected at the bottom of the river catchments reflect the integration of critical zone processes from orographic precipitation to storage in the subsurface and include coupled biological and physical processes. By using water stable isotopes to track the elevational origin of water on the expanded scale of the entire mountain range, confirmed by spatially distributed mass balance results, our results on the mountain range scale support previous findings in the Kings River Basin (Bales et al., 2018; Goulden & Bales, 2014; Hunsaker et al., 2012; Safeeq & Hunsaker, 2016).

Meanwhile, variability across the range was greater than variability within individual catchments. The Merced, American and Cosumnes river stable isotope signatures showed less variability than the Sierra wide river signatures (Figure 4-5) and the standard deviation of predicted source elevations was also higher when calculated from river stable isotope signatures across the range.

Low variability in tracer predicted source elevations for the Merced and American rivers throughout the transition from wet season to dry season suggests that the rivers were composed of mixed source water (Table A4-5). In the dry season, subsurface storage primarily from above mean catchment elevation sustains river runoff because snowpack melted during previous months. Furthermore, river source water reflects higher elevation subsurface storage rather than high elevation snowmelt because the predicted source elevations are relatively steady; if there was a much larger contribution of very high elevation snowmelt, we would expect to see a shift to lower isotopic values. Previously, it was found that the Merced River had a higher portion of groundwater on rising limbs of the hydrograph compared to falling limbs; the contribution of groundwater varies on shorter timescales than we show here (Shaw et al., 2014). Groundwater contributions to the Merced River included both shallow and deep reserves (Liu et al., 2017). These deeper flow paths may recharge from higher elevations. Comparing groundwater in Yosemite valley to snow deuterium signatures from the immediate Yosemite area with a δ^2H lapse rate with a slope of -63.5 ‰/km (offset of 51.2) result in mean estimated recharge elevation of 2.2 km (± 0.12 km standard deviation) (Liu et al., 2017). Even with a higher mean catchment elevation, compared to the American river, the Merced river tracer predicted source elevation was slightly lower than that of the American river, suggesting that differences in source elevation depends on both catchment hypsometry and other characteristics. Indeed, the distribution of vegetation, differences in subsurface storage, topographic complexity and elevation gradients likely affect differences among mean river source elevations and these variables warrant further investigation. Additionally, geology in the Northern Sierra contains more volcanic and meta-sedimentary rocks and the Southern Sierra is composed primarily of granitic rocks, yet the elevational origin of river water across the entire range is consistent. Isotopic lapse rates led to similar results in the semi-arid Kherlen River basin in Mongolia, showing that most of the river was composed of precipitation

that fell in headwater catchments above 1.65 km, which confirms the importance of orographic effects on water resources (Tsujimura et al., 2007).

Low-elevation groundwater input may have resulted in river samples with high $\delta^{18}O$ and $\delta^{2}H$ values, resulting in tracer predicted source elevations that were negative. Rivers during fall sampling that had very high values and, for which fractionation compensation did yield reasonable results, also had high lc-excess. As a result, the values did not shift in dual-isotope space to reasonable values. The resulting predicted source elevation values were also not reasonable, and were negative. This could have resulted from a low elevation groundwater source. Upstream water releases from reservoirs or diversions at the time of sampling may also have contributed to these results. For example, in the spring, the Yuba river had isotopic values of -5.8 ‰ and -28.0 ‰ in $\delta^{18}O$ and $\delta^{2}H$, which yields a very high lc-excess value of 10.8 ‰ because both $\delta^{18}O$ and $\delta^{2}H$ values are high and plot close to the LMWL. Additionally, Englebright Lake is located upstream of the sampling location and may have affected sample values. During spring sampling, the Tuolumne river also had high isotopic values (-9.0 and -61.5 ‰ in $\delta^{18}O$ and $\delta^{2}H$, respectively), with and lc-excess value of 0.2 ‰. The tracer predicted source elevation was very low, 0.87 km, considering the hypsometric mean catchment elevation is 2.1 km. The low tracer predicted source elevation could have been influenced by releases or diversions to/from Hetch Hetchy Reservoir, upstream of the sampling site. On the other hand, the Stanislaus River during spring had very low isotopic values of -14.8 and -111.7 ‰ in $\delta^{18}O$ and $\delta^{2}H$ resulting in a tracer predicted source elevation of 3.3 km, which is higher than the entire catchment. One explanation could be high elevation fracture flow or larger contributions of groundwater. During the 2017 fall season, several river $\delta^{18}O$ and $\delta^{2}H$ values were very high, including the Kings, Tuolumne, Mokelumne, Cosumnes, Yuba and feather rivers; these rivers' tracer predicted source elevations were all negative. Generally, Southern Sierra rivers, including the Kern, Tule, Kaweah and some of the central Sierra rivers, including the American, Merced, San Joaquin had isotopic signatures that resulted in tracer predicted source elevations that were reasonable (see Table A4-5).

The Cosumnes river predicted source elevations showed a consistent relationship with mean catchment elevation on a finer scale, shown through measurements at multiple sampling elevations (Figure 4-6), confirming that although the mean source elevation is above the mean catchment elevation, water from all elevations contribute to the river. In May the slope was lower than in August (Figure 4-6), which reflects a higher portion of snowmelt compared to higher portion of baseflow in August. Previous analysis showed that silica was derived from above 0.25 km in the Cosumnes River catchment in dry years (Ahearn et al., 2006), suggesting that higher elevation water stored in the subsurface provided baseflow in dry years, which is consistent with findings of Bales et al., 2018, in the Kings River Basin. Tracer predicted groundwater recharge elevations were generally higher than the sampling elevation, suggesting that the Sierra Nevada groundwater was not dominated by local recharge and that upper elevations are important to groundwater resources across the Sierra Nevada.

We observed evaporative signals across the Cosumnes River basin that suggest in-stream evaporation during the dry season, which was enhanced at the lower elevation sampling sites. The Cosumnes river stable isotope lapse rate constructed of measured, uncorrected values was steeper in August compared to May, and, likewise lc-excess was lower in August compared to May, suggesting that the river isotopic lapse rate was enhanced by evaporation during the dry season (Figure 4-7). Previous isotopic evidence has shown that enhanced evaporation at low elevations strengthened the isotopic lapse rate in the North Platte river, in Colorado (Zhu et al., 2018). Lower lc-excess values in the Cosumnes River in August also suggest that the corresponding increase in $\delta^{18}O$ and $\delta^{2}H$ values were caused by evaporative processes, rather than an increase in lower elevation contributions to the river. Indeed, after all data points were corrected through

fractionation compensation, the predicted source elevations in May and August were similar (Figure 4-6). In May 2018, the mean predicted source elevation from combining all elevations was 2.3 (± 0.3) km and in August was 2.4 (± 0.2) km. The top of the catchment is near 2.4 km, which suggests that the tracer-predicted elevation for August was slightly biased, possibly due to uncertainty in the fractionation compensation. Cosumnes River evaporation during August corresponded with higher temperatures (Figure 4-7), even though the temperature lapse rate in August was lower than the temperature lapse rate in May, suggesting that the overall seasonal temperature increase affected river stable isotope signatures more than the lapse rate, because the higher temperature lapse rate in May did not correspond to a similar correlation in lc-excess. Overall weather conditions affected river stable isotope signatures more than the temperature lapse rate, suggesting that stable isotopes values collected from surface water in warm, dry climates can lead to biased results. The evaporative signal also does not originate in upstream water because samples directly upstream have higher lc-excess (less evaporation). It is unlikely that low elevation shallow flow paths of soil water would lead to these strong evaporative signal in the river, either, because soil evaporation generally is limited to the top 100 cm (Or et al., 2013) and water is not flowing laterally to the river in the top 100 cm of soil in the dry season in the Sierra Nevada. Consequently, we conclude that the evaporative signals observed in low elevation August river samples from the Cosumnes river are a result of in-river evaporation. The Camp Creek Headwater sampling site, located near the top of the basin, deviated from the pattern in which higher elevation river samples had high lc-excess (indicating low evaporation). The Camp Creek Headwater samples had low lc-excess indicating higher evaporation. Similarly, in the Qinghai Lake basin, tributaries were observed to experience more evaporation than the main streams, which was attributed to higher volumes of unevaporated groundwater contributions to the main stream compared to the tributaries (Cui and Li, 2013).

In other locations, changes in summer surface water signatures have been attributed to evaporation and enriched summer precipitation (Ala-aho et al., 2018), but the Sierra Nevada experiences dry summers, with little summer precipitation. On the other hand, low elevation evaporative signals in stable isotope data in Rocky Mountain rivers have been attributed to contributions from groundwater and vadose zone processes (Zhu et al., 2018). Similarly measured d-excess increased with elevation in the semi-arid Kherlen River and the increasing evaporative signal was attributed to evaporation from the surface of the river (Tsujimura et al., 2007). By comparing d-excess values in precipitation, groundwater and river water, we are able to provide evidence to explain that surface water evaporation affects Sierra Nevada river isotopic signatures.

As climate change is predicted to cause the rain-snow transition zone to move up in elevation, cause increases in evapotranspiration at upper elevations, cause snow to melt earlier and lead to more extreme precipitation conditions including drought and rain on snow events, the elevation at which most Sierra Nevada river water originates may be affected (Kapnick and Hall, 2011; Goulden and Bales, 2014; Berghuijs et al., 2014; Belmecheri et al., 2016; Guan et al., 2016; Bales et al., 2018). The tracer predicted source elevations for major rivers presented here show the importance of mid and upper elevation zone of the Sierra Nevada. Evapotranspiration is an important component affecting the source elevation of major rivers in California, seen in the results from the mass balance approach. Vegetation at the mid and upper elevations, which is most likely to increase both spatially, upslope, and temporally, as the growing season expands, evapotranspiration will presumably continue to access water that makes up the majority of downstream river water.

4.5 Conclusions

We used isotopic data to determine the source elevation of major Sierra Nevada rivers, and confirmed these results with mean water source elevations determined from spatially distributed mass balance methods. Using evaporative signals in rivers during wet and dry seasons and at different elevations, compared with evaporative signals in precipitation and groundwater, we found that evaporation affected dry season river water and likely originated in surface water processes rather than precipitation or groundwater processes. By using water stable isotopes, we were able to determine elevational origin of river water, even after that water traveled a path through complex critical zone interactions including coupled biological-physical and geological processes. Our findings confirm that water stable isotopes provide valuable information in river systems or mountain ranges where limited data is available. Our results confirm that high elevation precipitation, often in the form of snow, is an important source of river flows whereas water storage in the subsurface of the critical zone can continue to deliver streamflow into the dry season of a Mediterranean climate.

References

Ala-aho, P., Soulsby, C., Pokrovsky, O. S., Kirpotin, S. N., Karlsson, J., Serikova, S., et al. (2018). Using stable isotopes to assess surface water source dynamics and hydrological connectivity in a high-latitude wetland and permafrost influenced landscape. *Journal of Hydrology, 556*, 279-293.

Archuleta, C. M. (2017). The National Map seamless digital elevation model specifications. In E. W. Constance (Ed.), *U.S. Geological Survey Techniques and Methods*. https://earthexplorer.usgs.gov/.

Bales, R. C., Goulden, M. L., Hunsaker, C. T., Conklin, M. H., Hartsough, P. C., O'Geen, A. T., et al. (2018). Mechanisms controlling the impact of multi-year drought on mountain hydrology. *Scientific Reports, 8*.

Barnett, T. P., Adam, J. C., & Lettenmaier, D. P. (2005). Potential impacts of a warming climate on water availability in snow-dominated regions. *Nature, 438*(7066), 303-309.

Belitz, K., Jurgens, B., Landon, M. K., Fram, M. S., & Johnson, T. (2010). Estimation of aquifer scale proportion using equal area grids: Assessment of regional scale groundwater quality. *Water Resources Research, 46*.

Belmecheri, S., Babst, F., Wahl, E. R., Stahle, D. W., & Trouet, V. (2016). Multi-century evaluation of Sierra Nevada snowpack. Nature Climate Change, 6(1), 2.

Benettin, P., Volkmann, T. H. M., von Freyberg, J., Frentress, J., Penna, D., Dawson, T. E., et al. (2018). Effects of climatic seasonality on the isotopic composition of evaporating soil waters. *Hydrology and Earth System Sciences, 22*(5), 2881-2890.

Berghuijs, W. R., Woods, R. A., & Hrachowitz, M. (2014). A precipitation shift from snow towards rain leads to a decrease in streamflow. Nature Climate Change, 4(7), 583.

Cayan, D. R. (1996). Interannual climate variability and snowpack in the western United States. *Journal of Climate, 9*(5), 928-948.

Cui, B. L., & Li, X. Y. (2015). Characteristics of stable isotopes and hydrochemistry of river water in the Qinghai Lake Basin, northeast Qinghai-Tibet Plateau, China. Environmental earth sciences, 73(8), 4251-4263.

Clark, I., & Fritz, P. (1997). Environmental Isotopes in Hydrogeology.

Dansgaard, W. (1964). Stable isotopes in precipitation. *Tellus, 16*(4), 436-468.

Dettinger, M., Redmond, K., & Cayan, D. (2004). Winter orographic precipitation ratios in the Sierra Nevada - Large-scale atmospheric circulations and hydrologic consequences. *Journal of Hydrometeorology, 5*(6), 1102-1116.

Ferrari, M. (2008). G*round-water Quality Data in the Central Sierra Study Unit, 2006*. In M. Fram (Ed.), *Results from the California GAMA Program*. USGS.

Goulden, M. L., & Bales, R. C. (2014). Mountain runoff vulnerability to increased evapotranspiration with vegetation expansion. *Proceedings of the National Academy of Sciences of the United States of America, 111*(39), 14071-14075.

Griffin, D., & Anchukaitis, K. J. (2014). How unusual is the 2012-2014 California drought? *Geophysical Research Letters, 41*(24), 9017-9023.

Guan, B., Waliser, D. E., Ralph, F. M., Fetzer, E. J., & Neiman, P. J. (2016). Hydrometeorological characteristics of rain-on-snow events associated with atmospheric rivers. Geophysical research letters, 43(6), 2964-2973.

PRISM (2004). Parameter-elevation Regressions on Independent Slopes Model (PRISM). Oregon State University.

House, M. A., Wernicke, B. P., & Farley, K. A. (1998). Dating topography of the Sierra Nevada, California, using apatite (U-Th)/He ages. *Nature, 396*(6706), 66-69.

Hunsaker, C. T., Whitaker, T. W., & Bales, R. C. (2012). Snowmelt Runoff and Water Yield Along Elevation and Temperature Gradients in California's Southern Sierra Nevada. *Journal of the American Water Resources Association, 48*(4), 667-678.

Kapnick, S., & Hall, A. (2012). Causes of recent changes in western North American snowpack. Climate Dynamics, 38(9-10), 1885-1899.

Landwehr, J. M., Coplen, T.B. (2006). *Line-conditioned excess: a new method for characterizing stable hydrogen and oxygen isotoperatios in hydrologic systems*. Paper presented at the Isotopes in Environmental Studies, Aquatic Forum 2004.

Liu, F. J., Conklin, M. H., & Shaw, G. D. (2017). Insights into hydrologic and hydrochemical processes based on concentration-discharge and end-member mixing analyses in the mid-Merced River Basin, Sierra Nevada, California. *Water Resources Research, 53*(1), 832-850.

Lucas, R. (2016). *Evapotranspiration and groundwater patterns in montane meadows of the Sierra Nevada, CA.* PhD Dissertation, University of California, Merced, eScholarship.

Molotch, N. P., & Meromy, L. (2014). Physiographic and climatic controls on snow cover persistence in the Sierra Nevada Mountains. *Hydrological Processes, 28*(16), 4573-4586.

Mote, P. W., Li, S. H., Lettenmaier, D. P., Xiao, M., & Engel, R. (2018). Dramatic declines in snowpack in the western US. *Npj Climate and Atmospheric Science, 1*.

O'Geen, A., Safeeq, M., Wagenbrenner, J., Stacy, E., Hartsough, P., Devine, S., et al. (2018). Southern Sierra Critical Zone Observatory and Kings River Experimental Watersheds: A Synthesis of Measurements, New Insights, and Future Directions. *Vadose Zone Journal, 17*(1).

Or, D., Lehmann, P., Shahraeeni, E., & Shokri, N. (2013). Advances in Soil Evaporation Physics-A Review. *Vadose Zone Journal, 12*(4).

Rice, R., Bales, R. C., Painter, T. H., & Dozier, J. (2011). Snow water equivalent along elevation gradients in the Merced and Tuolumne River basins of the Sierra Nevada. *Water Resources Research, 47*.

Rungee, J. (2019). Estimating plant-accessible water storage through evaluating evapotranspiration in the semi-arid western United States using eddy-covariance, remote sensing, and spatially distributed data. PhD Dissertation. University of California, Merced: eScholarship.

Rungee, J., Bales, R., & Goulden, M. (2019). Evapotranspiration response to multiyear dry periods in the semiarid western United States. *Hydrological Processes, 33*(2), 182-194.

Safeeq, M., & Hunsaker, C. T. (2016). Characterizing runoff and water yield for headwater catchments in the Southern Sierra Nevada. *Journal of the American Water Resources Association, 52*(6), 1327-1346.

Shaw, G. D., Conklin, M. H., Nimz, G. J., & Liu, F. J. (2014). Groundwater and surface water flow to the Merced River, Yosemite Valley, California: 36Cl and Cl2 evidence. *Water Resources Research, 50*(3), 1943-1959.

Shelton, J. (2010). G*roundwater-quality data for the Sierra Nevada study unit, 2008*. In M. Fram (Ed.), *Results from the California GAMA program*.

Skrzypek, G., Mydlowski, A., Dogramaci, S., Hedley, P., Gibson, J. J., & Grierson, P. F. (2015). Estimation of evaporative loss based on the stable isotope composition of water using Hydrocalculator. *Journal of Hydrology, 523*, 781-789.

Tsujimura, M., Abe, Y., Tanaka, T., Shimada, J., Higuchi, S., Yamanaka, T., et al. (2007). Stable isotopic and geochemical characteristics of groundwater in Kherlen River basin, a semi-arid region in eastern Mongolia. *Journal of Hydrology, 333*(1), 47-57.

Wakabayashi, J., & Sawyer, T. L. (2001). Stream incision, tectonics, uplift, and evolution of topography of the Sierra Nevada, California. *Journal of Geology, 109*(5), 539-562.

Zhu, L., Fan, M. J., Hough, B., & Li, L. (2018). Spatiotemporal distribution of river water stable isotope compositions and variability of lapse rate in the central Rocky Mountains: Controlling factors and implications for paleoelevation reconstruction. *Earth and Planetary Science Letters, 496*, 215-226.

Appendix for Chapter 4

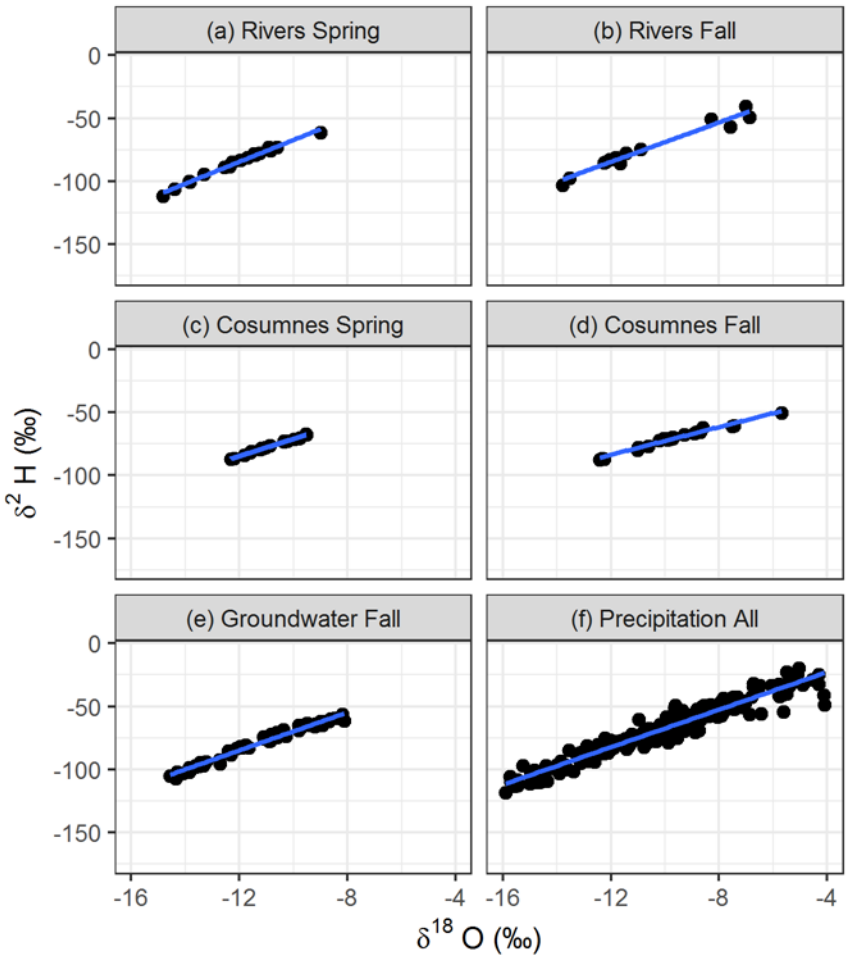

Figure A4-1. Dual isotope plots for (a) Major Sierra Nevada rivers, sampled in spring, 2017, (b) Major Sierra Nevada rivers, sampled in fall, 2017, (c) Cosumnes river sampled in May, 2018, (d) Cosumnes river sampled in August, 2018, (e) groundwater sampled in fall (August through October), (f) All precipitation collected from the Sierra Nevada, including the American and Kings Transects, the Southern Sierra Critical Zone Observatory P301 and Shorthair sites and Mt. Whitney. All groundwater samples were collected through the Groundwater Ambient Monitoring and Assessment (GAMA) program from 2006 through 2008 during months of August through October.

Table A4-1. Water lines for sample groups corresponding to Figure A1.

Sample Group	Slope	σ	Intercept	σ	R^2	p-value
Cosumnes Fall	5.49	0.20	-17.73	1.97	0.97	< 0.0001
Cosumnes Spring	6.82	0.13	-2.85	1.41	0.99	< 0.0001
All Rivers 2017 Fall	7.82	0.48	9.26	5.21	0.96	< 0.0001
All Rivers 2017 Spring	8.66	0.24	19.40	2.94	0.99	< 0.0001
Fall Groundwater	7.54	0.17	5.66	1.94	0.97	< 0.0001
Precipitation All	7.20	0.12	3.13	1.24	0.94	< 0.0001

Table A4-2. Cosumnes River May 2018 measured, uncorrected $\delta^{18}O$ and $\delta^{2}H$ values, fractionation-compensated values and predicted source elevations for each sampling location.

Latitude	Longitude	Mean Catchment Elevation	$\delta^{18}O$ (‰)[1]	$\delta^{2}H$ (‰)[1]	$\delta^{18}O$ (‰)[2]	$\delta^{2}H$ (‰)[2]	Predicted Source Elevation (km)
38.37155	-121.32486	0.730	-9.76	-70.16	-10.46	-72.20	1.58
38.49426	-121.07146	0.931	-9.98	-71.48	-10.62	-73.34	1.63
38.49841	-121.06250	0.931	-9.81	-70.71	-10.56	-72.87	1.61
38.55405	-120.84727	1.115	-10.22	-72.79	-10.76	-74.37	1.68
38.59091	-120.84261	1.142	-10.22	-72.62	-10.72	-74.08	1.66
38.54601	-120.75767	0.926	-9.54	-67.25	-9.93	-68.39	1.42
38.63743	-120.75748	1.273	-10.34	-73.39	-10.82	-74.79	1.70
38.61591	-120.73246	1.349	-11.10	-78.37	-11.47	-79.44	1.90
38.62651	-120.70014	1.354	-11.18	-78.93	-11.54	-79.98	1.92
38.53182	-120.69912	0.980	-9.52	-67.54	-10.01	-68.97	1.44
38.65289	-120.62706	1.409	-11.03	-77.76	-11.38	-78.81	1.87
38.63887	-120.58914	1.445	-11.14	-78.29	-11.43	-79.16	1.89
38.63934	-120.58414	1.445	-11.17	-78.70	-11.50	-79.70	1.91
38.62710	-120.57374	1.322	-10.34	-72.84	-10.70	-73.93	1.66
38.69149	-120.54625	1.593	-10.87	-76.27	-11.14	-77.08	1.80
38.72375	-120.52437	1.644	-11.22	-79.23	-11.60	-80.36	1.94
38.56392	-120.42881	1.748	-11.61	-82.06	-11.99	-83.20	2.06
38.65272	-120.41283	1.821	-11.55	-81.20	-11.83	-82.04	2.01
38.68242	-120.34819	1.953	-11.82	-84.03	-12.31	-85.50	2.16
38.63647	-120.24178	2.263	-12.20	-86.50	-12.64	-87.85	2.26
38.59759	-120.24006	2.164	-12.32	-87.32	-12.75	-88.64	2.30

[1] Measured, uncorrected values. [2] Fractionation-compensated values.

Table A4-3. Cosumnes River August 2018 measured, uncorrected $\delta^{18}O$ and $\delta^{2}H$ values, fractionation-compensated values and predicted source elevations for each sampling location.

Latitude	Longitude	Mean Catchment Elevation	$\delta^{18}O$ (‰)[1]	$\delta^{2}H$ (‰)[1]	$\delta^{18}O$ (‰)[2]	$\delta^{2}H$ (‰)[2]	Predicted Source Elevation (km)
38.63647	-120.24178	2.263	-12.41	-87.39	-12.71	-88.36	2.29
38.59759	-120.24006	2.164	-12.31	-86.61	-12.59	-87.54	2.25
38.59759	-120.24006	2.164	-12.26	-86.99	-12.74	-88.58	2.30
38.68242	-120.34819	1.953	-11.01	-79.86	-11.96	-83.01	2.05
38.65272	-120.41283	1.821	-10.62	-76.96	-11.52	-79.83	1.91
38.56392	-120.42881	1.748	-11.00	-77.95	-11.47	-79.46	1.90
38.56392	-120.42881	1.748	-10.97	-78.12	-11.53	-79.91	1.92
38.69149	-120.54625	1.593	-9.96	-70.61	-10.47	-72.26	1.59
38.72375	-120.52437	1.644	-10.20	-72.35	-10.71	-73.96	1.66
38.63934	-120.58414	1.445	-10.00	-71.25	-10.58	-73.03	1.62
38.63887	-120.58914	-	-9.93	-70.72	-10.51	-72.51	1.60
38.62710	-120.57374	1.322	-10.04	-71.05	-10.50	-72.49	1.60
38.65289	-120.62706	1.409	-9.73	-69.79	-10.43	-71.98	1.57
38.53182	-120.69912	0.980	-8.61	-61.99	-9.37	-64.36	1.24
38.62651	-120.70014	1.354	-9.81	-71.36	-10.75	-74.25	1.67
38.61591	-120.73246	1.349	-9.70	-70.82	-10.70	-73.90	1.66
38.61591	-120.73246	1.349	-9.90	-71.96	-10.83	-74.86	1.70
38.63743	-120.75748	1.273	-9.30	-67.67	-10.24	-70.58	1.51
38.54601	-120.75767	0.926	-5.68	-50.68	-8.83	-60.44	1.07
38.55405	-120.84727	1.115	-8.69	-65.89	-10.27	-70.79	1.52
38.55405	-120.84727	1.115	-8.92	-66.69	-10.28	-70.91	1.53
38.59091	-120.84261	1.142	-8.85	-65.76	-10.11	-69.68	1.47
38.49841	-121.06250	0.931	-7.52	-61.27	-10.02	-69.02	1.44
38.49426	-121.07146	0.931	-7.45	-60.76	-9.95	-68.51	1.42

[1] Measured, uncorrected values. [2] Fractionation-compensated values.

Table A4-4. 2017 Sierra Nevada river sampling locations and mean catchment elevations.

River	Latitude	Longitude	Mean Catchment Elevation
Kern	35.754488	-118.423296°	2.582
Tule	36.13453	-118.810427°	1.706
Kaweah	36.41164	-118.939458°	1.996
Kings	36.87907	-119.151483°	2.275
San Joaquin	37.072849	-119.562091°	2.2
Merced Bric	37.605005	-119.967136°	2.082
Merced Bag	37.610651	-120.135162°	-
Tuolumne	37.876952	-120.295153°	2.091
Stanislaus	38.136734	-120.373106°	1.945
Mokelumne	38.311427	-120.721651°	1.629
Cosumnes	38.550735	-120.849986°	1.296
American Ice	38.771041	-120.448444°	1.873
American Col	38.800579	-120.889024°	1.658
American Aub	38.915637	-121.040270°	1.573
Yuba	39.220773	-121.334313°	-
Feather Oro	39.497525	-121.579564°	-
Feather Bald	39.792557	-121.452310°	1.466
Feather Pulga	39.792557	-121.452310°	1.572

[1] Measured, uncorrected values. [2] Fractionation-compensated values.

Table A4-5. 2017 River measured, uncorrected $\delta^{18}O$ and $\delta^{2}H$ values, fractionation-compensated values, lc-excess and tracer predicted source elevations for each sampling location. Partial second words on River names indicates sampling location to distinguish between rivers sampled in multiple locations, for example, Merced "Bric" stands for Briceburg, Merced "Bag" stands for Bagby, American "Aub" stands for Auburn, American "Col" stand for Coloma, Feather "Oro" indicates sample from below Oroville dam, Feather "Bald" indicates Bald Rock.

Sampling Date	River	$\delta^{18}O$ (‰)[1]	$\delta^{2}H$ (‰)[1]	$\delta^{18}O$ (‰)[2]	$\delta^{2}H$ (‰)[2]	Lc-excess (‰)	Tracer Predicted Source Elevation
3/25/2017	Kern	-13.84	-100.70	-15.31	-107.12	-4.2	3.2
3/25/2017	Tule	-11.25	-77.71	-11.57	-80.19	0.2	1.8
3/26/2017	Kaweah	-13.84	-99.85	-15.44	-108.02	-3.3	3.2
3/25/2017	Kings	-14.40	-106.33	-16.28	-114.10	-5.8	3.5
3/26/2017	San Joaquin	-13.30	-94.32	-14.14	-98.66	-1.7	2.8
3/26/2017	Merced Bric	-10.85	-75.78	-11.39	-78.89	-0.8	1.7
3/27/2017	Merced Bag	-12.35	-88.18	-13.33	-92.86	-2.4	2.5
3/27/2017	Tuolumne	-9.01	-61.52	-9.01	-61.52	0.2	0.9
3/28/2017	Stanislaus	-14.81	-111.71	-14.81	-111.71	-8.2	3.3
3/27/2017	Mokelumne	-12.34	-86.82	-13.00	-90.50	-1.1	2.4
3/27/2017	Cosumnes	-10.61	-72.96	-10.88	-75.19	0.3	1.6
4/1/2017	American Ice	-12.26	-84.94	-12.60	-87.59	0.2	2.2
4/6/2017	American Col	-11.70	-81.41	-12.15	-84.34	-0.3	2.1
4/7/2017	American Aub	-11.46	-78.15	-11.52	-79.82	1.2	1.8
4/7/2017	Yuba	-5.83	-28.03	-5.83	-28.03	10.8	-0.6
4/7/2017	Feather Oro	-10.93	-73.29	-10.99	-76.00	2.3	1.6
4/7/2017	Feather Bald	-11.95	-83.44	-12.46	-86.58	-0.5	2.2
4/7/2017	Feather Pulga	-11.41	-79.22	-11.83	-82.02	-0.2	2.0
8/23/2017	Kern	-11.82	-81.19	-12.88	-89.59	0.8	2.3
8/24/2017	Tule	-10.90	-74.40	-11.82	-81.97	0.9	1.9
8/24/2017	Kaweah	-12.25	-85.08	-13.85	-96.56	0.0	2.6
8/26/2017	Kings	-3.99	-29.70	-5.52	-36.60	-4.1	-0.4
8/27/2017	San Joaquin	-13.79	-102.92	-15.89	-111.31	-6.8	3.4
8/29/2017	Merced Bric	-11.45	-77.56	-12.23	-84.94	1.8	2.1
8/29/2017	Merced Bag	-13.54	-97.37	-14.72	-102.83	-3.0	3.0
8/30/2017	Tuolumne	-7.02	-40.55	-7.02	-40.60	6.9	0.0
8/30/2017	Stanislaus	-12.20	-84.75	-13.50	-94.08	0.0	2.8
8/31/2017	Mokelumne	-3.68	-21.23	-3.68	-22.40	2.1	-1.1
8/31/2017	Cosumnes	-3.52	-21.81	-3.71	-23.57	0.4	-1.1
9/11/2017	American Ic	-8.28	-50.54	-8.28	-52.25	5.9	0.5
9/5/2017	American Col	-12.03	-82.92	-13.16	-91.62	0.6	2.4
9/5/2017	American Aub	-11.65	-85.62	-14.08	-98.23	-4.9	2.7
9/5/2017	Yuba	-4.40	-27.38	-4.58	-29.84	1.2	-0.8
9/6/2017	Feather Oro	-6.88	-49.04	-8.26	-56.32	-2.6	0.6
9/6/2017	Feather Bald	-7.57	-56.92	-9.73	-66.92	-5.5	1.1
9/6/2017	Feather Pulga	-0.22	-5.08	-1.87	-10.33	-6.6	-1.7
3/27/2017	American Ic	-12.71	-90.43	-12.71	-90.43	-2.0	2.3
3/31/2017	American Ic	-12.86	-91.22	-12.86	-91.22	-1.8	2.3
4/1/2017	American Ic	-12.26	-84.94	-12.26	-84.94	0.2	2.1
5/14/2017	American Ic	-13.04	-92.14	-13.23	-92.15	-1.4	2.4
5/24/2017	American Ic	-12.83	-91.37	-13.53	-94.27	-2.1	2.5
5/30/2017	American Ic	-13.11	-92.34	-13.55	-94.41	-1.1	2.5
6/17/2017	American Ic	-12.08	-82.94	-12.08	-83.58	0.9	2.0
6/26/2017	American Ic	-12.07	-84.21	-12.66	-88.02	-0.4	2.2

7/6/2017	American Ic	-11.80	-82.24	-12.38	-86.02	-0.4	2.1
7/17/2017	American Ic	-12.98	-92.45	-14.31	-99.91	-2.1	2.8
7/21/2017	American Ic	-12.77	-91.64	-14.27	-99.59	-2.8	2.8
7/28/2017	American Ic	-12.66	-90.20	-14.00	-97.65	-2.2	2.7
8/11/2017	American Ic	-12.53	-89.87	-14.01	-97.73	-2.8	2.7
8/15/2017	American Ic	-12.39	-90.83	-14.35	-100.16	-4.8	2.8
8/18/2017	American Ic	-12.16	-88.07	-13.84	-96.50	-3.6	2.6
8/22/2017	American Ic	-12.24	-88.08	-13.78	-96.11	-3.1	2.6
2/12/2017	Merced Bric	-10.89	-77.79	-11.18	-77.79	-2.5	1.7
2/26/2017	Merced Bric	-10.96	-77.24	-10.98	-77.24	-1.5	1.6
3/19/2017	Merced Bric	-13.09	-91.86	-13.09	-91.86	-0.7	2.4
3/26/2017	Merced Bric	-10.85	-75.78	-10.85	-75.78	-0.8	1.6
5/8/2017	Merced Bric	-12.72	-89.41	-12.82	-89.41	-1.0	2.3
5/21/2017	Merced Bric	-13.08	-94.20	-14.03	-97.86	-3.2	2.7
6/4/2017	Merced Bric	-11.90	-81.18	-11.90	-81.51	1.4	1.9
6/11/2017	Merced Bric	-11.84	-82.18	-12.63	-87.82	-0.1	2.2
8/8/2017	Merced Bric	-12.39	-88.12	-13.98	-97.56	-2.0	2.7
8/29/2017	Merced Bric	-11.45	-77.56	-12.06	-83.74	1.8	2.0

[1] Measured, uncorrected values. [2] Fractionation-compensated values.

Table A4-6. GAMA groundwater sampling dates, locations

Sampling Date	Latitude	Longitude	$\delta^{18}O$ (‰)[1]	$\delta^{2}H$ (‰)[1]	Predicted Source Elevation (km)
7/7/2008	35.3117	-118.4111	-9.47	-68.90	1.17
6/6/2006	35.3126	-118.4068	-9.95	-70.80	1.31
6/6/2006	35.3464	-118.3787	-10.06	-78.00	1.51
6/14/2006	35.5881	-118.4676	-10.62	-77.60	1.60
6/25/2008	35.5881	-118.4676	-10.73	-76.80	1.60
6/29/2006	35.6659	-118.292	-11.09	-83.60	1.84
6/25/2008	35.6659	-118.292	-11.07	-82.10	1.80
6/26/2008	35.6772	-118.4894	-9.99	-76.30	1.46
6/14/2006	35.7051	-118.4566	-10.52	-77.10	1.57
6/13/2006	35.7074	-118.4734	-10.05	-74.20	1.41
6/12/2006	35.7244	-118.552	-11.07	-75.50	1.63
7/8/2008	35.7244	-118.552	-11.12	-73.50	1.59
7/8/2008	35.7248	-118.6801	-9.49	-65.20	1.08
6/5/2006	35.7441	-118.4225	-13.34	-100.00	2.66
7/7/2008	35.7441	-118.4225	-13.59	-99.40	2.69
6/7/2006	35.798	-118.4518	-13.94	-101.00	2.80
6/12/2006	35.8299	-118.4567	-14.20	-104.00	2.92
7/9/2008	35.8793	-118.6794	-10.06	-69.10	1.28
6/21/2006	35.9268	-118.494	-12.72	-92.80	2.37
7/9/2008	35.9277	-118.493	-12.92	-93.50	2.42
7/16/2008	36.1004	-118.851	-9.22	-66.20	1.06
7/16/2008	36.1421	-118.627	-11.95	-81.60	1.94
7/15/2008	36.4285	-118.9056	-8.70	-62.10	0.86
7/15/2008	36.442	-118.9011	-8.86	-62.10	0.89
8/7/2008	36.4493	-118.6071	-13.59	-96.80	2.63
7/24/2008	36.6957	-118.8776	-12.42	-85.20	2.12
7/14/2008	36.7009	-119.0101	-11.10	-74.20	1.60
10/16/2008	37.0277	-118.9977	-13.33	-96.90	2.58
7/23/2008	37.1051	-119.3196	-11.77	-80.50	1.88
5/17/2006	37.1235	-119.8738	-8.94	-66.50	1.02
5/8/2006	37.1596	-119.8469	-8.73	-63.10	0.89
5/23/2006	37.1702	-119.7574	-9.08	-64.90	1.00
5/22/2006	37.1946	-119.4658	-11.94	-83.90	2.00
5/24/2006	37.1988	-119.7726	-8.63	-62.70	0.86
5/23/2006	37.2088	-119.7807	-8.60	-61.50	0.83
5/9/2006	37.2134	-119.6816	-9.49	-66.20	1.11
5/22/2006	37.2225	-119.4828	-11.02	-76.40	1.64
5/11/2006	37.2257	-119.5105	-11.92	-82.50	1.96
5/9/2006	37.2263	-119.7206	-9.64	-67.90	1.18
5/22/2006	37.2269	-119.5063	-11.92	-81.90	1.94
5/25/2006	37.2519	-119.7921	-8.64	-61.40	0.83
5/23/2006	37.2563	-119.7169	-9.35	-66.70	1.09
5/18/2006	37.2634	-119.6961	-9.35	-65.30	1.06
7/22/2008	37.2736	-119.6202	-10.83	-72.20	1.50
5/8/2006	37.2744	-119.5336	-11.19	-77.00	1.69
5/18/2006	37.2778	-119.6232	-10.66	-71.30	1.45
5/17/2006	37.2923	-119.5207	-10.78	-73.20	1.52
5/11/2006	37.3141	-119.5348	-12.24	-85.30	2.09
5/23/2006	37.3277	-119.6485	-10.16	-72.40	1.39

5/16/2006	37.3294	-119.6361	-9.55	-67.30	1.15
5/15/2006	37.3329	-119.5812	-10.58	-73.00	1.48
7/22/2008	37.3329	-119.5812	-10.84	-73.50	1.54
5/25/2006	37.3439	-119.4789	-11.64	-78.20	1.80
5/24/2006	37.3456	-119.7633	-9.22	-65.20	1.03
5/25/2006	37.3476	-119.4878	-11.94	-82.10	1.95
5/10/2006	37.3542	-119.6879	-10.06	-70.60	1.32
5/12/2006	37.3576	-119.7214	-11.24	-78.10	1.73
5/31/2006	37.3877	-119.6291	-11.95	-83.90	2.00
5/15/2006	37.4144	-119.7306	-10.48	-71.70	1.42
5/24/2006	37.4194	-119.6052	-11.59	-80.20	1.84
5/16/2006	37.4514	-119.6381	-12.93	-90.20	2.34
7/21/2008	37.4621	-119.7313	-11.65	-82.60	1.91
7/21/2008	37.6124	-120.1272	-8.98	-64.30	0.97
8/13/2008	37.7419	-119.5966	-12.72	-95.60	2.44
8/12/2008	37.7951	-119.3418	-14.36	-107.00	3.03
8/13/2008	37.8181	-120.0587	-10.62	-74.40	1.52
8/14/2008	37.8451	-120.1416	-10.28	-73.60	1.44
8/14/2008	37.8568	-119.9485	-10.90	-77.50	1.65
7/30/2008	37.9312	-120.3732	-8.92	-65.00	0.97
7/30/2008	37.9734	-120.3414	-9.20	-64.00	1.00
10/15/2008	38.0394	-120.1993	-11.08	-75.60	2.45
8/5/2008	38.0444	-120.5219	-8.49	-59.20	1.69
7/29/2008	38.088	-120.1922	-10.85	-77.00	2.45
7/31/2008	38.1475	-120.0731	-12.31	-88.40	2.92
7/28/2008	38.3264	-119.7544	-14.08	-103.00	3.52
10/15/2008	38.3576	-120.8269	-8.20	-56.40	1.58
8/18/2008	38.4436	-120.6316	-9.37	-65.20	1.96
8/6/2008	38.4746	-120.8336	-8.34	-59.60	1.68
8/18/2008	38.581	-120.5771	-10.65	-74.40	2.36
8/21/2008	38.6573	-120.6041	-9.80	-69.20	2.11
8/26/2008	38.8004	-120.0961	-13.61	-97.90	3.33
7/30/2007	38.8328	-120.0447	-13.44	-94.40	3.23
7/30/2007	38.8483	-120.0687	-13.25	-93.90	3.19
8/25/2008	38.8816	-120.0775	-13.50	-97.40	3.31
9/8/2008	38.8861	-121.2656	-8.13	-61.20	1.68
8/25/2008	38.9235	-120.3856	-12.09	-83.10	2.77
10/22/2008	39.0121	-120.9936	-9.50	-63.60	1.94
10/22/2008	39.0563	-120.7313	-10.62	-71.60	2.29
9/18/2008	39.1428	-121.1465	-8.62	-59.90	1.73
7/17/2007	39.1635	-120.2338	-13.85	-98.50	3.38
10/8/2008	39.2765	-120.9327	-10.60	-70.60	2.26
10/9/2008	39.3158	-120.7909	-10.96	-74.10	2.40
7/18/2007	39.3201	-120.1234	-13.86	-102.00	3.46
7/10/2007	39.3207	-120.2082	-12.73	-92.30	3.07
8/28/2008	39.3226	-120.6146	-11.89	-83.00	2.74
7/9/2007	39.3249	-120.2918	-13.61	-96.90	3.31
7/16/2007	39.345	-120.2503	-14.56	-105.00	3.64
7/9/2007	39.3514	-120.2688	-14.31	-102.00	3.53
10/8/2008	39.5176	-121.1966	-10.38	-68.80	2.19
10/7/2008	39.6251	-121.3751	-9.70	-66.60	2.04
9/17/2008	39.6964	-120.667	-12.39	-86.10	2.88
10/6/2008	39.74	-121.6788	-9.01	-61.90	1.83
10/7/2008	39.8152	-121.5976	-9.80	-64.90	2.02

10/6/2008	39.8786	-121.167	-11.95	-82.20	2.73

[1] Measured, uncorrected values. [2] Fractionation-compensated values.

Chapter 5 Summary Conclusion

Precipitation stable isotope signatures were affected by elevation, season and canopy interception, which were characterized in this dissertation through analysis of new precipitation and snowmelt data at expanded spatial and temporal scales. The LMWL for the entire Sierra Nevada had a slope of 7.20 (±0.12) and offset of 3.13 (± 1.25). The mean $\delta^{18}O$ input was -9.80 (± 4.25). The volume weighted LMWL for the Southern Sierra Critical Zone Observatory, with a slope of 6.54 (± 0.39) and an offset of -9.08 (± 4.91) was not significantly different from the non-weighted LMWL with a slope of 5.93 (± 0.35) and offset of -12.64 (± 3.87). The LMWL varied by season, with slopes ranging from 4.7 (± 0.2) in summer to 9.0 (± 0.1) in winter. However, interannual variation was low, and the slope for the water year 2016 LMWL 7.5 (± 0.5) and the slope of the water year 2017 LMWL 7.7 (± 0.4). Canopy intercepted snowmelt signatures were significantly higher than snowmelt measured in open areas in both water year 2016 and water year 2017 ($p < 0.001$). Through the 2016 and 2017 melt seasons, snowmelt did not increase over time. Precipitation input signatures decreased with elevation at both elevational transects sampled, the American Transect and Kings Transect, however, variability over time was high. Amount weighted isotopic lapse rates were -3.3 (±1.8) ‰/km in the American Transect and -2.8 (± 1.8) ‰/km in the Kings Transect.

Vegetation xylem water was analyzed for both water stable isotopes and tritium and compared with measurement of precipitation, saturated zone meadow water and runoff in a central Sierra headwater catchment. Vegetation changed water sources depending on availability, based on stable isotope signatures. Furthermore, tritium concentrations in vegetation confirm that vegetation accesses "younger" water, compared to groundwater, which is composed of a mix of water ages, including "older" water from deeper flow paths. Both vegetation and groundwater were composed of water that originated as snowmelt in forest gaps, that had not been intercepted by forest canopy, based on stable isotope signatures.

Mean vegetation xylem stable isotope signatures measured during eight field sampling campaigns ranged from -12.5 (± 0.55) ‰ in $\delta^{18}O$ during winter snowmelt season to -9.6 (± 0.32) ‰ in $\delta^{18}O$ following fall rain. During winter snowmelt season, both headwater catchment groundwater and xylem water stable isotope signatures were consistent with signatures of snowmelt that was not intercepted by forest canopy. ^{3}H concentrations in vegetation were distinct from the ^{3}H concentrations in groundwater, with mean concentrations of 22.3 (± 5.9) pCi/L and 6.8 (± 0.7) pCi/L, respectively. Furthermore, the distinction between vegetation and groundwater concentrations was consistent throughout winter and summer seasons. Major rivers in California had ^{3}H concentrations similar to groundwater from the Southern Sierra Critical Zone Observatory headwater catchment. This dissertation showed that using a multi-tracer approach ($\delta^{18}O$, $\delta^{2}H$ and ^{3}H) enhanced the scales at which we were able to investigate ecohydrologic connectivity within a headwater catchment.

River source elevation on the mountain range scale was estimated by combining river stable isotope data and isotopic lapse rates, finding that the source elevation of spring 2017 major rivers, was 2.5 km (± 0.7) km. Individual river source predictions using this tracer method were compared to results from an independent mass balance approach, finding that one the mountain range scale, river water consistently originated above mean catchment elevation, even though subsurface geology and topography varied across basins.

Limitations to this dissertation include time in which samples were collected, limitations in the ability to collected and process soil and vegetation sample for tritium and stable isotopes, and limitations to access samples, such as high elevation snow and water within bedrock fractures. Although this dissertation relies on new isotopic data at a higher spatial and temporal resolution than previously published, longer term data collection, collecting samples from inaccessible

locations and collecting vegetation samples in higher numbers would lead to new insights in isotope hydrology and ecohydrology. A longer-term record of Sierra Nevada snowpack stable isotopes could determine if the differences measured here, (mean $\delta^{18}O$ in WY 2016, -92‰ and in WY 2017 -80‰ and from the entire Sierra the mean $\delta^{2}H$ was -67.39) compared to precipitation measurements in the 1960s, -122.5‰ in $\delta^{2}H$ (Friedman & Smith, 1972), were due to climate change. Differences in the isotopic lapse rates between the American Transect and the Kings Transect suggest that microclimate and storm source can have a large effect on precipitation stable isotope signatures. Therefore, additional precipitation stable isotope data at higher spatial resolution and sampling throughout many distinct storms, could determine the effects and feedback among microclimate, storm source and characteristics. Additionally, the years that this study took place included extreme hydrometeorological conditions, including severe drought in 2015 and extreme precipitation in 2017.

The time required to process soil and vegetation samples for stable isotopes and tritium limited the sample size for this study; additionally, the lack of standard methods to measure stable isotopes in soil water present challenges and limited my confidence in soil water stable isotope results. The small sample size for each vegetation species precluded statistical analysis to determine species differences in vegetation water use strategies and competition. Furthermore, the number of times a single tree can be resampled is limited. Recent research has revealed challenges in reliably determining stable isotope signatures of soil water. Extraction time, temperature, vacuum pressure mineral properties and soil characteristics can affect stable isotope signatures from extracted soil water (Gaj et al., 2019; Meik Meissner et al., 2014; Oerter et al., 2014; Orlowski, Breuer, et al., 2016; Orlowski, Pratt, et al., 2016; Orlowski et al., 2018; Oshun et al., 2016; Sprenger et al., 2015).

The research findings here point to the significance of deep flow paths, containing older water, contributing to runoff, which can provide drought resilience. Although I sampled subsurface water from each layer of soil and weathered bedrock, and meadow groundwater, sampling subsurface unsaturated water with a hand augur limits spatial sampling to the penetrable area and does not facilitate sampling from bedrock fractures, which could provide deep storage for water. Sierra Nevada bedrock fractures have been observed containing roots (Hubbert et al., 2001) and fractures that had previously been filled with roots that could provide a conduit for water to flow deep into the subsurface. It has been estimated that as much as $3.7 \times 10^{7}\ m^{3}$ of water per year can flow through fractured and faulted bedrock in the southern Sierra Nevada, which has recharged desert basins on the southeastern side of the Sierra Nevada (Thyne et al., 1999), although we would expect differences in the rain-shadowed eastern Sierra compared to the leeward, western side of the Sierra Nevada.

Through use of a strategic combination of hydrologic tracers, we estimated the elevational origin of major Sierra Nevada rivers following complex critical zone interactions including coupled biological-physical and geological processes, determined forest vegetation water sources on new temporal dimensions and provide a baseline of precipitation input signals affected by elevation, season and canopy interception. As climate change affects the coupled biological and physical processes governing the flux of water through the Sierra Nevada critical zone, this dissertation provides a baseline to compare with future conditions.

References

Friedman, I., & Smith, G. I. (1972). Deuterium content of snow as an index to winter climate in Sierra-nevada area. *Science, 176*(4036), 790-&.

Gaj, M., Lamparter, A., Woche, S. K., Bachmann, J., McDonnell, J. J., & Stange, C. F. (2019). The Role of Matric Potential, Solid Interfacial Chemistry, and Wettability on Isotopic Equilibrium Fractionation. *Vadose Zone Journal, 18*(1).

Hubbert, K. R., Graham, R. C., & Anderson, M. A. (2001). Soil and weathered bedrock: Components of a Jeffrey pine plantation substrate. *Soil Science Society of America Journal, 65*(4), 1255-1262.

Meissner, M., Koehler, M., Schwendenmann, L., Hoelscher, D., & Dyckmans, J. (2014). Soil water uptake by trees using water stable isotopes (delta H-2 and delta O-18)-a method test regarding soil moisture, texture and carbonate. *Plant and Soil, 376*(1-2), 327-335.

Oerter, E., Finstad, K., Schaefer, J., Goldsmith, G. R., Dawson, T., & Amundson, R. (2014). Oxygen isotope fractionation effects in soil water via interaction with cations (Mg, Ca, K, Na) adsorbed to phyllosilicate clay minerals. *Journal of Hydrology, 515*, 1-9.

Orlowski, N., Breuer, L., & McDonnell, J. J. (2016). Critical issues with cryogenic extraction of soil water for stable isotope analysis. *Ecohydrology, 9*(1), 3-10.

Orlowski, N., Pratt, D. L., & McDonnell, J. J. (2016). Intercomparison of soil pore water extraction methods for stable isotope analysis. *Hydrological Processes, 30*(19), 3434-3449.

Orlowski, N., Winkler, A., McDonnell, J. J., & Breuer, L. (2018). A simple greenhouse experiment to explore the effect of cryogenic water extraction for tracing plant source water. *Ecohydrology, 11*(5).

Oshun, J., Dietrich, W. E., Dawson, T. E., & Fung, I. (2016). Dynamic, structured heterogeneity of water isotopes inside hillslopes. *Water Resources Research, 52*(1), 164-189.

Sprenger, M., Herbstritt, B., & Weiler, M. (2015). Established methods and new opportunities for pore water stable isotope analysis. *Hydrological Processes, 29*(25), 5174-5192.

Thyne, G. D., Gillespie, J. M., & Ostdick, J. R. (1999). Evidence for interbasin flow through bedrock in the southeastern Sierra Nevada. *Geological Society of America Bulletin, 111*(11), 1600-1616.

Chapter 6 Future Research

I sampled sulfur-35 and tritium in the fourteen major rivers discussed in Chapter 3 of this dissertation during both wet and dry seasons and have performed laboratory analysis on these samples. This data will be used to determine the percent new water (PNW), which is water that fell as precipitation within the water year (Uriostegui et al., 2017). Preliminary analysis of sulfur-35 measurements from fourteen major Sierra Nevada rivers revealed that over 60% of the river runoff in 2017 was composed of snow that fell during winter 2017 and about 40% was stored in the mountain watersheds before winter 2017, suggesting the importance of water stored in a form other than snowpack. All rivers had similar mean residence times between 8 and 14 years based on tritium concentrations with little seasonal variation. Meanwhile, the portion of river runoff made up of the most recent winter's snowpack varied considerably from river to river and season to season, with some catchments releasing large amounts of young water in spring and other river catchments showing a lag in snow melt contributions. The amount of yearly snowpack has previously been the focus of determining river runoff, however, these results highlight the importance of subsurface storage in headwater catchments that provide water to major rivers years after snow has melted.

Understanding Sierra Nevada subsurface storage by determining how runoff is stored, either as groundwater or snowpack, will inform water resources management facing climate change. In the Sierra Nevada "new" water is stored as snowpack, and in runoff, the portion of new water can be determined using sulfur-35, and stable isotopes (Jasechko et al., 2016). Water storage in the Sierra Nevada is either stored as snowpack or stored in the subsurface. By determining when catchments release new (recent snowmelt), or older water (more than one year old) stored in the subsurface, we can predict how streamflow may be sustained or falter under emerging climate conditions.

The concept of "young" water in the field of hydrology and ecohydrology is garnering substantial interest because of its fundamental importance to both theoretically-based hydrology and water resource management (Jasechko et al., 2016; Kirchner, 2016a, 2016b; McDonnell et al., 2010). Measuring tracers and hydrograph information together is essential to understand how catchments respond to perturbations by storing and releasing water (McDonnell & Beven, 2014). How fast water flows through systems is fundamental to biogeochemical cycling, chemical weathering and water quality (Bieroza & Heathwaite, 2016; Brunke et al., 1998; Hyer et al., 2001; Zimmer & McGlynn, 2018). Californians are critically dependent on water from the Sierra Nevada (Gilbert & Maxwell, 2018; Rhoades et al., 2018), yet the fate of how each winter's snowmelt is delivered to rivers is difficult to predict (Bales et al., 2018; Lundquist et al., 2015; Rheinheimer et al., 2016). Future climate conditions will likely include increased temperatures, evaporative demand (Pierce et al., 2013; Williams et al., 2013), evapotranspiration(Goulden & Bales, 2014), rain-on-snow events and flooding (Huang et al., 2018; Musselman et al., 2018).

The ideal location to understand how rain and snow are either stored or released to rivers is in the Tule and Kaweah Rivers, which are both located in the Southern Sierra Nevada, but the Kaweah River headwaters are located at a higher elevation. How the Kaweah and Tule rivers, in the lower latitude of the Sierra Nevada, store and release rain and snow will help forecast future river runoff and storage and would provide insights into how other Sierra Nevada rivers, as well as mountain-fed rivers and lakes, globally, will respond as the global reservoir of snow continues to decline.

Existing river discharge, precipitation, snow level, geology and elevation data can be analyzed. Historical streamflow data for the Kaweah and Tule are available through the Department of Water Resources California Data Exchange Center from May 2007 on and January 2010 on, respectively. Snow level (S-band radar) data is available through NOAA Earth System Research Laboratory and is collected at Pine Flat (2011 – present) and Kernville (2013 – present), which are

located north and south of the Tule and Kaweah rivers. Previously, S-band radar derived snow level data has been used to accurately determine the rain snow transition in the northern Sierra Nevada4. Analysis of precipitation amounts relative to catchment hypsometry can be performed using PRISM data and digital elevation models. Geology within each catchment will be characterized using data from the California Department of Conservation. By complementing these existing measurements with the use of novel tracer data, the goal would be to understand how water is stored in upper elevations in terms of subsurface storage versus snowpack.

Understanding relationships between elevation, weathering and regolith production are also important to understanding how mountains store water in the subsurface and act as key critical zone feedbacks. In mountain systems weathering and recharge-discharge are coupled processes at the critical zone surface-subsurface interface that regulate and determine water residence times and the availability of water resources downstream. In mountain catchments the fraction of water that falls as precipitation within a year, "young water", is the most sensitive to interannual precipitation variability and drought; consequently, as high elevation snowpack declines due to climate warming, understanding the storage and release of young water through subsurface flowpaths in mountain systems is critical (Hamlet et al., 2005; Leung et al., 2004; Mankin et al., 2015; Rango & Martinec, 1995). Furthermore, elevation controls much of the heterogeneity in mountain climates through temperature and orographic precipitation. Climate contributes to the heterogeneity in bedrock weathering and regolith development, factors affecting subsurface water storage capacity. Likewise, high elevation areas are characterized by lower temperatures, more exposed rock, less vegetation and thinner soils, factors that affect chemical weathering rates (Drever & Zobrist, 1992; Velbel, 1993) that may lead to lower water storage capacity and shorter flowpaths. On the other hand, bedrock fractures can serve as subsurface water storage compartments and conduits for flow (Ajami et al., 2011; Paillet, 1993); indeed, frost cracking occurs in cold, high elevation areas (Hales & Roering, 2007). Incidentally, (Jasechko et al., 2016) found that steeper landscapes had less young streamflow and attributed this to deeper vertical infiltration, however further research is warranted to better understand these processes in mountain systems. Research is needed to understand elevational effects on weathering related to hydrologic flow paths, specifically flowpaths of vulnerable young water portions in mountain systems. Young water portions can be determined using sulfur-35 (Uriostegui et al., 2017), elevation water source using stable isotope lapse rates, combined with measurements of ^{10}Be and U–Th–Ra disequilibria at different elevations to determine elevation - weathering and regolith production rate relationships.

References

Ajami, H., Troch, P. A., Maddock, T., Meixner, T., & Eastoe, C. (2011, Apr). Quantifying mountain block recharge by means of catchment-scale storage-discharge relationships. *Water Resources Research*, *47*, Article W04504. https://doi.org/10.1029/2010wr009598

Bales, R. C., Goulden, M. L., Hunsaker, C. T., Conklin, M. H., Hartsough, P. C., O'Geen, A. T., Hopmans, J. W., & Safeeq, M. (2018, Jan). Mechanisms controlling the impact of multi-year drought on mountain hydrology. *Scientific Reports*, *8*, Article 690. https://doi.org/10.1038/s41598-017-19007-0

Bieroza, M. Z., & Heathwaite, A. L. (2016, Dec). Unravelling organic matter and nutrient biogeochemistry in groundwater-fed rivers under baseflow conditions: Uncertainty in in situ high-frequency analysis. *Science of the Total Environment*, *572*, 1520-1533. https://doi.org/10.1016/j.scitotenv.2016.02.046

Brunke, M., Gonser, T., & Grieder, E. (1998). Environmental gradient patterns in hyporheic interstices: A model based on hydrologic exchange processes. *Advances in River Bottom Ecology*, 23-30.

Drever, J. I., & Zobrist, J. (1992, Aug). Chemical-weathering of silicate rocks as a function of elevation in the southern swiss alps. *Geochimica Et Cosmochimica Acta, 56*(8), 3209-3216. https://doi.org/10.1016/0016-7037(92)90298-w

Gilbert, J. M., & Maxwell, R. M. (2018, Jul). Contrasting warming and drought in snowmelt-dominated agricultural basins: revealing the role of elevation gradients in regional response to temperature change. *Environmental Research Letters, 13*(7), Article 074023. https://doi.org/10.1088/1748-9326/aacb38

Goulden, M. L., & Bales, R. C. (2014, Sep). Mountain runoff vulnerability to increased evapotranspiration with vegetation expansion. *Proceedings of the National Academy of Sciences of the United States of America, 111*(39), 14071-14075. https://doi.org/10.1073/pnas.1319316111

Hales, T. C., & Roering, J. J. (2007, Jun). Climatic controls on frost cracking and implications for the evolution of bedrock landscapes. *Journal of Geophysical Research-Earth Surface, 112*(F2), Article F02033. https://doi.org/10.1029/2006jf000616

Hamlet, A. F., Mote, P. W., Clark, M. P., & Lettenmaier, D. P. (2005, Nov). Effects of temperature and precipitation variability on snowpack trends in the western United States. *Journal of Climate, 18*(21), 4545-4561. https://doi.org/10.1175/jcli3538.1

Huang, X. Y., Hall, A. D., & Berg, N. (2018, Jun). Anthropogenic Warming Impacts on Today's Sierra Nevada Snowpack and Flood Risk. *Geophysical Research Letters, 45*(12), 6215-6222. https://doi.org/10.1029/2018gl077432

Hyer, K. E., Hornberger, G. M., & Herman, J. S. (2001, Dec). Processes controlling the episodic steamwater transport of atrazine and other agrichemicals in an agricultural watershed. *Journal of Hydrology, 254*(1-4), 47-66. https://doi.org/10.1016/s0022-1694(01)00497-8

Jasechko, S., Kirchner, J. W., Welker, J. M., & McDonnell, J. J. (2016, Feb). Substantial proportion of global streamflow less than three months old. *Nature Geoscience, 9*(2), 126-+. https://doi.org/10.1038/ngeo2636

Kirchner, J. W. (2016a, 2016). Aggregation in environmental systems - Part 1: Seasonal tracer cycles quantify young water fractions, but not mean transit times, in spatially heterogeneous catchments. *Hydrology and Earth System Sciences, 20*(1), 279-297. https://doi.org/10.5194/hess-20-279-2016

Kirchner, J. W. (2016b, 2016). Aggregation in environmental systems - Part 2: Catchment mean transit times and young water fractions under hydrologic nonstationarity. *Hydrology and Earth System Sciences, 20*(1), 299-328. https://doi.org/10.5194/hess-20-299-2016

Leung, L. R., Qian, Y., Bian, X. D., Washington, W. M., Han, J. G., & Roads, J. O. (2004, Jan-Feb). Mid-century ensemble regional climate change scenarios for the western United States. *Climatic Change, 62*(1-3), 75-113. https://doi.org/10.1023/b:clim.0000013692.50640.55

Lundquist, J. D., Hughes, M., Henn, B., Gutmann, E. D., Livneh, B., Dozier, J., & Neiman, P. (2015, Aug). High-Elevation Precipitation Patterns: Using Snow Measurements to Assess Daily Gridded Datasets across the Sierra Nevada, California. *Journal of Hydrometeorology, 16*(4), 1773-1792. https://doi.org/10.1175/jhm-d-15-0019.1

Mankin, J. S., Viviroli, D., Singh, D., Hoekstra, A. Y., & Diffenbaugh, N. S. (2015, Nov). The potential for snow to supply human water demand in the present and future. *Environmental Research Letters, 10*(11), Article 114016. https://doi.org/10.1088/1748-9326/10/11/114016

McDonnell, J. J., & Beven, K. (2014, Jun). Debates-The future of hydrological sciences: A (common) path forward? A call to action aimed at understanding velocities, celerities and residence time distributions of the headwater hydrograph. *Water Resources Research, 50*(6), 5342-5350. https://doi.org/10.1002/2013wr015141

McDonnell, J. J., McGuire, K., Aggarwal, P., Beven, K. J., Biondi, D., Destouni, G., Dunn, S., James, A., Kirchner, J., Kraft, P., Lyon, S. W., Maloszewski, P., Newman, B., Pfister, L., Rinaldo, A., Rodhe, A., Sayama, T., Seibert, J., Solomon, K., Soulsby, C., Stewart, M., Tetzlaff, D., Tobin, C., Troch, P., Weiler, M., Western, A., Worman, A., & Wrede, S. (2010, Jun 15). How old is streamwater? Open questions in catchment transit time conceptualization, modelling and analysis. *Hydrological Processes*, *24*(12), 1745-1754. https://doi.org/10.1002/hyp.7796

Musselman, K. N., Lehner, F., Ikeda, K., Clark, M. P., Prein, A. F., Liu, C. H., Barlage, M., & Rasmussen, R. (2018, Sep). Projected increases and shifts in rain-on-snow flood risk over western North America. *Nature Climate Change*, *8*(9), 808-+. https://doi.org/10.1038/s41558-018-0236-4

Paillet, F. L. (1993, Oct). Using borehole geophysics and cross-borehole flow testing to define hydraulic connections between fracture-zones in bedrock aquifers. *Journal of Applied Geophysics*, *30*(4), 261-279. https://doi.org/10.1016/0926-9851(93)90036-x

Pierce, D. W., Westerling, A. L., & Oyler, J. (2013, 2013). Future humidity trends over the western United States in the CMIP5 global climate models and variable infiltration capacity hydrological modeling system. *Hydrology and Earth System Sciences*, *17*(5), 1833-1850. https://doi.org/10.5194/hess-17-1833-2013

Rango, A., & Martinec, J. (1995, Aug). Revisiting the degree-day method for snowmelt computations. *Water Resources Bulletin*, *31*(4), 657-669.

Rheinheimer, D. E., Bales, R. C., Oroza, C. A., Lund, J. R., & Viers, J. H. (2016, May). Valuing year-to-go hydrologic forecast improvements for a peaking hydropower system in the Sierra Nevada. *Water Resources Research*, *52*(5), 3815-3828. https://doi.org/10.1002/2015wr018295

Rhoades, A. M., Jones, A. D., & Ullrich, P. A. (2018, Sep). Assessing Mountains as Natural Reservoirs With a Multimetric Framework. *Earths Future*, *6*(9), 1221-1241. https://doi.org/10.1002/2017ef000789

Uriostegui, S. H., Bibby, R. K., Esser, B. K., & Clark, J. F. (2017, Mar 15). Quantifying annual groundwater recharge and storage in the central Sierra Nevada using naturally occurring S-35. *Hydrological Processes*, *31*(6), 1382-1397. https://doi.org/10.1002/hyp.11112

Velbel, M. A. (1993, Dec). Temperature-dependence of silicate weathering in nature - how strong a negative feedback on long-term accumulation of atmospheric CO2 and global greenhouse warming. *Geology*, *21*(12), 1059-1062. https://doi.org/10.1130/0091-7613(1993)021<1059:tdoswi>2.3.co;2

Williams, A. P., Allen, C. D., Macalady, A. K., Griffin, D., Woodhouse, C. A., Meko, D. M., Swetnam, T. W., Rauscher, S. A., Seager, R., Grissino-Mayer, H. D., Dean, J. S., Cook, E. R., Gangodagamage, C., Cai, M., & McDowell, N. G. (2013, Mar). Temperature as a potent driver of regional forest drought stress and tree mortality. *Nature Climate Change*, *3*(3), 292-297. https://doi.org/10.1038/nclimate1693

Zimmer, M. A., & McGlynn, B. L. (2018, Mar). Lateral, Vertical, and Longitudinal Source Area Connectivity Drive Runoff and Carbon Export Across Watershed Scales. *Water Resources Research*, *54*(3), 1576-1598. https://doi.org/10.1002/2017wr021718